Cranfield University

A. P. Moody

A Peroxide Sensor for the Food and Beverages Industry

Institute of Bioscience and Technology

PhD Thesis

Cranfield University

Institute of Bioscience and Technology

PhD Thesis

Academic Years 2001 – 2002

A. P. Moody

A Peroxide Sensor for the Food and Beverages Industry

Supervisor: Professor S. Saini

November 2001

This thesis is submitted for the degree of Doctor of Philosophy

God grant me the serenity to accept things I cannot change,
the courage to change things I can
and wisdom to know the difference.

Reinhold Biebuhr (1892 - 1971)

Abstract

Due to desirable environmental reasons, peroxides have replaced halogenated substances for disinfection purposes in the food and beverage industry. However, cost issues and the requirement to completely remove these agents after disinfection necessitates simple, low-cost and sensitive test methods with a wide dynamic range and on-line capability. The development and performance of such a method is detailed in this thesis. The novelty of this work was in the simplified production of the sensor by pre-mixing all active components before application onto a screen-printed graphite base electrode in a single step.

Having established the principle of pre-mixing all the components, the proportions were optimised with regard to a balance between cost and required performance in the industrial application. Once this had been established, the performance and stability was evaluated in the laboratory, a comparative study was performed against other methods for hydrogen peroxide determination and finally the sensor was demonstrated to work in a small-scale industrial field trial.

Some of the available mass-production processes for the sensor were considered for suitability and a recommendation made. The relative analytical performances of sensors produced manually and by the recommended process were compared to their visual appearance under a microscope and a possible quality control process suggested for the manufacturing stage.

Finally, a scanning electrochemical microscope was commissioned and a method for producing ultramicroelectrodes for use with it developed. This was then used to study the variation of the sensor surface coating with the aim of facilitating the optimisation of the composition, production and quality control processes.

Acknowledgements

I would like to express my gratitude to my supervisor, Professor. S. Saini for the help and guidance I have received throughout my work on this thesis.

I also acknowledge the financial support of the European Union Standards, Measurements and Testing programme, Europerox project (SMT4 - CT97 - 2153) and the cooperation of partners therein: especially Cees Bonis and Lauren Plevier from Skalar Analytical BV; for the on-line testing studies and loan of equipment; Dr. Diedrich Harms & Dr. Frank Nitzsche of the König-Brauerei GmbH & Co. KG for the comparative study and on-line testing facilities.

I would also like to thank all my colleagues and friends in IBST for their support whilst I have been working on this thesis, to list them all would take too many pages. However, I must include a special thank-you to the sadly deceased David Weston who encouraged us all be 'mad for it' and got me hooked (should I admit it here?) on 'Buffy the vampire slayer'; may he rest in peace.

A special thank-you to Heather Cole for reminding me of the rules of English grammar, spelling and generally encouraging me to make the text comprehensible.

Finally, a big thank-you to my family and all my musician friends, once again too many to name individually, who have helped me maintain my sanity (?) when I was not actually working.

Contents

List of Figures

List of Tables

1. General Introduction

The origin of this thesis was to develop a biosensor for on-line monitoring of hydrogen peroxide concentrations in industrial processes where it is used for disinfection and bleaching.

This chapter will introduce the background of the project and explain why the sensor was required by industry followed by a brief description of some of the current methodologies for determining hydrogen peroxide. The overall objectives of the thesis are then described.

The different techniques used throughout the work are then introduced along with a brief introduction to sensor technology and screen-printing as they relate to this thesis. The production processes used to produce the sensor are then described and finally the scanning electrochemical microscope is introduced as a technique for surface characterisation of the sensor. The literature for these areas will be reviewed during the relevant chapters where the discussions will have more relevance.

1.1. Background

1.1.1 Industrial Requirements

Hydrogen peroxide is used for disinfection in the food and beverages industry where reliable disinfection methods have to be used to guarantee consumer safety. It is also used for bleaching in the textile and paper production industries where they are looking for cost-effective and environmentally acceptable bleaching procedures.

A wide range of chemical agents are routinely used for disinfection purposes in industrial processes, including alcohols, aldehydes, gaseous agents, phenolics and halogenated compounds, with the latter group being most widely employed for reasons of cost and efficiency (Wurster, 1992; Krüßmann & Bohnen, 1994).

In recent years however, peroxides such as hydrogen peroxide and peroxyacetic acid have been increasingly used since they are more potent oxidising agents than many of

the routinely used halogenated disinfectants. Hydrogen peroxide readily decomposes into water and oxygen and therefore poses no threat to the environment and reduces the possibility of disinfectant contamination due to inadequate rinsing of production vessels. The halogenated compounds however, remain permanently toxic to the environment.

Unfortunately, the environmental benefits of using peroxides are commercially countered by the expense since peroxides typically cost up to three times more than their halogenated counterparts (Krüßmann & Bohnen, 1994). Therefore, in order for peroxide disinfection to be cost-effective, industrial users require simple, low-cost and effective methods for monitoring and thus controlling their usage and waste (Forber, 1992; Wurster, 1992; Krüßmann & Bohnen, 1994). Furthermore, since manufacturers achieve error free disinfection and avoid biological contamination by working with excess levels of disinfectant, on-line measurement procedures would allow the manufacturer to accurately maintain disinfectant levels above a desired threshold value thereby minimising excess disinfectant usage. Such on-line measurement procedures would also allow the end-user to rapidly and routinely confirm that all disinfectant residues have been removed from the production vessel prior to commencement of the next production cycle.

The EUROPEROX project consortium was formed (with European Union funding) to develop new selective and reliable methods for peroxide analysis. The consortium partners from five European Union countries were from a mix of industrial and academic institutions to give a range of backgrounds and outlooks on the problem. Cranfield University was an academic partner with the task of developing a bioelectrochemical sensor for continuous liquid phase hydrogen peroxide monitoring. Other partners had tasks to develop methods for hydrogen peroxide monitoring in the gas phase and peroxyacetic acid in gas and liquid phases.

An example of current cleaning process practice is that used at the König brewery, an industrial partner in the EUROPEROX project. They have a process controlled such that the concentration of peroxide does not fall below 30 $mmol.l^{-1}$ during the disinfection process. To achieve this they currently start the process with a 220 $mmol.l^{-1}$ peroxide concentration. To facilitate the removal of organic material during the cleaning cycle,

the wash solution also contains 0.5 $mol.l^{-1}$ sodium hydroxide and is heated to between 60 and 80 degrees Celsius (Harms, 2001 personal communication).

This initial concentration of hydrogen peroxide is considered sufficient to compensate for the losses that occur due to its breakdown during the disinfection process. The operators must add this extra quantity because the current analytical methods (titration, photometry) are not suitable for on-line monitoring at the concentrations and speed needed. Thus, an adequate on-line detection method would reduce their consumption and thus costs considerably.

The chemical methods currently available for the determination of peroxides in solution are all based upon the production of a coloured product that can be quantified spectrophotometrically and related to the concentration of hydrogen peroxide (Frew *et al*, 1983). However, the inherent electroactivity of these compounds also allows their simple measurement using electroanalytical techniques, notably amperometry in which an electrode is set at a suitable operating potential and the current due to the reduction of the peroxide measured.

The hot, caustic nature of the wash solution will pose a problem for most analytical methods but it is easily cooled and neutralised. However, the organic debris such as yeast cells will pose a random problem for any spectrophotometric method because of the light scattering properties these particles will have. Also, when the process begins the wash solution is clear and colourless but gradually becomes dark brown as the organic material is charred. Regardless of the detection wavelength, this will also cause a variable level of interference. The advantage of an electrochemical biosensor is that its response is not affected by changes in colour or particulates.

1.1.2 Current Methodologies

Current methods for hydrogen peroxide determination in solution are varied but are all based upon the production of a coloured product that can be quantified spectrophotometrically and related to the concentration of hydrogen peroxide (Frew *et al*, 1983). All can be used for concentrations of 1 to 10 $\mu mol.l^{-1}$ in aqueous solution.

The relevant points are summarised below and the reader should refer to Frew *et al*, 1983 for further detail if required.

1) Hydrogen peroxide forms a yellow complex with titanium (IV) sulphate under acidic conditions but this is somewhat insensitive compared to the other methods with a molar absorptivity of 720 l mol^{-1} cm^{-1} at 410 nm. Also, as the industrial wash process uses an alkaline wash, this would not be the ideal reaction to utilise

2) Potassium iodide is oxidised by hydrogen peroxide and organic hydroperoxides in the presence of an ammonium molybdate catalyst. The triiodide produced is then measured spectrophotometrically. This is a more sensitive method with a molar absorptivity of 2.5 x 10^4 l mol^{-1} cm^{-1} at 350 nm.

3) Iron (II) is oxidised to Iron (III) by peroxides and the Iron (III) then forms a coloured complex with xylenol orange that has a molar absorptivity of 2.68 x 10^4 l mol^{-1} cm^{-1} at 540 nm.

4) Iron-porphyrin complexes (ferrihaems) catalyse the decomposition of peroxides in a two-stage process. The iron-porphyrin complex is activated by reaction with hydroperoxide to form an oxidised iron-porphyrin intermediate. This intermediate then reacts with suitable electron donors; the extent of the oxidation of the donor is then used as a measure of the peroxide. The first stage is pH dependent (greater than pH 10 being favoured) but with the sequential reactions taking place, there is a greater risk of unintended side reactions.

5) Peroxides will oxidise phenolphthalin to phenolphthalein in the presence of a Cu^{2+} catalyst. The phenolphthalein is then measured spectrophotometrically under alkaline conditions with a molar absorptivity of 3.3 x 10^4 l mol^{-1} cm^{-1} at 552 nm. This method has been successfully used in industrial processes but the reaction is slow compared to the other methods.

6) Horseradish peroxidase coupled oxidations with various substrates can be used and are highly selective for hydrogen peroxide. 4-aminoantipyrene and phenol give a product with a molar absorptivity of 6.4 x 10^3 l mol^{-1} cm^{-1} at 505 nm.

Overall, none of the above methods are simple and straightforward. They also require reagent preparation and sequential reagent additions followed by spectrophotometry. A sensor device requiring only a dilution in buffer with concentration read-out would be a big advantage by not only simplifying the monitoring system set-up and maintenance but also the simplicity and relatively low cost of reagent preparation.

1.1.3 Objectives

The objective of this thesis is to take the reader through the development and testing stages of a sensor for hydrogen peroxide that can meet the requirements of a food or beverage production facility such as the König brewery in Germany. The brewery, being an industrial partner in the EUROPEROX project that funded much of this work, also made available materials and facilities for field-testing.

The key requirements that were taken into account during the development were:

1) A commercially viable sensor should have relatively low production costs. To achieve this, the design had to be compatible with current mass production technologies and use readily available and inexpensive materials.

2) Operating costs should be kept as low as possible.

3) The sensor should be readily incorporated into the on-line monitoring systems used for temperature, particulates and fluid flow that are already in place at a production facility.

4) Routine maintenance should be minimal and simple enough for a semi-skilled operator to perform.

Having developed a working sensor, light microscopy and the relatively new technique of scanning electrochemical microscopy were assessed for usefulness in the characterisation of the sensor surface. By characterising the surface, it was hoped that the information could be used to aid in the development of a suitable mass production process for the final sensor.

1.2 Sensors and their Composition

The following definitions are from the International Union of Pure and Applied Chemistry (IUPAC, 2000).

A chemical sensor is a device that transforms chemical information, ranging from the concentration of a specific sample component to total composition analysis, into an analytically useful signal. Chemical sensors contain usually two basic components connected in series: a chemical (molecular) recognition system (receptor) and a physico-chemical transducer. Biosensors are chemical sensors in which the recognition system utilises a biochemical mechanism.

An electrochemical biosensor is a self-contained integrated device, which is capable of providing specific quantitative or semi-quantitative analytical information using a biological recognition element (biochemical receptor) which is retained in direct spatial contact with an electrochemical transduction element.'

Turner (1987) gave a more concise definition that still remains valid: 'A Biosensor is a device incorporating a biological sensing element which is either intimately connected to or integrated within a transducer.'

1.2.1 Chemical Sensors for Hydrogen Peroxide

The inherent electroactivity of peroxides will allow their amperometric measurement using just simple carbon electrodes. The problem using these types of electrodes is the applied potential required for the reduction process to occur. The operating potential can be reduced using noble metals such as gold or platinum or more inexpensively using electrocatalytic materials such as metallised carbons (Kröger & Turner, 1997; Newman *et al*, 1995; Sampath & Lev, 1997; Selkirk, 1997; Wang, J. *et al*, 1995).

However, even with these materials, a significant potential is required and signal interference due to the presence of other electroactive compounds in a given sample can occur. Whilst a further reduction in operating potential will reduce the magnitude of the interference signal, this will also be at the expense of the analyte signal.

1.2.2 Biosensors for Hydrogen Peroxide

The interference problem can be effectively eliminated by the use of biological rather than electrochemical catalysts, allowing the application of very low operating potentials. For hydrogen peroxide, this is routinely achieved using the redox enzyme horseradish peroxidase. Horseradish peroxidase is able to reduce hydrogen peroxide to water with the concomitant oxidation of a suitable electron donor usually called a mediator (see section 1.2.5). The biological catalyst improves the selectivity, whilst the mediator lowers the required operating potential.

1.2.3 Enzyme Biosensors

An enzyme is a protein that is synthesised in a living cell and catalyses or speeds up a thermodynamically possible reaction. The enzyme in no way modifies the equilibrium constant or free energy change of the reaction. The specificity of the enzyme is due to the highly complex structure of the enzyme protein which provides both the environment for a particular reaction mechanism and the template function to recognise a limited set of substrates (Conn & Stumpf, 1976).

The specificity of certain enzymes and their high turnover rate make them favourable components for biosensors. In general, they are also inexpensive and readily available, thus making them desirable in a commercial application.

For more specialised devices, some enzymes can be linked to other biological components such as antibodies or antigens, thus allowing an alternative measurement or signal amplification technique. Then, when the antibody or antigen is involved in an immunological reaction, the enzyme will be attached to the antibody-antigen complex. After removing any excess of labelled antigen or antibody, the activity of the remaining enzyme is used to estimate the amount of complex and thus analyte in the original sample.

During the reaction, the enzyme structure changes due to the loss or gain of electrons. This can also be a complex process but is simplified in figure 1.1 below

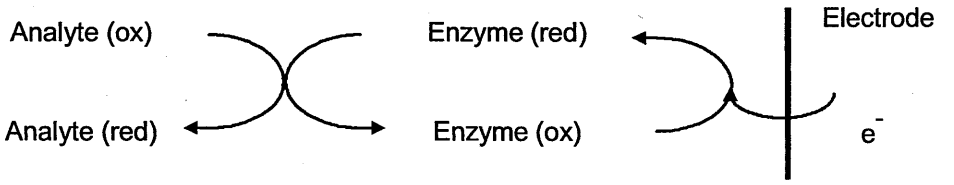

Figure 1.1 Electrochemical principle of an enzyme biosensor

1.2.4 Peroxidases

Peroxidases are classified as the group of enzymes that catalyse the oxidation of numerous organic and inorganic compounds by peroxides. Most peroxidases contain ferriprotoporphyrin IX as prosthetic group (the non-protein component of a conjugated protein), of the few that do not, most contain some other hemin derivative. Thus they are large molecules with horseradish peroxidase having a molecular weight of about 42,000 excluding any bound water (Dunford, 1982) and a physical size of 6 nm (Okawa *et al*, 1999). The large size of the enzyme causes problems linking the enzyme to the electrode as will be discussed in the next section.

Peroxidases catalyse the following sequence of reactions

$$\text{Native Enzyme} + H_2O_2 \longrightarrow \text{Compound I} + H_2O \qquad (1.1)$$

$$\text{Compound I} + \text{AH} \longrightarrow \text{Compound II} + {}^{\bullet}\text{A} \qquad (1.2)$$

$$\text{Compound II} + \text{AH} \longrightarrow \text{Native Enzyme} + {}^{\bullet}\text{A} \qquad (1.3)$$

AH is a reducing substrate (electron donor) and $^{\bullet}$A is a free radical

Compound I is formed in the two-electron oxidation of the native enzyme by hydrogen peroxide. Compound I is then reduced by the substrate AH, in a one-electron transfer to yield compound II. To complete the cycle, native enzyme is then produced from compound II in a second one-electron reduction by the substrate (Dunford, 1982).

Figure 1.2 develops the process shown in figure 1.1 with the analyte being hydrogen peroxide, the electron donor being the electrode and the process expanded to show the two-stage reduction back to the native enzyme.

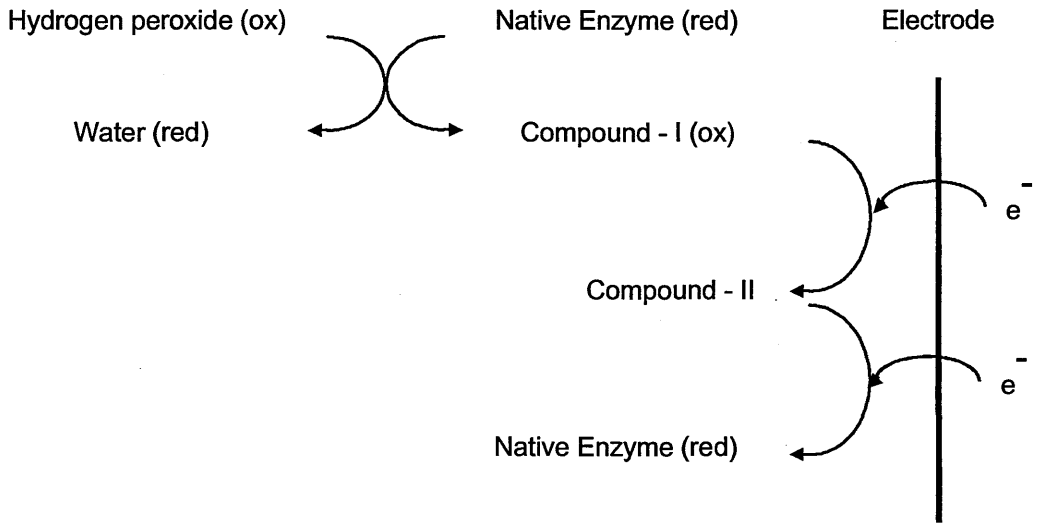

Figure 1.2 Electrochemical principle of a peroxidase biosensor

More recently, a similar mechanism involving the formation of a supervalent iron-oxo-porphyrin cation radical has been postulated (Lotzbeyer *et al*, 1994)

$$[(HN)Fe^{III}] + H_2O_2 \longrightarrow [(HN)Fe^{IV}{=}O]^{\bullet +} + H_2O \qquad (1.4)$$

This is then reduced by a two-stage electron transfer from the electrode

$$[(HN)Fe^{IV}{=}O]^{\bullet +} + e^- + H^+ \longrightarrow [(HN)Fe^{IV}\text{-}OH] \qquad (1.5)$$

$$[(HN)Fe^{IV}\text{-}OH] + e^- + H^+ \longrightarrow [(HN)Fe^{III}] + H_2O \qquad (1.6)$$

1.2.5 Mediators for Enzyme Biosensors

The dictionary definition of a mediator is 'something that serves as a medium for causing a result or transferring objects or information etc' (Collins English Dictionary, 1979). In this electrochemical usage, a mediator performs the function by facilitating the transfer of electrons between an electrode and an enzyme.

Incorporating enzymes into sensors can improve their selectivity and sensitivity. However, due to their physical size, under normal conditions enzymes cannot make direct contact with the metallic component of the electrode. This slows down the transfer of electrons from the reaction site to the electrode. In addition, when the sample solution is a complex mixture, there may be other components with electrochemical activity at the same electrode potential as the analyte.

In electroanalytical systems, it is common practice to incorporate a fast electron transfer mediator into the system to overcome this problem. This acts as a medium for speeding up electron transfer from the enzyme to the electrode and lowering the potential required for the transfer to take place.

To develop further the electrochemical process taking place at the biosensor surface, if one refers back to figure 1.2, the electrochemical principle of a peroxidase biosensor, this can be further developed for the mediated peroxidase biosensor and is shown in figure 1.3.

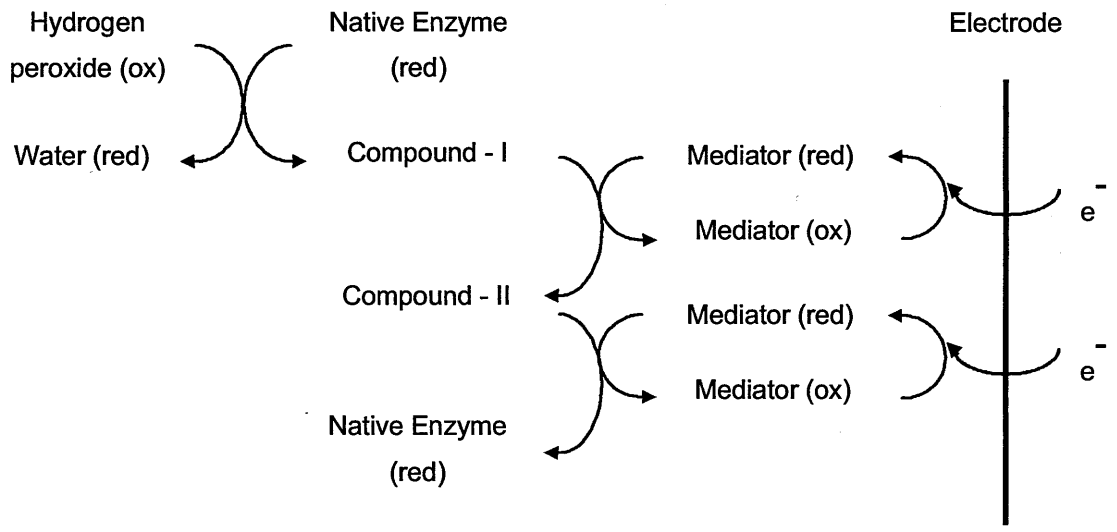

Figure 1.3 The electrochemical principle of a mediated peroxidase biosensor

1.2.6 Immobilisation and Membranes

Enzymes and many mediators are soluble in aqueous solution. For a single use sensor, it is possible that all the active components will remain on the surface of the sensor long enough to make a measurement. However, in a monitoring situation, the sensor needs to be stable over a long period and the continuously changing sample will remove some of the soluble components of the sensors. Immobilisation of these components or the application of a membrane over them will retain them on the surface to give a longer active lifetime. Also, depending on the choice of membrane material, there is a good possibility that the membrane will add to the selectivity of the sensor by stopping some potential interferents from reaching the active components. Membranes have also been used to reduce surface fouling and extend the electrode linear range (Vadgama, 1990). Membranes also improve biocompatibility when sensors are used *in-vivo* or *in-vitro* by reducing complement activation and surface coagulation (Vadgama, 1992).

1.3 Electrochemistry

Throughout this section the general texts: Instrumental methods in electrochemistry (Southampton electrochemistry group 1990) and Electrode Dynamics (Fisher 1996) were used.

Electrochemistry is the study of electron transfer reactions between electrodes and reactant molecules. Many parameters have been found to influence the dynamics of these reactions. In principle, the following can all control the rate of the charge transfer process:

1) The electrode potential.
2) The reactivity (ease of oxidation or reduction) of the solution species.
3) Transport of material between the electrode and bulk solution.
4) The nature of the electrode surface.
5) The structure of the interfacial region over which the electron transfer occurs.

1.3.1 The Electrochemical Cell.

There are two types of electrochemical cell.

1) Galvanic cell.
   This converts the energy produced by a physical or chemical change into electrical energy (the principle of the domestic battery) and is not used in this work.

2) Electrolytic cell.
   This requires an external supply of electrical energy to bring about a physical or chemical change to take place at the electrode surface. This is the type of cell used throughout this work.

1.3.2 The Electrode Potential

An electrode process involves the transfer of charge across the interface between a solution and an electrode (usually of metallic composition). For example:

$$\underset{\textit{solution}}{\text{Oxidised}} + \underset{\textit{electrode}}{ne^-} \rightleftharpoons \underset{\textit{solution}}{\text{Reduced}} \qquad (1.7)$$

For this reaction to proceed, the electrode must act as a source (supplier) or a sink (acceptor) of electrons. This depends upon the relative concentrations of the oxidised and reduced species and thus the direction of the reaction.

Since this reaction involves the transfer of electrons between the electrode and solution, as it moves towards equilibrium, a charge separation must develop between the electrode and solution. This in turn creates a potential difference at the interface called the potential drop.

If Φs represents the solution potential
Φm the electrode potential and
$\Delta\Phi m/s$ the potential drop.

Then $$\Delta\Phi_{m/s} = \Phi_m - \Phi_s \qquad (1.8)$$

This will have a fixed and precise value for any particular system. However, direct measurement of $\Delta\Phi_{m/s}$ is not possible as it is at a single interface and measurement of a potential difference requires a complete, conducting, electrical circuit. Thus, at least one other electrode is required to complete the circuit. This will also have a potential drop and thus any voltage-measuring device connected to the system will monitor the difference of the potential drops at the two electrode/solution interfaces. These two interfaces are then called half-cells and create a two-electrode electrochemical cell (figure 1.4).

By convention, the electrode supplying the electrons is called the cathode and the electrode accepting the electrons is called the anode.

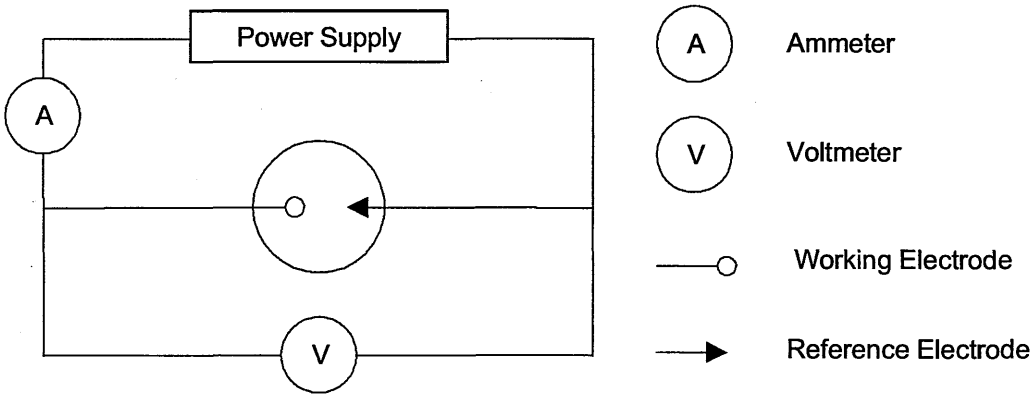

Figure 1.4 A two-electrode electrochemical cell

When a measurement of potential difference is made between two electrodes, the observed voltage (E) is given by

$$E = (\Phi m - \Phi s) + (\Phi m - \Phi s) \qquad (1.9)$$

measuring electrode *counter electrode*

or $\Delta\Phi_{m/s}$ (*measuring electrode*) + $\Delta\Phi_{m/s}$ (*counter electrode*) (1.10)

In this situation, there are now two unknown values. To overcome this, a counter electrode with a known potential is used. Because it has a known potential, it is called a reference electrode and will maintain a constant potential drop across its interface with the solution.

Provided no current is drawn through the cell, the potential difference between the two electrodes quickly reaches a steady equilibrium value (E_e) dependent upon the relative concentrations of the oxidised and reduced forms of the analyte.

Thus, the potential at the measuring electrode (E_e) can be represented by the equation

$$E_e = E\,(\textit{measured}) - \Delta\Phi_{m/s}\,(\textit{reference electrode}) \qquad (1.11)$$

As the potential of the reference electrode is known, this then becomes

$$E_e = E\,(\textit{measured}) - \text{Constant} \qquad (1.12)$$

If current is drawn through the cell, there will be a potential difference between the electrode and the solution. Up to about 2 mV, this reference electrode can still be used as the counter electrode, but as the voltage difference becomes greater, this is no longer the case. In these situations, a third electrode must be introduced into the system (figure 1.5). This extra electrode then acts as the counter electrode for the electrochemistry and the reference electrode is used to provide a stable reference potential. This arrangement allows the measurement of large currents above 10μA

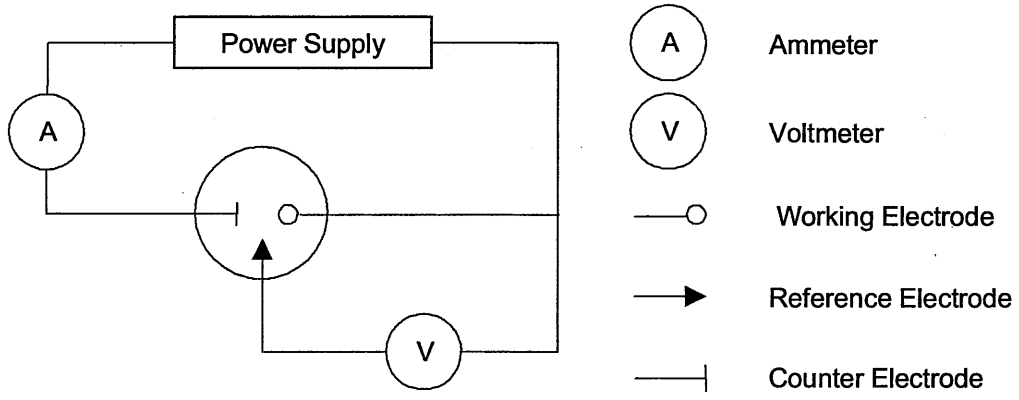

Figure 1.5 A three-electrode electrochemical cell

Referring back to equation (1.7), Nernst showed that the potential established at the electrode under equilibrium conditions is given by:

$$E_e = E^{\theta} + \ln \frac{RT}{nF} \cdot \frac{[\text{Oxidised}]}{[\text{Reduced}]} \qquad (1.13)$$

F is the Faraday constant (96485 C mol^{-1})

R is the Molar Gas constant (8.31451 J $mol^{-1}.K^{-1}$)

T is Absolute Temperature (K)

The equilibrium potential (E_e) of the electrode results from the standard electrode potential (E^{θ}) of the reaction and the activities of the oxidised and reduced components at the electrode surface, which are the same as the bulk solution activities when at equilibrium. (In a dilute solution, the activity of a species can be assumed to be the same as concentration)

1.3.3 The Electrode – Solution Interface

The presence of an electrode in a solution causes a phase boundary giving rise to two types of solute molecules: those molecules that cannot feel the presence of the electrode and those which are close enough to the electrode to participate in the electrochemical reactions.

The region of solution interacting with the electrode is considered as consisting of three separate planes. Firstly, at the inner Helmholtz plane (IHP), the solute molecules are specifically adsorbed to the electrode surface and therefore cannot be fully hydrated by the solvent. Next, the outer Helmholtz plane (OHP) contains molecules carrying their primary hydration shell, separated from the electrode by a monolayer of solvent molecules. Finally, in the diffuse layer, the solute molecules experience equilibrium between attraction to the ions in the OHP and the opposing random forces of thermal motion.

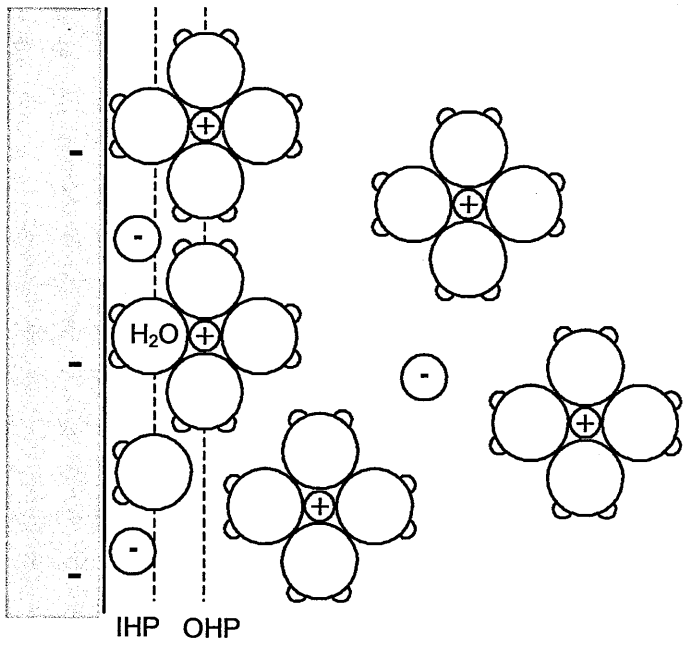

Figure 1.6 Schematic diagram of solute molecule distribution at the electrode solution interface (Southampton electrochemistry group 1990).

1.3.4 Reference Electrodes

A reference electrode is made of non-polarisable material such that there is little change in the potential when a small current is passed. This means that there is no charge build up on the surface and thus the potential remains stable. Conversely, the working electrode is made of a polarisable material such that there is no charge transfer across the electrode-solution interface regardless of the applied potential.

Reference electrodes all have a known potential referenced back to the standard hydrogen electrode, which by convention has an absolute potential of zero. Commonly used reference electrodes are the saturated calomel electrode and the silver / silver chloride electrode.

1.3.5 Amperometry

Amperometry is the simplest electrochemical measurement technique; it is where the current that flows at a fixed potential (different to the equilibrium potential, E_e) is measured. As a relatively long time scale is used, the solution is stirred to remove the effects of natural convection within the solution (or it may be used in a flowing system where the sample at the electrode surface is continuously changing). The steady state current at this known potential is then measured using a potentiostat with circuitry based on that shown in figure 1.5 to give a quantitative value that is proportional to the analyte concentration.

This current induces the exchange of electrons between the electrode and the solute molecules thus altering their oxidation state. This electron transfer can be in either direction.

Thus either reduction (electron gain) at the cathode

$$[\text{Oxidised}] + e^- \longrightarrow [\text{Reduced}] \qquad (1.14)$$

Or oxidation (electron loss) at the anode can occur

$$[\text{Reduced}] \longrightarrow [\text{Oxidised}] + e^- \qquad (1.15)$$

The reactions at the electrode surface can be shown as:

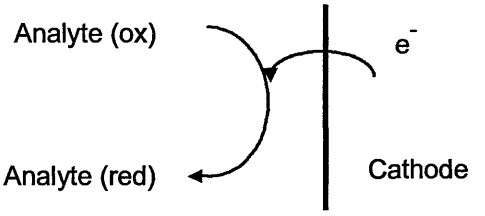

Figure 1.7 Reduction at a cathode

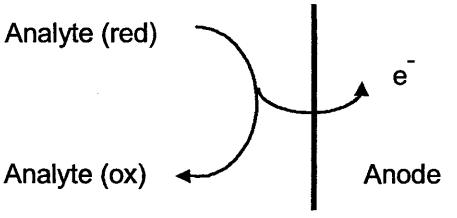

Figure 1.8 Oxidation at an anode

To summarise

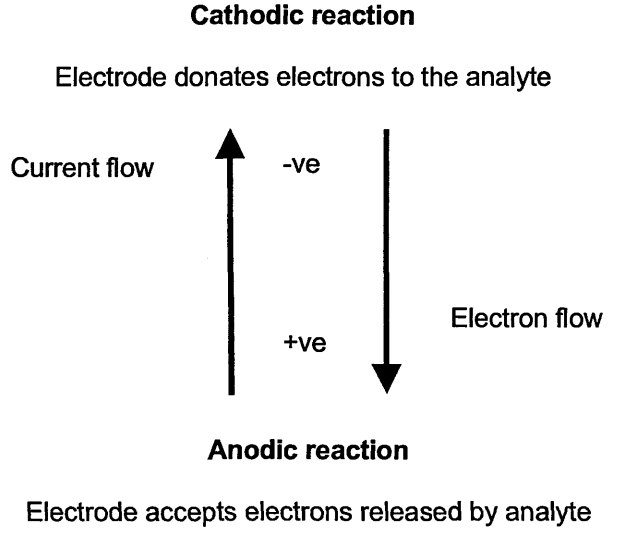

Figure 1.9 Summary of the redox processes seen at electrodes

The magnitude of the current that flows (i) is given by

$$i = AFj \qquad (1.16)$$

A is the electrode area (cm^2)

j is the 'flux' of analyte reaching the electrode surface ($M.cm^{-2}.s^{-1}$)

j is dependent upon many factors beyond the needs of this thesis. However, in a continuously stirred homogeneous solution, or a flowing system, the current can be regarded as proportional to the concentration of analyte.

1.3.6 Linear Sweep Voltammetry

Linear sweep voltammetry is the measurement of current with respect to a changing potential in a single direction at a known sweep rate ($V.s^{-1}$), i.e. the potential starts at E_1 and changes to E_2.

Consider the simple reversible reaction of the type described by equation (1.17) and assume that only the reduced species, R is present initially.

$$R \rightleftharpoons O + n e^- \qquad (1\text{-}17)$$

If a very slow linear potential sweep is applied to the system, a voltammogram similar to that in figure 10. at 0.05 $V.s^{-1}$ will be obtained. As the sweep rate is increased, a peak of increasing height is obtained as shown again by the faster scans in figure 1.10 at 0.10, 0.50 and 1.00 $V.s^{-1}$.

This can be explained by considering what is happening to R at the electrode surface. Until the equilibrium potential (E_e) has been reached there is no reaction, but once this is exceeded, R is oxidised to O. This will produce a measurable current that increases with the increase in the applied potential. However, diffusion of O away from the electrode and its replacement by more R is limited due to the quiescent nature of the solution and this in turn limits the current. At a faster scan rate, the bulk of the initial R is oxidised rapidly giving a peak current that then falls as diffusion fails to replace it.

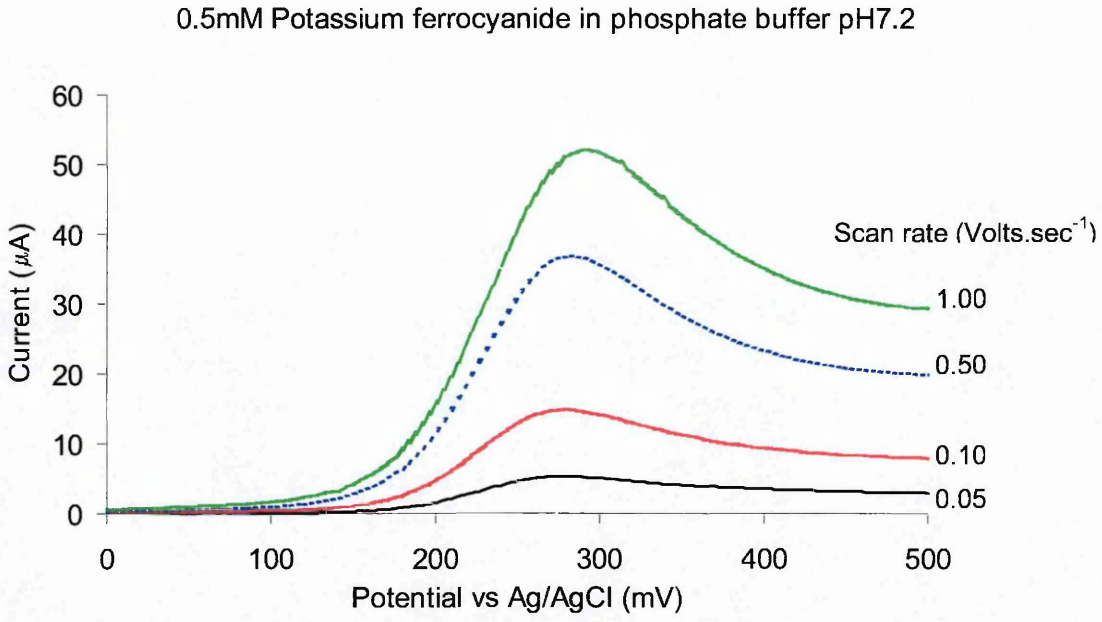

Figure 1.10 Idealised linear sweep voltammograms

1.3.7 Cyclic Voltammetry

Cyclic voltammetry is similar to linear sweep voltammetry, but when potential E_2 is reached, the direction is reversed and returns to potential E_1, usually at the same sweep rate.

With cyclic voltammetry, an 'electrochemical spectrum' is obtained and the relationships between scan rate, peak potential and peak current, can be used to give information about processes such as diffusion, adsorption and coupled homogeneous reactions

Considering the reversible reaction 1.17 again and following on from the explanation for linear sweep voltammetry, there will be a high concentration of O at the electrode once the linear scan has reached E_2. This is reduced back to R as the potential returns to E_1.

As for linear sweep voltammetry, at very slow potential sweeps there will not be a significant peak. However, for faster sweeps on reversal, there is a significant concentration of O near the electrode and it is still being formed until the potential nears the equilibrium potential (E_e). Thus, a peak current will be observed for the same reasons as on the forward scan.

If the reactions are quasi-reversible or irreversible due to the rate of mass transport being greater than the rate of electron transfer or the species not being stable, then the cyclic voltammogram changes. The peaks will separate by more than 59 mV, one peak will be missing or the peak heights will not increase with increased scan rate.

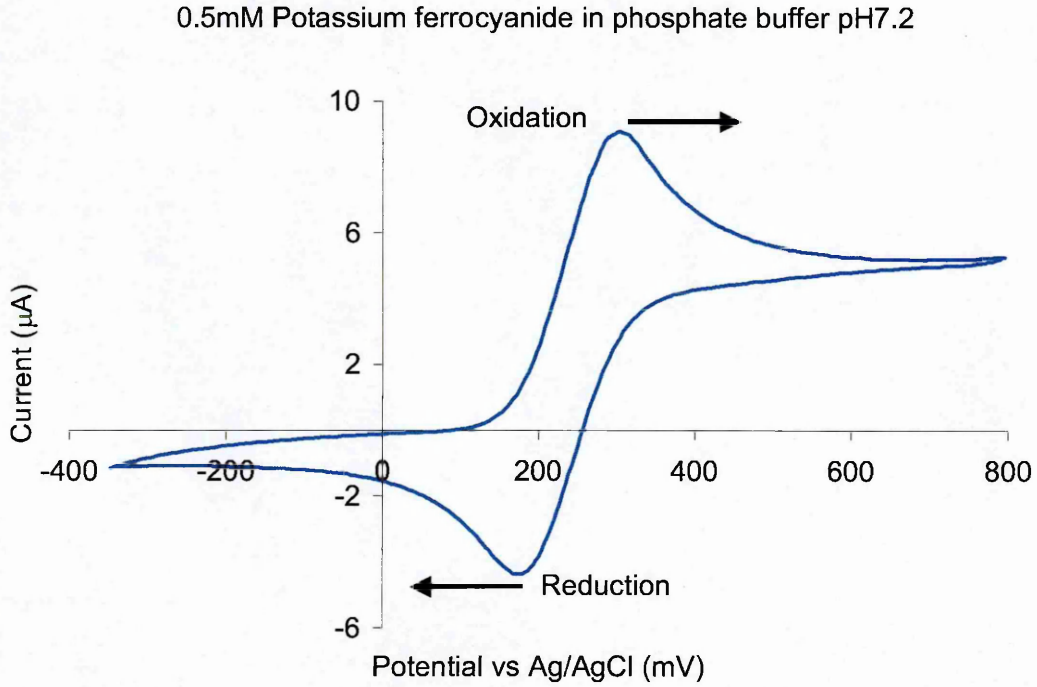

Figure 1.11 Idealised cyclic voltammogram (scan rate $1V.s^{-1}$)

1.4 Screen and Ink-jet Printing

With the widespread establishment of screen-printing processes in the microelectronics and printing industries, the basic materials for the cheap mass production of sensors are readily available (Newman *et al* 1995; Hart *et al*, 1996; Rohm *et al*, 1996; Kröger & Turner, 1997).

Screen-printing is a form of graphic reproduction where a quantity of ink or other viscous compound is forced through a mesh screen onto a surface; parts of this screen are blocked off or 'masked' to prevent the ink passing through. Thus, an image or repeatable pattern of controlled thickness is printed onto the surface. Complex images or multi-layered devices may be built up by using a series of screens with different masking patterns.

Ink-Jet Printing operates by forcing fluid under pressure through a very small nozzle. As the fluid passes through the print head, a drive rod actuated by an oscillating piezoelectric crystal produces a shock wave, which breaks the jet into a series of regular droplets. This occurs at a frequency of about 64 000 Hz, dependent on the modulation voltage. Printing is achieved by charging individual droplets via a charge electrode, which is controlled by a microprocessor. The printed pattern is constructed in a dot matrix format.

1.5 Scanning Electrochemical Microscopy (SECM)

The scanning electrochemical microscope is a scanned probe microscope related to the scanning tunnelling and atomic force microscopes. These microscopes all operate by scanning or "rastering" a very small probe over the surface to be imaged. In scanning electrochemical microscopy, the tip is an ultramicroelectrode and imaging occurs in an electrolyte solution. In most cases, the monitored tip signal is the current resulting from the electrolysis of solution species. The features that distinguish scanning electrochemical microscopy from its related techniques of electrochemical scanning tunnelling microscopy and atomic force microscopy is the chemical sensitivity of its tip and the use of solution phase ions or molecules to produce the imaging signal (Wipf, D. O., 2001).

The first use of such a system to investigate surface reactivity was by Liu and co-workers (Liu *et al*, 1986), who when working with the scanning tunnelling microscope at ultrahigh vacuum looked at the use of a solution as an alternative to the vacuum. Engstrom and co-workers (Engstrom *et al*, 1987) used the amperometric response of a tiny carbon fibre electrode positioned at between 1 μm and 75 μm from the surface of a platinum electrode to investigate the nature of the diffusion layer of the electrode/solution interface.

Bard and co-workers (Bard *et al*, 1989) introduced the term 'scanning electrochemical microscopy' in 1989 when they described the instrumentation, theory and applications of the technique. Since its introduction, it has been used to investigate localised surface reactivity at a variety of solid/liquid interfaces ranging from biomaterials, polymers and minerals to electrode surfaces (Scott *et al*, 1991; Lee *et al*, 1991; Mirkin and Horrocks, 2000). Ion and electron transfer processes occurring at a liquid/liquid interface have also been studied (Barker *et al*, 1999).

A simple example of what can be shown using this technique when investigating localised surface reactivity is given below. Figure 1.12, shows a photomicrograph of a gold array with 15 μm spacing on a glass base and figure 1.13 shows a scanning electrochemical microscope scan obtained by rastering a 10 μm platinum probe over a 100 μm square of the same array using a 100 $mmol.l^{-1}$ hexacyanoferrate solution to provide the electrochemical redox system. The bands of higher current flow correspond to the gold stripes and the lower current flow to the glass insulator. It cannot be a sharp differentiation due to the limited resolution possible with the relatively large probe diameter and the effect of the diffusion layer.

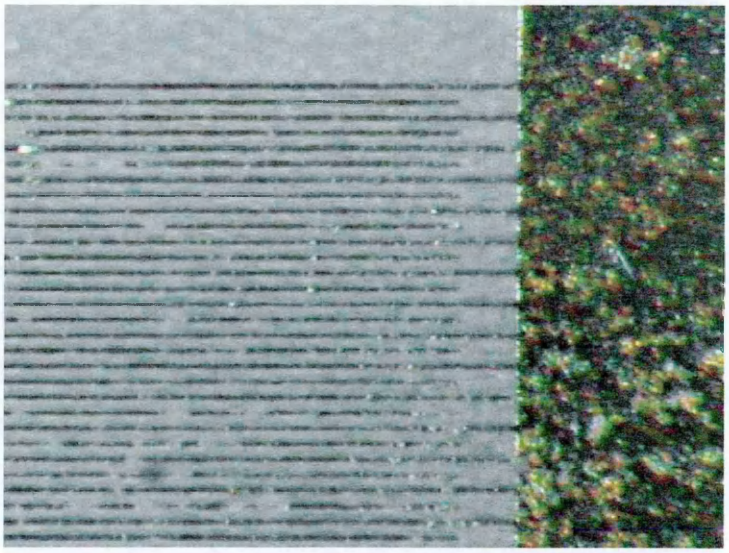

Figure 1.12 Photomicrograph of a gold on glass array with 15 μm spacing (ABTECH Scientific, Inc. Virginia USA)

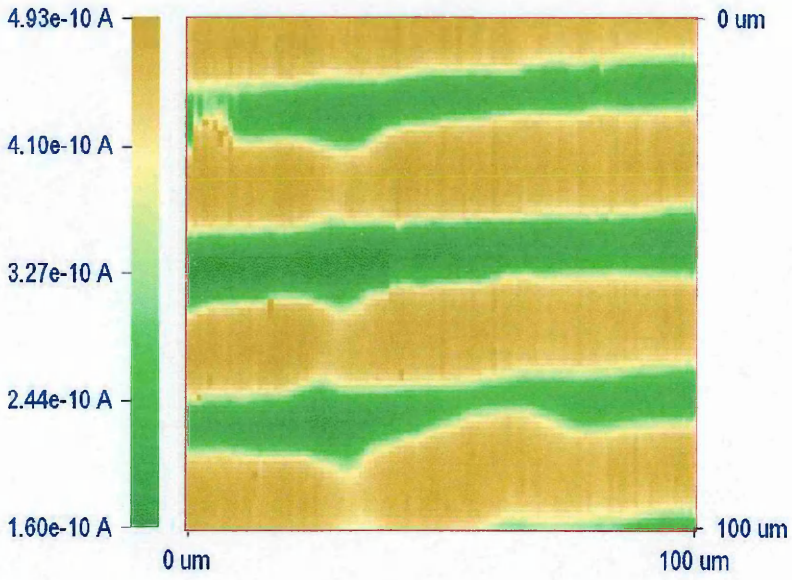

Figure 1.13 Scanning electrochemical micrograph of a gold on glass array with 15 μm spacing (false colour map, green corresponding to the glass and dark yellow to the gold stripes)

The resolution of this technique depends primarily upon the size and shape of the ultramicroelectrode tip and this will be discussed further in chapter 5. The mass and charge transfer process rates that affect the current density distribution and the solution resistance have a lesser, but important influence.

If possible, this technique will be developed to allow the characterisation of different sensor surfaces and optimise their production to give a more even response over the whole surface of a single electrode and thus better reproducibility between sensors. There is little published work so far in this area of the application, but direct electron transfer between microperoxidase and electrodes has been visualised with this technique (Kranz *et al*, 1997)

In addition to imaging, the scanning electrochemical microscope tip can be used as a microscopic source or sink of electrons and chemical reagents. When the tip is positioned close to the surface, these reagents will modify it on a microscopic scale, thus turning the scanning electrochemical microscope into a versatile microfabrication device. In the micro-reagent mode, a reaction at the scanning electrochemical microscope tip changes the local solution composition to provide a driving force for chemical reactions at the surface. Electrolytic generation of an oxidising agent at the tip can precisely etch metal and semiconductor surfaces and local pH changes caused by electrolysis at the tip have been used to deposit metal oxides and polymers (Borgwarth *et al*, 1995).

2. Sensor Construction

2.1 Introduction

As stated in the general introduction to this thesis, some of this work was funded by the European Union as part of the EUROPEROX project. As a consequence of this, the sensor was developed in two stages:

1) A single use sensor was developed and tested to show suitability for the intended industrial application.

2) This single use sensor was then further developed for continuous monitoring in the intended industrial setting with the potential for commercial production being considered at all times.

This chapter describes how the sensor was built-up with discussion regarding the available choices and selections of materials made at each stage.

2.2 General Methods

2.2.1 Materials

Acetone, dipotassium phosphate, hydrogen peroxide (30% w/v), monopotassium phosphate and potassium chloride, all of analytical grade (Merck Eurolab, Poole, UK). Ascorbic acid, horseradish peroxidase (EC 1.11.1.7. 200 U/mg solid. One unit will form 1.0 mg purpurogallin from pyrogallol in 20 sec at pH 6.0 at 20°C, This purpurogallin (20 sec) unit is equivalent to approx. 18 μM units per min at 25°C.) and potassium hexacyanoferrate (II) (Sigma, Poole, UK). 1,1'-dimethylferrocene and tetrathiafulvalene (Aldrich, Gillingham, UK). Cellulose acetate in four different average molecular weights, Nafion (5%w/v in lower aliphatic alcohols and 10% water) and peroxyacetic acid (Fluka Chemie AG, Buchs, Switzerland).

Polyester sheet, 250 μm thick ICI Melinex ST275 (Cadillac Plastic Ltd., Swindon, UK). Graphite ink, Electrodag 423SS (Acheson Colloids, Plymouth, UK). 15% silver

chloride in silver paste, Ag/AgCl (MCA Services Ltd., Cambridge, UK). Blue epoxy-based protective coating ink 242-SB (Agmet ESL Ltd., Reading, UK).

Water was purified by deionisation and reverse osmosis using an Elgastat system (Elga, High Wycombe, UK).

0.1M Phosphate buffer (pH 7.2, containing 0.1 M Potassium Chloride to ensure the presence of sufficient electrolyte) was used throughout the development and testing.

Wash solution from a cleaning process at the König brewery containing unidentified debris in approximately 0.5 M sodium hydroxide.

2.2.2 Safety Considerations

Hydrogen peroxide and peroxyacetic acid are powerful oxidants. Mixtures or solutions of aqueous peroxides with organic compounds are hazardous due to the danger of explosion. Skin contact leads to immediate irritation and whitening (cutaneous emphysema) and longer contact will lead to burns. Contact with the eye leads to serious injury. Peroxide vapors cause irritation or damage to the upper respiratory tract and lungs. The threshold concentration for acute irritative effects of gaseous hydrogen peroxide on the respiratory tract is 10 $mg.m^{-3}$. (Ullman's Encyclopedia of Industrial Chemistry, 1991)

As a precaution, all handling of the concentrated peroxide solutions was carried out in a fume hood and safety glasses and gloves were worn.

2.2.3 Cyclic Voltammetry and Amperometry Procedures

All Cyclic Voltammetry and Amperometry measurements were made with an Autolab Electrochemical Analyser (Autolab) with the general-purpose electrochemical software GPES3 (Ecochemie, Utrecht, Netherlands). All potentials were referenced to a silver/silver chloride reference electrode or the printed silver chloride in silver paste on the sensors. The data files from this were then imported into the spreadsheet software package, Excel (Microsoft Corp., USA) for graphing and analysis. The screen-printed electrodes were connected to the Autolab by using an IDE edge connector from Maplin Electronics plc (Wombwell, South Yorkshire, UK) insulated at one side to give a tighter fit and thus better connection.

For the development and early testing stages, the electrodes were then immersed into 8 ml of the phosphate buffer in a 10 ml beaker, this being the smallest beaker that was large enough to take the sensor and in all cases 2 µl of sample was pipetted into this. All these experiments were performed at ambient temperature between 17 and 21 °C. In the later development and testing stages, a small perspex flow cell was custom built to our design (Model products, Wooton, UK) enabling the experiments to be performed at 25 °C by immersion in a water bath. The individual settings for the Autolab will be given when appropriate in the text.

2.2.4 Screen Printing

Screen-printing is a form of graphic reproduction where a viscous compound (usually ink) is deposited as a film onto a surface in a controlled manner to give a repeatable pattern of controllable thickness (Alvarez-Icaza & Bilitewski, 1993; Goldberg *et al.*, 1994).

This is achieved by pushing the ink through a mesh onto the surface to be covered. The mesh can he made of Nylon, polyester or stainless steel. Blocking areas of the mesh where no ink is required to pass through with an ultra-violet light-sensitive polyvinyl chloride emulsion creates the print pattern.

The distance between the threads of the mesh is usually less than three times the particle size of the ink and the minimum definition of line that can he printed is approximately three times the mesh thread diameter. Figure 2.1 shows a typical stainless steel screen mesh at low and high magnification.

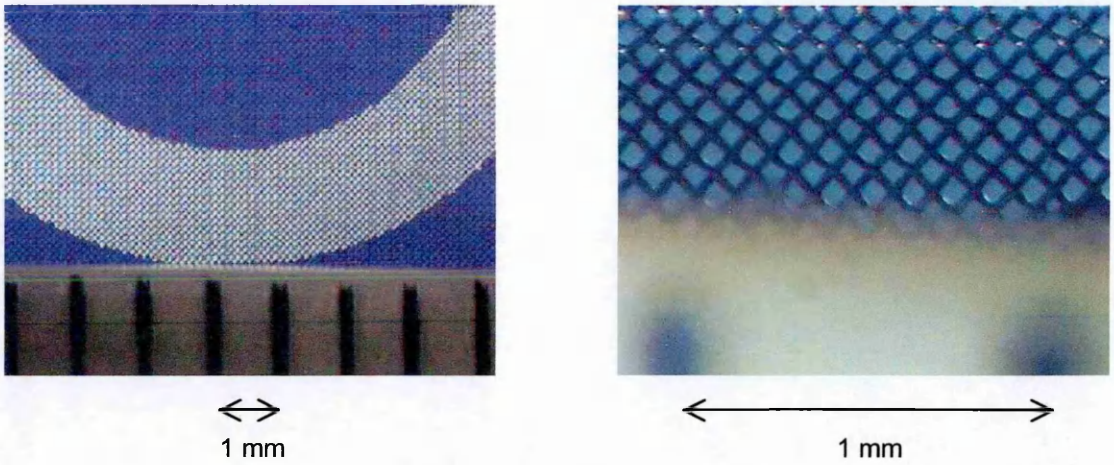

Figure 2.1. Screen-printing mesh.

This mesh is stretched over a rigid aluminium frame (wood and most plastics would not have sufficient strength and durability) to produce the screen. For complex patterns with different inks, a series of matching screens are used with different parts of the pattern blocked on the mesh and then the layers of ink applied in sequence.

The frame is held securely in place and covered with an excess of the ink to be printed. The substrate to be printed is placed on a moving platform that is then moved under the screen and raised until it almost touches it.

When the substrate is in place, a flexible yet firm blade (usually made of polyurethane) called a 'squeegee' is pushed across the screen. As it goes across, the squeegee pushes the screen down onto the substrate and forces ink through the open mesh areas onto it. As the squeegee continues across, it removes excess ink and releases the screen contact with the substrate. At the end of a pass, the squeegee is raised slightly, moved further forward and lowered again so that as it returns to its origin it will pull any excess unused ink back to the origin. Just before the origin, it is raised again and moved back behind the ink ready for the next cycle. At the same time, the substrate platform is lowered and moved out from under the screen so that a fresh substrate can be made ready for printing. Figure 2.2 shows the general layout of this process.

Controlling the speed and pressure of the squeegee has a significant effect on the thickness of the printed layer. A high-speed pass of the squeegee results in a thick

deposit of ink and high pressure results in a thin deposit of ink. Ideally, the squeegee should move across the screen at an angle between 45-60° and have a sharp edge for good definition of the pattern.

As a guideline, the distance between the screen and the substrate (print gap) can he gauged using the width of the screen multiplied by: 0.004 for stainless steel mesh, 0.006 for polyester, or 0.01 for Nylon.

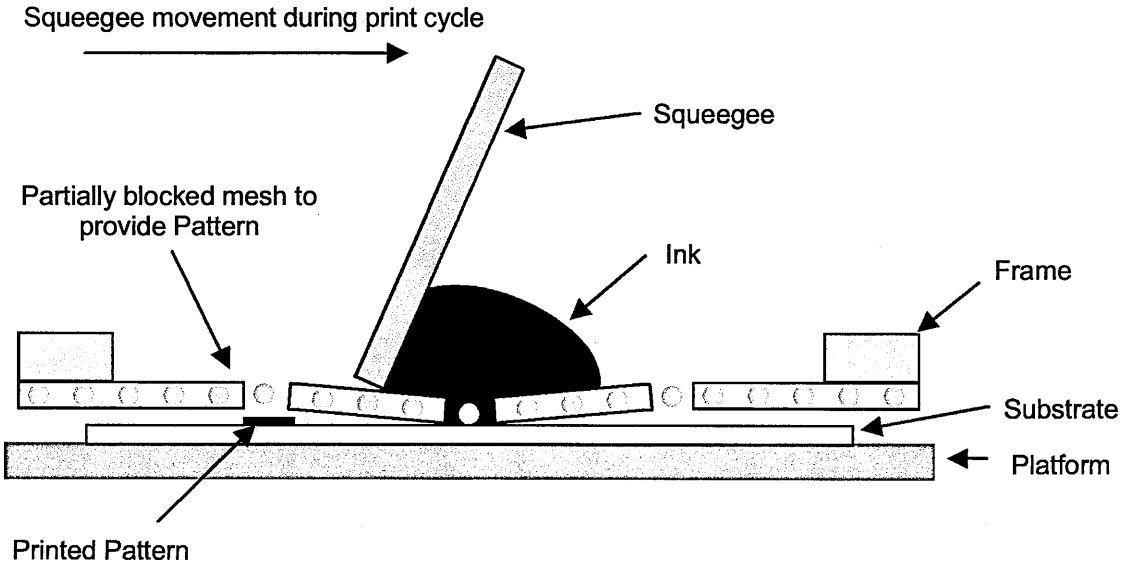

Figure 2.2. General layout of the screen-printing procedure

2.3 Base Electrode Fabrication

Regardless of the final choices for sensor composition, a base electrode structure that was easy and cheap to manufacture was needed. In order to meet this requirement, a three-electrode device was mass-manufactured in-house by a multi-stage screen-printing process.

Screen-printed electrodes are not like metallic or carbon electrodes because they contain binding materials that are not removed during production even by firing processes (Kalab & Skladal, 1995).

With this difference being borne in mind and the requirement for a commercially viable product at the end of the work, the development was done at all times using the screen-printed electrodes. The graphite ink used was the same as would be recommended for production and the physical design of the screens and thus base electrodes was the same as had been previously used by other groups within the department. (Kröger & Turner, 1997; Newman *et al*, 1995 & 1997; Cardosi & Birch, 1993; Hart *et al*, 1996).

This approach had the following three advantages:

1) A new screen design was not required for the production of prototype sensors and thus helped to keep development costs as low as possible.

2) Development time was saved by not having to wait for a new design to be produced.

3) The physical dimensions of the sensor design could be readily changed to fit industrial requirements in the final application should this have become necessary.

The base electrodes were screen-printed in three stages (see figure 2.3) onto 250 μm thick polyester sheets using a DEK 248 automated screen-printing machine (DEK, Weymouth UK); the printer settings are given in table 2.1.

Table 2.1. Parameters for printing electrodes on the DEK 248 screen-printing machine

Print parameter	**Setting**
Print mode	Print/Flood
Squeegee Pressure	4 kg.
Print gap	2.5 mm
Deposits	1
Forward Carrier Speed	50 mm.s-1
Reverse Carrier Speed	50 mm.s-1
Front Limit	38 mm
Rear Limit	402 mm
Separation Speed	70%

The three screens had been produced by the DEK precision screen division and had 60 stencil designs per screen. The stainless steel screen mesh was mounted at 45° to the print stroke with an emulsion thickness of 13 μm.

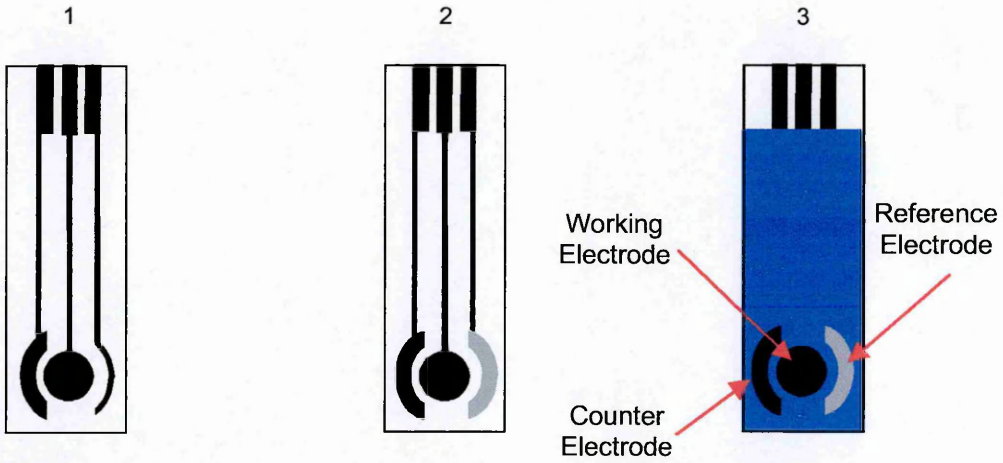

1) Three Graphite tracks were printed onto the plastic backing sheet using a stainless steel stencil with 125 wires per cm.
2) A reference electrode was then printed over one of these tracks using the silver/silver chloride ink and a stainless steel stencil with 77 wires per cm.
3) Finally, an insulating layer was then printed over the graphite tracks using the epoxy-based protective coating ink and a stainless steel stencil with 77 wires per cm to give reproducible working electrode dimensions.

Figure 2.3 The three printing stages of sensor production

The electrodes were then heat-treated at 125°C for 2 hours to cure the epoxy resin to allow prolonged device usage in solution.

If required, other layers can be over-printed sequentially before the insulating ink but it must be born in mind that they must be stable to the heat treatment stage. Insulating inks that are cured by non-heating means are available but do not have the same resistance to water penetration (Selkirk, 1997). The circular working electrode had a planar area of 0.16 cm^2 and with the design used, 60 sensors were produced on each sheet (Figure 2.4).

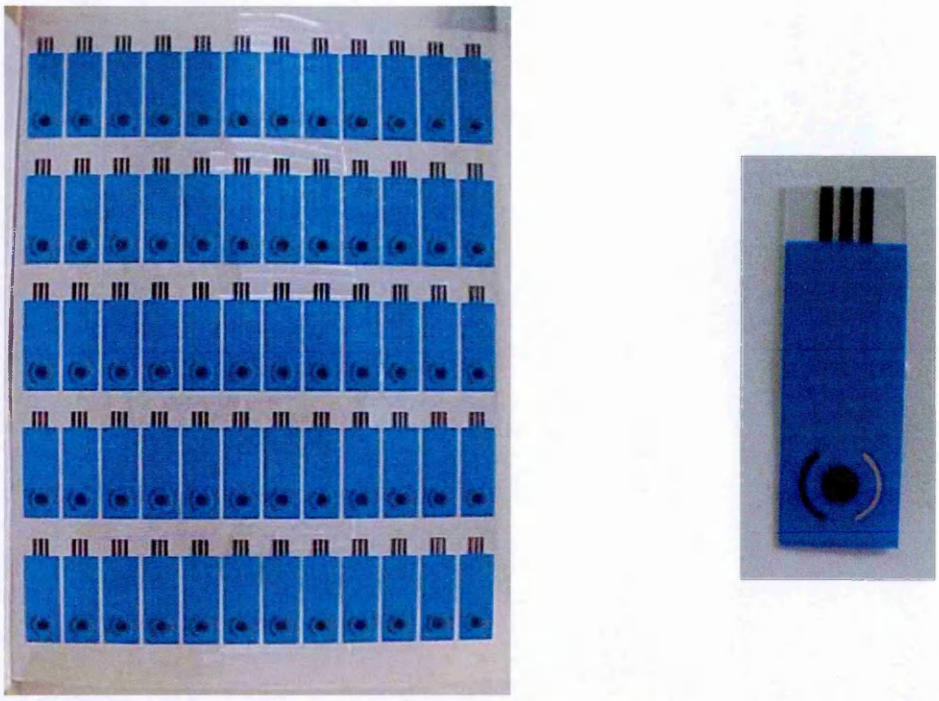

Figure 2.4 Photograph of a sheet of sensors with a single sensor at actual size

2.4 Metallised Carbons or Enzyme Biosensor?

According to Lowe (1985), a biosensor transducer should include the following features:

1) High specificity for the analyte and response in the relevant concentration range.
2) Fast response time (typically 1-60 s).
3) Amenable to minaturisation and designed for practical application.
4) It should not be adversely affected by environmental changes like temperature.

Carbon has the above features and for sensing applications is attractive because it has a wide potential range, low electrical resistance with a low background current and is relatively inexpensive (Gilmartin & Hart, 1995; Wang *et al.* 1996)

Carbon based printing inks offer the advantages of carbon but the printing process requires them to have a low carbon content and the resulting printed surface is complex. This compromises the analytical performance and redox activity (Wang *et al.* 1996).

Carbon alone also requires a high potential to reduce hydrogen peroxide (Frew & Hill, 1988; Wring & Hart, 1992). However, by modifying the surface of the carbon particles with chemical or biological components, the selectivity and sensitivity of the sensor can he enhanced (Gorton, 1985; Wang, 1991).

Chemical modification can facilitate the charge transfer process between the electrode and biological component significantly reducing the overpotential by providing electrocatalytic effects (Wring & Hart, 1992).

For selective amperometric detection, the optimum operating potential should ideally be in the range of –100 mV to 0 mV since most common interfering compounds that may be found in food industry applications (e.g., ascorbic acid or dissolved oxygen) are neither electrochemically oxidised or reduced at these potentials (Cosgrove *et al* 1988). Also, the background current for most materials switches signs in this potential region facilitating sensitive and relatively noise-free detection (Gorton *et al.* 1991).

2.4.1 Metallised Carbons

As stated in the introduction (section 1.1.1), the inherent electroactivity of peroxides will allow their amperometric measurement using just simple carbon electrodes. The problem using these types of electrodes is the high applied potential required for the reduction process to occur. The operating potential can be reduced using noble metals such as gold, platinum or rhodium or less expensively using electrocatalytic materials such as metallised carbons (Kröger & Turner, 1997, Newman *et al.* 1995, Sampath & Lev, 1997, Selkirk, 1997, Wang, J. *et al.* 1995). Highly dispersed noble metals bound with carbon have an electrocatalytic effect due to synergistic and electronic interactions (Mukerjee, 1990).

Use of these metallised carbon electrodes lowers the potential required for the reduction of hydrogen peroxide whilst the potential for many of the common interferents remains higher. Metallised carbon electrodes also offer a fast response with high sensitivity and uncomplicated manufacture (Wang, J. *et al.,* 1995).

Rhodium on carbon (rhodinised carbon) was seen as the most interesting of these electrocatalytic materials as it has been shown it to be more sensitive and selective towards hydrogen peroxide than platinised carbon (White *et al.,* 1994).

Rhodinised carbon is commercially available as a powder and is readily incorporated into an ink for screen-printing. For this reason, a simple comparison was made of rhodinised carbon sensors against the base graphite ink.

2.4.2 Rhodinised Carbon or Graphite as Base Electrode

In order to evaluate the possible use of rhodinised carbon, a sheet of electrodes with a rhodinised carbon ink screen printed over the graphite base of the working electrode area prior to the insulating ink were kindly donated by a colleague, S. Jawaheer.

The only expected chemical interferents to the sensor in its intended industrial applications were ascorbic acid and peroxyacetic acid. The presence of ascorbic acid was considered unlikely in the brewery, but if adopted for other areas of the food industry then it would become a possibility. Peroxyacetic acid is sometimes used along with hydrogen peroxide in the disinfection process and the solutions used are an equilibrium mixture of hydrogen peroxide, peroxyacetic acid and ethanoic acid (Schneider, 1993). Thus, ascorbic acid, peroxyacetic acid and ethanoic acid were also tested to see if either electrode responded them.

At this stage, it was decided to characterise the electrochemical activity of both the rhodinised carbon sensors and the base graphite sensors using cyclic voltammetry and amperometry. It would help in the decision process and provide comparative data for later use.

The cyclic voltammograms were recorded between –1 and +1 V at a scan rate of 0.05 $V.s^{-1}$ following the general procedure given in section 2.2.3. Each sensor type was tested in triplicate by immersing the sensors into phosphate buffer solutions containing 2.4 $mmol.l^{-1}$ of hydrogen peroxide, ascorbic acid, peroxyacetic acid or ethanoic acid. This concentration was chosen as Johansson *et al,* (1993) and Gorton *et al,* (1991) have reported that horseradish peroxidase is inactivated by hydrogen peroxide concentrations

greater than 2.5 $mmol.l^{-1}$. The other analytes were tested at the same concentration to simplify any comparisons in electrochemical response if this were necessary.

The comparative amperometric responses of the rhodinised carbon sensors and the base graphite sensors were then determined using the same concentrations of analytes with the potentials and timings given in table 2.2.

Table 2.2. Autolab settings for amperometric comparison of base sensors

Time (seconds)	Potential (Volts)
1 – 60	-0.4
61 – 120	-0.3
121 – 180	-0.2
181 – 240	-0.1
241 – 300	0.0
301 – 360	+0.1
361 – 420	+0.2

The cyclic voltammogram for the graphite sensor is shown in figure 2.5 and for the rhodinised carbon sensor in figure 2.6. There was good agreement between the sensors, but the data from just one sensor is shown in the figures for clarity.

From the cyclic voltammograms, it was apparent that at negative potentials beyond –0.4 V the reduction current was due to background factors such as dissolved oxygen. Also, electro-reduction did not start until the potential was below +0.2 V. In view of this outcome, the comparative amperometric responses of the rhodinised carbon sensors and the base graphite sensors were determined between –0.4V and +0.2V

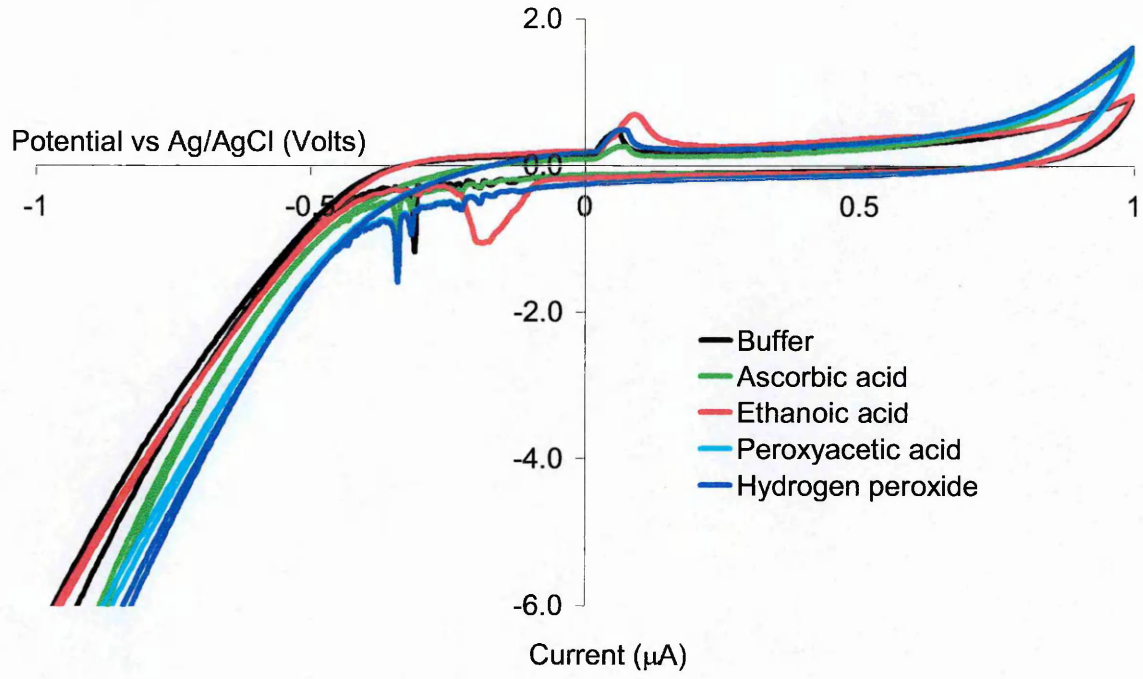

Figure 2.5 Cyclic Voltammetry at a Graphite electrode. Scan speed 0.05 $V.s^{-1}$

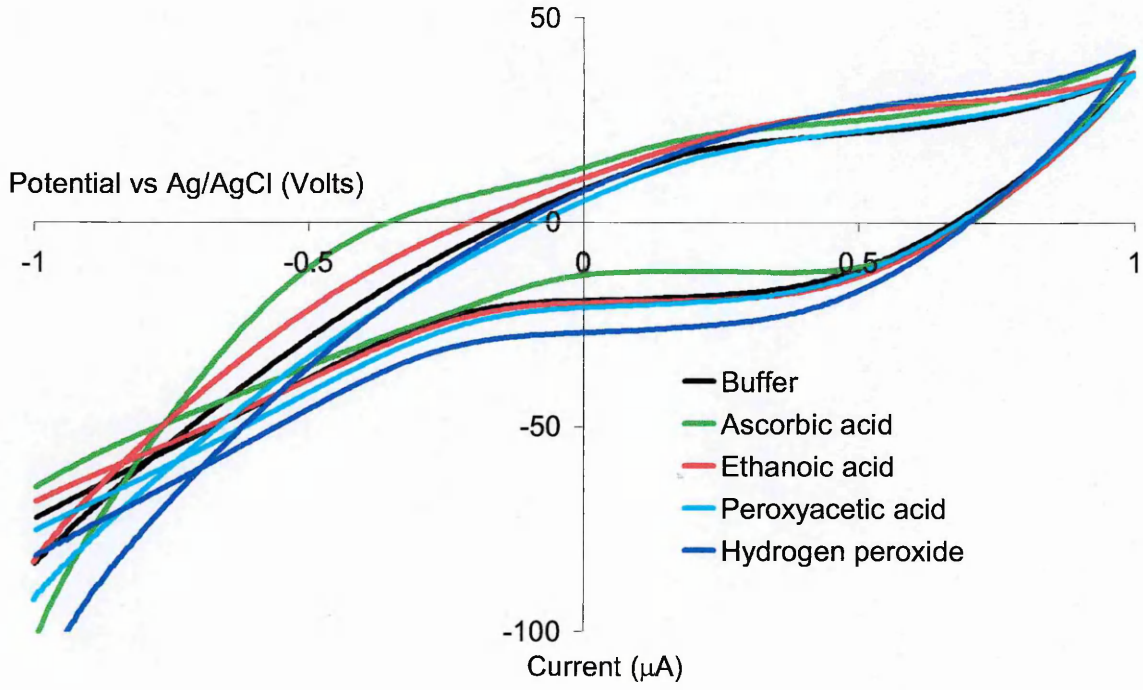

Figure 2.6 Cyclic Voltammetry at a Rhodinised Carbon electrode. Scan speed 0.05 $V.s^{-1}$

The results for amperometric response obtained with the graphite sensors are shown in figure 2.7 and with the rhodinised carbon sensors in figure 2.8. Again, three sensors of each type were tested with good agreement and the data from just one sensor is shown in the figures for clarity.

At positive potentials, the graphite sensors showed a response to all four analytes. At negative potentials, hydrogen peroxide gave a relatively greater response than peroxyacetic acid; the ascorbic acid only showed a response below –0.3 V. As the buffer also showed a response below this potential, it was probably due to dissolved oxygen. As expected, the ethanoic acid did not give a response at negative potentials, as organic acids do not show electrochemical reduction.

The responses obtained with the rhodinised carbon sensors showed little differentiation between the analytes at all potentials probably due to their greater catalytic properties. Between –0.1 V and –0.3 V the response to ascorbic acid became more significant relative to the other three analytes. In addition, the response to peroxyacetic acid was always greater than for hydrogen peroxide. It is possible that this is a catalytic effect on the equilibrium mixture of peroxyacetic acid, ethanoic acid and hydrogen peroxide but it was not considered a significant enough finding for further investigation as part of this work.

Although it was thought unlikely that there would be any other electroactive compounds present in the industrial wash solutions, with the regular advances and changes being made, it was considered better to develop a more selective device at the outset.

It can be seen that the sensor shows similar responses to hydrogen peroxide and peroxyacetic acid at the potentials studied. It is important to consider at this stage that one of the breakdown products of peroxyacetic acid is hydrogen peroxide. This means that the sensor may in fact be responding to hydrogen peroxide produced from the peroxyacetic acid as well as the peroxyacetic acid itself. In addition, the applied potential may be promoting this break down.

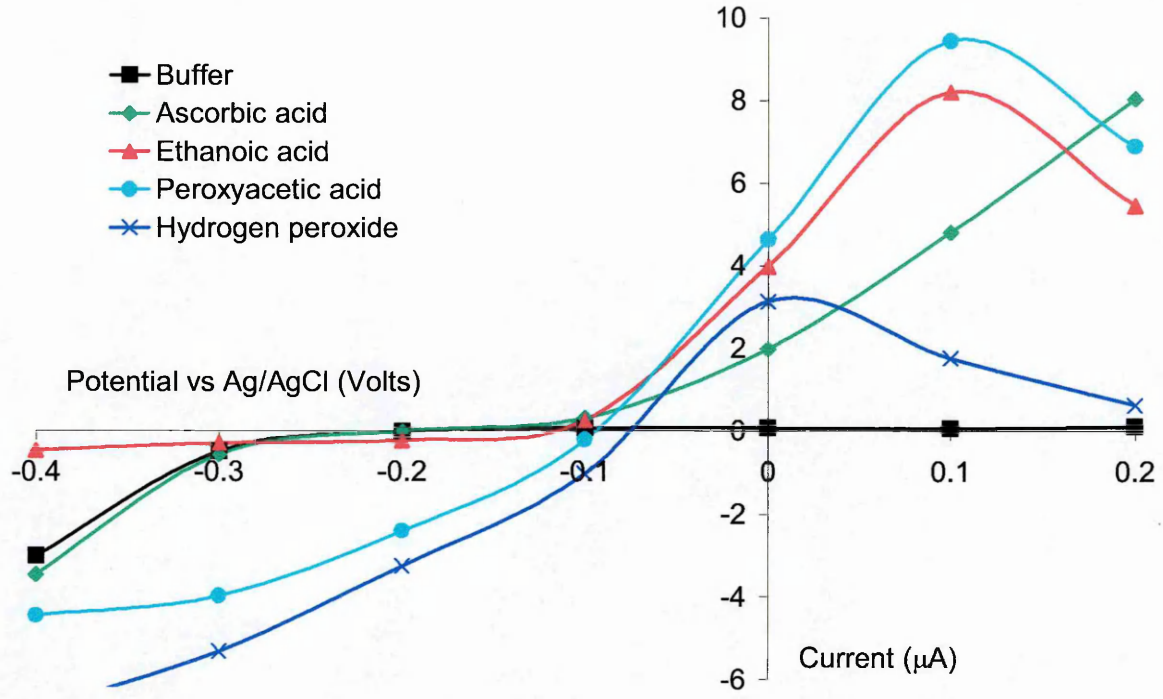

Figure 2.7 Steady state response of graphite electrodes as a function of applied potential

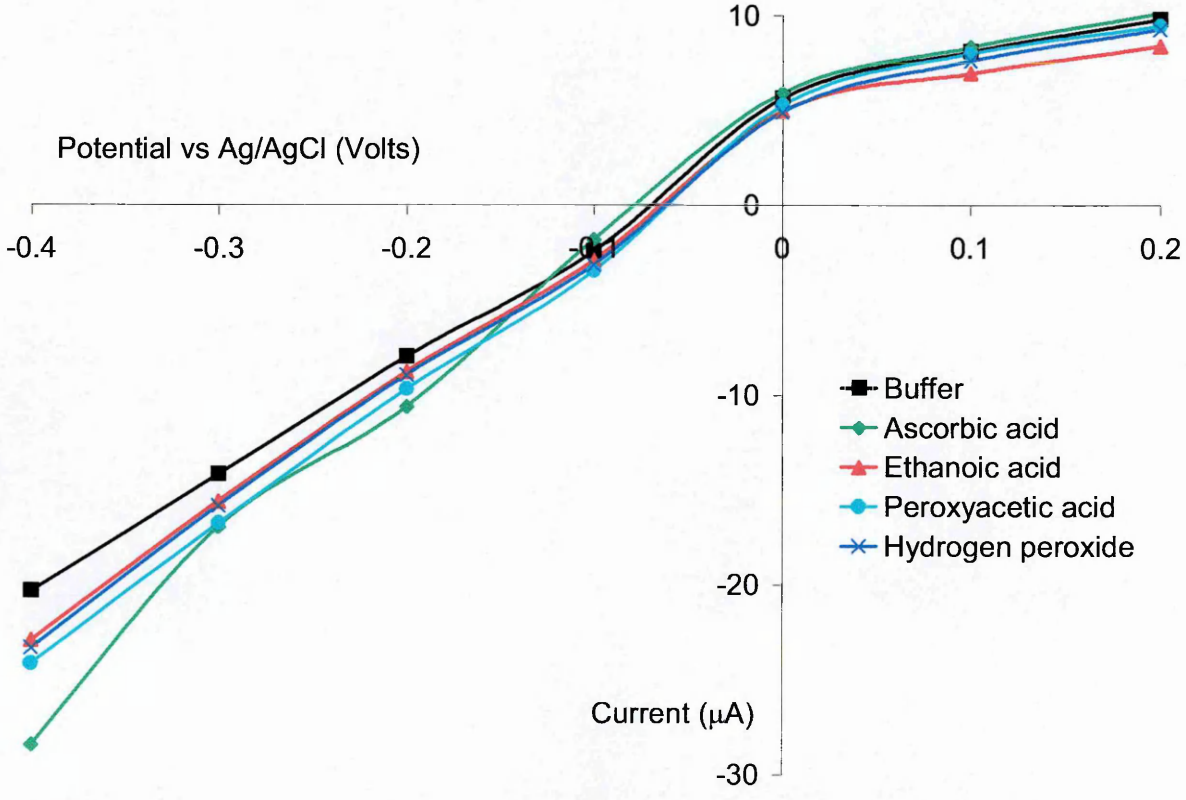

Figure 2.8 Steady state response of rhodinised carbon electrodes as a function of applied potential

2.4.3 Selection

Although the rhodinised carbon sensors have been found more sensitive and selective by other workers (section 2.4.1), it was considered that the extra expense of the rhodinised carbon, the labour involved in manufacture and the failure of the donated batch to give the sort of responses required, indicated that the modified graphite sensor would be a more robust and reproducible option.

Also, even with the rhodinised carbon a significant potential is still required and signal interference due to the presence of other electroactive compounds in a given sample can occur. Whilst a further reduction in operating potential will reduce the magnitude of the interference signal it will be at the expense of the analyte signal.

Thus, from the above results, it was decided to proceed with a graphite base electrode for the final sensor.

2.5 Enzyme Biosensors

As stated in section 1.3.2, the use of a biological rather than electrochemical catalyst can effectively eliminate the problem of interference from other electroactive compounds. The use of an enzyme along with a mediator will allow the use of a low operating potential, for peroxides, this is routinely achieved using the redox enzyme horseradish peroxidase. There are other peroxidases available and the choice of enzyme will be discussed below. All peroxidases are able to reduce hydrogen peroxide to water with the concomitant oxidation of a suitable electron donor. For these reasons, development continued on an enzyme biosensor.

2.5.1 Selection of the Enzyme

Various enzymes have been used in the production of biosensors for hydrogen peroxide. Some of the commonest are catalase (Cosgrove *et al*, 1988), microperoxidase (Lotzbeyer *et al*, 1994; Moore *et al*, 1996; Spohn *et al*, 1997) and horseradish peroxidase (Csoregi *et al*, 1994a & 1994b; Popescu *et al*, 1995; Spohn *et al*, 1997).

Catalase converts hydrogen peroxide to oxygen and water; the oxygen thus produced being monitored with an oxygen electrode (Dunford, 1982, Cosgrove *et al*, 1988).

As the dissolved oxygen content of the solutions that will be presented to the sensor cannot be standardised, it was decided that catalase would not be a suitable enzyme component for this sensor.

Peroxidases and microperoxidases also convert hydrogen peroxide to oxygen and water but the redox changes to the enzyme can be directly monitored electrochemically (Csoregi *et al*, 1994a & 1994b; Lotzbeyer *et al*, 1994; Popescu *et al*, 1995; Moore *et al*, 1996; Spohn *et al*, 1997).

Microperoxidases such as MP-8 and MP-11 have a lower electrocatalytic efficiency per molecule (Spohn *et al*, 1997), they are not readily available from the usual sources and are more expensive per unit of activity. Horseradish peroxidase is readily available, cheap and well characterised. Thus, it was decided to develop the sensor using horseradish peroxidase as the enzyme of choice.

A possible concern with this selection was the report that horseradish peroxidase is inactivated by hydrogen peroxide concentrations greater than 2.5 $mmol.l^{-1}$ (Johansson *et al,* 1993 and Gorton *et al,* 1991). This would not be a problem during development as it is easily controlled and as the maximum possible concentration would be known in an industrial cleaning process, the dilution could be guaranteed to be sufficient such that this level is not exceeded in practice.

2.5.2 Validating the Choice of Horseradish Peroxidase

As a simple trial to show that this would work in principle, the working electrode surface of three base graphite electrodes were each coated with 5µl of a 5 $U.ml^{-1}$ solution of horseradish peroxidase in buffer to give a coating of 25 U per sensor. This was then allowed to dry for 1 hour at room temperature before running cyclic voltammetry between –1 V and +1 V in buffer and 2.4 $mmol.l^{-1}$ hydrogen peroxide in buffer. The results are shown in figure 2.9. However, for clarity, the scales have been cropped to show the response between –0.6 V and +0.6 V and the result from only one electrode is shown, as the results were almost identical.

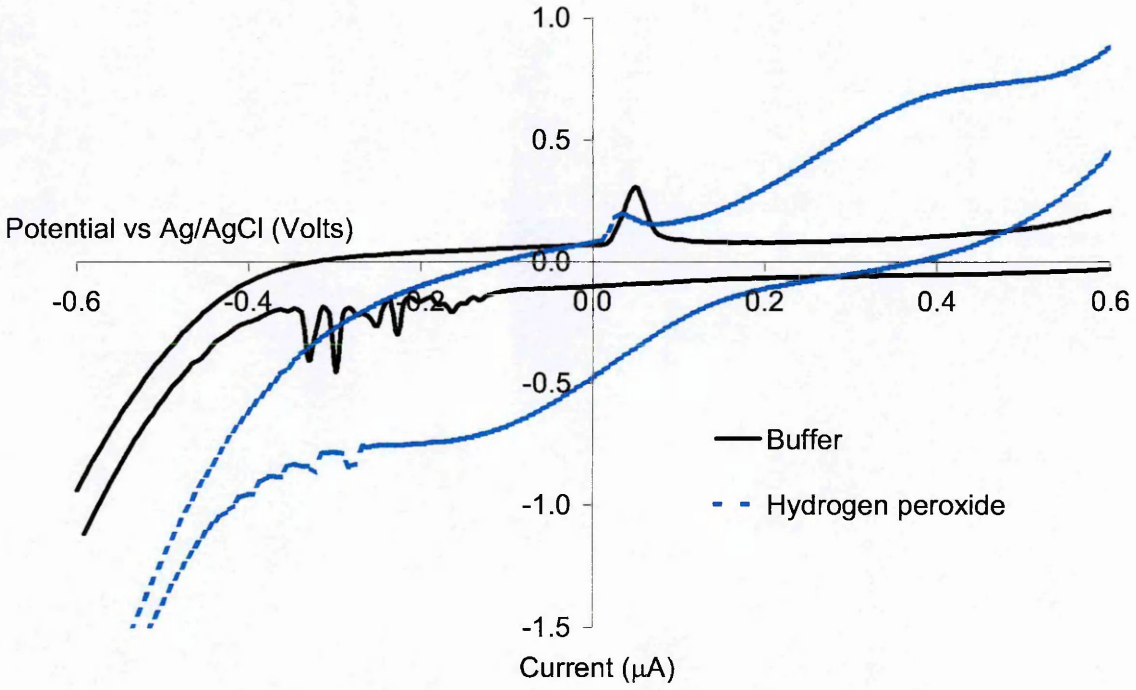

Figure 2.9 Cyclic voltammetry of the base electrode coated with horseradish peroxidase. Scan speed 0.05 $V.s^{-1}$

From this data, it can be seen that there is some evidence to suggest that when there was hydrogen peroxide present in the solution, there was some reduction of the oxidised horseradish peroxidase at a potential in the region of –0.1V (see figures 1.9, 1.10 and 1.11). This suggests that there was some direct electron transfer between the enzyme and graphite electrode as described by others (Frew & Hill, 1988; Lötzbeyer *et al*, 1994).

It has been suggested that this electron transfer is due to other active groups on the surface of the electrode acting as mediators (Lötzbeyer *et al* 1994) and as the current measured at this point was low, suggesting a slow rate of electron transfer, it was decided to investigate other possibilities for the final sensor design.

2.5.3 Linking the Enzyme to the Electrode

There are two main approaches for linking redox enzymes directly to an electrode (Cardosi & Turner, 1987; Frew & Hill, 1988 and Cardosi & Birch 1993)

1) Direct and unmediated electron transfer.

2) Indirect and mediated electron transfer.

However, a protective protein and glycoprotein shell surrounds the active centre of redox enzymes and has two important functions (Heller, 1990).

1) It stabilises the enzyme structure,

2) It prevents indiscriminate electron exchange between natural redox macromolecules.

If direct or unmediated electron transfer is to be used then the enzyme must be immobilised onto the surface of the electrode. Various methods have been used for this including:

1) Self-assembled monolayers:
   Various enzymes have been immobilised covalently to the self-assembled monolayers of 3-mercaptopropionic acid on a gold electrode. The self-assembled monolayer is claimed to make electron transfer more likely and quicker. Self-assembly works but it is not applicable to mass production process at present. (Dong and Li, 1997)

2) Glutaraldehyde cross-linking.
   Various enzymes have been immobilised on the surface of a metal electrode by covalent cross-linking with glutaraldehyde and bovine serum albumin as a stabiliser. Gold electrodes are regarded to be better for this process (Cosgrove *et al*, 1988;

Csoregi *et al*, 1994b; Abdel-Hamid *et al*, 1995; Kalab and Skladal, 1995; Liu *et al*, 1995a). Immobilisation using such a technique can lead to lower enzyme activity. This could be due to changes in the tertiary structure of the enzyme or blockage of the active site by the glutaraldehyde.

3) Covalent bonding with biotin/avidin.

   Horseradish peroxidase has been bound to carbon fibres via biotin/avidin/biotin (Csoregi *et al*, 1994a). This is also a multi stage process and requires a coupling agent.

4) Sol-gel immobilisation

   Sol-gel immobilisation of enzymes within metal oxides results in thin composite layers that are useful for biosensors. These have pore sizes that can be controlled by the formation process but unfortunately; the process is not currently suited to mass production of sensors (Kunzelmann & Bottcher, 1997; Sampath & Lev, 1997).

5) Direct Wiring.

   There have also been reports of 'wired' peroxidase by cross-linking it with redox polymers. Yang *et al* (1995) and Kenausis *et al* (1997) both used an Osmium poly(vinylpyridine) polymer, the osmium-containing redox centres allowing direct electrical communication between the electrode surface and the heme centres of the peroxidase (Kenausis *et al*, 1997). Cardosi (1994) used cyanuric chloride to covalently attached horseradish peroxidase to the surface of platinized carbon particles

   Ferapontova *et al*, (2001), working with recombinant horseradish peroxidases containing a six-histidine tag at the C- or N-terminus, have demonstrated an interaction of the histidine tag with the electrode surface, showing that enhanced catalytic activity of the enzyme can be achieved by genetic engineering design of the enzyme molecules.

None of the above techniques are applicable to a simple production process. It has been shown that the rate of electron transfer decays exponentially with distance when the distance substantially exceeds atomic dimensions (greater than 0.3 nm) in accordance

with theory (Heller, 1990). As stated in the introduction (section 1.4.4) horseradish peroxidase has a molecular weight of about 42,000 excluding any bound water (Dunford, 1982) and a physical size of 6 nm (Okawa *et al*, 1999). As this is 20 times greater than the atomic dimensions, the rate of electron transfer will be considerably reduced (figure 2.9). The direct wiring technique may overcome this but the manufacturing difficulties and material costs were considered to outweigh the advantages. Also, as shown in section 2.5.2, the low current measured for the apparent direct electron transfer indicated that a faster rate of electron transfer should be sought for the final sensor design.

It was therefore decided to investigate the use of mediated electron transfer and then use a membrane or entrapment technique. Hopefully, this would also have the advantage of increasing sensitivity, reducing the effects of potential interferents by reducing the required potential for electrocatalysis, and speeding up the analysis time.

2.6 Selection of Mediator

An artificial mediator must be reduced more rapidly than oxygen and be electroactive at low potentials in order to be successful in an amperometric sensing device (Cardosi & Turner, 1987).

2.6.1 Suitable Mediators Reported in the Literature

From a search of the literature regarding mediators for peroxide sensors there were many possible choices available. Most were readily rejected for this application due to their unsuitability for incorporation into a mass-produced product. This decision was made on the basis of availability, cost or ease of manipulation at manufacture.

Those that were considered and rejected on this basis included: N,N-diethylaminomethylferrocene, Medola blue [8-dimethylamino-2,3-benzophenoxazine] (Kulys *et al*, 1992), Prussian blue (made from $K_3[Fe(CN)_6]$ + $FeCl_3$) (Karyakin *et al*, 1996), N-methyl phenazine methosulphate (Liu *et al*, 1997), Nickelocene (Liu *et al*, 1995b) and Tetracyanoquinodimethane [TCNQ] (Pandey *et al*, 1997).

Ferrocene [bis(cyclopentadienyl)iron] was one of the preferred choices and has been successfully used by many groups (Green *et al*, 1986; Sanchez *et al*, 1991; Kulys *et al*, 1992; Chut *et al*, 1997; Kunzelmann & Bottcher, 1997). It is only slightly soluble in water, stable in air but readily oxidised to ferricinium in acidic solution. Adding a substituent onto the n-cyclopentadienyl ring reduces the rate of oxidation (Epton *et al*, 1978). It has also been shown that the rate-limiting step of the steady-state oxidation of ferrocenes is the electron transfer between horseradish peroxidase II and the ferrocene (Goral, V. N. & Ryabov, A. D, 1998) and that steric hindrance increases the electron transfer distance (Ryabov, A. D. *et al*, 1999). Thus, a balance between molecular size and the addition of substituents onto the n-cyclopentadienyl ring was considered. For this reason 1,1'-dimethylferrocene, readily available at a cost of about £1.80 per mM was selected for further study as a representative of the ferrocene group.

The other two that were selected for further investigation were tetrathiafulvalene at a cost of about £23 per mM (although expensive, well favoured in the literature) and potassium hexacyanoferrate (II) at a cost of about 3p per mM. Based on cost, potassium hexacyanoferrate (II) was the obvious preferred choice.

2.6.2 Potassium hexacyanoferrate (II)

Potassium hexacyanoferrate (II) is a pale yellow, water soluble, crystalline solid with the formula: $K_4Fe(CN)_6.3H_2O$ and formula weight: 422.4, it is a popular choice as a mediator and thus its electrochemistry is well described (Johansson *et al*, 1993; Ortiz *et al*, 1997). For a monitoring device however, it has a disadvantage by being water-soluble. Although the final device would probably have a membrane or some form of protective cover, this would still reduce the likely operational stability.

A simple trial to show how this mediator would work in principle was performed in a similar to way to that for the enzyme in section 2.5.2. The working electrode surfaces of three base graphite electrodes were each covered with 5µl aqueous (20 $mg.ml^{-1}$) potassium hexacyanoferrate (II). This was allowed to dry for 1 hour at room temperature and gave a coating of 0.24 µmol per electrode. After drying, each sensor was covered with 5 µl of a 5 $U.ml^{-1}$ solution of horseradish peroxidase in buffer to give a coating of 25 U per sensor. This was also allowed to dry for 1 hour at room

temperature before running cyclic voltammetry between –1 V and +1 V in buffer and 2.4 mmol.l^{-1} hydrogen peroxide in buffer.

The results are shown in figure 2.10. For clarity, the scales have been cropped to show the response between –0.6 V and +0.6 V and the result from only one electrode is shown, as the results were almost identical for all electrodes.

The use of potassium hexacyanoferrate (II) as a mediator showed a four-fold increase in current response compared to the horseradish peroxidase alone and thus amperometry was performed in the same way as in section 2.4.2 (on the base electrodes) to investigate further,. The potentials and timings are given in table 2.3 and each of the three sensors being tested with a blank buffer solution and solutions of 0.8, 1.6 & 2.4 mM hydrogen peroxide in buffer.

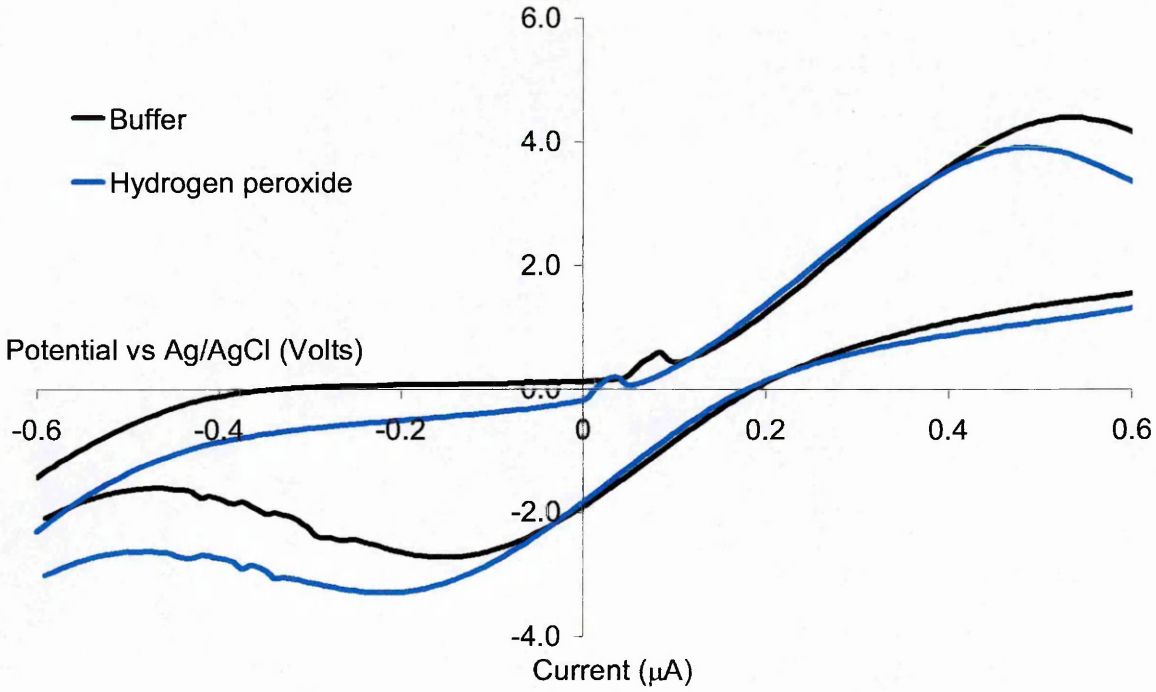

Figure 2.10 Cyclic voltammetry of potassium hexacyanoferrate (II) as a mediator. Scan speed 0.05 V.s^{-1}

Table 2.3. Autolab settings for amperometric evaluation of mediators.

Time (seconds)	Potential (Volts)
1 – 60	-0.6
61 – 120	-0.4
121 – 180	-0.2
181 – 240	0.0
241 – 300	+0.2
301 – 360	+0.4

The results obtained are shown in figure 2.11, good visual agreement was seen, but at this stage, statistical analysis was not performed, as it was only a trial study. Also, for clarity the data from just one sensor is shown in the figure.

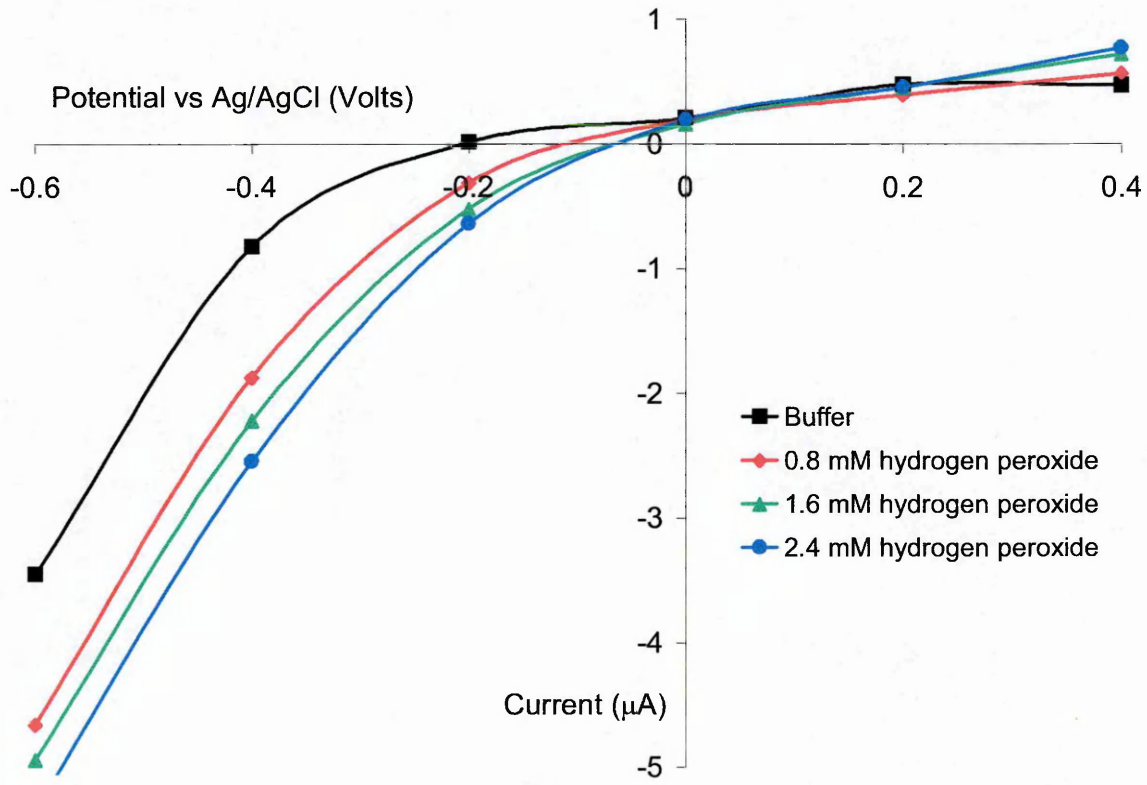

Figure 2.11 Steady state response using a potassium hexacyanoferrate (II) mediator as a function of applied potential

At the end of each series, it was apparent from the yellow colouration of the buffer solutions that some of the potassium hexacyanoferrate (II) had leached off the sensor and dissolved into the buffer solution. The cyclic voltammetry indicated that electro-reduction started at about +0.1 V and electro-oxidation at about 0.0 V. Amperometry indicated that a useable electro-reduction signal could be obtained from somewhere between 0.0 and –0.2 V down to –0.6 V. This would be studied further and optimised if selected.

2.6.3 1,1'-dimethylferrocene

1,1'-Dimethylferrocene has the formula: $(C_5H_4.CH_3)_2$ Fe, a formula weight of 214.09 and is a dark red crystalline solid. It is a relatively stable substance and is only slightly soluble in water. It has a catalytic process that appears to be highly dependent on the amount present with kinetic control, internal diffusion control and external diffusion control being obtained by varying the amount incorporated in the sensor (Amine *et al*, 1993). It has been successfully used by others (Kulys *et al*, 1992; Pandey *et al*, 1997)

A simple trial to show how this mediator would work in principle was performed in a similar way to that for potassium hexacyanoferrate (II). The working electrode surfaces of three base graphite electrodes were each covered with 4 µl of 12.5 $mg.ml^{-1}$ 1,1'-dimethylferrocene in acetone to give a coating of 0.24 µmol per electrode. Only 4 µl were required due to the better spreading properties of the acetone solution compared to the buffer and also only 10 minutes evaporation were needed due to its being volatile. After drying, each sensor was covered with 5 µl of a 5 $U.ml^{-1}$ solution of horseradish peroxidase in buffer to give a coating of 25 U per sensor. This was allowed to dry for 1 hour at room temperature before running cyclic voltammetry between –1 V and +1 V in buffer and 2.4 $mmol.l^{-1}$ hydrogen peroxide in buffer.

The results are shown in figure 2.12. Again, for clarity, the scales have been cropped to show the response between –0.6 V and +0.6 V and the result from only one electrode is shown, as the results were almost identical for all electrodes.

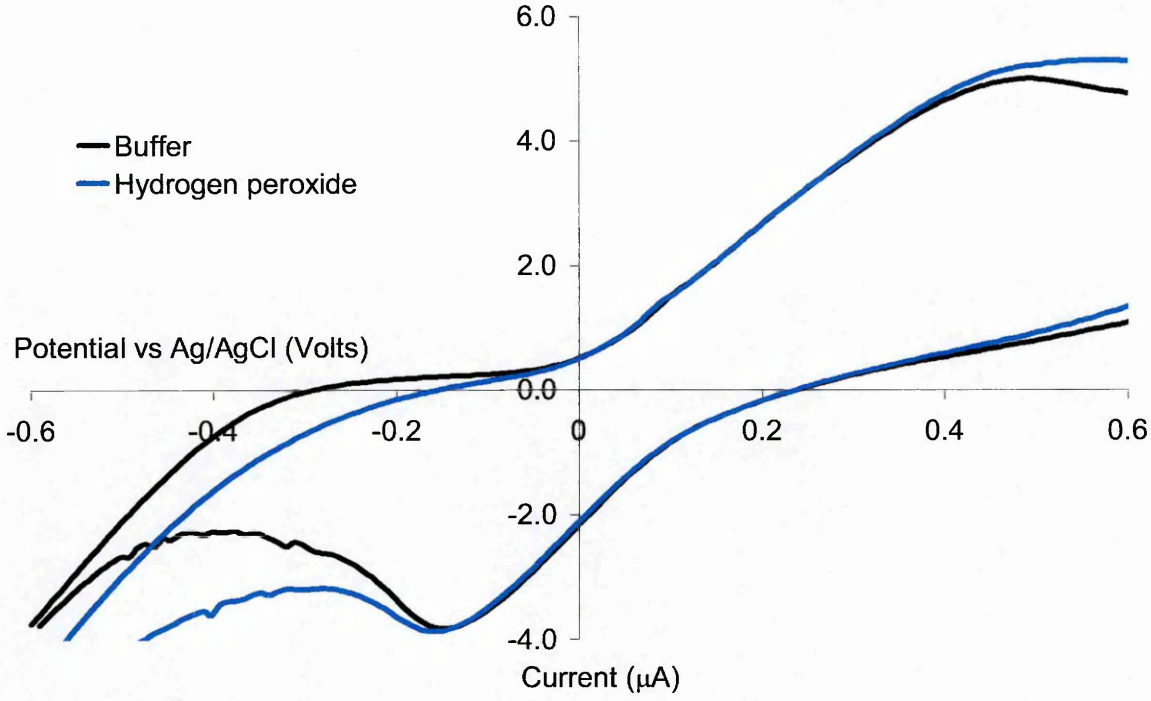

Figure 2.12 Cyclic voltammetry of 1,1'-dimethylferrocene as a mediator
Scan speed 0.05 $V.s^{-1}$

As with the potassium hexacyanoferrate (II), the 1,1'-dimethylferrocene showed a four-fold increase in current response compared to the horseradish peroxidase alone and to investigate further, amperometry was performed as in section 2.6.2.

The results obtained are shown in figure 2.13. Again, good visual agreement was seen, statistical analysis was not performed as it was only a trial study and just one sensor is shown in the figure for clarity.

As with the potassium hexacyanoferrate (II), the cyclic voltammetry indicated that electro-reduction started at about +0.1 V and electro-oxidation at about 0.0 V. Amperometry indicated that a useable electro-reduction signal could be obtained from somewhere between 0.0 V and –0.2 V down to –0.6 V. This would be studied further and optimised if this mediator was selected. There was no apparent colouration of the buffer solutions at the end of each series, suggesting that the mediator had remained on the sensor surface. Had there been significant leaching into solution a red colouration would have been expected.

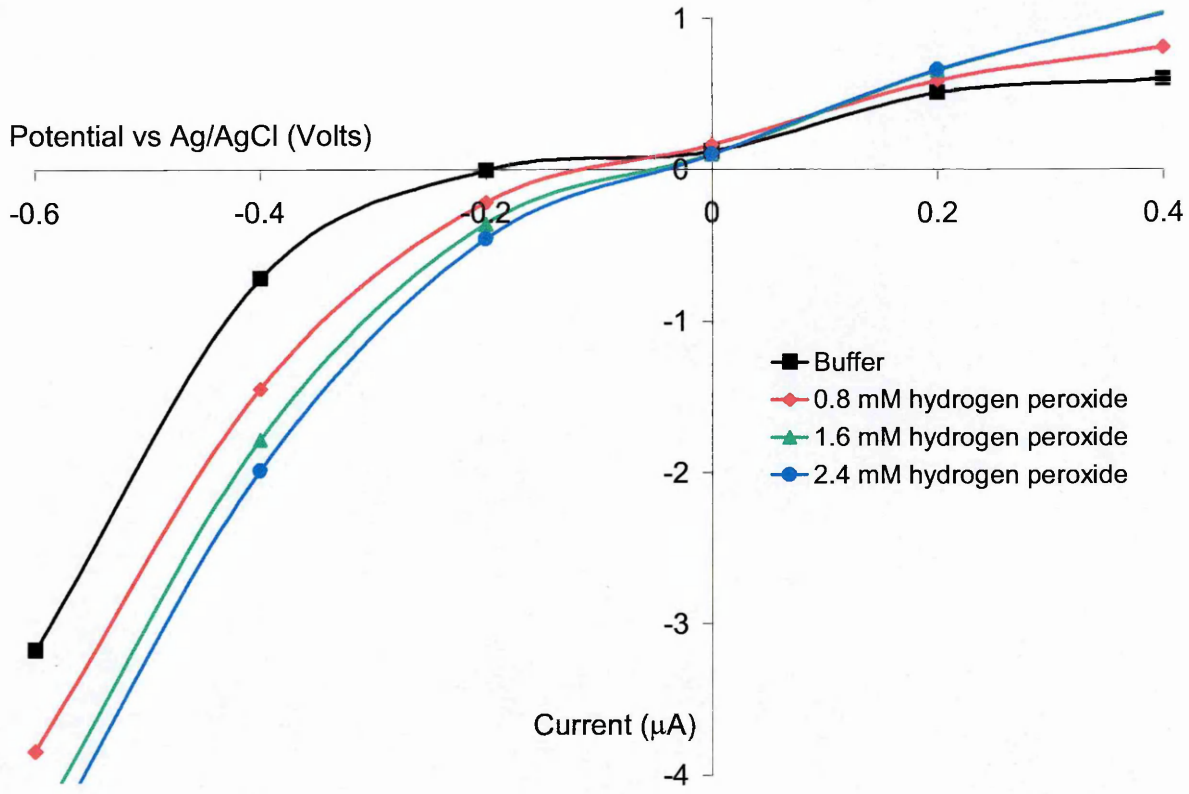

Figure 2.13 Steady state response using a 1,1'-dimethylferrocene mediator as a function of applied potential

2.6.4 Tetrathiafulvalene

Tetrathiafulvalene is a dark orange crystalline solid with the formula: $C_6H_4S_4$ and formula weight: 204.3.

Tetrathiafulvalene is insoluble in water but can be dissolved in aqueous solution containing Tween 80.

Pandey *et al* (1997) found it the best choice for the development of a peroxide biosensor when compared with tetracyanoquinodimethane, and 1,1'-dimethylferrocene. It was more stable and gave more reproducible results. Bilitewski *et al* (1993), however, found that it had a lower response than 1,1'-dimethylferrocene and did not last as long in continuous use, only two to three days compared to the fourteen days that they obtained for 1,1'-dimethylferrocene.

The chemistry of tetrathiafulvalene is more complex than the previous two mediators in that it undergoes two successive one-electron oxidation processes in aqueous solution

bringing about the formation of tetrathiafulvalene^{+} and tetrathiafulvalene^{2+}. The redox potentials for these two oxidised forms vary greatly with the method of immobilisation and supporting electrolyte. The first oxidation process is reversible but the second oxidation process is not (Liu *et al*, 1995a). Other workers have used it successfully as an organic conducting salt with p-tetracyanoquinodimethane in the development of a peroxide biosensor (Korell & Spichiger, 1994).

A simple trial to show how this mediator would work in principle was again performed in a similar way to that for potassium hexacyanoferrate (II). The working electrode surfaces of three base graphite electrodes were each covered with 4 µl of 13 mg.ml^{-1} tetrathiafulvalene in acetone to give a coating of 0.24 µmol per electrode. As with 1,1'-Dimethylferrocene, only 4 µl were required due to the better spreading properties of acetone compared to the buffer used for the potassium hexacyanoferrate (II) and also only 10 minutes evaporation were needed.

After drying, each sensor was covered with 5 µl of a 5 U.ml^{-1} solution of horseradish peroxidase in buffer to give a coating of 25 U per sensor. This was allowed to dry for 1 hour at room temperature before running cyclic voltammetry between –1 V and +1 V in buffer and 2.4 mmol.l^{-1} hydrogen peroxide in buffer. The results are shown in figure 2.14. However, for clarity, the scales have been cropped to show the response between –0.6 V and +0.6 V and the result from only one electrode is shown, as the results were almost identical for all electrodes.

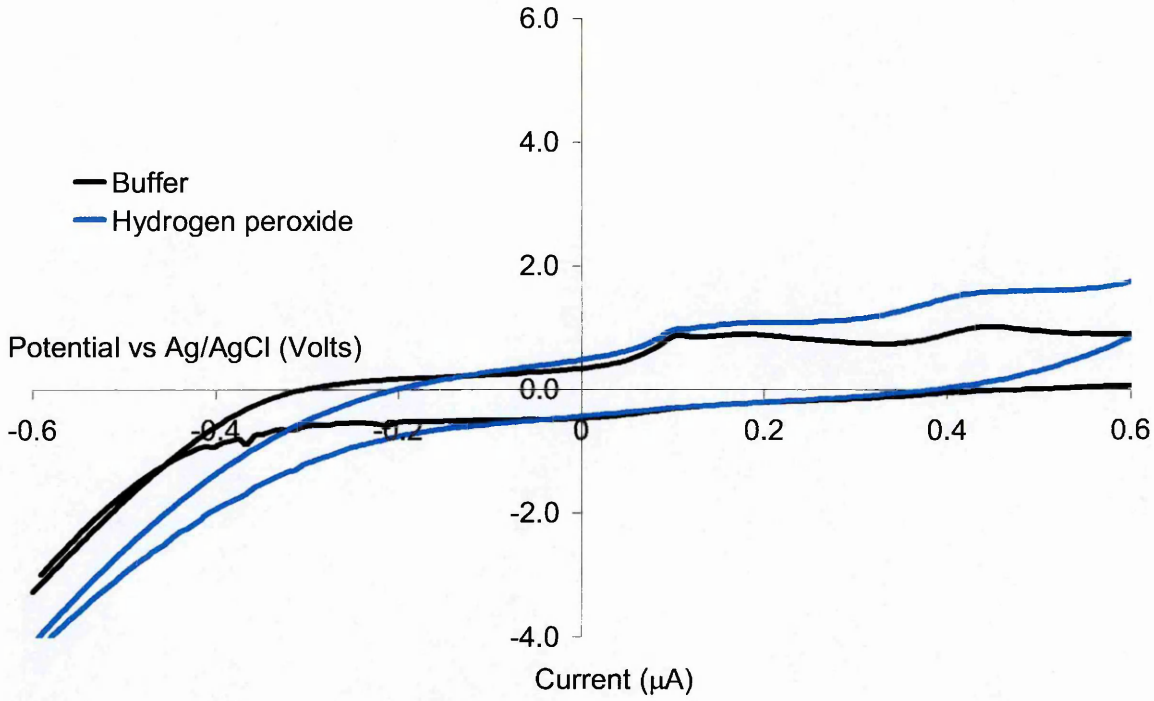

Figure 2.14 Cyclic voltammetry of tetrathiafulvalene as a mediator
Scan speed 0.05 $V.s^{-1}$

On addition of tetrathiafulvalene to the buffer, the forward sweep of the cyclic voltammetry produced two peaks corresponding to the two oxidation stages of tetrathiafulvalene to tetrathiafulvalene^{+} and then tetrathiafulvalene^{2+}. As there was no reduction current, it is in agreement with the findings of Liu *et al* (1995a), who showed that the second step is irreversible. As the operating potential would be controlled at a reduction potential below 0.3 V, it would not be a problem, although it does demonstrate the relative instability of tetrathiafulvalene compared to potassium hexacyanoferrate (II) and 1,1'-dimethylferrocene when considering the storage stability of the final sensor. The cyclic voltammogram of tetrathiafulvalene between –0.6 V and +0.3 V is shown in figure 2.15 to demonstrate the oxidation of tetrathiafulvalene to tetrathiafulvalene^{+} and reduction back to tetrathiafulvalene.

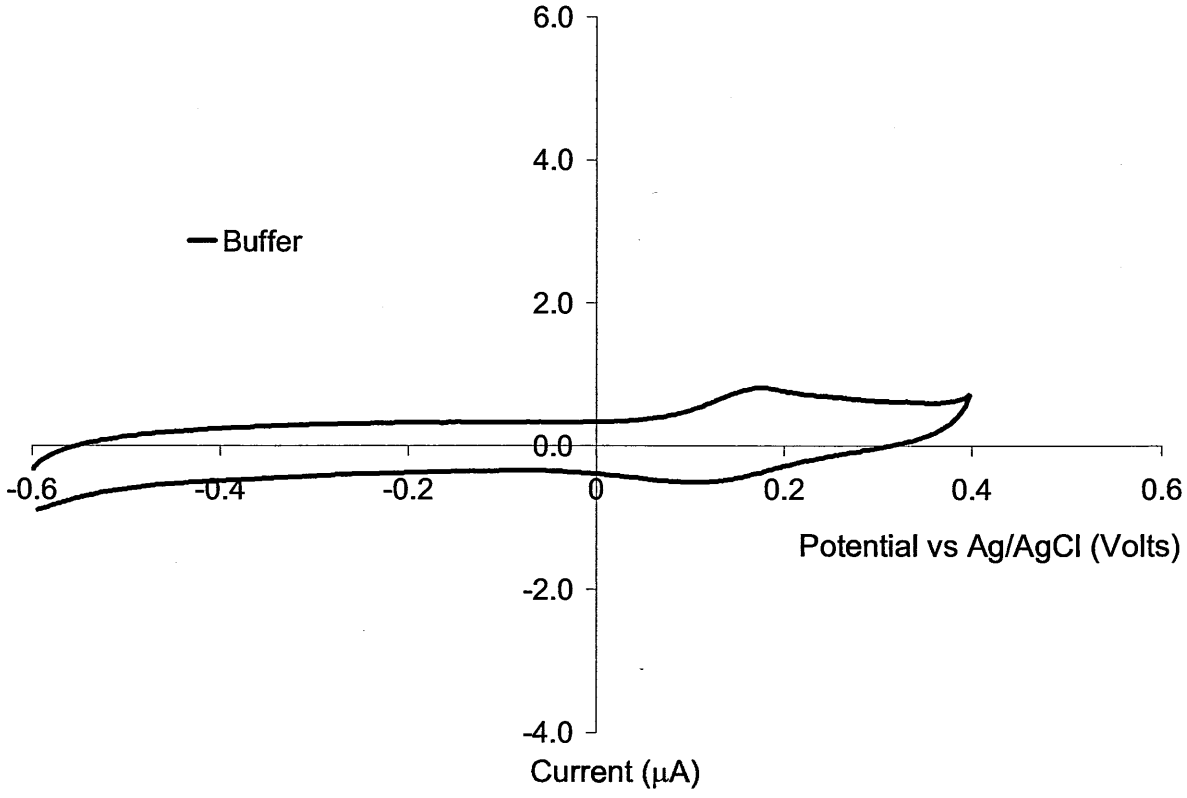

Figure 2.15 Cyclic voltammetry of tetrathiafulvalene between –0.6 V and +0.3 V Scan speed 0.05 $V.s^{-1}$

To investigate further, amperometry was performed using the same procedure as before with potassium hexacyanoferrate (II) and 1,1'-dimethylferrocene.

The results obtained are shown in figure 2.16, and again, good visual agreement was seen although subjectively there did appear to be more noise. As this was just an initial trial, statistical analysis was not performed and just one sensor is shown in the figure for clarity.

As with the potassium hexacyanoferrate (II), the cyclic voltammetry indicated that electro-reduction started at about +0.1 V and electro-oxidation at about 0.0 V. Amperometry indicated that a usable electro-reduction signal could be obtained from somewhere between 0.0 V and –0.2 V down to –0.6 V. This would be studied further and optimised if selected. There was no apparent colouration of the buffer solutions at the end of each series, suggesting that the mediator had remained on the sensor surface.

Had there been significant leaching into solution an orange colouration would have been expected.

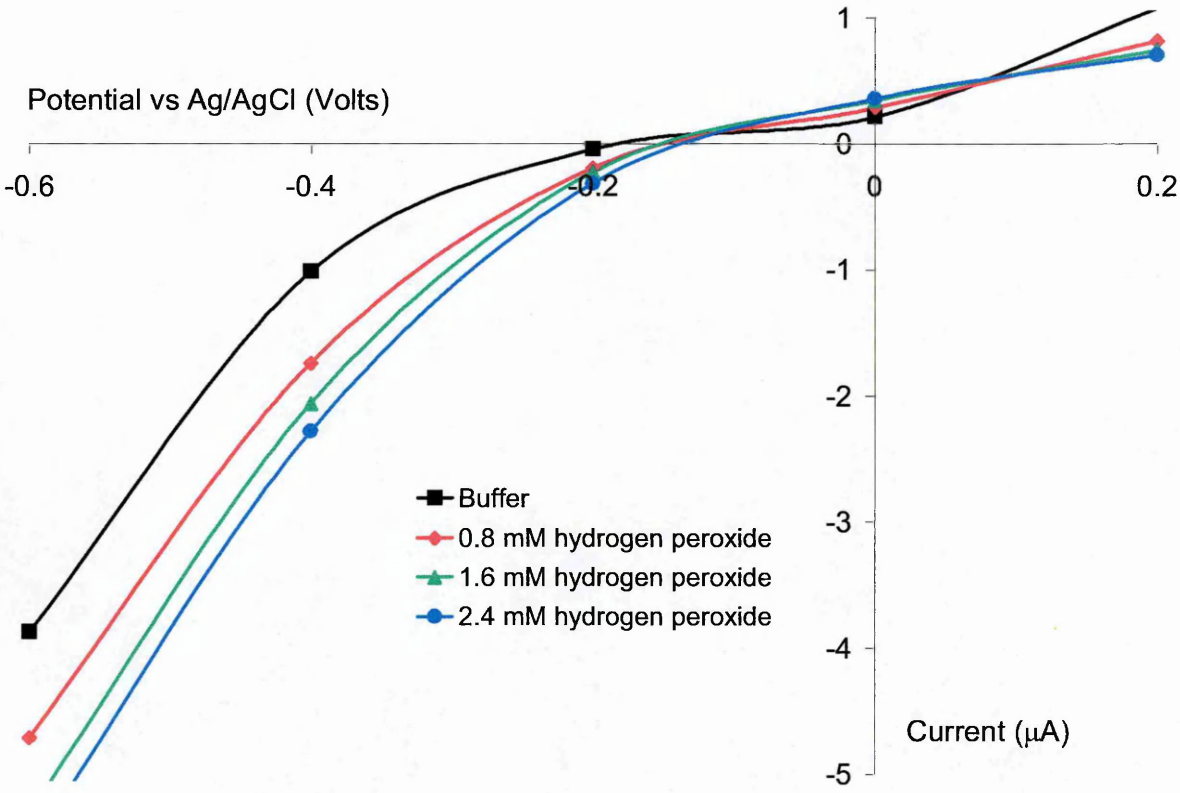

Figure 2.16 Steady state response using a tetrathiafulvalene mediator as a function of applied potential

2.6.5 Selection

To summarise the mediator performances, the current responses at –0.2V, -0.4V and –0.6V were taken from the data displayed in figures 2.11, 2.13 and 2.16 and plotted against the hydrogen peroxide concentration (figure 2.17a,b,c).

From these figures, it can be seen that there is a considerable shift in baseline signal between the applied potentials. To enable a clearer comparison, these results were plotted again with the baseline current subtracted from the current responses for each level of hydrogen peroxide and the error bars removed (figure 2.18).

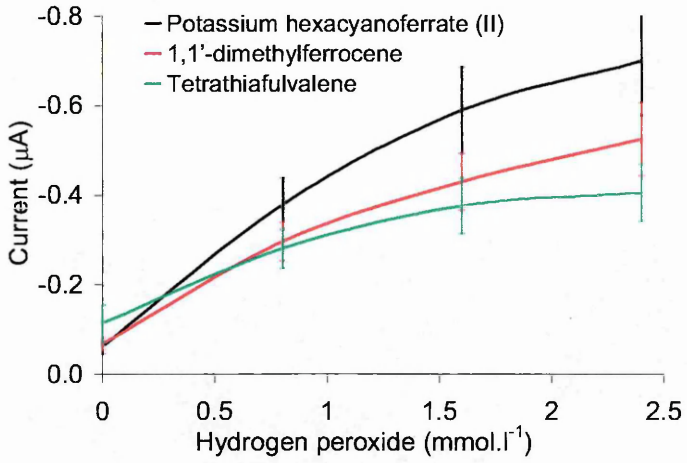

a) Potential –0.2V vs Ag/AgCl

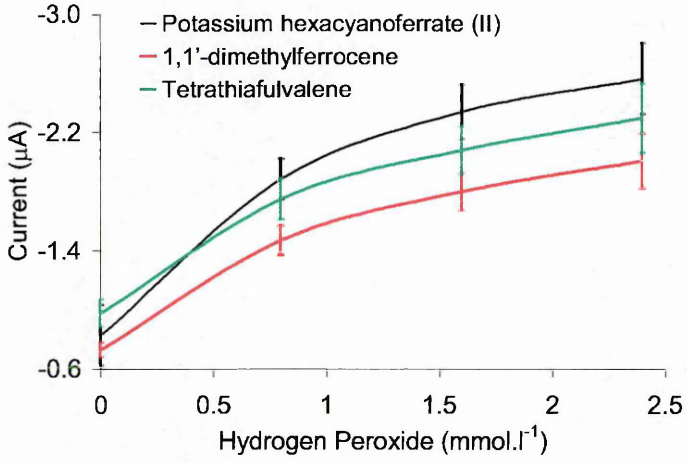

b) Potential –0.4V vs Ag/AgCl

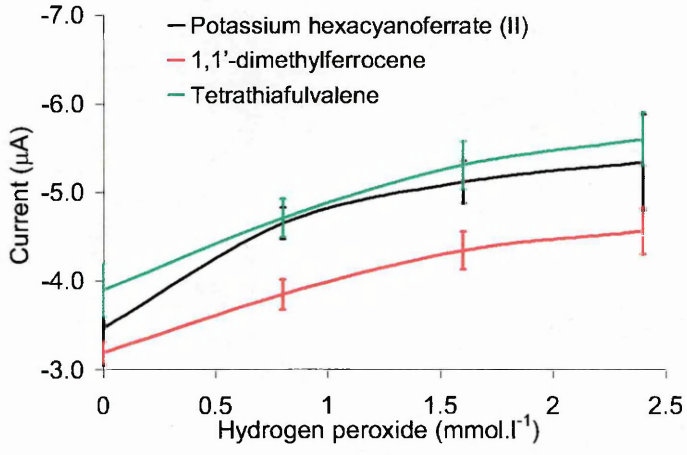

c) Potential –0.6V vs Ag/AgCl

Figure 2.17 Comparison of sensor responses using the different mediators

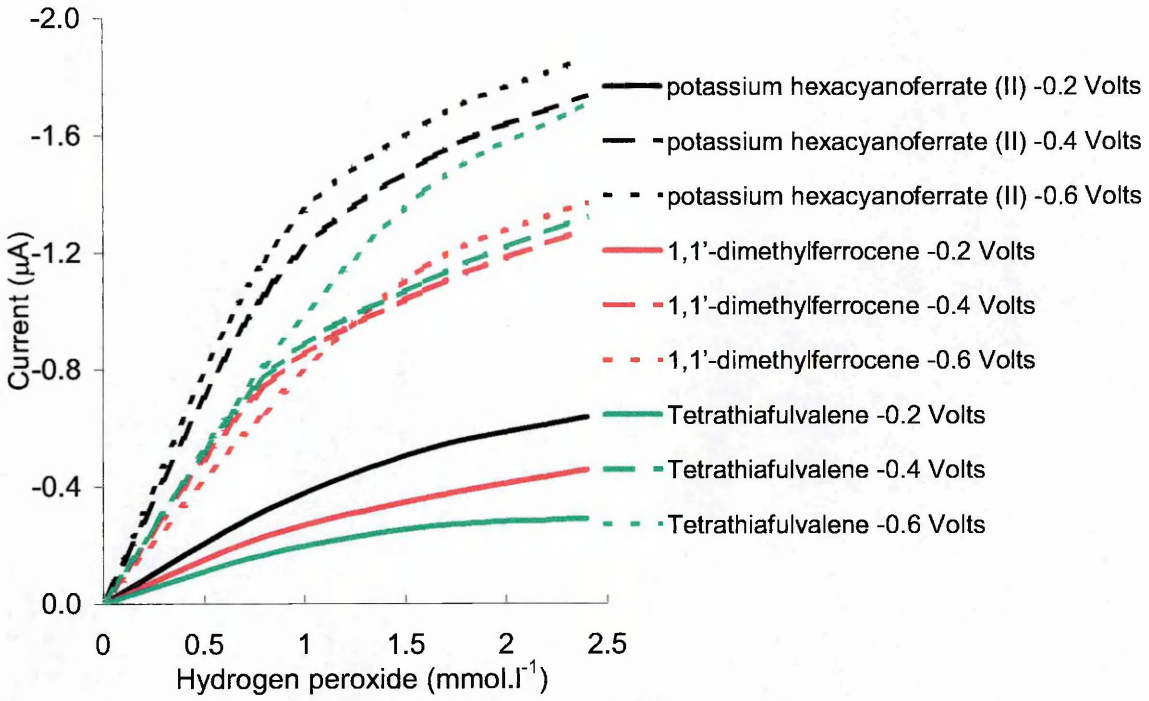

Figure 2.18 Baseline corrected sensor responses using the different mediators

From these results, it can be seen that when using potassium hexacyanoferrate (II) as the mediator there was a larger response to the hydrogen peroxide at all three potentials.

However, it was felt that even if a membrane were used to cover the sensor, there would still be too great a risk of mediator loss from the sensor surface when used in an on-line application. The larger response was not considered sufficient to allow for the loss that may be seen over an extended period. For these reasons, despite its low cost at £0.03 per mM, potassium hexacyanoferrate (II) was not used for further development.

The difference between the responses seen for sensors using 1,1'-dimethylferrocene and tetrathiafulvalene as mediator varied depending on the applied potential. At –0.2V the response seen with tetrathiafulvalene was about 30% lower than with 1,1'-dimethylferrocene and was in agreement with Bilitewski *et al* (1993). At –0.4V the responses were about the same, but at –0.6V the response with tetrathiafulvalene was about 25% higher than with 1,1'-dimethylferrocene. Bilitewski *et al* (1993) also found that tetrathiafulvalene did not last as long in continuous use, only two to three days compared to fourteen days for 1,1'-dimethylferrocene. The final factor considered

was the relative costs, at current prices, 1,1'-dimethylferrocene costs £1.80 for 1mM compared to £23.90 for tetrathiafulvalene

As the object of this development was to produce a commercially viable sensor with relatively low production costs, it was decided that this was sufficient evidence to reject tetrathiafulvalene as a potential mediator.

Thus, to summarise the advantages of 1,1'-dimethylferrocene:

1) 1,1'-dimethylferrocene is only very slightly soluble in aqueous solution. When compared to potassium hexacyanoferrate (II) it will be easier to retain on the surface of a sensor.

2) 1,1'-dimethylferrocene is soluble in volatile organic solvents (viz. acetone) and will thus be much quicker and easier to deposit onto the manufactured sensor.

3) The responses seen for sensors using 1,1'-dimethylferrocene and tetrathiafulvalene were very close and thus the significantly lower cost of 1,1'-dimethylferrocene gives it a big advantage.

4) 1,1'-dimethylferrocene is reported to be more stable than tetrathiafulvalene in continuous use.

Thus, from this study it was decided to develop the sensor using 1,1'-dimethylferrocene as the mediator.

2.7 Selection of the Operating Potential for Amperometry

As shown in section 2.4.2, peroxyacetic acid showed similar behaviour to hydrogen peroxide towards the base sensor. Although not a requirement of the sensor for the EUROPEROX project, it was decided to look at the response of the sensor to peroxyacetic acid as well as hydrogen peroxide whilst optimising the potential used for amperometry. As some manufacturers use peroxyacetic acid in their cleaning processes, it may prove possible to use the sensor in these applications, thus increasing the commercial viability of the final sensor.

To determine the optimal operating potential, a calibration curve up to 2.5 $mmol^{-1}$ was generated for the amperometric response of both hydrogen peroxide and peroxyacetic acid at different potentials. Each data point was produced using a fresh sensor made with a loading of 25U horseradish peroxidase and 0.24 μmol 1,1'-dimethylferrocene. The sensor was immersed in buffer until a stable baseline current was obtained (generally within 20 seconds) and the average from ten measurements over the next ten seconds taken as the value. The sensor was then transferred to the standard of either hydrogen peroxide or peroxyacetic acid in buffer until a stable current was again obtained (generally within 30 seconds) and again, the average from ten measurements over the next ten seconds taken as the value. The current used for producing the calibration curve was the difference between the buffer blank and standard. The results obtained for hydrogen peroxide are shown in figure 2.19 and for peroxyacetic acid in figure 2.20.

As each point was generated with a fresh sensor and the data points all fell into a linear pattern, it was considered adequate at this stage not to make replicate measurements. From the results, it was decided to use –0.3 V as the operating potential for future work with hydrogen peroxide and –0.2 V for peroxyacetic acid. Although these chosen potentials may not have been the perfect optimal value, it was decided that there would not be a significant increase in sensitivity by making slight adjustments such as 50 mV in either direction. Also, with a separation of 100 mV between hydrogen peroxide and peroxyacetic acid, it may prove possible if required in the future to differentiate between the two in a mixture.

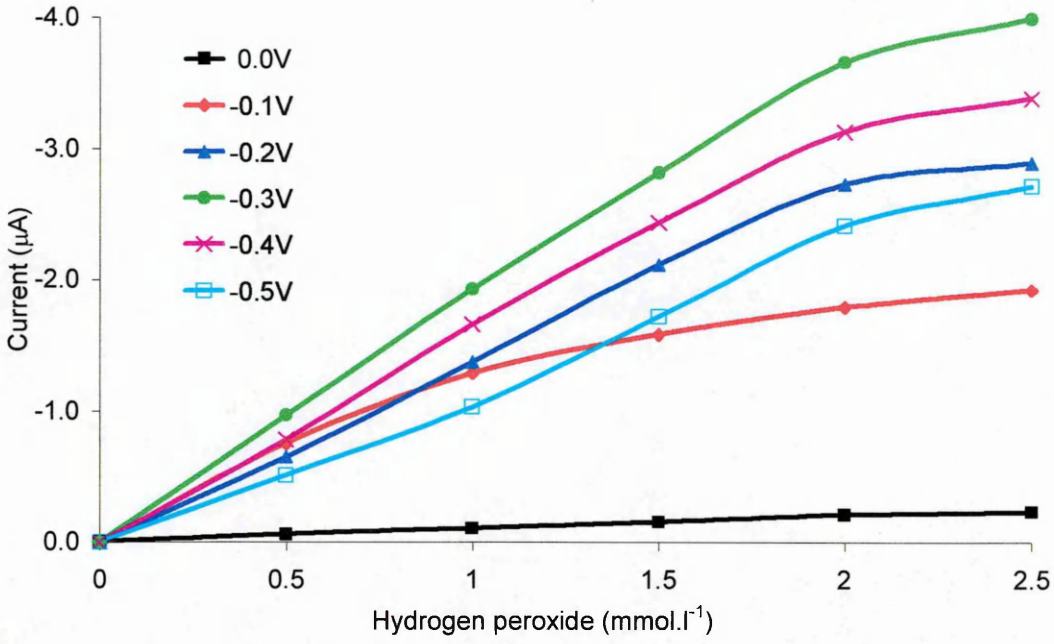

Figure 2.19 Amperometry of hydrogen peroxide at varying operating potentials vs Ag/AgCl

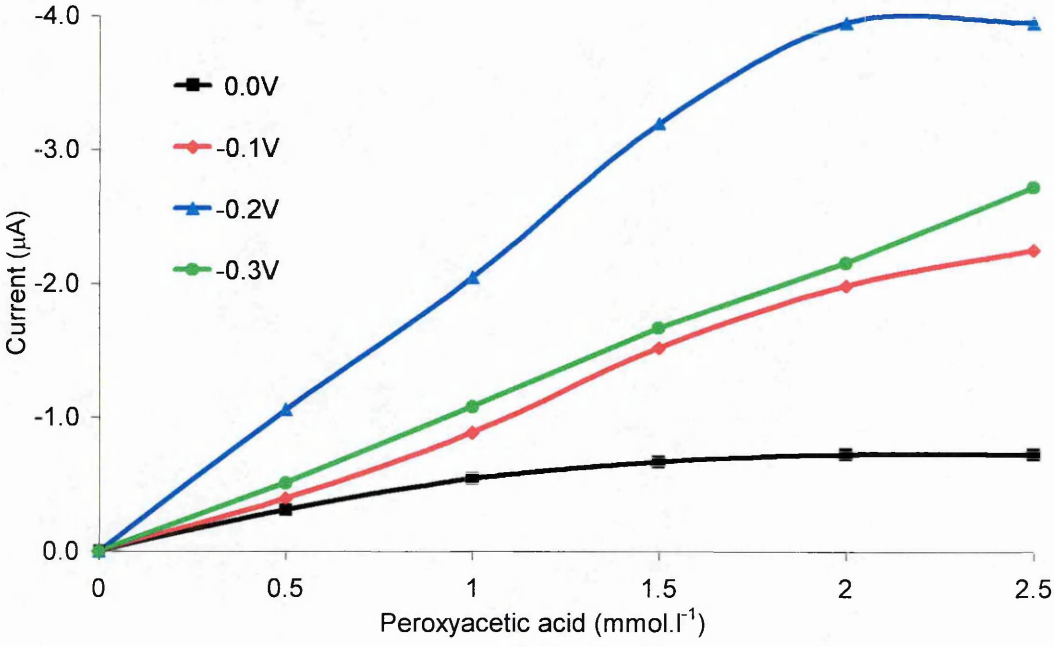

Figure 2.20 Amperometry of peroxyacetic acid at varying operating potentials vs Ag/AgCl

2.8 Evaluation as a Single-Use Sensor

As stated in the introduction to this chapter (section 2.1), a single use sensor was developed and tested to show suitability for the intended industrial application. This was part of the requirement of the European Union funding of the EUROPEROX project.

Having decided on the development of a 1,1'-dimethylferrocene mediated peroxidase biosensor, this was briefly tested by producing a calibration curve to show a changing response that could be simply related to the concentration of hydrogen peroxide. The essential requirement at this stage was that the sensor should have a low enough limit of detection to allow a large dilution of the wash solution reducing the problem of it being strongly alkaline.

All measurements were made at –0.3 V using the same sensor loading and procedure as used in section 2.7. The results obtained are given in table 2.4 and plotted in figure 2.21.

Table 2.4. Calibration data for single use peroxide sensors

Peroxide concentration $mmol.l^{-1}$	Number of sensors used	Mean Current Amps	Standard Deviation	Coefficient of Variation %
3.00	6	-2.35E-06	-8.15E-07	17
1.50	6	-2.65E-06	-8.70E-07	16
0.30	6	-7.97E-07	-1.27E-07	8
0.15	6	-4.13E-07	-1.91E-07	23
0.06	6	-1.29E-07	-3.94E-08	15
0.03	6	-1.09E-08	-2.68E-08	123

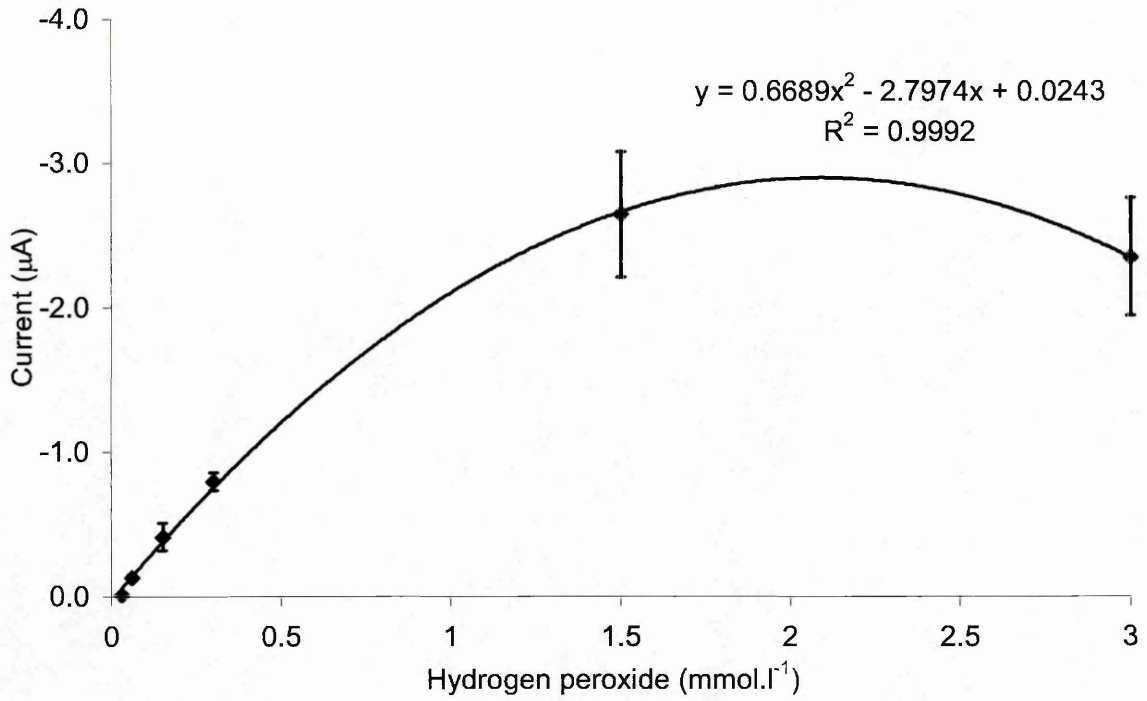

Figure 2.21 Calibration curve for single use peroxide sensors

The coefficient of variation at all levels of hydrogen peroxide seen in table 2.4 is too large for a usable device. However, this will be improved by work described in later sections with the application of a membrane and improved production of the sensor.

The fall in response and precision seen at the higher concentrations of hydrogen peroxide (and thus upper analytical limit) was probably due to inactivation of the horseradish peroxidase as described by Johansson *et al* (1993) and Gorton *et al* (1991). It was not investigated further at this stage, as the focus of this trial was to show that the sensor could respond at low levels of peroxide. Also, as the expected levels of hydrogen peroxide for the cleaning process are about 30 mmol.l^{-1} the final dilution required could easily be adjusted provided the analytical range is large enough with a low limit of detection.

2.9 Retention of Sensor Components

One of the greatest difficulties in developing a biosensor is stability. Having a biological component poses problems such as irreversible inactivation of the enzyme by extremes of heat or pH. In addition to this, as the sensor will be used in aqueous solutions in which the enzyme is soluble, some means of retaining it on the electrode surface is needed. As well as minimising the loss of horseradish peroxidase activity or 1,1'-dimethylferrocene due to desorption, covering the sensor surface with a membrane will increase its stability (Johansson *et al*, 1993) and will also minimise electrode fouling (Vadgama, 1990).

As the application of a simple membrane also keeps the manufacturing processes to a minimum, it was regarded as an attractive solution to the problem.

2.9.1 Available Membrane Materials

Various polymers have been used as membrane materials (Vadgama, 1990). From the literature search, there were many materials and techniques worthy of investigation and as in previous sections; cost and ease of manufacturing the final device were taken into account.

1) Polyurethane.
   Horseradish peroxidase has been immobilised in a polyurethane membrane (Abdel-Hamid *et al*, 1995, Wang, F. *et al*, 1995). Also, 1% polyurethane dissolved in tetrahydrofuran has been used to form an outer membrane as a diffusion control layer (Xu *et al*, 1997; Marzouk *et al*, 1997)

2) Nylon.
   Kalab and Skladal (1995) used a nylon net membrane activated by heating in dimethylsulphate and incubating in lysine to provide a free amino acid group for coupling.

3) Epoxy resin.

An epoxy resin has been used to produce a horseradish peroxidase-graphite-epoxy biocomposite. With this report, it was also claimed that the proximity of the redox centres of the enzyme with the conductive sites at the surface of the electrode permitted a direct regeneration of the enzyme (Morales *et al*, 1996)

4) Polycarbonate and cellulose acetate butyrate.

Koochaki *et al* (1991) in a study of different membranes for hydrogen peroxide sensors, found that a polycarbonate membrane of 2-μm pore size showed no selectivity but reduced all electrode responses to about 10-20% of the bare electrode value. Cellulose acetate membranes gave smaller responses, but were selective and acetate butyrate membranes showed a further reduction in response with the same pattern of selectivity as cellulose acetate.

5) Other polymers.

Other polymers have also been investigated: poly(vinyl chloride) (Reddy *et al*, 1994; Abdel-Hamid *et al*, 1995; Benmakroha *et al*, 1996); polysulphone (PS) and sulphonated polyether-ether sulphonepolyether sulphone (Benmakroha *et al*, 1996). Gooding *et al* (1997) showed that the presence of an enzyme in an acrylate emulsion polymer film increases its permeability.

6) Polymers formed by electropolymerisation.

Various polymers formed by electropolymerisation to give an ultra-thin layer have been used: poly(o-phenylenediamine) (Johansson *et al*, 1993; Myler *et al*, 1997); poly(1,3-phenylenediamine) (Wang *et al*, 1997); poly m-phenylenediamine (Xu *et al*, 1997; Marzouk *et al*, 1997); polypyrrole (Guerrieri *et al*, 1998). It has been shown that these films result in an accelerated oxidation of hydrogen peroxide, with the electrocatalytic behaviour being affected by the electropolymerisation potential, time, monomer structure and pH (Wang *et al*, 1997).

7) Nafion™

Nafion is a highly negatively charged perfluorinated sulphonate polymer that acts as a strongly acidic cation-exchanger. It tends to repel anionic species whilst allowing the passage of cations, particularly divalent hydrophobic cations (Gilmartin & Hart, 1995). It can be used alone (Amine *et al*, 1993; Gilmartin & Hart, 1995; Newman *et al*, 1995; Karyakin *et al*, 1996) or with cellulose acetate (Zhang *et al*, 1994). Ink-jet printing can be used for the deposition of Nafion, giving membranes of defined and reproducible geometry.

8) Cellulose acetate

Cellulose acetate works by size exclusion with the thickness of the coating affecting the response time of the sensor (Abdel-Hamid *et al*, 1995). It can be used alone (Koochaki *et al*, 1991; Abdel-Hamid *et al*, 1995; Gilmartin & Hart, 1995; Kröger & Turner, 1997) or in combination with other membrane types: poly(vinyl chloride) (Reddy *et al*, 1994) and Nafion (Zhang *et al*, 1994). The various molecular weight variants available for cellulose acetate also exhibit differences in permeability to hydrogen peroxide (Jawaheer, 1999). Sensors can be dip coated or ink jet printed with solutions of cellulose acetate and thus, are suited to mass production.

Because of cost, availability and suitability to mass production processes it was decided to investigate the use of Nafion and cellulose acetate.

2.9.2 Nafion

A simple trial to show if Nafion would work in principle was performed in a similar way to that for the enzyme and mediator. The working electrode surfaces of three base graphite electrodes were each covered with 4 µl of 12.5 $mg.ml^{-1}$ 1,1'-dimethylferrocene in acetone to give a coating of 0.24 µmol per electrode. After being left at room temperature for 10 minutes to allow the acetone to evaporate, 5µl of a 5 $U.\ ml^{-1}$ solution of horseradish peroxidase in buffer was pipetted over this to give a coating of 25 U per sensor. This was then allowed to dry for 1 hour at room temperature. 4 µl of Nafion (5%w/v in lower aliphatic alcohols and 10% water) was then pipetted over the top. The sensors were then stored at 4°C overnight whilst the alcohols evaporated off.

For testing, the sensors were immersed in buffer until a stable baseline current was obtained. Initially there was a drift in the baseline but it was generally constant and slight within 60 seconds.

Once considered stable, the average from ten measurements over the next ten seconds was taken as the current response. The sensor was then transferred to the first hydrogen peroxide standard in buffer (using the same concentrations as in section 2.8), until a stable current was once more obtained (generally within 30 seconds) and again, the average from ten measurements over the next ten seconds taken as the current response. The sensor was then transferred back to a fresh buffer aliquot to return the response to baseline. Once the sensors had conditioned to being in solutions rather than dry, these changes only required about 30 seconds before a stable response was observed. This cycle was repeated until responses for all the standards had been obtained.

The current used for producing the calibration curve was the difference between the buffer blank and standard; the results obtained are shown in figure 2.22 along with those from the cellulose acetate sensors.

2.9.3 Cellulose Acetate

A simple trial to show if cellulose acetate would work in principle was performed in the same way as for Nafion. The enzyme and mediator were applied as above in section 2.9.2. After drying for 1 hour at room temperature, 4 µl of a $20g.l^{-1}$ solution of cellulose acetate in acetone was then pipetted over the top and the sensors stored at 4°C overnight whilst the acetone evaporated off.

The same testing procedure was followed as above in section 2.9.2 with the observation that the baseline drift settled much sooner to a lower level or none at all.

There were 4 molecular weight variants of cellulose acetate studied; the results obtained being shown in figure 2.22 along with those from the Nafion sensors.

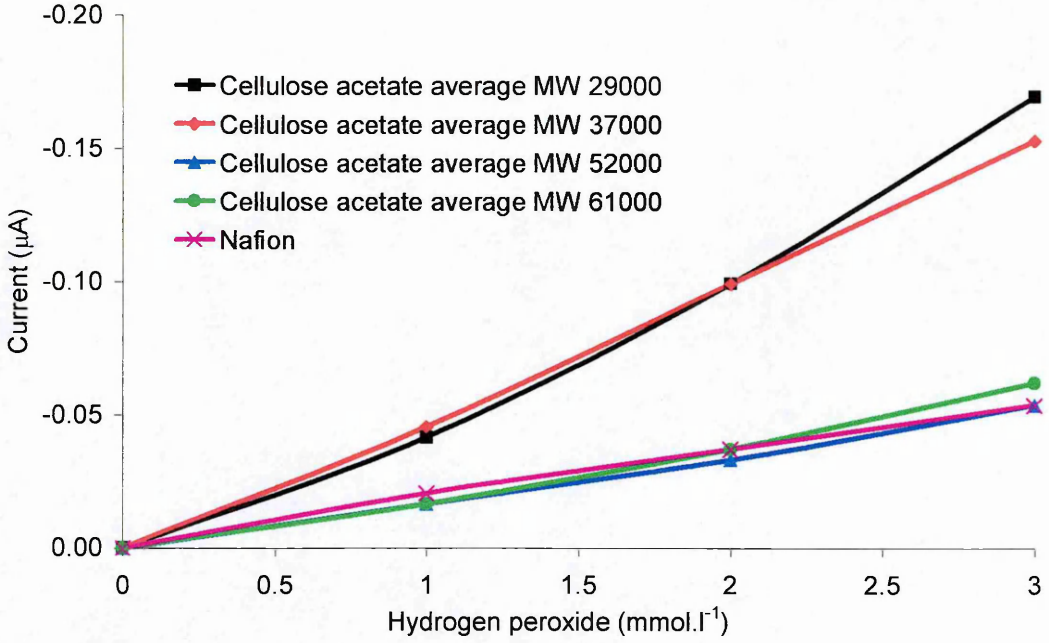

Figure 2.22 Comparison of Nafion with varying molecular weight variants of cellulose acetate

2.9.4 Selection

The initial results showed cellulose acetate to be more suitable for membrane fabrication purposes than Nafion. It demonstrated a lower baseline drift, faster stabilisation of response and had the benefit of a lower cost (0.001p per sensor compared to 0.8p per sensor for Nafion). Thus, further development was directed towards the optimisation of the sensor with this as the membrane. These initial results also showed that there might be benefit in using the lower average molecular weight variants.

2.10 Summary

In this chapter a biosensor device that will meet the requirements in the intended industrial application has been developed.

A screen-printed bare carbon working electrode surface has been adapted for hydrogen peroxide detection using the enzyme, horseradish peroxidase as the biological sensing element and 1,1'-dimethylferrocene to mediate electron transfer between the enzyme and electrode.

In order to minimise electrode fouling and loss of enzyme activity due to desorption whilst the final device is functioning in a flowing stream, the working electrode is to be covered with a cellulose acetate membrane.

The components have all been selected based on evidence from the literature; trial studies, cost, and ease of use for a manufacturing process.

In the following chapters this sensor's performance will be optimised, tested and the production process refined.

3. Sensor Optimisation

3.1 Introduction

In the previous chapter, components for the sensor were selected from the literature on the basis of suitability for simple manufacture. Those selected were then tested for their suitability such that a final selection could be made based on relative performance with consideration of cost.

This chapter will describe the optimisation of the sensor performance using the selected components.

3.2 Application of Components

The first consideration for the optimisation process was that of the application of the 1,1'-dimethylferrocene, horseradish peroxidase and cellulose acetate onto the base graphite electrode. The ideal outcome for simplicity of production would be that of a single mixed reagent application rather than layers, but this would require the enzyme to be in an organic solvent during the process.

The use of enzymes in organic media is well documented (Saini, *et al.*, 1991; Saini & Turner, 1991; Schubert *et al.*, 1991; Saini, 1993;) and the key points relative to the application of the enzyme to the base electrode are discussed below.

3.2.1 Enzymes and organic solvents

Enzymes often unfold and lose some of their activity in organic solvents but will maintain better operational stability in more hydrophobic solvents (Reslow *et al*, 1987). It is the concentration of water on the enzyme that determines its activity in a particular solvent (Zaks & Russell, 1988) and thus enzymes in hydrophobic solvents appear to require less water for maximum activity than those in hydrophilic ones (Zaks & Klibanov, 1988a) as the more hydrophobic solvents will leave more water available for the enzyme molecule.

Maximum activity in organic solvents requires roughly 1000 molecules of water per enzyme molecule, equating to roughly a monolayer of water on the surface (Zaks & Klibanov, 1988a). The loss of this essential water has a detrimental effect on enzymatic activity, but when the water is replenished, the catalytic activity is restored with less than a monolayer of water effectively screening the surface charge of a protein (Zaks & Russell, 1988). Increasing the water layer from 0.5 to 1.1 % can increase the enzymatic activity by up to 1000 fold (Zaks & Klibanov, 1988b). The effect of the organic solvent on the enzymatic activity is primarily due to interactions with the enzyme bound essential layers of water rather than the enzyme itself and thus the enzyme produces a suspension in the solvent rather than dissolving in it (Zaks & Klibanov, 1988a).

The enzyme will also remember the pH of its last aqueous solvent but the substrate specificity may change between organic and aqueous solvents, in some instances the enzyme also becomes more thermo-stable in organic solvents (Zaks & Russell, 1988),

Adeyoju *et al* (1995) made a study involving horseradish peroxidase electrodes in organic solvents. In agreement with the above, they found that the reactivities of the electrodes in acetonitrile, methanol and acetone using butanone peroxide as a substrate, decreased as the hydrophilic nature of the solvent increased (methanol > acetonitrile > acetone). They also attributed this to the ability of the hydrophilic solvents to desorb essential water of hydration from the enzyme active site.

Schubert *et al*, 1992 developed an organic-phase enzyme electrode for the determination of hydrogen peroxide and phenol that could operate in dioxane, chloroform and chlorobenzene requiring only a small amount of aqueous buffer for activity.

3.2.2 Testing

From the above studies, it was considered feasible to dissolve the horseradish peroxidase in buffer so that the pH of its last aqueous solvent was the same as the operating pH and then mix with the 1,1'-dimethylferrocene and cellulose acetate in acetone. Provided that the enzyme was dissolved in buffer it could be assumed that there was sufficient water to maintain the water layer whilst saturating the acetone. Any

dehydration effects would be countered once the sensor was in use with just the possibility of a required conditioning period.

Also, it was hoped that by mixing the enzyme and mediator before application to the electrode surface it would hopefully facilitate a more intimate contact with the electrode than could be achieved by applying sequential layers as in the previous chapter. Additionally, by mixing the enzyme and mediator with the cellulose acetate it could be regarded as an entrapment within the cellulose acetate rather than a membrane layer. This could give rise to improvements in diffusion and transfer within the reagent layer on the electrode surface and thus give a significant improvement in performance.

To investigate this, six protocols were produced for the application process. Each component application was made in a single and a double coating to validate that the manual pipetting technique was giving a good coverage of the electrode surface. The protocols were devised such that they resulted in the same component loading on all electrodes, with 5 µl of aqueous solution required to cover the electrode, but only 4 µl required if there was acetone present. When the enzyme was dissolved in the buffer it produced a dark brown solution. However, when this was mixed with the 1,1'-dimethylferrocene or cellulose acetate in acetone, it produced a lighter brown solution that was probably due to the formation of a suspension rather than a solution.

In addition, there are four molecular weight variants of cellulose acetate available (29000, 37000, 52000 and 61000) and these were all tested to determine the optimal choice for this sensor.

After the coating process, all sensors were left at room temperature for 1 hour to ensure that all the acetone and water had evaporated off before being stored at -20°C until testing.

1) Single application of mediator, enzyme and membrane in sequence.
   4 µl of 0.06 µmol.µl^{-1} 1,1'-dimethylferrocene in acetone was pipetted onto the surface of the base graphite electrode to give a coating of 0.24 µmol per electrode and left for 10 minutes to allow the acetone to evaporate off. This was followed by 5 µl of a 5 U.µl^{-1} solution of horseradish peroxidase in buffer to give a coating of

25 U per sensor that was allowed to dry for 1 hour at room temperature. Finally, 4 µl of a 20 $\mu g.\mu l^{-1}$ solution of cellulose acetate in acetone was pipetted over the top to give a membrane cover of 80 µg per sensor.

2) Double application of mediator, enzyme and membrane in sequence.
4 µl of 0.03 $\mu mol.\mu l^{-1}$ 1,1'-dimethylferrocene in acetone was pipetted onto the surface of the base graphite electrode to give a coating of 0.12 µmol per electrode and left for 10 minutes to allow the acetone to evaporate off. This was then repeated to give a final coating of 0.24 µmol per electrode as above. This was followed by 5 µl of a 2.5 $U.\mu l^{-1}$ solution of horseradish peroxidase in buffer to give a coating of 12.5 U per sensor. This was allowed to dry for 30 minutes at room temperature before repeating to give a coating of 25 U per sensor and allowing it to dry for a further 1 hour. Next, 4 µl of a 10 $\mu g.\mu l^{-1}$ solution of cellulose acetate in acetone was pipetted over the top to give a membrane. Finally, after being left for 10 minutes to allow the acetone to evaporate, another 4 µl of the 10 $\mu g.\mu l^{-1}$ cellulose acetate was pipetted over the top giving a final cellulose acetate coverage of 80µg per sensor.

3) Single application of pre-mixed enzyme and mediator followed by the membrane.
Equal volumes of 0.12 $\mu mol.\mu l^{-1}$ 1,1'-dimethylferrocene in acetone and 12.5 $U.\mu l^{-1}$ solution of horseradish peroxidase in buffer were mixed to give the suspension. 4 µl of this were immediately pipetted onto the electrode surface to give the same loading as above and allowed to dry for 30 minutes. Finally, 4 µl of a 20 $\mu g.\mu l^{-1}$ solution of cellulose acetate in acetone was pipetted over the top to give an 80 µg membrane.

4) Double application of pre-mixed enzyme and mediator followed by the membrane.
Equal volumes of 0.06 $\mu mol.\ \mu l^{-1}$ 1,1'-dimethylferrocene in acetone and 6.25 $U.\mu l^{-1}$ solution of horseradish peroxidase in buffer were mixed to give the suspension. 4 µl of this were immediately pipetted onto the electrode surface to give the half the required loading and allowed to dry for 30 minutes. After drying, another mix of the 1,1'-dimethylferrocene and horseradish peroxidase was made fresh and pipetted to give the final loading as above. Next, 4 µl of a 10 $\mu g.\mu l^{-1}$ solution of cellulose acetate in acetone was pipetted over the top to give a membrane. Finally, after being left for

10 minutes to allow the acetone to evaporate, another 4 µl of the 10µg.µl^{-1} cellulose acetate was pipetted over the top to give an 80 µg coverage.

5) Single application after pre-mixing all components.
Equal volumes of 0.24 µmol.µl^{-1} 1,1'-dimethylferrocene in acetone and 80 µg.µl^{-1} cellulose acetate in acetone were mixed together. An aliquot of this was then mixed with an equal volume of 12.5 U.µl^{-1} solution of horseradish peroxidase in buffer to give a similar suspension to that in 3 and 4 above. 4 µl of this mix were immediately pipetted onto the electrode surface to give the same loading as above.

6) Double application after pre-mixing all components.
The mixture of 1,1'-dimethylferrocene and cellulose acetate used in 5 above was diluted 1 to 1 with acetone. An aliquot of this was then mixed with an equal volume of 6.25 U.µl^{-1} solution of horseradish peroxidase in buffer and 4 µl immediately pipetted onto the electrode surface. After being allowed to dry for 30 minutes, this was repeated to give the final loading.

Each of the sensors was then tested for their amperometric response to hydrogen peroxide at an operating potential of –0.3 V. Each sensor was placed in buffer until a stable baseline signal was obtained; once the baseline signal had been established the sensor was placed into a series of the standard hydrogen peroxide solutions in buffer, starting at the lowest concentration. The sensor was returned to the buffer between each standard to re-establish the baseline signal.

The calibration curves for single application protocols are shown in figure 3.1 and for double application protocols in figure 3.2.

From these curves, it is clear that there is an enhanced response obtained by pre-mixing the 1,1'-dimethylferrocene, horseradish peroxidase and cellulose acetate prior to application. To evaluate the single and double application protocols, the data from the pre-mixing of all components are plotted together in figure 3.3.

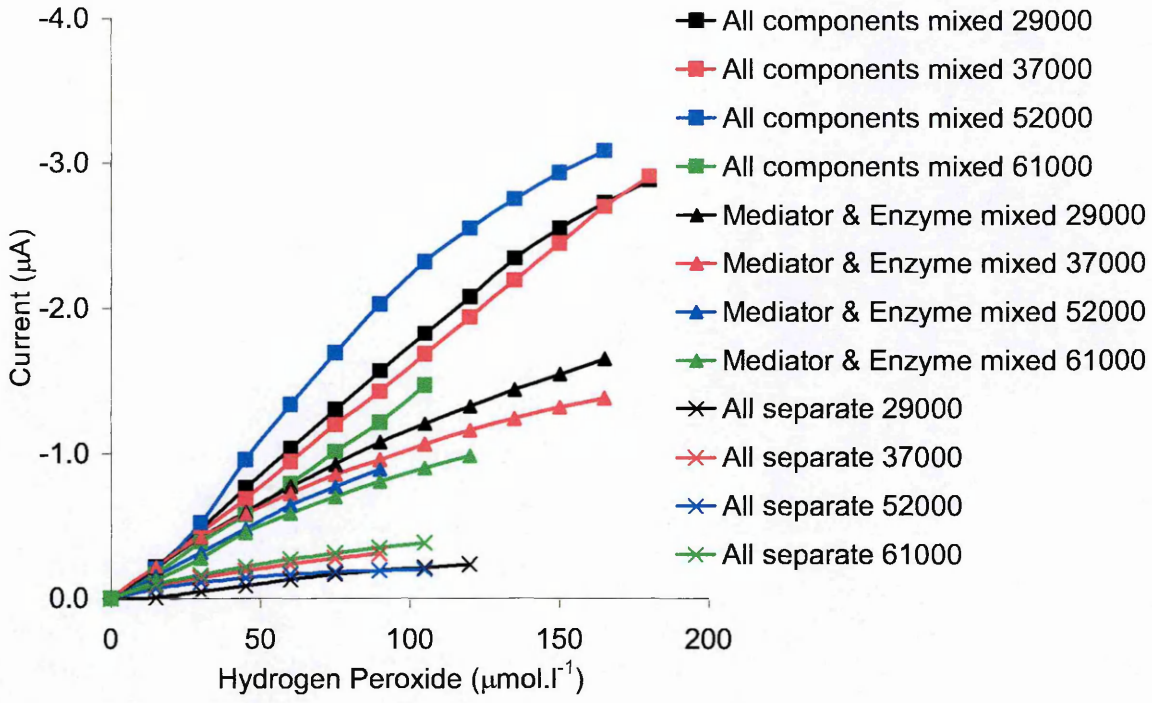

Figure 3.1 Single application of sensor components.

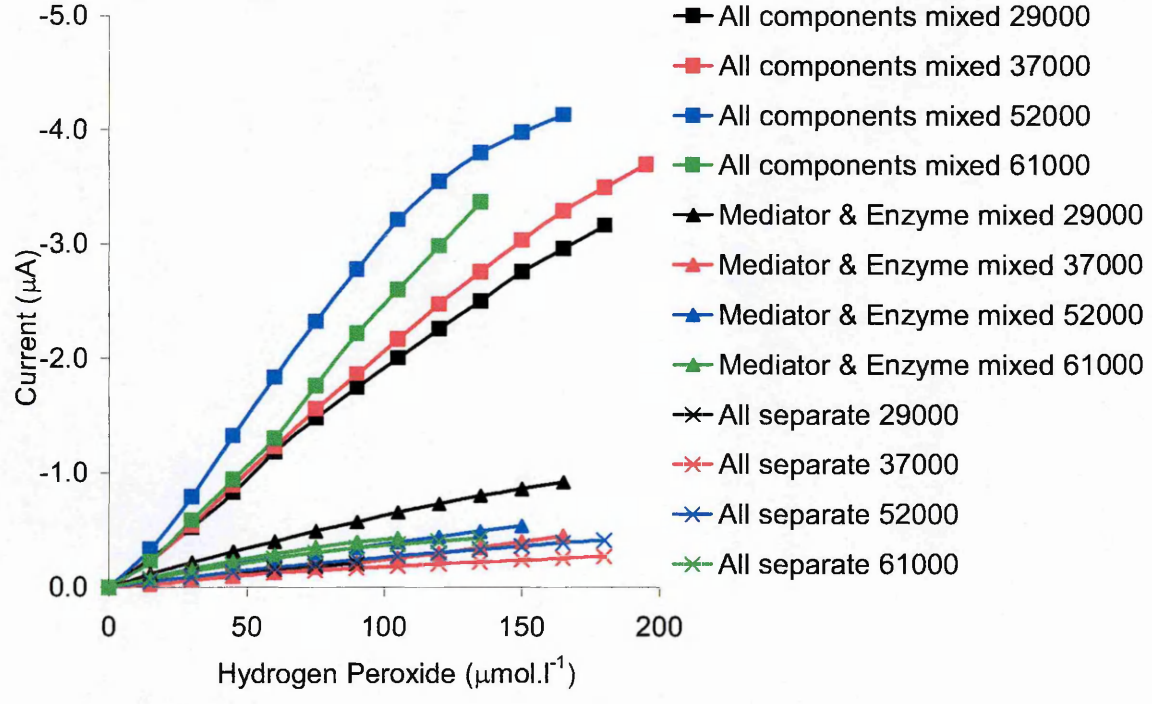

Figure 3.2 Double application of sensor components.

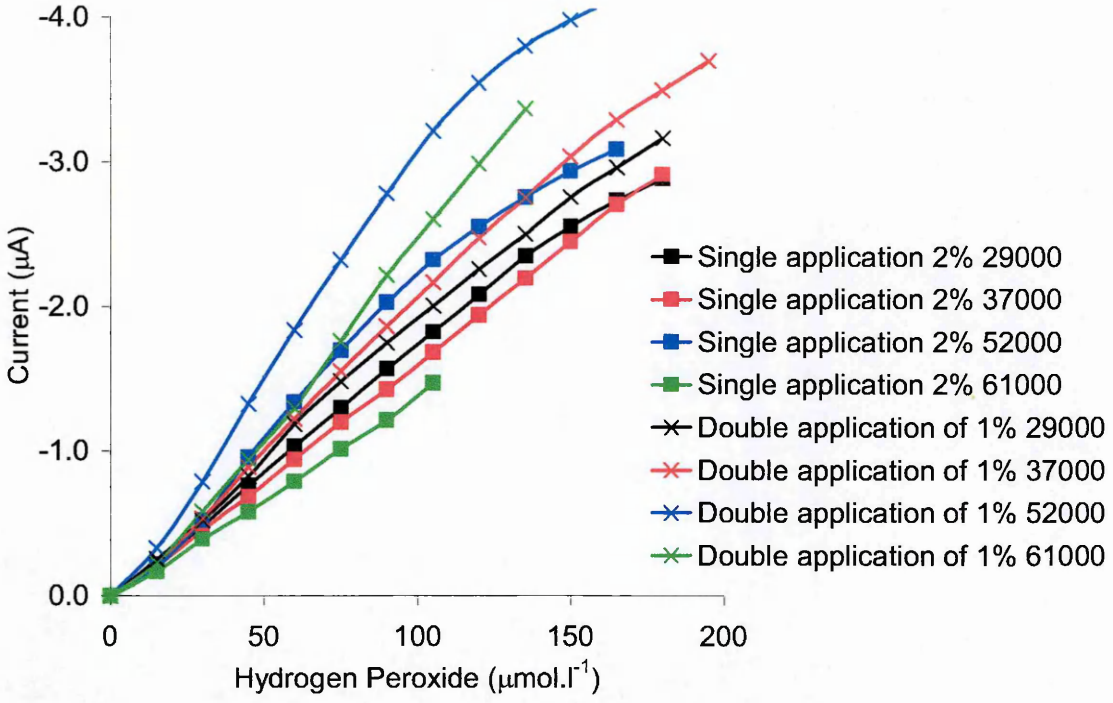

Figure 3.3 Single and Double application of pre-mixed sensor components.

3.2.3 Discussion

Not all of the sensors had sufficient operating lifetime to continue giving a response to establish the full calibration curve. In some instances, when the sensor failed, it was apparent that the components or at least the cellulose acetate had become detached from the electrode surface. In other cases, the level of noise became too great to establish the response current. It appeared that the higher molecular weight cellulose acetate was more prone to this problem, as were sensors produced by the sequential application of 1,1'-dimethylferrocene, horseradish peroxidase and cellulose acetate. As the final selection was to apply the components as a single pre-mixed dose (see below) and use the 37,000 molecular weight variant of cellulose acetate (section 3.4.3) this observation was not studied further.

The current versus concentration gradients ($A.\mu mol^{-1}$) for the sensors across the hydrogen peroxide concentration range of 0 - 180 $\mu mol.l^{-1}$ (or as far as they responded) are given in table 3.1.

Table 3.1. The effect of the component application protocol on the sensor response

		Cellulose acetate MW			
		29 000	37 000	52 000	61 000
	Application	**Trendline ($A.\mu mol^{-1}$)**			
All components pre-mixed	**Single**	1.68×10^{-8}	1.62×10^{-8}	2.04×10^{-8}	1.36×10^{-8}
	Double	1.84×10^{-8}	1.99×10^{-8}	2.79×10^{-8}	2.43×10^{-8}
Enzyme and mediator pre- mixed	**Single**	1.09×10^{-8}	9.50×10^{-9}	1.03×10^{-8}	8.82×10^{-9}
	Double	5.99×10^{-9}	2.58×10^{-9}	3.78×10^{-9}	4.51×10^{-9}
Individual application of all components	**Single**	2.06×10^{-9}	3.80×10^{-9}	2.35×10^{-9}	4.08×10^{-9}
	Double	2.54×10^{-9}	1.69×10^{-9}	2.49×10^{-9}	3.60×10^{-9}

For both single and double application protocols, it is clear that the sensor responses were enhanced by pre-mixing the 1,1'-dimethylferrocene, horseradish peroxidase and cellulose acetate prior to application. It is possible that this enhanced response is a result of entrapment of the enzyme and mediator within, as opposed to under the membrane film, presumably enhancing the accessibility of the substrate to the enzyme and then the mediator to both the enzyme and the electrode. Furthermore, applying the reagents in two discrete doses as opposed to a single dose further enhanced the signal. A number of factors may contribute to this effect, including the fact that the membrane pore size, which is a function of drying time, will be influenced by the amount of liquid deposited on the electrode.

Although there was a slight increase in the current versus concentration gradients ($A.\mu mol^{-1}$) for a double application of the components, given the fact that ease and economy of mass-manufacture is an important factor in this development, single dose reagent application was selected over the double dose method.

In producing the sensors, care had to be taken regarding evaporation of the acetone before application; in the initial testing phases this can be overcome, but will present issues that will have to be considered for the mass production process.

3.3 Required Analytical Range

As stated in the introduction, the final application of this sensor will require it to monitor the level of hydrogen peroxide in the wash solution to ensure that the concentration does not fall below 30 $mmol.l^{-1}$. At present, the process starts at a concentration of 220 $mmol.l^{-1}$ and thus the sensor should also be able to work at this level. As stated earlier, horseradish peroxidase is inactivated at hydrogen peroxide levels greater than 2.5 $mmol.l^{-1}$, thus the wash needs to be diluted a minimum of 100 fold. As the wash solution is also 0.5 M sodium hydroxide, the dilution also needs to be sufficient that the buffer can control the pH to 7.2.

To check the ability of the buffer to achieve this, 100ml of buffer was placed in a beaker and the pH monitored whilst the alkaline wash solution from the König brewery was added in 100 µl steps. The results are shown in figure 3.4.

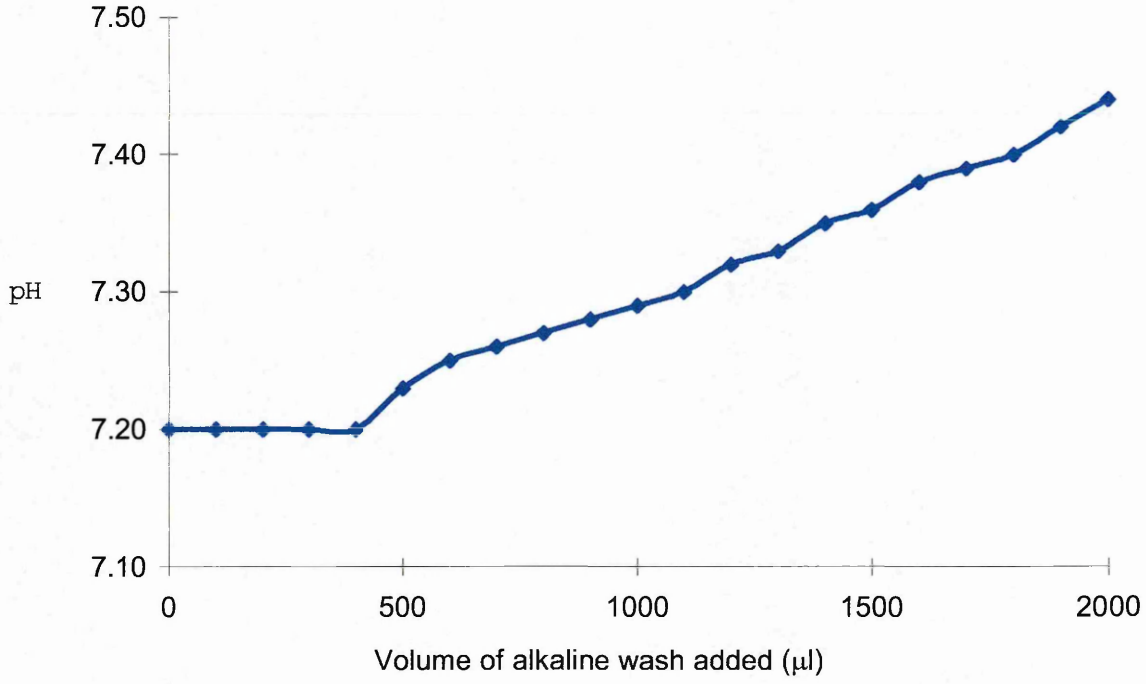

Figure 3.4 Titration of wash solution against 100 ml buffer

From this, it can be seen that the buffer was effective for the addition of up to 400 µl of the wash solution before the pH was affected. This is equivalent to a minimum dilution

of 1 in 250. Thus, a minimum dilution factor of 1000 needed to be adopted to guarantee that the buffer maintained the pH at 7.2.

This dilution factor thus required that the analytical range of the sensors should have a lower limit well below 30 $\mu mol.l^{-1}$ and an upper limit above 220 $\mu mol.l^{-1}$. From this, it was decided to test the sensors over the range of 0 to 368 $\mu mol.l^{-1}$ in the experiments described in the following sections. The upper limit was determined for a convenient dilution of the stock hydrogen peroxide standard whilst being well above the desired limit.

3.4 Component Optimisation

A large-scale optimisation experiment was performed in which all combinations of the sensor components were assessed, in triplicate, across a suitable range of values over the desired hydrogen peroxide concentration range. That combination of components giving the highest signal versus reproducibility ratio coupled to an acceptable dynamic range and limit of detection was considered optimal with regard to sensor performance. The following sections detail the effect of varying each of these three variables in turn, with the remaining two variables being maintained at the optimum levels determined by the overall large-scale experiment.

The sensors were all made from the same stock solutions of horseradish peroxidase, 1,1'-dimethylferrocene and cellulose acetate suitably diluted such that the same mix of buffer and acetone was pipetted onto all the electrode surfaces. This removed the risk of variation due to any changes that the buffer and acetone mix may make to the surface characteristics of the graphite base, thus ensuring that the observed differences were due to component proportions.

As the testing had to take place over several days, once fabricated, the sensors were all stored at –20°C. Testing was then performed at random so that any storage changes would reduce the precision rather than the relative performance.

To encompass the required analytical range and test the lower limit, standards containing 0.22, 2.2, 22, 220 and 368 µmol/l of hydrogen peroxide in buffer were used.

3.4.1 Horseradish peroxidase loading

The most important consideration for horseradish peroxidase loading was to ensure that there was sufficient enzyme present such that it was not the rate-limiting factor. Equally, as it is a large protein molecule (6 nm), if too much is applied to the surface of the electrode it could act as a diffusion barrier.

Sensors were fabricated using the 37 000 molecular weight variant of cellulose acetate and a 1,1'-dimethylferrocene loading of 0.03 μmol per sensor. The horseradish peroxidase was applied to give a final covering of 0, 10, 20, 25, 30, 40 Units per sensor.

The analytical responses of the sensors over the tested range of hydrogen peroxide concentrations are shown in figure 3.5 with the coefficient of variation plotted against concentration in figure 3.6. To clarify the responses at the lower hydrogen peroxide concentrations, the same data are shown in figures 3.7 and 3.8 but with the concentration scale going up to 2.2 μmol/l.

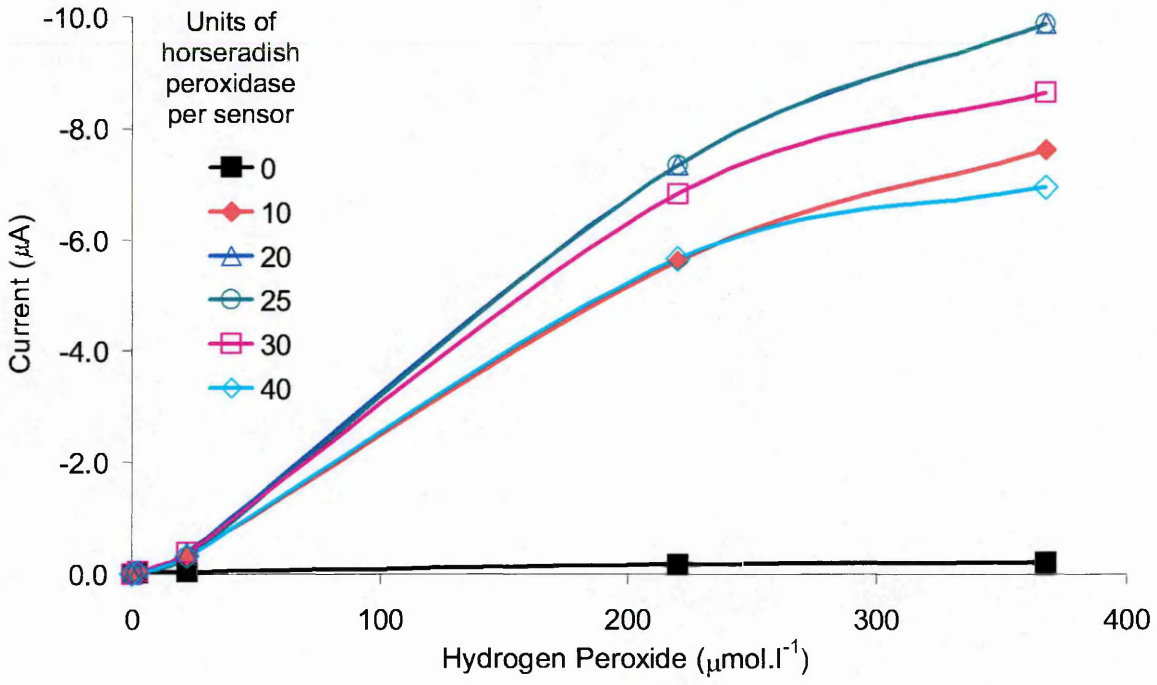

Figure 3.5 The effect of horseradish peroxidase loading on the sensor response to hydrogen peroxide

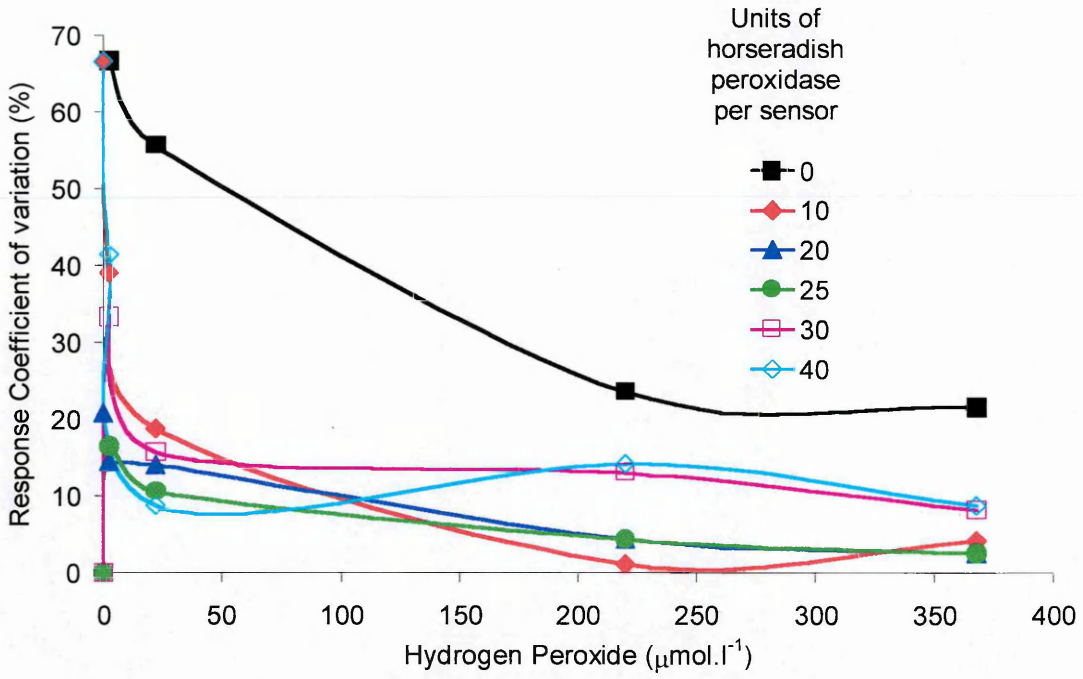

Figure 3.6 The coefficient of variation of the sensor response to hydrogen peroxide at a range of horseradish peroxidase loadings

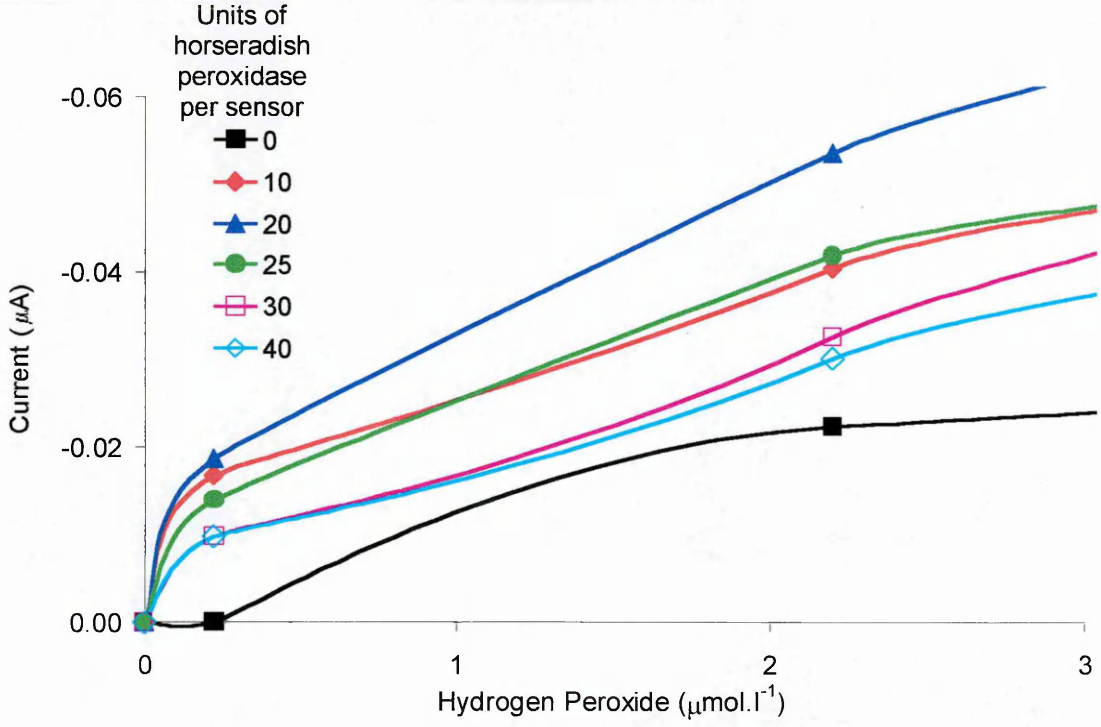

Figure 3.7 The effect of horseradish peroxidase loading on the sensor response to low levels of hydrogen peroxide (lower range of figure 3.5 enlarged)

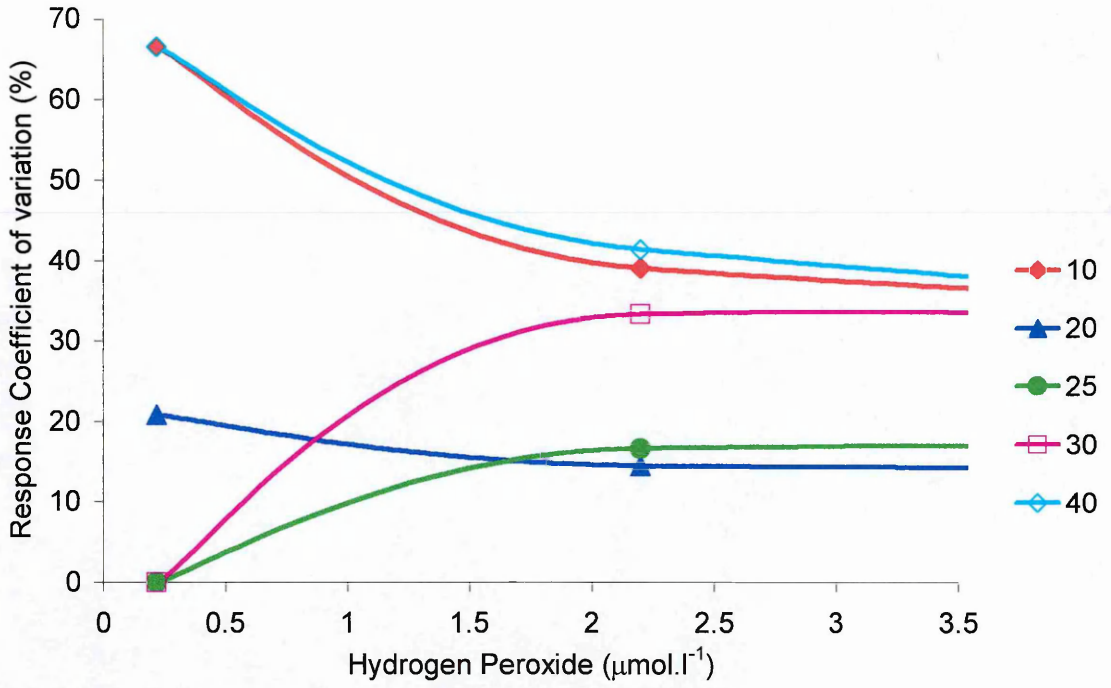

Figure 3.8 The coefficient of variation of the sensor response to low levels of hydrogen peroxide at a range of horseradish peroxidase loadings (lower range of figure 3.6 enlarged)

Looking at the figures, it can be seen that the enzyme loadings of 20 and 25 units per sensor gave the larger current responses at the higher concentrations of hydrogen peroxide and with the exception of the 10 units per sensor enzyme loading they also showed lower coefficient of variation values. At lower concentrations of hydrogen peroxide the 20 units per sensor enzyme loading showed a slightly larger response and lower coefficient of variation values than the 25 units per sensor enzyme loading. However, the at the lowest concentration of hydrogen peroxide 0.22 $\mu mol.l^{-1}$ the 25 units per sensor enzyme loading showed a significantly lower coefficient of variation indicating a lower limit of detection.

Table 3.2 gives the coefficient of variation values (%) at each standard level and trend-line data for the desired analytical range 0 to 220 $\mu mol.l^{-1}$ to ascertain the enzyme loading offering the most suitable overall dynamic range and limit of detection.

Table 3.2. Sensor response data at varying horseradish peroxidase loadings

Horseradish peroxidase loading (Units per electrode)	Hydrogen peroxide (µmol.l^{-1})					Equation for linear region in figure 3.5
	0.22	2.2	22	220	368	
	Coefficient of variation (%)					
0		67	56	24	22	$y = -8.42 \times 10^{-10}x$
10	67	39	19	1	4	$y = -2.54 \times 10^{-08}x$
20	21	14	14	4	3	$y = -3.32 \times 10^{-08}x$
25	0	17	11	4	3	$y = -3.32 \times 10^{-08}x$
30	0	33	16	13	8	$y = -3.09 \times 10^{-08}x$
40	67	41	9	14	9	$y = -2.56 \times 10^{-08}x$

Visual examination of the calibration plots had indicated that the largest responses were obtained at enzyme loadings of 20 and 25 units per sensor and the trend-line data confirmed this. However, the 25 units per sensor loading was selected, based on the lower coefficient of variation at the lower level of hydrogen peroxide.

3.4.2 1,1'-dimethylferrocene loading

It has already been shown that the rate of oxidation of 1,1'-dimethylferrocene is highly dependant on the amount incorporated into the electrode (Amine *et al*, 1993).

Sensors were fabricated using the 37 000 molecular weight variant of cellulose acetate and a horseradish peroxidase loading of 25 units per sensor. The 1,1'-dimethylferrocene was applied to give a final covering of 0, 0.01, 0.03, 0.06, 0.1 and 0.3 µmol per sensor

The analytical responses of the sensors over the tested range of hydrogen peroxide concentrations are shown in figure 3.9 with the coefficient of variation plotted against concentration in figure 3.10. To clarify the responses at the lower hydrogen peroxide concentrations, the same data are shown in figures 3.11 and 3.12 but with the concentration scale going up to 2.2 µmol/l.

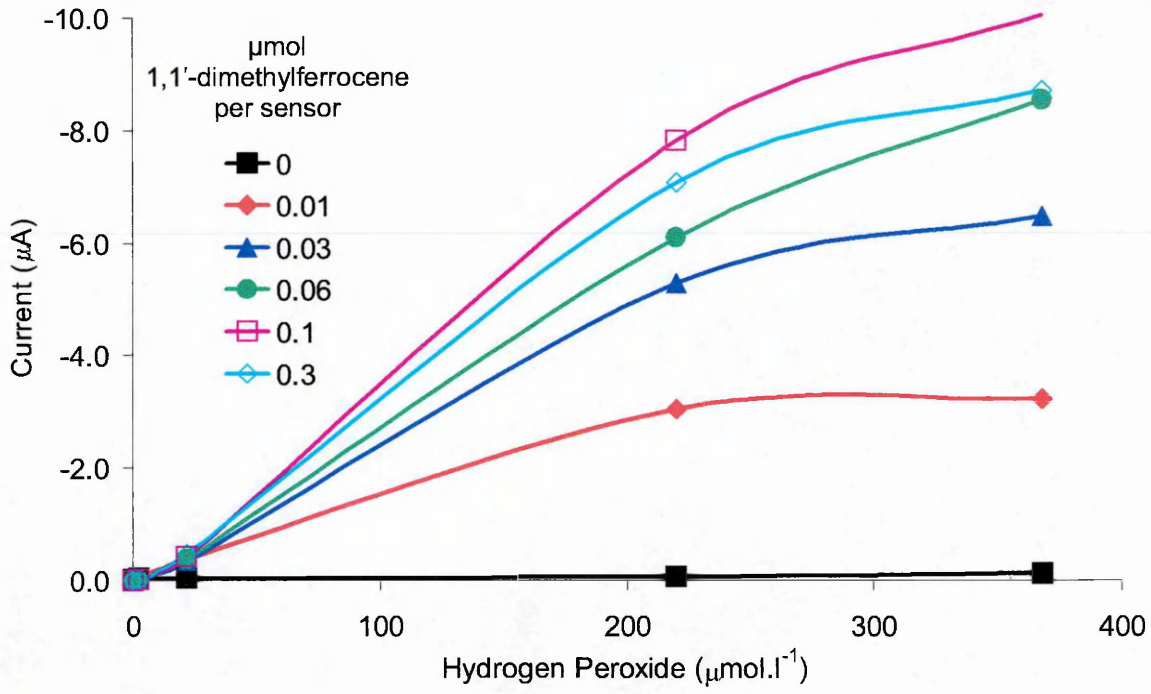

Figure 3.9 The effect of 1,1'-dimethylferrocene loading on the sensor response to hydrogen peroxide

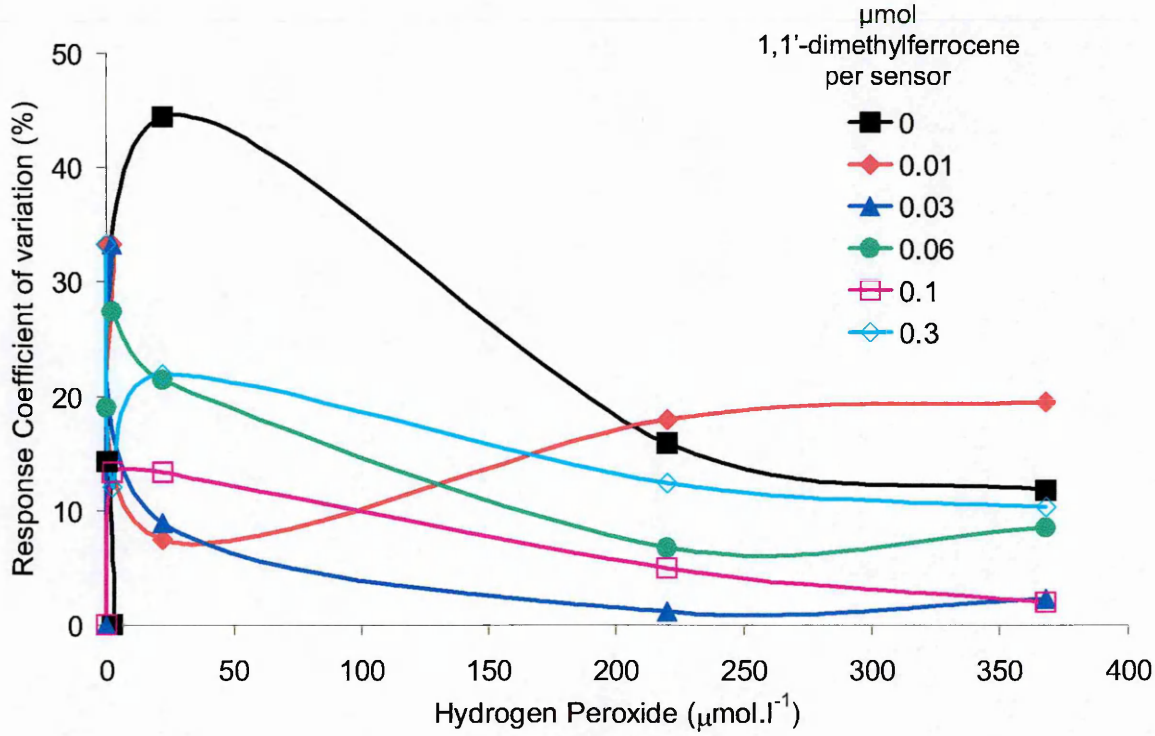

Figure 3.10 The coefficient of variation of the sensor response to hydrogen peroxide at a range of 1,1'-dimethylferrocene loadings

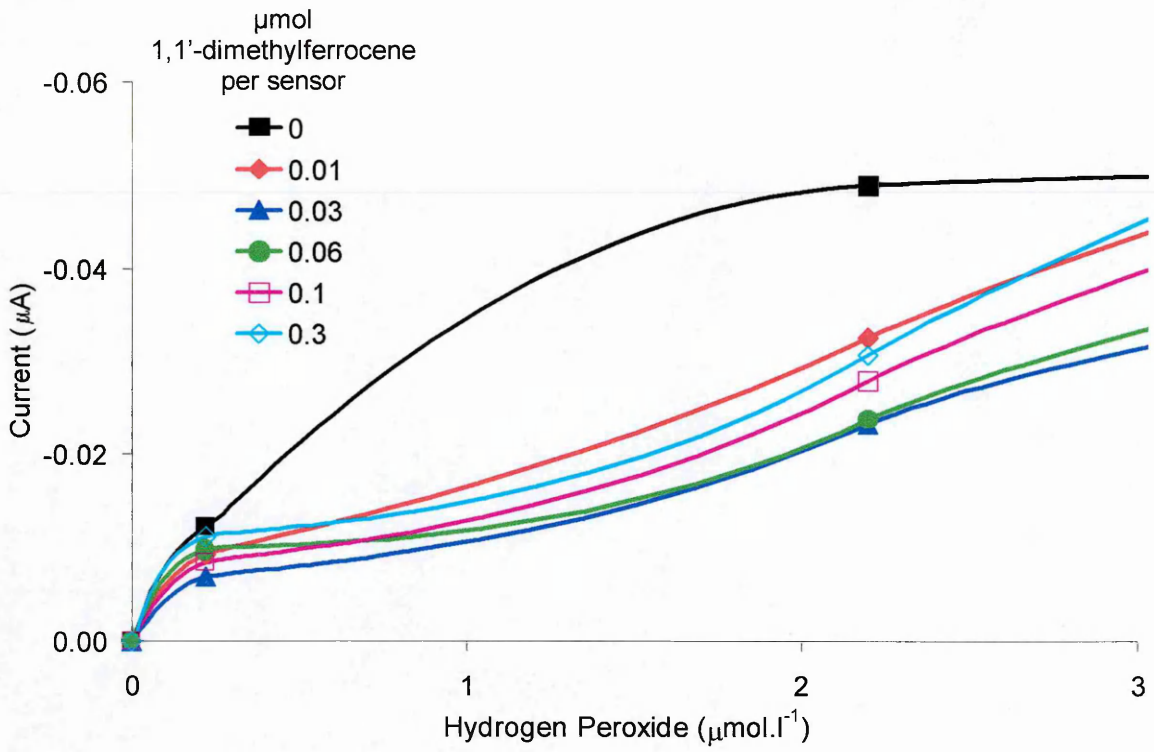

Figure 3.11 The effect of 1,1'-dimethylferrocene loading on the sensor response to low levels of hydrogen peroxide (lower range of figure 3.9 enlarged)

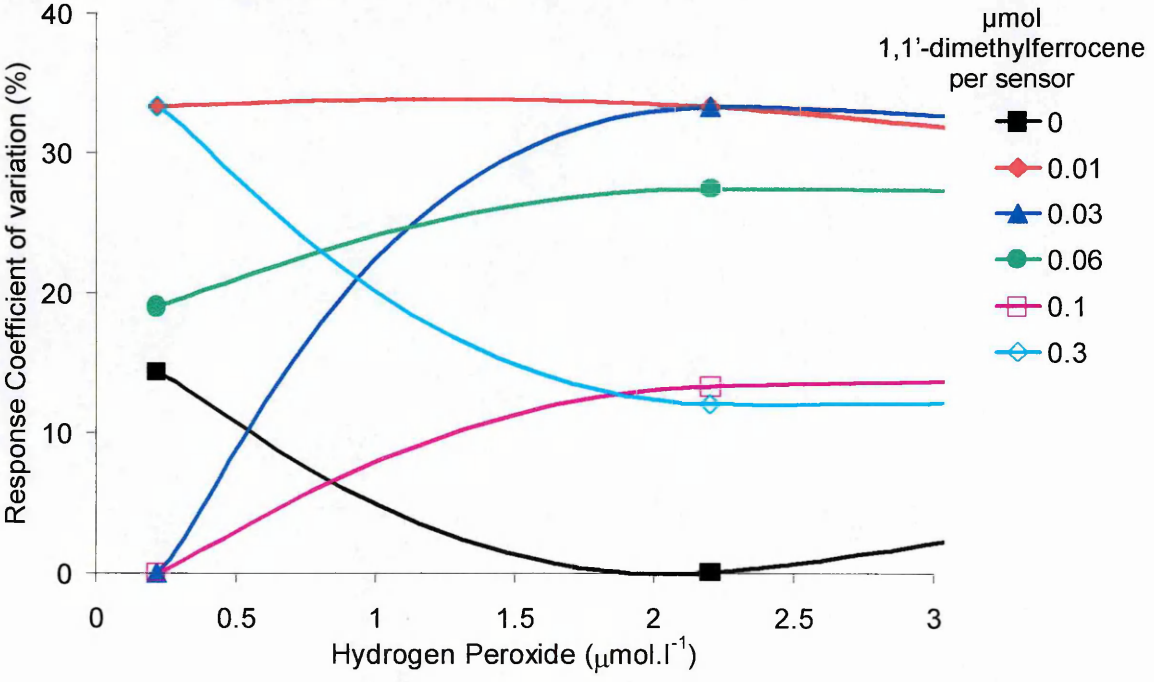

Figure 3.12 The coefficient of variation of the sensor response to low levels of hydrogen peroxide at a range of 1,1'-dimethylferrocene loadings (lower range of figure 3.10 enlarged)

Looking at the figures, it can be seen that the higher 1,1-dimethylferrocene loadings gave the larger current responses. However, the 0.03 μmol per sensor loading showed a significantly lower coefficient of variation. At lower concentrations of hydrogen peroxide the current responses were all fairly similar with the higher 1,1-dimethylferrocene loadings demonstrating lower coefficients of variation.

Table 3.3 gives the coefficient of variation values (%) at each standard level and trend-line data for the desired analytical range 0 to 220 $\mu mol.l^{-1}$ to ascertain the 1,1-dimethylferrocene loading offering the most suitable overall dynamic range and limit of detection.

Table 3.3. Sensor response data at varying 1,1-dimethylferrocene loadings

1,1-dimethylferrocene loading (μmol per electrode)	**Hydrogen peroxide ($\mu mol.l^{-1}$)**					**Equation for linear region in figure 3.9**
	0.22	2.2	22	220	368	
	Coefficient of variation (%)					
0	14	0	44	16	12	$y = -3.35 \times 10^{-10}x$
0.01	33	33	7	18	20	$y = -1.38 \times 10^{-08}x$
0.03	0	33	9	1	2	$y = -2.40 \times 10^{-08}x$
0.06	19	27	21	7	8	$y = -2.76 \times 10^{-08}x$
0.10	0	13	13	5	2	$y = -3.54 \times 10^{-08}x$
0.30	33	12	22	12	10	$y = -3.21 \times 10^{-08}x$

Visual examination of the calibration plots had indicated that the largest responses were obtained at higher 1,1-dimethylferrocene loadings and the trend-line data confirmed this. However, the 0.03 μmol per sensor loading was selected, based on the lower coefficient of variation at the levels of hydrogen peroxide for which the sensor is being developed.

At low hydrogen peroxide concentrations (0-2.2 μmol.l^{-1}), the data suggests an optimum mediator loading of 0.10 μmol per sensor. Thus, the optimum choice of mediator loading is therefore dependent upon the level of analyte in the sample and is in agreement with the report of Amine *et al*, 1993.

3.4.3 Cellulose acetate molecular weight

Sensors were fabricated using a horseradish peroxidase loading of 25 units per sensor and a 1,1'-dimethylferrocene loading of 0.03 μmol per sensor. Four mean cellulose acetate molecular weights were examined: 29 000, 37 000, 52 000 and 61 000.

The analytical responses of the sensors over the tested range of hydrogen peroxide concentrations are shown in figure 3.13 with the coefficient of variation plotted against concentration in figure 3.14. To clarify the responses at the lower hydrogen peroxide concentrations, the same data are shown in figures 3.15 and 3.16 but with the concentration scale going up to 2.2 μmol/l.

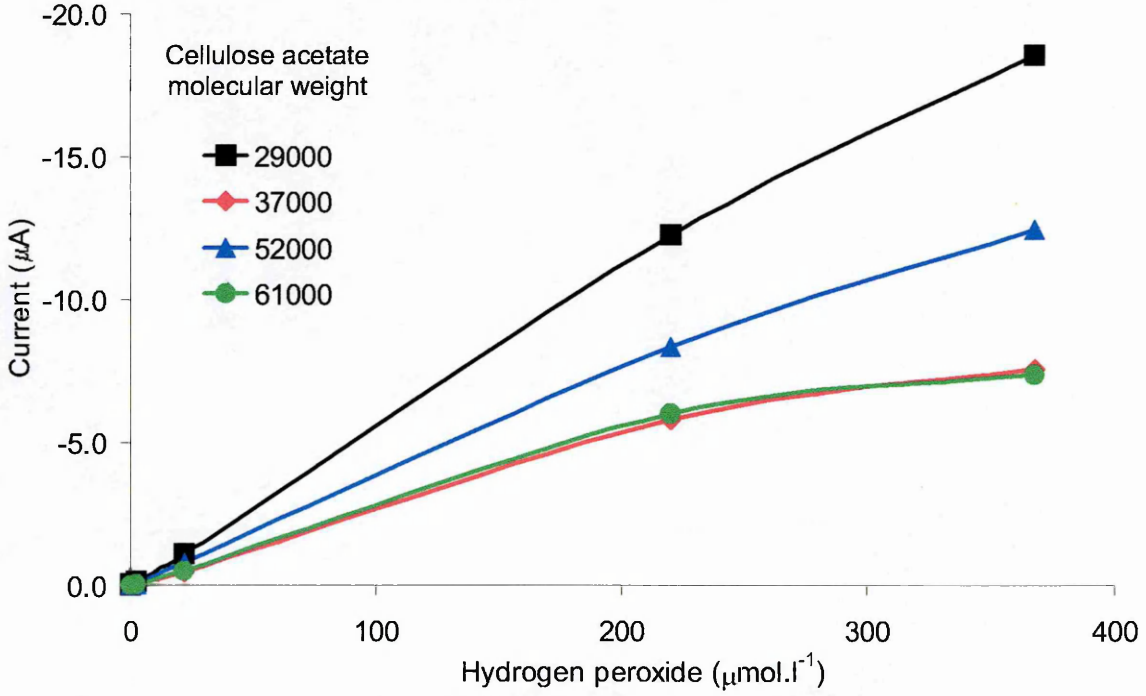

Figure 3.13 The effect of cellulose acetate membrane molecular weight on the sensor response to hydrogen peroxide

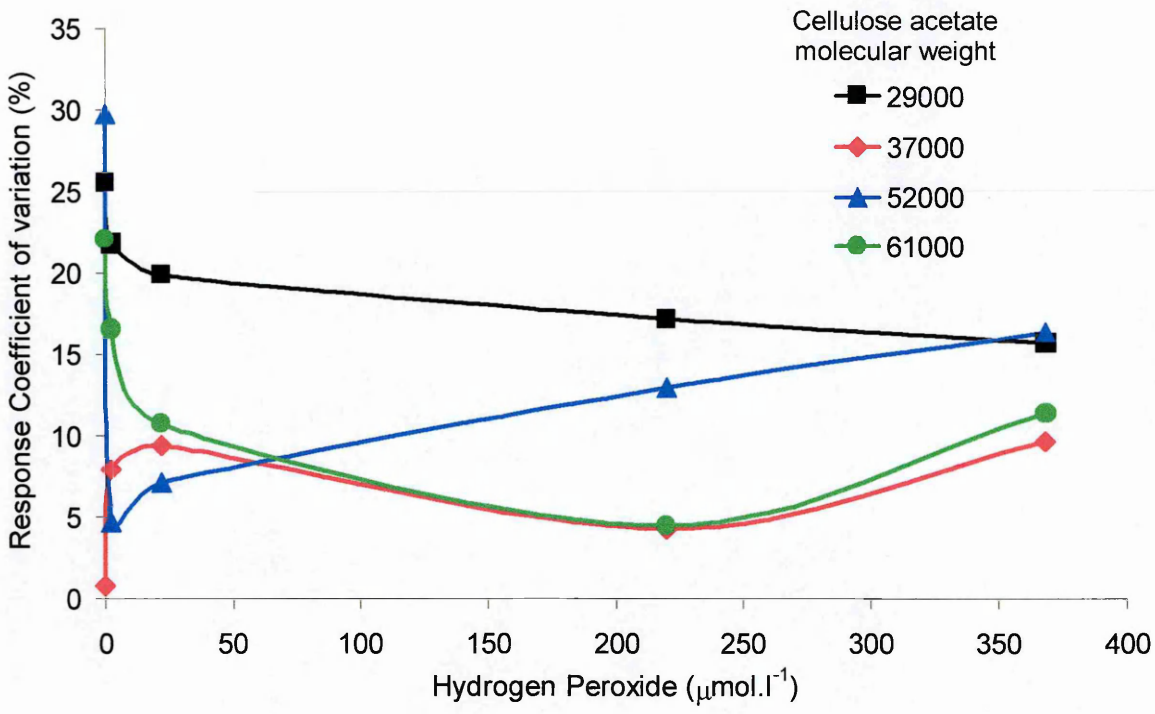

Figure 3.14 The coefficient of variation of the sensor response to hydrogen peroxide with a range of cellulose acetate membrane molecular weights

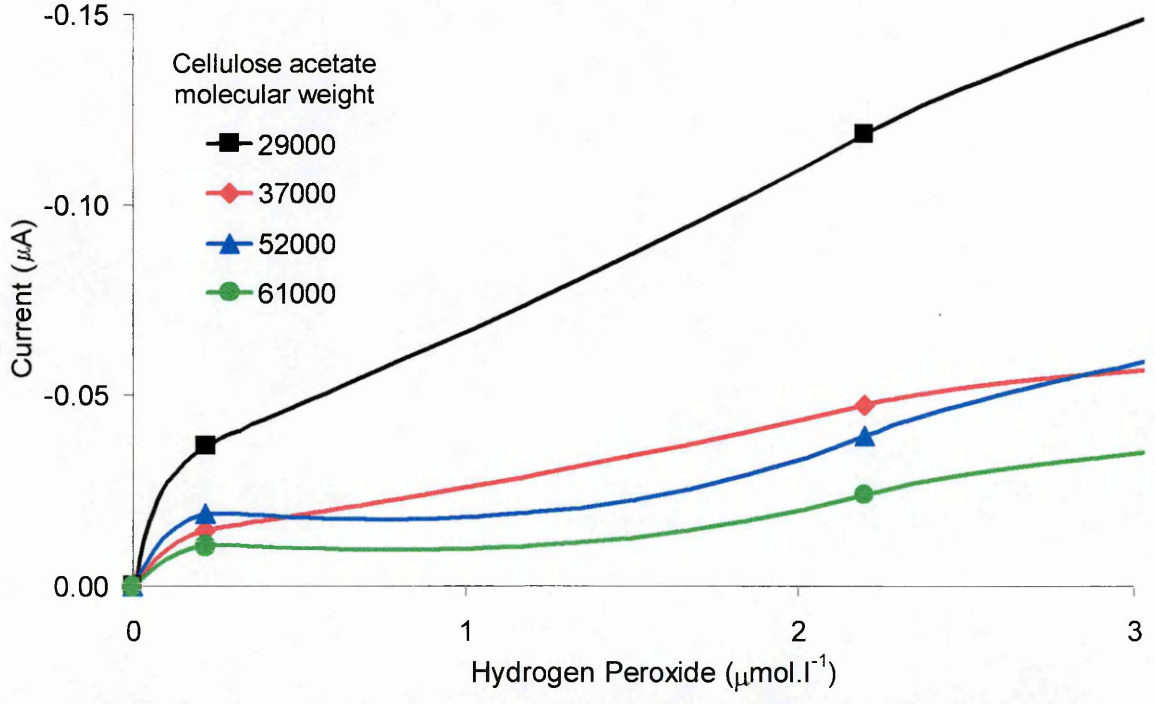

Figure 3.15 The effect of Cellulose acetate membrane molecular weight on the sensor response to low levels of hydrogen peroxide (lower range of figure 3.13 enlarged)

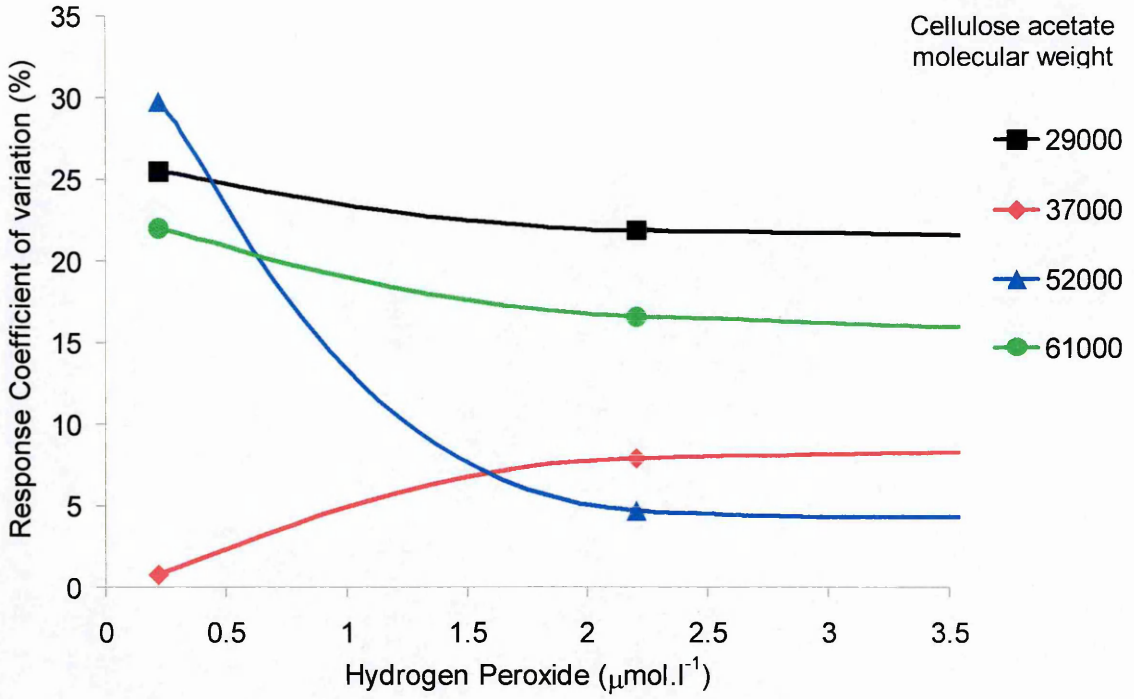

Figure 3.16 The coefficient of variation of the sensor response to low levels of hydrogen peroxide with a range cellulose acetate membrane molecular weights (lower range of figure 3.14 enlarged)

Looking at the figures, it can be seen that the responses were higher using the 29,000 and 52,000 average molecular weight variants. However, the 37,000 variant showed a significantly lower coefficient of variation in the desired analytical range.

Table 3.4 gives the coefficient of variation values (%) at each standard level and trend-line data for the desired analytical range 0 to 220 $\mu mol.l^{-1}$ to ascertain the average molecular weight variant offering the most suitable overall dynamic range and limit of detection.

Visual examination of the calibration plots had indicated that the largest responses were obtained using the 29,000 average molecular weight variant with the 37,000 variant giving the lowest responses and this was confirmed by the trend-line data. However, if the coefficient of variation is considered, over most of the levels of hydrogen peroxide for which the sensor is being developed, the 37,000 variant gave a considerable better reproducibility. This is especially significant at the lower levels of hydrogen peroxide and therefore, it was decided to select the 37,000 molecular weight variant on the basis

of better reproducibility. Although the overall responses were the lowest, as there are no problems with the sensitivity of the sensor, it was considered to be acceptable.

Table 3.4. Sensor response data at varying cellulose acetate molecular weights

Cellulose acetate average molecular weight	Hydrogen peroxide ($\mu mol.l^{-1}$)					Equation for linear region in figure 3.13
	0.22	2.2	22	220	368	
	Coefficient of variation (%)					
29 000	25	22	20	17	16	$y = -5.57 \times 10^{-08}x$
37 000	1	8	9	4	10	$y = -2.62 \times 10^{-08}x$
52 000	30	5	7	13	16	$y = -3.79 \times 10^{-08}x$
61 000	22	17	11	5	11	$y = -2.73 \times 10^{-08}x$

3.5 Summary

In this chapter, the performance of the sensor has been optimised by selection of the component loadings and their application method.

Optimum sensor performance based mainly on the best reproducibility (lowest coefficient of variation) was obtained using 25 units of horseradish peroxidase and 0.03 μmol 1,1'-dimethylferrocene per electrode, entrapped within an 80 μg cellulose acetate membrane (mean molecular weight of 37 000) all three components being co-deposited in a single step.

4. Production and Testing

4.1 Introduction

This chapter describes the testing of the sensors developed in the previous two chapters. The sensors will be demonstrated to work in a continuous monitoring situation in the laboratory and then the difficulties of mass production are considered and a possible solution suggested. This final sensor is then evaluated against other methodologies and finally tested in an on-line experiment at the König brewery.

4.2 Set-up of Testing System

From this stage onwards, the aim was to reproduce the industrial operating conditions as closely as possible in a laboratory environment. Thus, dilution in a flowing buffer stream was required and therefore a sampler, pump and flow cell arrangement was devised.

4.2.1 Sampler and Pump Manifold

Skalar (Breda, NL) who were one of the industrial partners in the EUROPEROX project loaned their model SA2002 sampler and SA1000 pump to the department for this stage of the development. The SA1000 peristaltic pump had a fixed rate, but by the use of different internal diameter colour-coded tygon tubes the flow rate of sample and buffer could be controlled at a fixed and approximately known rate. The pump manifold was constructed to obtain a final dilution of the sample in buffer of about 1 in 1000 and is shown schematically in figure 4.1. The quoted flow rates are the nominal figures quoted by the manufacturers and will depend also on the pump motor speed. Using this data gives a dilution factor of 1 in 1109 and was considered satisfactory.

The purpose of the tubes pumping air is to introduce a regular air segment into the fluid flow. These air segments reduce carry-over and facilitate mixing as the stream passes through the mixing coils. In a continuous monitoring situation, the segments would still be needed when calibrating and will reduce the delay in the sensor responding to a

change in sample concentration. The de-bubbler removes the air just before the diluted sample stream enters the flow cell so that the air segments do not upset the sensor response. The rate of flow through the cell was set at 0.42 ml.min^{-1} as a compromise between available pump tubes, rapid change of cell contents and backpressure due to the small cell volume.

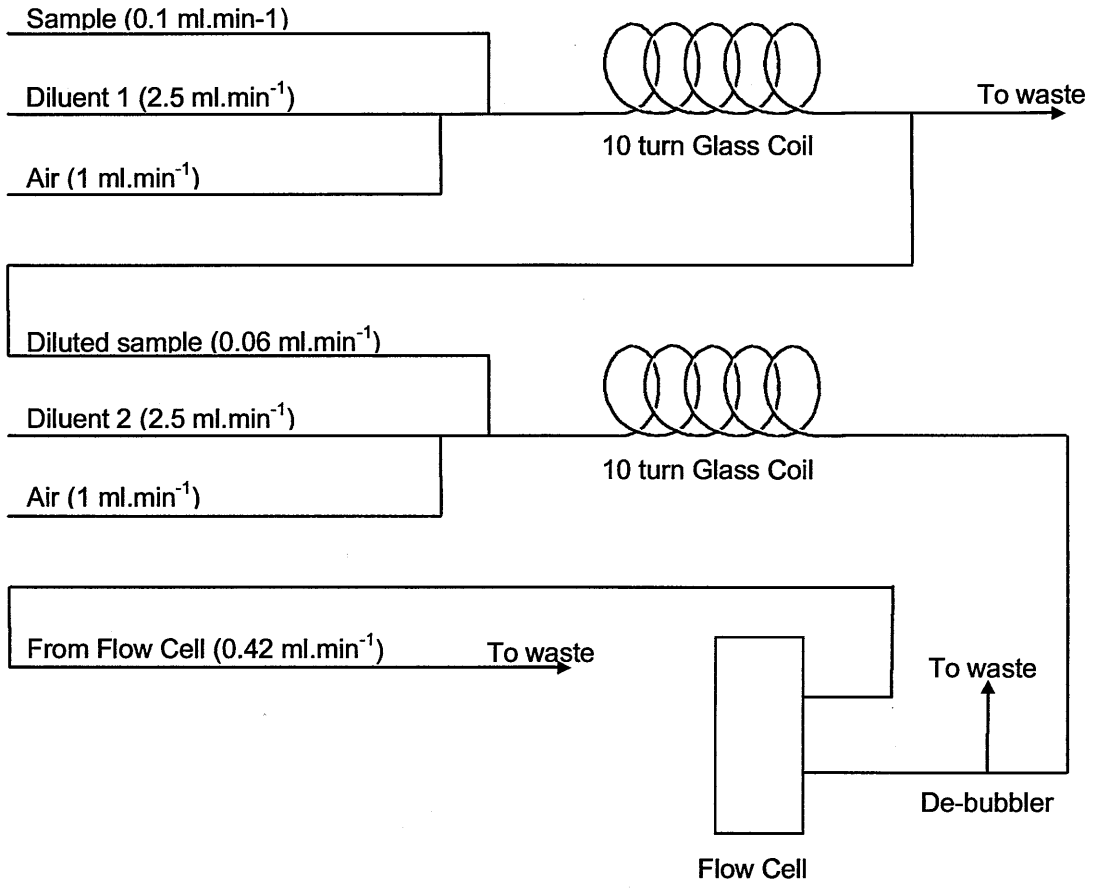

Figure 4.1 Pump manifold layout for laboratory evaluation

A two-step dilution process was required to dilute the sample sufficiently such that the diluted sample concentration of hydrogen peroxide fell within the analytical range of the sensor. This was based on the assumption that the sample was a brewery wash solution and thus in the range of 30 to 220 mmol.l^{-1}. It was not possible to achieve this magnitude of dilution in a single-step, as there is not the range of pump tubes available. Also, with this arrangement, buffer is used at 5 ml.min^{-1} and even with the sample pumped at the lowest possible rate (based on tube availability) of 0.015 ml.min^{-1}, buffer

would be used at the rate of 15 $ml.min^{-1}$ to achieve the dilution in a single step. Thus there are benefits in keeping the operating costs as low as possible.

The SA2002 sampler could be programmed via independent thumbwheels to sample or wash for periods of 1 to 999 seconds at 1 second intervals.

4.2.2 Flow-cell

The final sensor device was intended to function in a flowing stream during a complete disinfection cycle. For this reason, a perspex flow-cell to accommodate the sensor was designed in-house and custom made by Model Products Ltd. (Wooton, Bedfordshire. UK). A line diagram and the dimensions are given in figure 4.2. The cell comes in two halves; the 'O' ring seal sits in a groove and is slightly raised above the surface. Thus, with the sensor is in place, the 'O' ring creates a seal when the 4 clamping bolts are tightened. The approximate channel dimensions of the cell are 24 x 10 x 0.5 mm resulting in a cell volume of approximately 0.12 ml. This meant that the cell contents were replaced approximately every 17 seconds at the flow rate of 0.42 $ml.min^{-1}$ given above. A photograph of the flow cell with a sensor in place is shown in figure 4.3.

The sample is pulled through the cell in order that any bubbles that may get past the de-bubbler will not lodge in the flow cell. Also, should there be a blockage in the flow cell, there will not be a build up of pressure possibly resulting in a leakage; whatever is not pulled through the cell will simply run to waste via the de-bubbler outlet.

With this flow cell, it was possible to simulate the eventual operating environment very closely. The dilution with buffer was sufficient that in the brewery environment, the temperature and pH of the wash solution would be adjusted to that of the buffer.

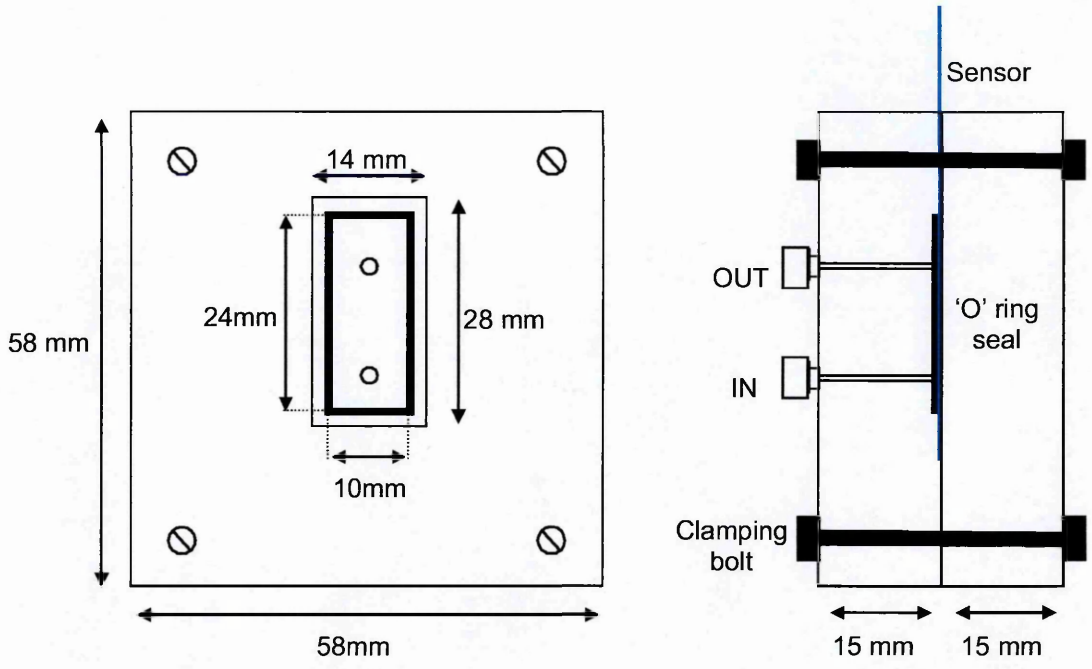

Figure 4.2 Line diagram of the flow cell for a continuous monitoring system

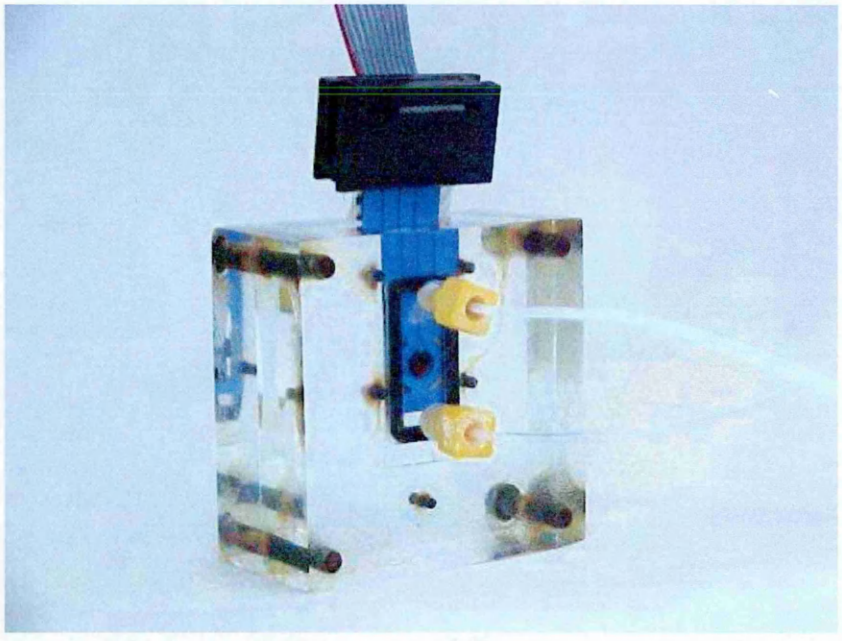

Figure 4.3 Photograph of the flow cell with sensor in place

4.2.3 Testing Rig

The sampler, pump and flow cell were all connected as shown by the photograph in figure 4.4, the flow cell was placed in a water bath to ensure that the sensor was maintained at the same temperature throughout. If the system were to be adopted into commercial use, the flow cell could be contained in a thermal jacket if the operating environment was not controlled at a suitable temperature. The fact that the pump tube flow rates and flow through the cell were approximate was not a problem as they were constant and the standard solutions were to be sampled in exactly the same manner as the test solution.

However, it was necessary to establish the timing parameters for the sampler. Although when immersed in a beaker, stable responses were established within a minute or less, it could not be assumed that it would be the same for the flow cell. Although the contents of the flow cell would be replaced almost four times every minute, there would be a delay in reaching full response and then falling back to the baseline between samples.

Figure 4.4 Sampler, pump and flow cell all connected as the testing rig

To test the length of the delay, buffer was sampled until the sensor had settled to give a stable baseline response. Then, the hydrogen peroxide standard with the highest concentration was sampled until a stable current response was obtained and finally buffer was sampled again until the response had returned to the baseline level. The outcome is shown in figure 4.5.

Due to the length of tubing used for the two-stage dilution and mixing, there was a delay of five minutes before the first response to the standard solution was seen. This was assumed inconsequential to the sampler timing but would have a considerable effect on real-time monitoring in the industrial setting. If adopted by industry, this delay would have to be investigated fully at the installation stage and allowances made for it in any control mechanisms.

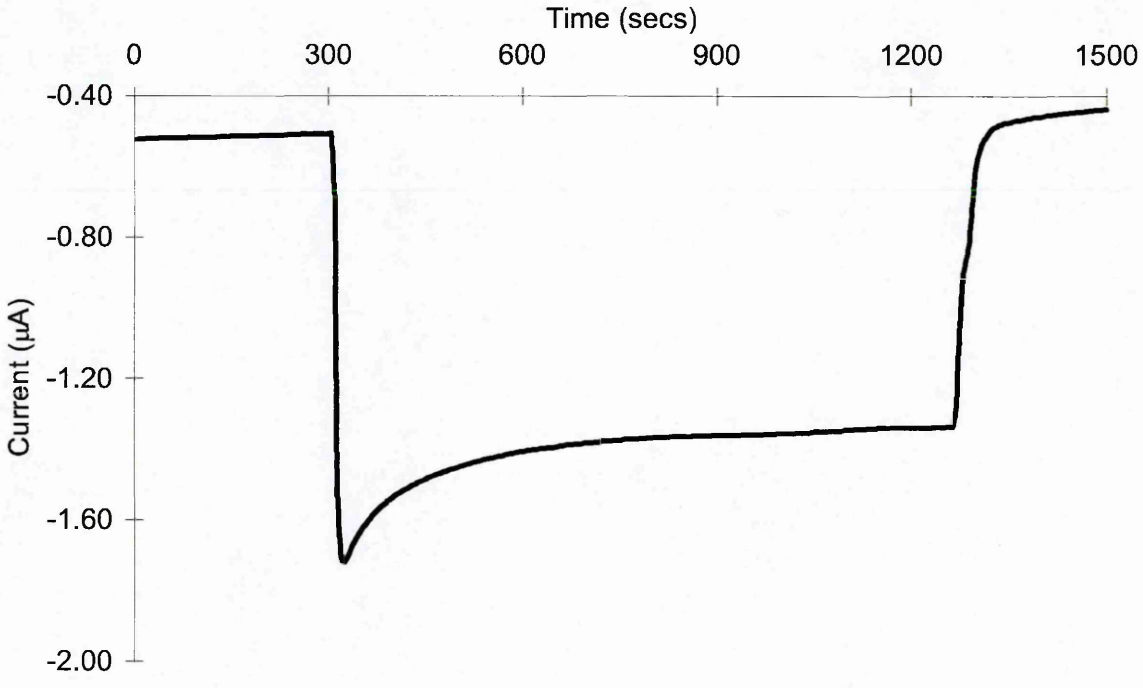

Figure 4.5 Timing curve for sensor response after sampling

When a sensor was used fresh from the freezer, it would take at least 10 minutes to attain a stable baseline. Then, on sampling the standard, the response would peak within 20 seconds of the first change in response and then take 5 minutes to stabilise. Over the first 2 hours of use, this response became quicker until a stable response was seen after 3 minutes. On re-sampling the buffer, a stable baseline was re-established after only 2 minutes (see figure 4.5).

If the sensor was allowed to warm up for an hour in a small beaker of buffer, it still took about 10 minutes for the stable baseline to be established. However, a stable response to the standard was obtained after 3 minutes from the outset. On re-sampling the buffer, a stable baseline was again re-established after only 2 minutes. The outcome of this was that the sampler timer was set to sample for 5 minutes and wash for 5 minutes to ensure a reproducible response even at high concentrations of hydrogen peroxide.

This conditioning of the sensor response can probably be attributed to the water layer around the enzyme as discussed in the section regarding enzymes in organic solvents in the previous chapter, section 3.2.1.

4.3 Testing Manually Produced Sensors

4.3.1 Calibration

The manifold layout in figure 4.1 resulted in an automatic 1000-fold dilution for all samples. Thus the highest concentration standard of hydrogen peroxide sampled was set at 880 $mmol.l^{-1}$. This meant that the level at the sensor would be about 0.88 $mmol.l^{-1}$ guaranteeing that the hydrogen peroxide level at the sensor would not go above 2.5 $mmol.l^{-1}$ and risk inactivating the horseradish peroxidase.

The sampler was set to sample standards for 5 minutes followed by a buffer wash for 5 minutes. A typical response is shown in figure 4.6 with each peak annotated with the hydrogen peroxide standard concentration.

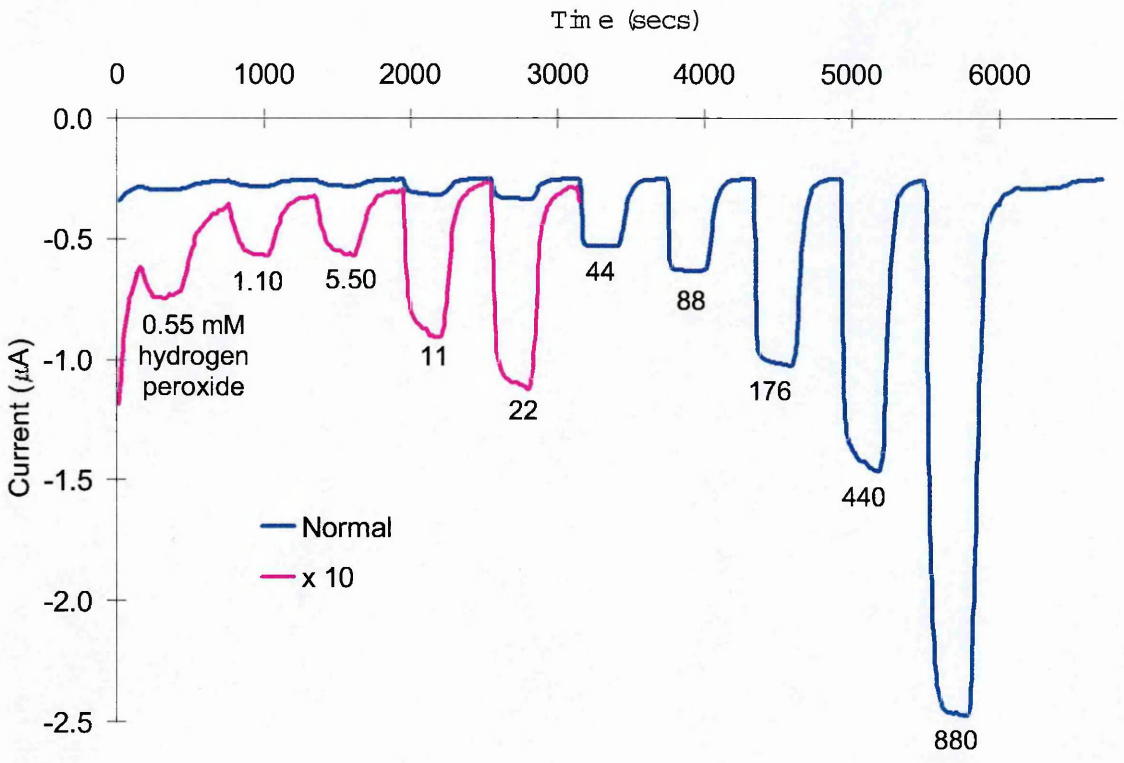

Figure 4.6 Sensor responses to a series of hydrogen peroxide standards.

Because of the large analytical range of the sensor, it was not possible to show all the peaks on the same scale, thus the peaks for the lower five standard solutions have been numerically multiplied by a factor of 10 and the baseline adjusted to bring them on-scale.

The calibration curve generated from the mean responses of six different sensors after the baseline responses had been deducted is shown for the whole range in figure 4.7 and for the range up to 100 mmol.l^{-1} in figure 4.8. The error bars represent one standard deviation either side of the mean response.

The numerical data is given in table 4.1 including the coefficient of variation at each concentration of hydrogen peroxide in order to compare the relative precision over the analytical range.

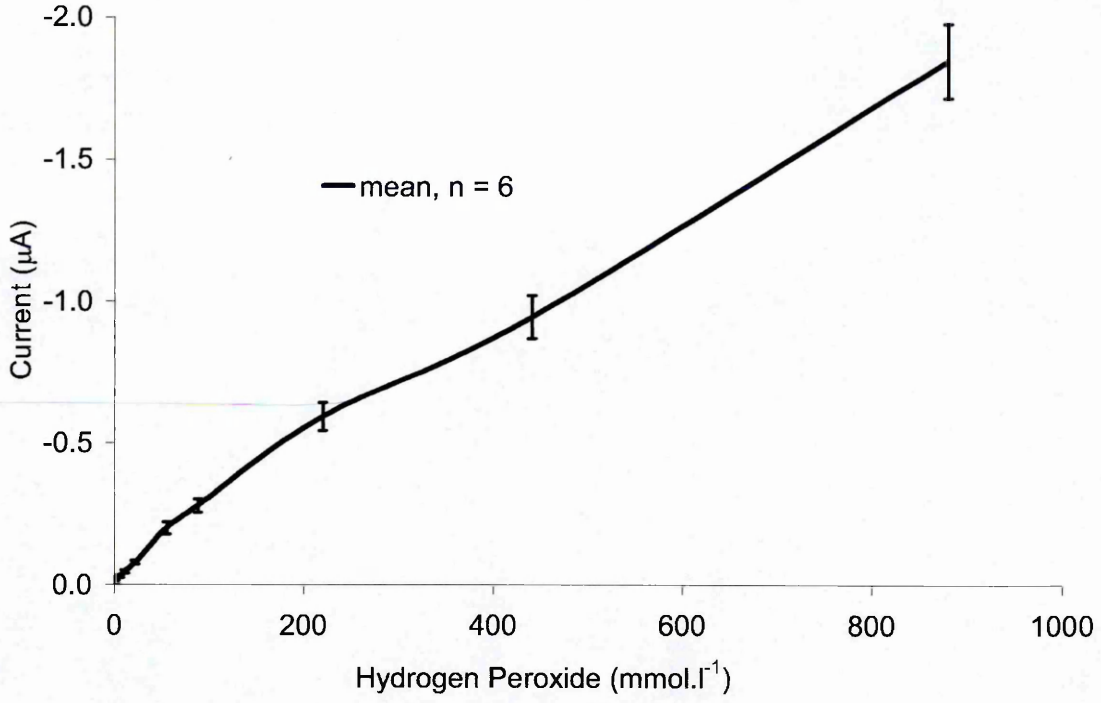

Figure 4.7 Calibration curve for hydrogen peroxide response with the sensor in the flow cell

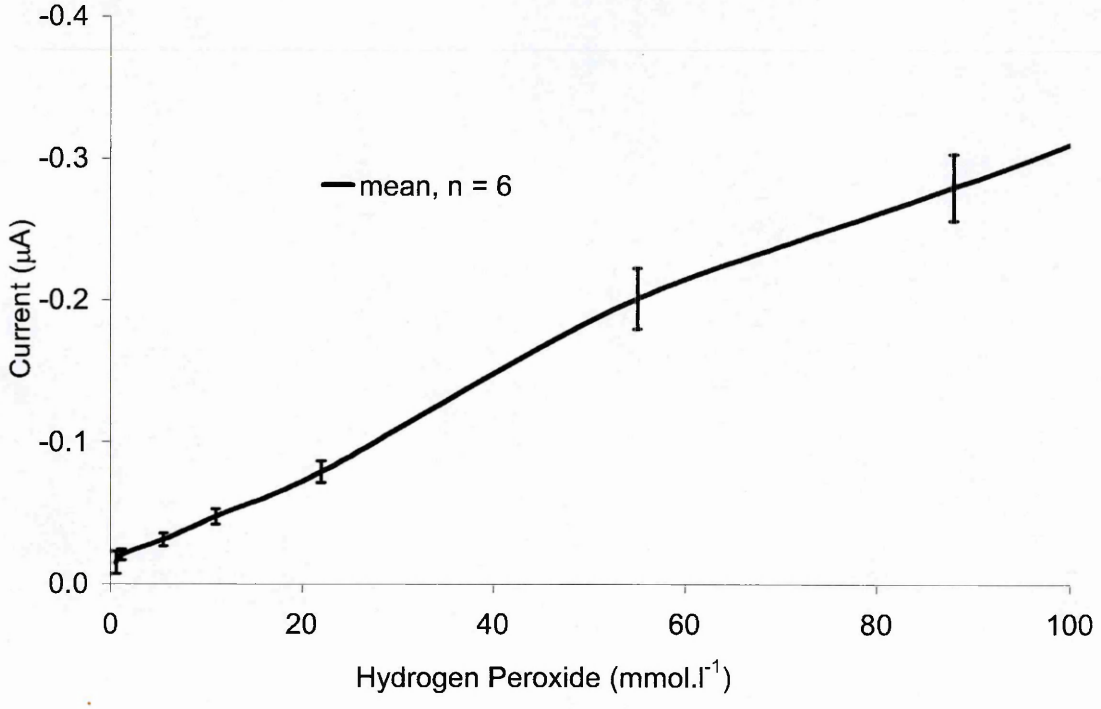

Figure 4.8 Calibration curve for hydrogen peroxide response up to 100 mmol.l^{-1} with the sensor in the flow cell.

Table 4.1. Data for the responses of six sensors in the flow cell

Hydrogen peroxide (mmol.l^{-1})	Response (Amps)		
	Mean	Standard deviation	Coefficient of Variation
0.55	-1.49 x 10-8	-7.94 x 10-9	53.3
1.1	-2.02 x 10-8	-3.77 x 10-9	18.6
5.5	-3.09 x 10-8	-4.69 x 10-9	15.2
11	-4.73 x 10-8	-5.25 x 10-9	11.1
22	-7.87 x 10-8	-7.61 x 10-9	9.67
55	-2.01 x 10-7	-2.15 x 10-8	10.7
88	-2.80 x 10-7	-2.35 x 10-8	8.41
220	-5.94 x 10-7	-4.98 x 10-8	8.39
440	-9.44 x 10-7	-7.59 x 10-8	8.04
880	-1.85 x 10-6	-1.31 x 10-7	7.08

From this data it can be seen that the better sensor-to-sensor precision figures were obtained at concentrations above 11 mmol.l^{-1}. With the brewery using a low cut-off level of 30 mmol.l^{-1} for the disinfection process, this is well within the desired analytical range. However, it does indicate that each sensor would have to be calibrated individually rather than for each batch as would be more desirable from a marketing standpoint.

In the flow cell, the sensor responses at the higher concentrations of hydrogen peroxide (allowing for the approximately 1000 fold dilution made by the pump) were about 10% of that seen in the previous chapter when the sensors were in a beaker of stirred buffer (figure 4.9). Also in the flow cell, the linear range of the sensor response was extended up to a much higher sampled concentration of hydrogen peroxide and at lower levels became proportionally closer to the response that was obtained in the beaker of stirred buffer (figure 4.10).

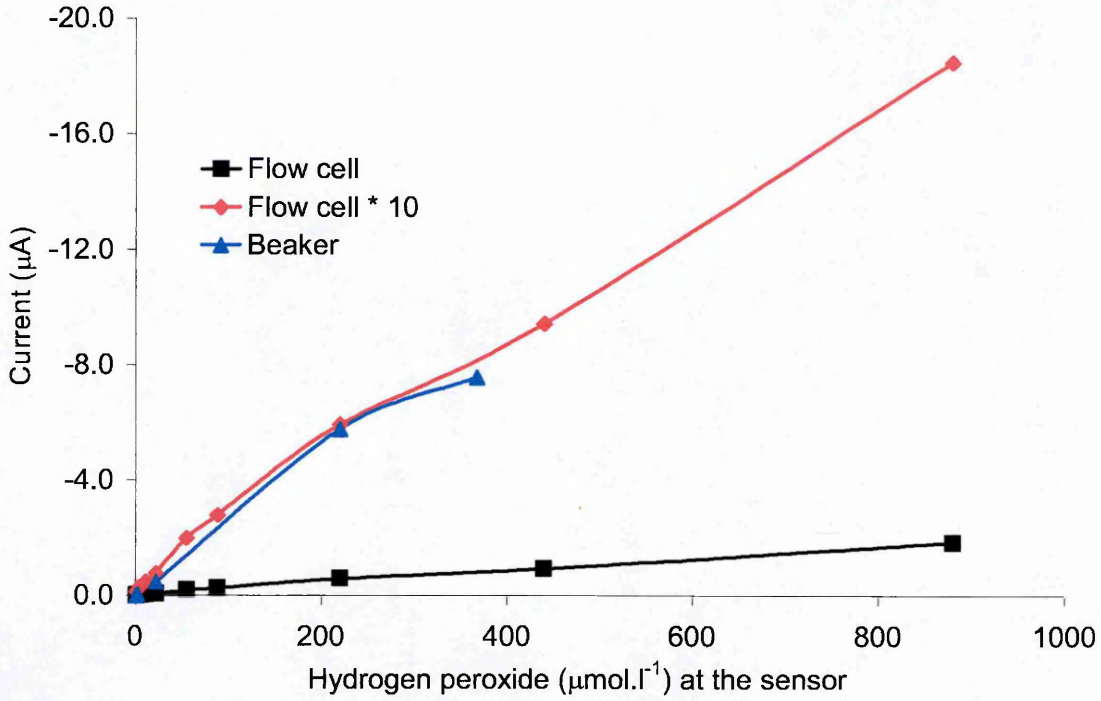

Figure 4.9 Comparison of sensor responses in a beaker and in a flow cell to hydrogen peroxide

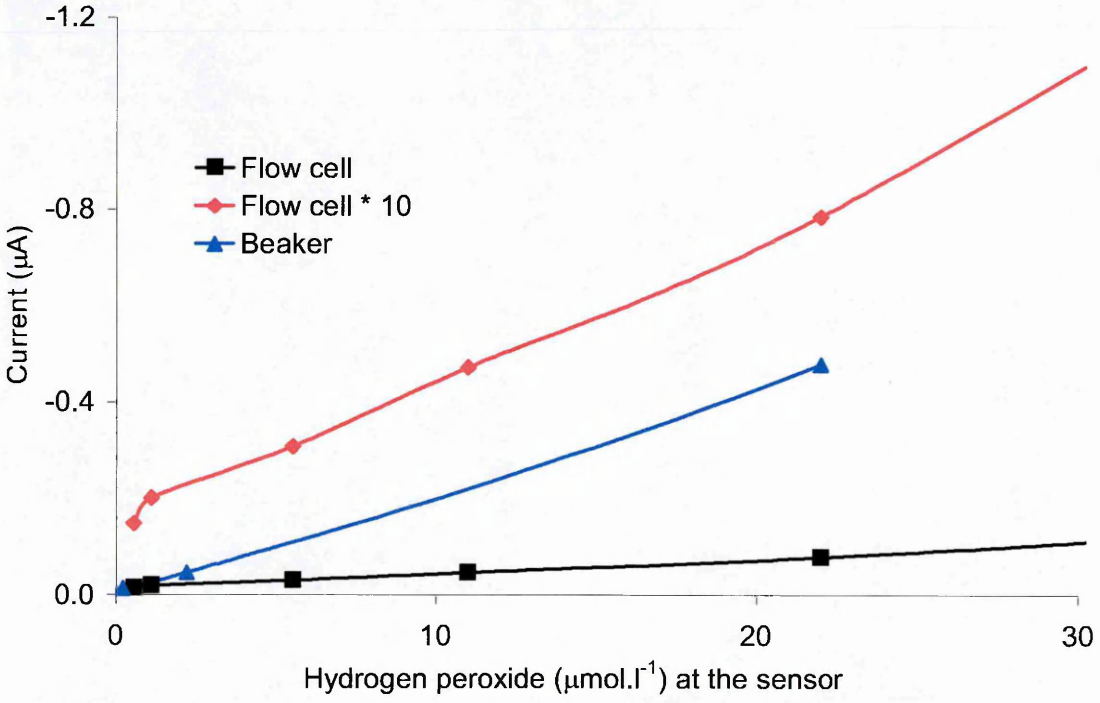

Figure 4.10 Comparison of sensor responses in a beaker and in a flow cell at low concentrations of hydrogen peroxide

This can probably be accounted for by the continual renewal of the diffusion layer on the sensor never allowing equilibrium to be reached in the flow cell, thus a lower proportion of the hydrogen peroxide is getting to the entrapped horseradish peroxidase. In the beaker, although it is being stirred, the diffusion layer on the sensor will not be as vigorously agitated and therefore it will be closer to equilibrium.

4.3.2 Stability Testing

In order to test the stability of the sensors, they were placed in the flow cell and immersed in a 25°C water bath to maintain a constant temperature throughout the testing period. Each sensor was allowed to equilibrate to the temperature and buffer flow until a stable baseline response was observed. The sampler was loaded with a shorter calibration series, as at higher concentrations, the hydrogen peroxide calibration solutions would show a significant fall in concentration whilst on the sample tray and this could not be controlled, especially overnight. The calibrators were replenished as needed and a fresh series made daily from the stock hydrogen peroxide solution.

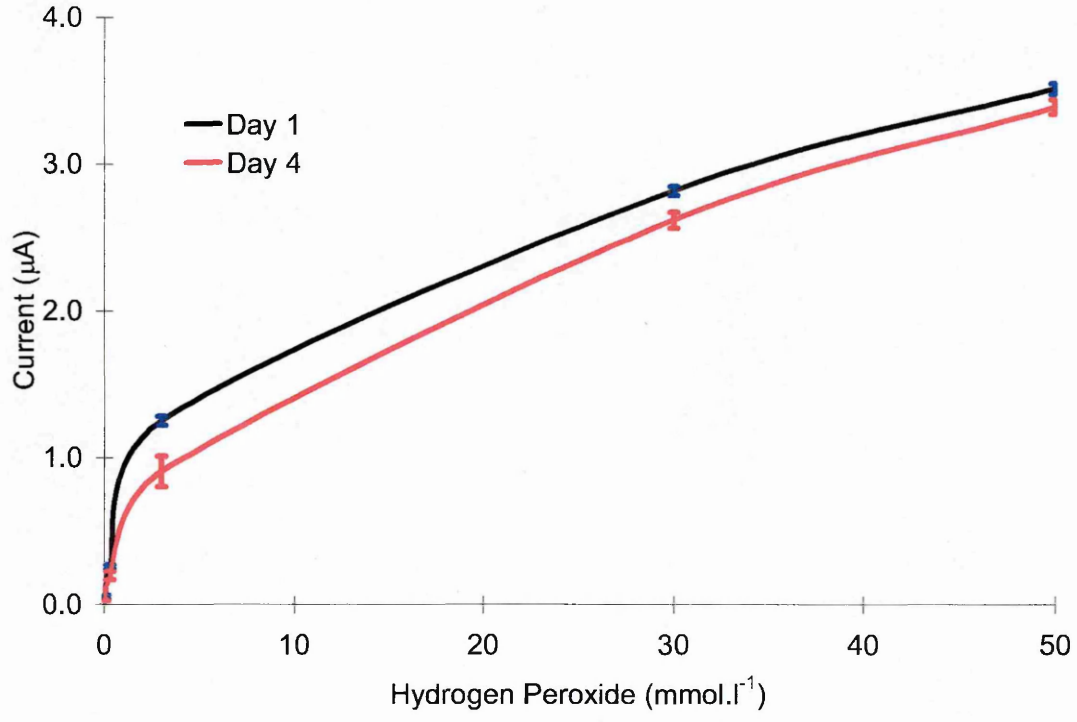

Figure 4.11 Comparison of sensor response when fresh and after four days continuous use.

There was considerable variation between the sensors, all lasted at least four days and one lasted four weeks in continuous use. Figure 4.11 shows the typical response of a sensor when fresh and after four days continuous use. The data from six consecutive calibration cycles on each day (using the fresh calibrator series) was used to assess the changing precision, as shown by the error bars in the figure. The coefficient of variation at each calibrator concentration was also calculated and this is given in table 4.2.

A very small decline in signal magnitude (<7.1%) was observed at the higher hydrogen peroxide concentrations (30 and 50 $mmol.l^{-1}$), but became more noticeable at lower hydrogen peroxide concentrations up to a 45.6% loss of signal at 0.03 $mmol.l^{-1}$. Since the disinfection process is completed in a matter of hours, the observed stability characteristics of the sensor were considered to be acceptable.

Table 4.2. Stability data for a fresh sensor and after four days continuous use.

	Day 1			Day 4		
Hydrogen peroxide ($mmol.l^{-1}$)	Current (Amps)		Coefficient of Variation	Current (Amps)		Coefficient of Variation
	Mean	Standard deviation		Mean	Standard deviation	
0.03	5.15×10^{-8}	1.15×10^{-8}	22.4	2.8×10^{-8}	2.13×10^{-9}	7.6
0.3	2.55×10^{-7}	1.39×10^{-8}	5.5	1.96×10^{-7}	2.92×10^{-8}	14.9
3	1.25×10^{-6}	3.02×10^{-8}	2.4	9.06×10^{-7}	1.07×10^{-7}	11.8
30	2.82×10^{-6}	3.02×10^{-8}	1.1	2.62×10^{-6}	5.48×10^{-8}	2.1
50	3.52×10^{-6}	3.82×10^{-8}	1.1	3.40×10^{-6}	4.81×10^{-8}	1.4

4.3.3 Discussion

The data gathered in this section shows that the linear analytical range of the sensor when used in the flow cell is from approximately 1 $\mu mol.l^{-1}$ up to at least 880 $\mu mol.l^{-1}$ subject to the inaccuracy of the pump dilution. This compares to a range of 1 $\mu mol.l^{-1}$ up to about 200 $\mu mol.l^{-1}$ when in a beaker of stirred buffer. Thus, there is an obvious advantage to be had using the flow cell arrangement. At concentrations above

220 $\mu mol.l^{-1}$ in the beaker of stirred buffer, the response was levelling off; this would probably not occur until the flow cell concentration reached 2000 $\mu mol.l^{-1}$ but has not been tested. As a consequence of this, there is less chance of the enzyme being inactivated by a random excessively high level of hydrogen peroxide.

The lower response and extended linear range seen in the flow cell arrangement could safely allow a smaller dilution and thus extend the limit of detection provided that the buffering capacity of the diluent could cope with the alkaline wash, or a larger dilution up to three fold if the upper sample concentration range needed to be increased.

The sensor to sensor precision figures with a coefficient of variation of 10% for hydrogen peroxide concentrations above 11 $mmol.l^{-1}$ is acceptable. It does however mean that each sensor will have to be individually calibrated. With improvements to the production process (the components for these sensors had been manually pipetted onto the working electrode surface) it may become possible to perform a full calibration for each batch of sensors with just a single or two-point check for each sensor thereafter.

The consecutive calibration cycles during the stability testing showed good precision with a coefficient of variation of less than 3% at 3 $mmol.l^{-1}$ and with it down to 1.1% at 30 $mmol.l^{-1}$, this would be acceptable for a production process.

The slight decline in sensor performance seen over four or more days may be due to a number of factors including leaching of enzyme and/or mediator, loss in enzyme activity and membrane and/or electrode fouling. It may also be due to deterioration of the tygon pump tubes; the very small tubes are prone to stretching resulting in a lower and irregular fluid flow, the larger tubes become flattened resulting in a lower fluid flow. This will cause the dilution factor to change in an unpredictable manner and thus the sensor response. In routine use, this would need to be assessed in order to define a calibration protocol.

4.4 Production processes

A prerequisite for commercial production is that the sensor must be fabricated at least on a medium batch scale, with appropriate quality assurance. In most cases, sensor systems are developed to solve specific research problems. Product engineering is not included as part of the development; the sensors can be produced only by research scientists and thus they are not suitable for large-scale production (Alvarez-Icaza and Bilitewski, 1993). Also, to be commercially viable the final selling price needs to be at a low enough level to compete with alternative methods. This can be aided by keeping the development costs and thus the development overhead component of the final selling price to a minimum.

The use of existing manufacturing processes will help to reduce the development time and thus costs. In addition, the transition from the development stage to production should be smoother. This has already been taken into account by using screen-printing to produce the base electrodes (section 2.3) and as such, by changing the printer specification and throughput, production can be readily altered to meet requirements.

The mediator, enzyme and membrane have been applied manually up to this stage and in this section, some options are considered for automating this process. Suitable automation would hopefully provide a rapid and reproducible deposition of the components onto the graphite electrode surface in a manner that would enable mass-production in the future.

There are several techniques available that can be used to print or coat the required components onto the surface of the electrode and the merits of some of these are considered below.

4.4.1 Langmuir Blodget Films

Langmuir Blodget films are widely used to produce monolayer surfaces. This technique cannot be realistically be used for mass production however, as it requires a complex series of actions involving the interaction of the transducer with the components to be immobilised on its surface (Weston, 1999).

4.4.2 Touch-off Printing

Touch-off printing uses a syringe pump to generate a positive pressure and a droplet at the tip of a needle. The needle is then brought into contact with the surface to be printed. The system is effective for printing relatively large volumes (greater than 10 μl) onto porous substrates and is liable to cause damage to the surface due to the direct contact required (Weston, 1999). As the print volume required is less than 10 μl and the graphite surface would be easily scratched, this technique was also considered unsuitable.

4.4.3 Spin-Coating

In spin-coating, the electrodes are individually mounted on a spigot and rotated at 2000 rpm. The component mixture is then pipetted onto the surface of the working electrode and left to rotate long enough to allow the acetone to evaporate. This then leaves a thin membrane deposited on the surface. This technique may possibly give a better reproducibility than manually pipetting, but is again not really suited to a mass-production process.

4.4.4 Dip-Coating

In dip-coating, the electrodes would be immersed in the component mixture and immediately removed. The electrodes would then be suspended vertically and left to dry long enough to allow the acetone to evaporate. This could be readily adapted to a production process, but there would be little control over the thickness of the coverage of the working electrode and as the whole sensor would be covered, there would be a large wasted excess of the components.

4.4.5 Ink-jet Printing

There are two methods of inkjet printing, continuous or drop on demand. Continuous inkjet printing can operate with either polar or non-polar solutions, and is simply a pressurised stream of reagent broken into droplets by a solenoid. Drop on demand requires the solution being printed to be polar, this is a requirement as it is passed between two high voltage plates that deflect the droplets as a function of the voltage, allowing a pattern to be deposited onto the surface. Whilst being a more complex technique than continuous inkjet printing, drop on demand has the big advantage that it can deliver very small volumes and print complex patterns. The electrical control of the printing means that any solution that is not used can be returned to the reagent reservoir, therefore the system can be economical when expensive reagents are being used (Weston, 1999).

4.4.6 Biodot Printing

The Biodot printer (Biodot Ltd, Huntingdon, Cambridgshire, UK) as in touch-off printing uses a syringe pump to generate a positive pressure to force the fluid through a small nozzle. In addition to this though, as the fluid passes through the print head, a drive rod actuated by an oscillating piezoelectric crystal (at 64 000 Hz, dependent on the modulation voltage) produces a shock wave that breaks the jet into a series of regular droplets.

The droplets are driven from the nozzle, and thus unlike touch-off printing, direct contact is not required. Equally, whilst it is similar to inkjet printing in the use of a solenoid to produce droplets, it is not currently possible to print as small a volume as with inkjet printing. The minimum syringe pump volume determines the minimum printable volume of the Biodot system. With the system available within the department, this was 8.3 nl, equivalent to 1 step of the syringe stepper motor.

4.4.7 Discussion

Of the six possible techniques considered above, the use of Langmuir Blodget films, and spin-coating were immediately rejected as being unsuitable for mass production. Touch-off printing was a possible technique to use, but it is liable to damage the surface

of the base graphite electrode, it was decided to look at the other possible techniques first. Dip coating was also suitable for this application but with the excess use of components and thus waste, this was considered the 'last option'. Both Ink-jet and Biodot printing were considered suitable techniques and as there was a Biodot printer available in the department, this was the obvious first line of testing.

4.5 The Application of Biodot Printing

4.5.1 The Biodot X-Y3000™ Dispensing Platform

The Biodot X-Y3000™ dispensing platform shown in figure 4.12 was the only model available in the laboratory and was thus used for an initial trial of this printing technique.

The programming and operation of the dispensing platform is done through the control pad. The syringe pump and valve are situated at the rear of the platform and a diagram is shown in figure 4.13. The dispenser containing the print head is mounted on a pneumatic cylinder with a micrometer adjustment for the height above the surface to be printed. Patterns can be generated on the surface by the movement of the platform in the X and Y-axes whilst printing.

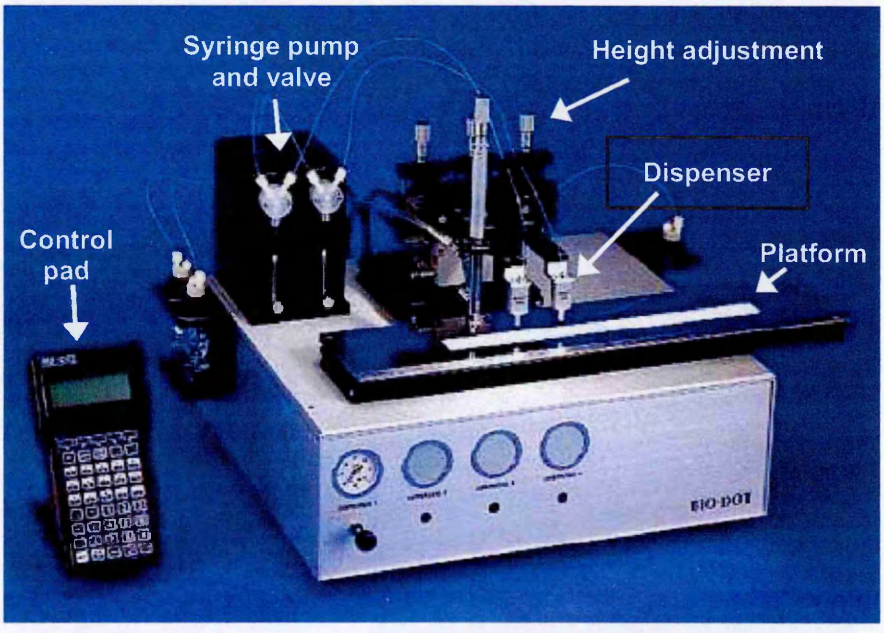

Figure 4.12 Biodot X-Y 3000™ dispensing platform

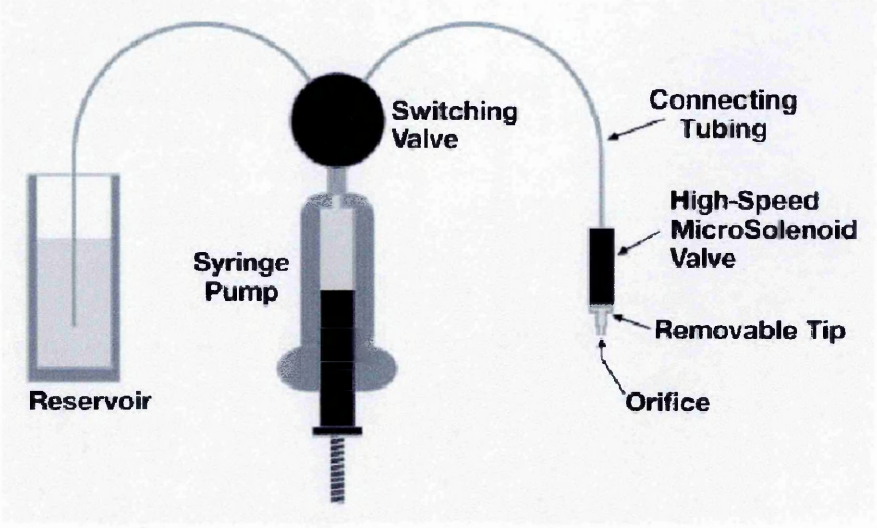

Figure 4.13 Syringe pump and valve

Due to the relatively large surface area of the base graphite electrode, it was thought that it would be better to print multiple dots in suitable patterns to cover the full area. Various patterns were investigated and four examples are shown in figure 4.14.

a) This sensor was produced by printing 4 dots of 1µl in a square pattern from 5 mm above the surface. It can be seen that the dots do not merge fully together and have not dispersed sufficiently to totally cover the graphite surface.

b) This sensor was produced by printing 4 dots of 1µl in a square pattern from 10 mm above the surface. It can be seen that the dots have merged together better but still leave a small hole in the middle and have still not dispersed sufficiently to totally cover the graphite surface.

Both of these sensors also show a 'coffee ring' effect at the edges indicating an uneven coverage. Combinations of up to nine dots of lower volumes arranged in different patterns were tried and similar results obtained. Thus a single dot application was tried.

c) This sensor was produced by printing 1 dot of 4 µl from 10 mm above the surface. There is no apparent 'coffee ring' but the dot has not dispersed to totally cover the graphite surface.

d) This sensor was produced by printing 1 dot of 4 µl from 15 mm above the surface. Again, there is no apparent 'coffee ring' and now the dot has dispersed to totally cover the graphite surface.

Unfortunately, on drying there was a mottled appearance to the surface that could not be overcome using this printer and it was therefore decided that a single dispense of 4 µl from 15 mm above the surface to allow sufficient dispersion of the jet gave the best coverage.

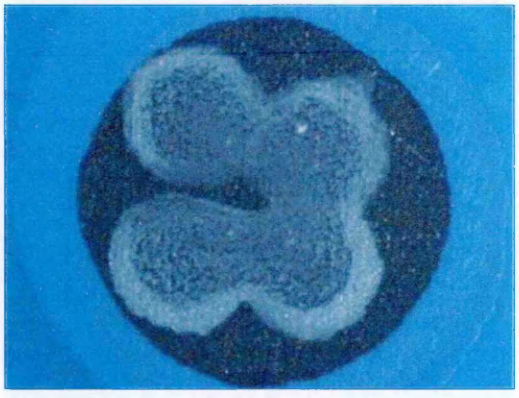

a) 4 dots of 1µl from 5 mm above the surface

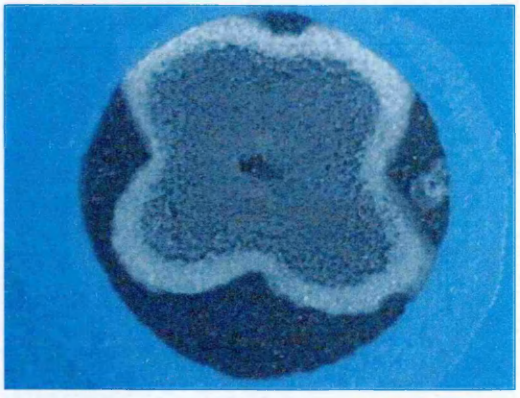

b) 4 dots of 1 µl from 10 mm above the surface

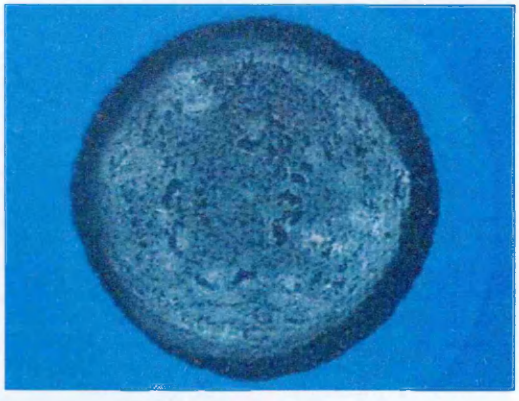

c) 1 dot of 4 µl from 10 mm above the surface

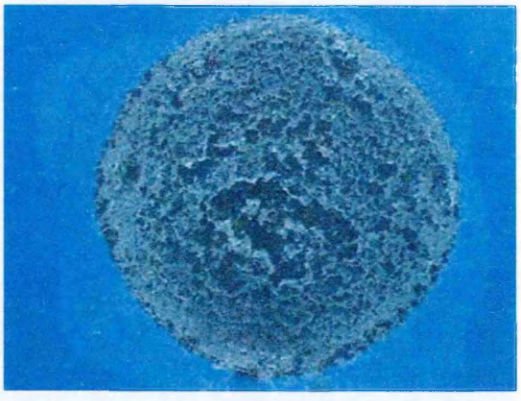

d) 1 dot of 4 µl from 15 mm above the surface

Figure 4.14 Various application patterns

Other problems in the use of this model printer were that the component mixture of 1,1'-dimethylferrocene, horseradish peroxidase and cellulose acetate in buffer and acetone had to be placed in a reservoir and primed through the syringe pump causing a significant waste of reagents. Also, the first few sensors would be produced satisfactorily but the enzyme suspension started to settle in the reservoir and tubing resulting in lower amounts being applied. This could be overcome by placing the reservoir in a small sonication bath to maintain good dispersion of the suspension, however it still settled in the tubing and as the acetone evaporated, the cellulose acetate started to coat the syringe pump and print head eventually blocking both.

4.5.2 The synQUAD™ Dispensing Platform

On contacting the local agents for Biodot inc., they arranged a visit to the office in Huntingdon to use another model of printer/dispenser, the synQUAD shown in figure 4.15. This was designed for coating the wells of microtitre plates using a new pump and valve arrangement shown in figure 4.16.

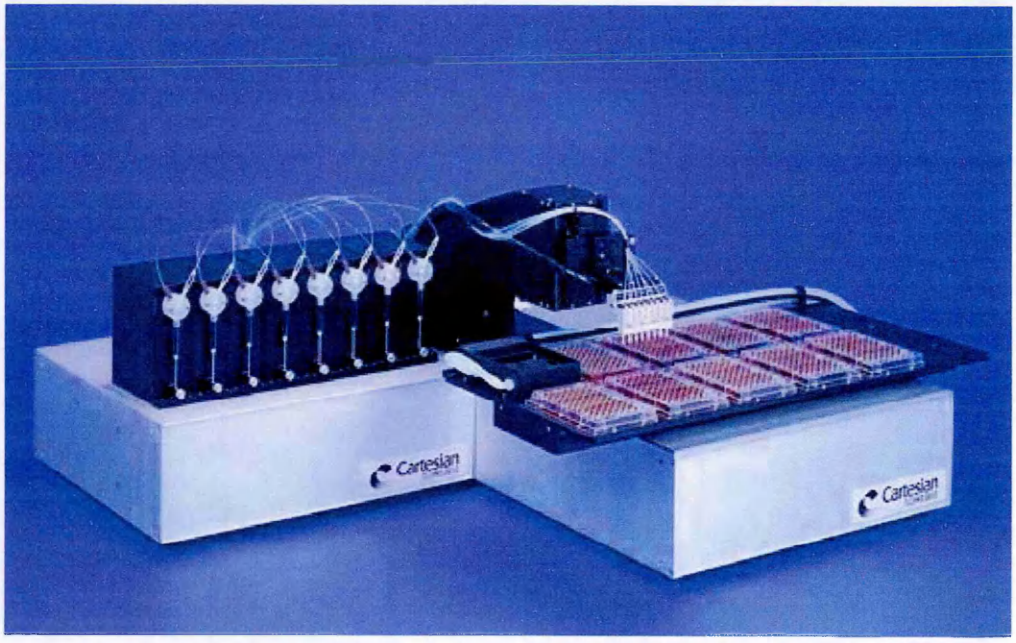

Figure 4.15 synQUAD™ dispensing platform.

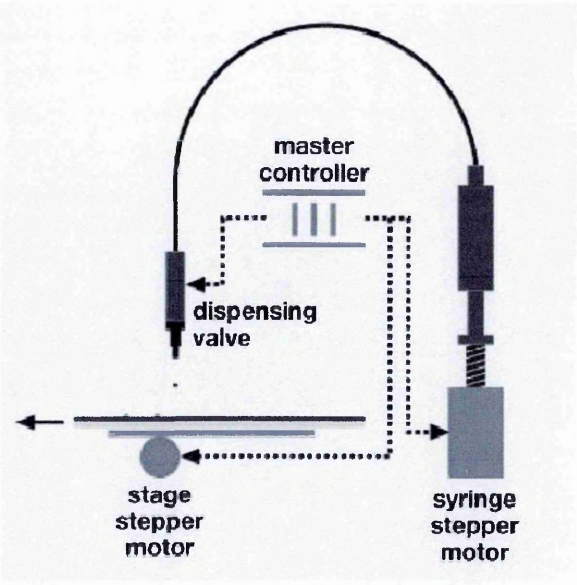

Figure 4.16 New syringe pump and valve arrangement.

This new pump and valve arrangement allows the quantitative aspiration and dispensing of volumes from 50 nl to 8 µl either in a continuous dispense or aspirate and dispense mode for pickup and transfer of multiple reagents.

For this trial, time was limited by the instrument availability and thus only a few sensors were produced. By using the aspirate and dispense mode and aspirating a small amount of acetone before the mixture and then dispensing it to waste after deposition of the mixture onto the sensor, allowed a flush after each cycle ensuring that there was no deposition of the component mixture in the tip. For this trial, it was only possible to produce one sensor in each cycle but the manufacturers claim that the instrument can be adapted to improve this throughput. Also, the reagent reservoir could be modified such that it is chilled to reduce evaporation of the acetone and a sonication device incorporated to prevent settlement of the suspension.

The optimal coverage using this instrument (based on visual observation as there was no microscope available) was obtained by dispensing four overlaid spots of 1 µl. Due to the small volume being dispensed, the acetone evaporated on contact with the graphite electrode giving a smooth even coat. An example is shown in figure 4.17

Figure 4.17 Photomicrograph of a sensor produced using the synQUAD™ dispensing platform

4.6 Testing the Biodot Printed Sensors and Field Study

An inter-method comparison of the determination of hydrogen peroxide and peroxyacetic acid in liquid samples was carried out at the König Brewery, in Germany within the framework of the EUROPEROX project from the 5th until the 7th June 2000. The sensors used in this field study had all been manufactured using the synQUAD™ dispensing platform to deposit the components on the working electrode. Unfortunately, time and conditions did not allow for manually produced sensors to be tested at the same time. The comparative performance of manually produced sensors should not be considered critical as these would not be viable as a commercial product even if their performance was superior, the important consideration is the question of sensors produced by a mass production technique meeting the precision requirements of an end user.

4.6.1 Inter-method Comparison Protocol

Although the sensor had been optimised for the determination of hydrogen peroxide, in the development stages it had been found to respond favourably to peroxyacetic acid at an applied potential of –0.2 V (section 2.7). Thus, as this inter-method comparison was for both hydrogen peroxide and peroxyacetic acid, it was considered a suitable opportunity to evaluate its performance to both analytes in comparison to other methods.

The other methods for hydrogen peroxide determination were:

1) Triphenyl phosphine is oxidised by hydrogen peroxide; the phosphine oxide produced was quantified using high performance liquid chromatography (Effkemann *et al*, 1998).

2) Hydrogen peroxide forms a coloured adduct with a dinuclear iron (III) complex; this coloured adduct was quantified using a micro-plate reader (Harms *et al*, 1999a & 1999b).

3) Hydrogen peroxide forms a coloured complex with Titanium (IV) chloride; this coloured complex was quantified using a micro-plate reader (Christensen *et al*, 2000).

4) 2,2′-Azino-bis(3-ethylbenzothiazoline)-6-sulphate is oxidised by hydrogen peroxide in the presence of a peroxidase and to give a green coloured radical cation (Meyer *et al*, (1999). The green coloured radical cation was quantified using a micro-plate reader and by flow injection analysis.

The other methods for peroxyacetic acid determination were:

1) 2-([3-{2-[4-amino-2-(methylsulphanyl)phenyl]-1-diazenyl}phenyl]sulphonyl)-1-ethanol dissolved in acetonitrile is oxidized by peroxyacetic acid to produce the corresponding sulphuloxide; 2-([3-{2-[4-amino-2-(methylsulphoxy)phenyl]-1-diazenyl}phenyl]sulphonyl)-1-ethanol; the sulphuloxide was quantified using high performance liquid chromatography (Effkemann *et al*, 1999).

2) 2,2′-Azino-bis(3-ethylbenzothiazoline)-6-sulphate is instantaneously oxidised by peroxyacetic acid to form an intensively coloured green radical cation which was quantified using a micro-plate reader (Pinkernell *et al*, 1997). In addition, this technique was used for continuous determinations using flow injection analysis.

3) Methyl *p*-tolyl sulphide dissolved in ethanol is oxidised by peroxyacetic acid; the oxidation product was quantified using high performance liquid chromatography (Pinkernell *et al*, 1996).

Aqueous standards were made from commercial stock solutions and three samples obtained from different stages of the brewery cleaning procedure were spiked with hydrogen peroxide and peroxyacetic acid at two different levels to give known concentrations. The purpose of analyzing aqueous hydrogen peroxide and peroxyacetic acid standard solutions was to distinguish between analytical errors and problems associated with potentially interfering components in the 'real' brewery samples.

Calibration standards were prepared individually by the appropriate dilution of the same stock solutions.

The 'real' samples obtained from the brewery cleaning processes (tanks and vessels) had to be spiked rather than sampled as the concentration of the peroxides declines very rapidly at the high temperatures used in the processes (unpublished results). The samples used were sampled from the vessels such that they contained no peroxides in advance and were allowed to cool to room temperature before spiking. The composition of the samples is given in table 4.3.

Table 4.3. The composition of the samples for the inter-laboratory comparison.

Samples A, B & C all contained 1-2 % sodium hydroxide (pH 14) and varying amounts of proteins, carbohydrates, minerals, polyphenols and organic acids				mmol.l^{-1}			
				Hydrogen peroxide		Peroxyacetic acid	
Sample	**Source**	**Matrix**	**Appearance**	**Low**	**High**	**Low**	**High**
Aqueous standard				7.8	141.3	2.6	13.2
Sample A	Wort vessel	Water and malt	Yellow/brown and turbid	138.7	141.1	-	-
Sample B	Separator tank	Beer, yeast and alcohol	Turbid and faintly yellow	28.2	141.1	-	-
Sample C	Yeast culture	0.1 % yeast	White and turbid	-	-	3.9	15.8

The concentration of hydrogen peroxide in the stock solution, standard solutions, and 'real' samples were also determined before and after each analysis by titration with

thiosulphate after the addition of potassium iodide. The thiosulphate was standardised by iodometric titration with dichromate and the error in the aqueous concentration of hydrogen peroxide was estimated to be ± 2.0%. The certificate of analysis for the peroxyacetic acid stock solution was used to calculate the concentration levels in standard solutions and 'real' samples. These concentrations were not revealed to the analysts until after the results had been collated to prevent the effect of operator bias.

No changes were observed in the peroxide concentrations of the standard solutions and 'real' samples over the time-span of the analysis. However, in order to eliminate this possible source of error, samples were processed by all methods at exactly the same time. Thus, any observed difference in the results could be attributed to the differences in analytical procedures. Six replicate measurements were performed for each sample solution.

Unfortunately it was not possible to use the flow cell for this study and thus the precision of the results obtained does not reflect what may be achieved with a more reproducible sampling procedure.

4.6.2 Inter-method Comparison Results

The results from this comparison are summarised in table 4.4.

The spiked value for hydrogen peroxide is that assigned by titration with thiosulphate after the addition of potassium iodide and for peroxyacetic acid it was calculated using the dilution factor and the value on the certificate of analysis for the stock solution.

The group mean and standard deviation were calculated for all methods after the removal of any results more than 50% from the spiked value.

From the data in table 4.4, it can be seen that the sensor performed comparably with the other methods for the determination of both hydrogen peroxide and peroxyacetic acid. It can also be concluded that the organic components in the samples did not significantly interfere with the hydrogen peroxide determination.

As it was not possible to use the flow cell with automatic dilution for this study, there was an increased error due to the manual pipetting of buffer and sample. The results in

section 4.3.1 showed that the flow cell environment gave better linearity and lower limit of detection. It can also be assumed that it gave a better precision.

Table 4.4. The results of the inter-method comparison.

	Hydrogen peroxide (mmol.l^{-1})						Peroxyacetic acid (mmol.l^{-1})			
	Aqueous standard		Sample A		Sample B		Aqueous standard		Sample C	
	Low	High	Low	High	Low	High	Low	High	Low	High
Spiked value	7.8	141.3	138.7	141.1	28.2	141.2	2.6	13.1	3.9	15.8
Group mean	8.0	145.8	139.6	146.1	28.6	134.2	2.4	12.5	3.8	15.1
Sensor mean	6.7	136.9	131.1	149.1	27.3	118.6	1.7	11.8	3.6	15.1
Sensor % error	-14.0	-3.1	-5.4	5.7	-3.4	-16.0	-35.0	-10.0	-10.0	-4.4
Group standard deviation	1.0	11.3	5.6	5.5	7.4	28.6	0.4	0.8	0.4	0.9
Sensor standard deviation	0.4	4.2	5.7	10.9	1.4	6.6	0.1	0.6	0.2	1.2
Coefficient of variation	6.7	3.1	4.3	7.3	5.2	5.6	8.1	5.3	6.6	7.9

The results in section 4.3.2 (table 4.2), showed that using the flow cell with an automatic dilution of 1 in 1109; a coefficient of variation of 1.1 % is achievable for aqueous standards containing between 30 mmol.l^{-1} and 50 mmol.l^{-1} hydrogen peroxide. After dilution, this represents a range of 27 μmol.l^{-1} to 45 μmol.l^{-1} at the sensor. With the manual dilution of 1 in 4000 used in this study, the 141.3 mmol.l^{-1} standard was diluted to 35 μmol.l^{-1} at the sensor and had a coefficient of variation of 3.1 %. If the assumption is made that the difference of 2 % is due to the error in pipetting, then the results can be considered acceptable. However, for a commercial system this would have to be validated properly.

4.6.3 Conclusions from the Inter-method Comparison

All the hydrogen peroxide determinations using the sensor were within ±16% of those determined by the standard permanganate titration method for both the synthetic and real samples at the higher and lower analyte concentrations. From this, it can be concluded that the sensor is suitable for use in the determination of hydrogen peroxide in the wash solutions used throughout the brewing process. If peroxyacetic acid were to be used as an alternative, then the sensor could also be used although it has not been established what proportions of the response are due to the peroxyacetic acid and the hydrogen peroxide present as part of the equilibrium mixture.

Furthermore, the good agreement between the sensor and standard methods for both analytes in the 'real' samples indicated no significant matrix or interference effects. In all cases the coefficient of variation of the measured samples (n=6) was 7.3% or less and this would be greatly improved with an automated sampling and dilution procedure.

4.6.4 On-line Study

Whilst at the König Brewery for the inter-method comparison, there was the opportunity to test the sensor mounted in the flow-cell within a real production environment for a scaled down cleaning process after a pilot brewing process.

There were restrictions to this study that affected the overall quality of the results.

1) The sample stream had to be diluted 1 in 51 with 10 mmol.l^{-1} ethanoic acid before it could be sampled for the sensor. This sample was further diluted using a pump tube of 0.06 ml.min^{-1} for the sample and 2.50 ml.min^{-1} for the buffer (dilution 1 in 42.67) to give an overall dilution of 1 in 2176.

2) The calibration standards had to be sampled from the most concentrated to the most dilute without a blank between each one thus reducing the differentiation between them.

3) There was little time to prepare the system and thus the sensor was not given sufficient time to equilibrate before processing either the calibration solutions or the sample line giving rise to a considerable baseline drift.

The fermentation vessel to be cleaned had a total capacity of 1000 litres and it contained approximately 10 litres of spent fermentation broth. For the wash, 180 litres of 0.5 $mmol.l^{-1}$ sodium hydroxide was added and this was heated to between 60° and 80° Celsius. The wash solution was stirred and pumped around the vessel and recycled such that the entire inner surface was being washed. A small sample-valve was available from the recycling pump for testing the cycling wash solution.

The standards containing 221, 147, 74, 29 and 15 $mmol.l^{-1}$ were sampled off-line whilst the wash solution was being heated, but were diluted through the same process as the sample-line. The monitored current response is shown in figure 4.18 and the calibration curve generated from this data is shown in figure 4.19.

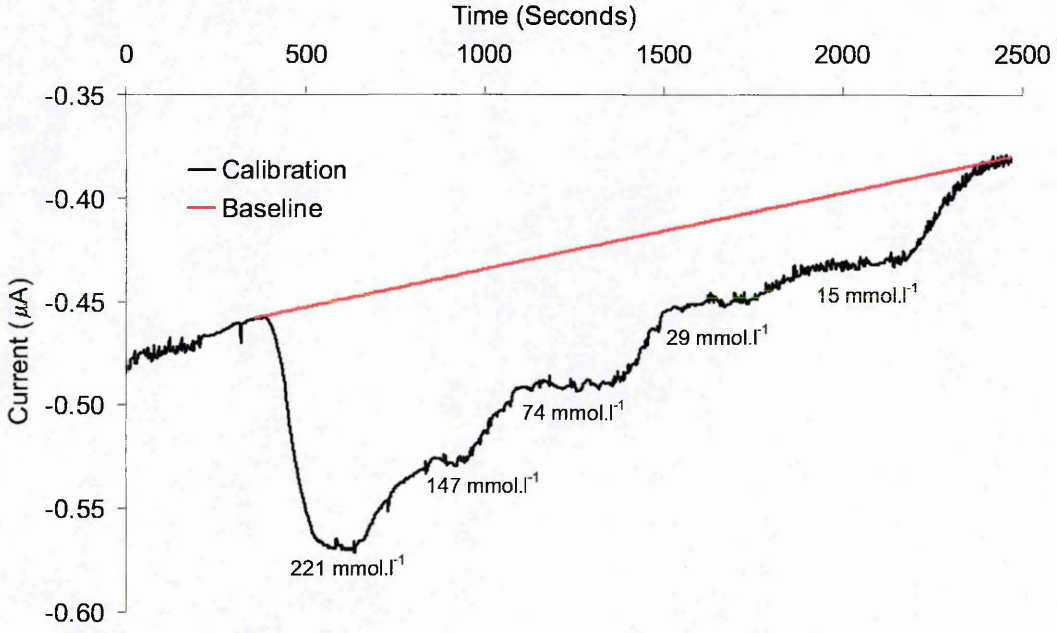

Figure 4.18 Current response to hydrogen peroxide calibration solutions

Once the wash solution had been heated to the desired temperature, the valve was opened and a small flow regulated by the valve was passed through a refrigeration unit before being diluted by the ethanoic acid and then sub-sampled and diluted by the phosphate buffer.

Once a baseline had been established (after 245 seconds), 1 litre of 8.8 mol.l^{-1} hydrogen peroxide was added to the wash solution followed by another 500 ml five minutes later. The monitored current response is shown in figure 4.20.

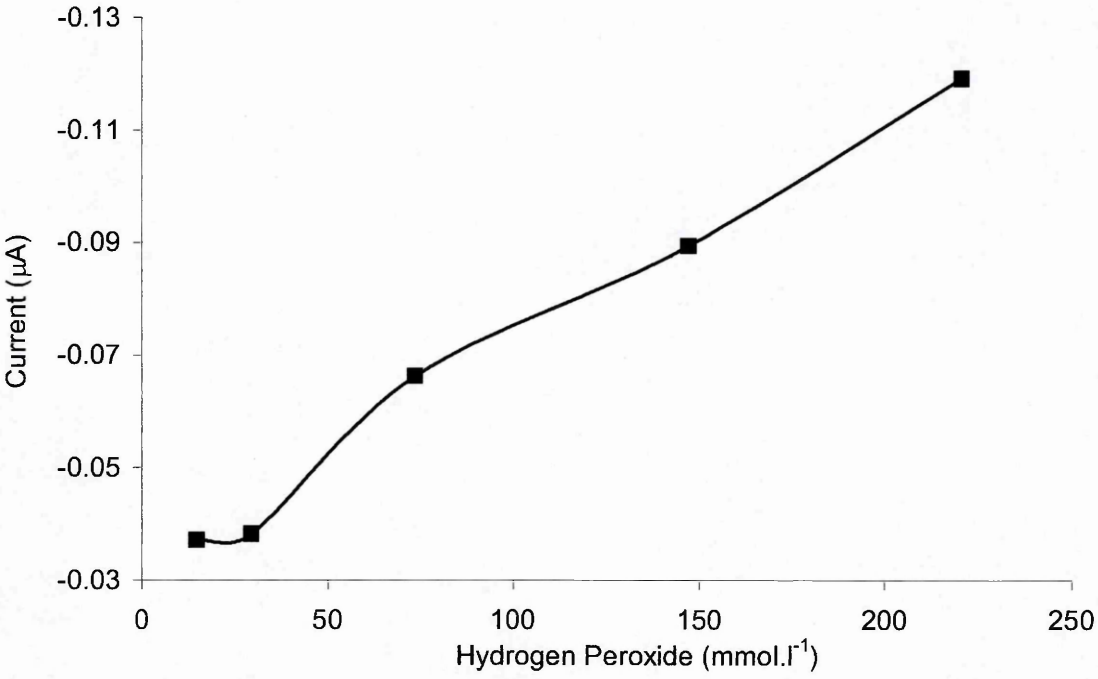

Figure 4.19 Calibration curve for the on-line study

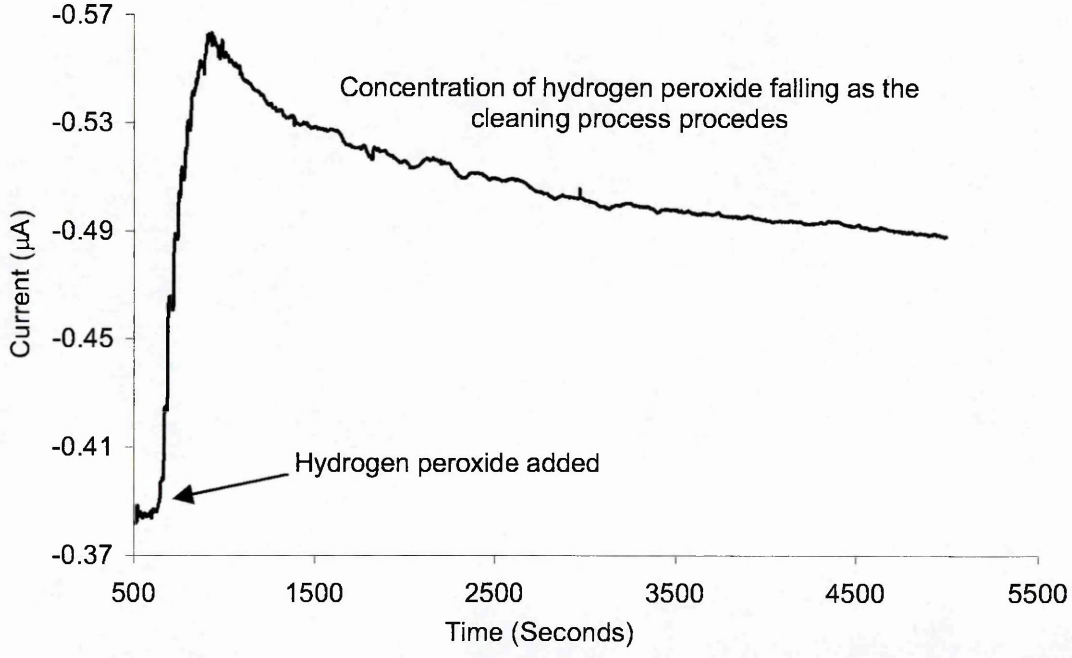

Figure 4.20 Current response to wash solution during wash cycle

4.6.5 Discussion

Despite the restraints imposed on this study, the response seen in figure 4.20 indicates that the sensor can be used for the monitoring of hydrogen peroxide concentrations in an industrial cleaning process.

If more time were available for a full trial, the calibration process would have to be altered to give a baseline between each calibration peak. Also, an equilibrium time would have to be established such that the performance of the sensors could be guaranteed after this time, or an algorithm would have to be developed such that an operator would be notified once there was a sufficiently stable baseline.

4.7 Visual Inspection and Comparison

In section 4.5, figures 4.14 and 4.17 showed images of sensors produced during the optimisation of the printing/deposition process. As there was a considerable difference in the visual appearance of all the sensors, it was considered to be a possible technique for assessing the quality of produced sensors.

There are already many applications of camera systems being used to monitor the quality of production lines, the brewery were using such a system to ensure that all bottles had labels correctly placed! It would therefore be possible to develop such a system to reject sensors that did not meet a predefined minimum coating level.

In order to investigate this possibility a Motic M700Z zoom stereomicroscope (Speed Fair Co. Ltd. Hong Kong) with a JVC TK-C401EG colour video camera (Victor Company of Japan, Ltd.) mounted on a double iris photo attachment was used. The video output was then captured using a miroVIDEO DC30 card (Pinnacle Systems GmbH, Braunschweig, Germany) installed in a HP Kayak XW PII/300 graphics PC Workstation (Hewlett Packard. USA). Single frames from the captured video sequences were then selected and converted into bitmap format images using Adobe Premier V5.1 (Adobe Systems Incorporated. USA).

Images of sensors from various production batches were then captured before the sensors were placed in the flow cell and a calibration cycle performed. Examples of sensors from each batch are shown in figure 4.21.

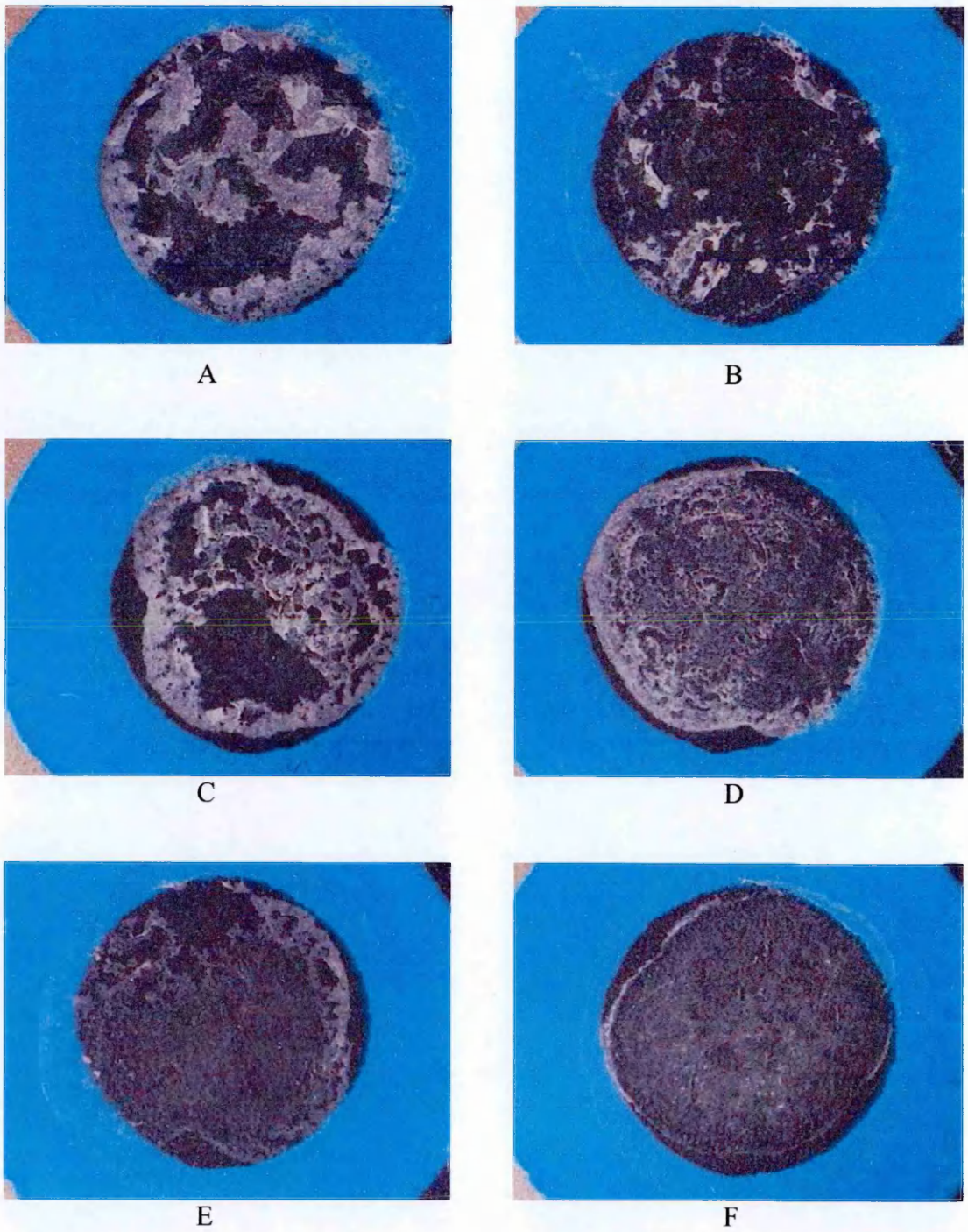

Figure 4.21 Images of sensors produced by different procedures

Batches A, B and C were produced by manually pipetting the component mix onto the base graphite electrode. Batch D was produced using the Biodot X-Y3000™ dispensing platform and batches E and F were produced using the synQUAD™ dispensing platform, batch E being a single application of 1 µl and batch F four overlaid applications of 1 µl.

The calibration curves based on the mean responses for 3 sensors of each batch are shown in figure 2.22 with the standard deviation at each level plotted in figure 4.23.

As was expected, the sensors produced by the automated deposition techniques (Biodot X-Y3000™ and synQUAD™ dispensing platforms) showed higher responses with a better sensor to sensor variation.

From these results, it can be seen that the automated deposition of the component mix onto the base graphite surface has both the advantages of speed and sensor to sensor reproducibility.

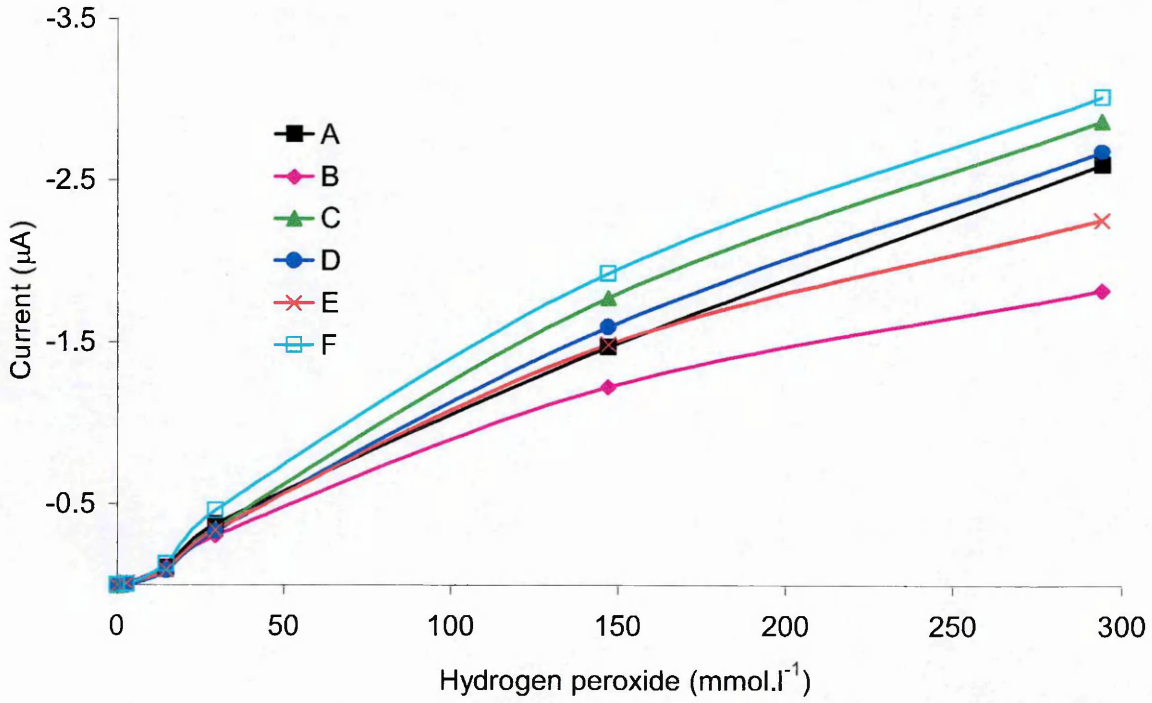

Figure 4.22 Calibration curves for sensors produced by different procedures

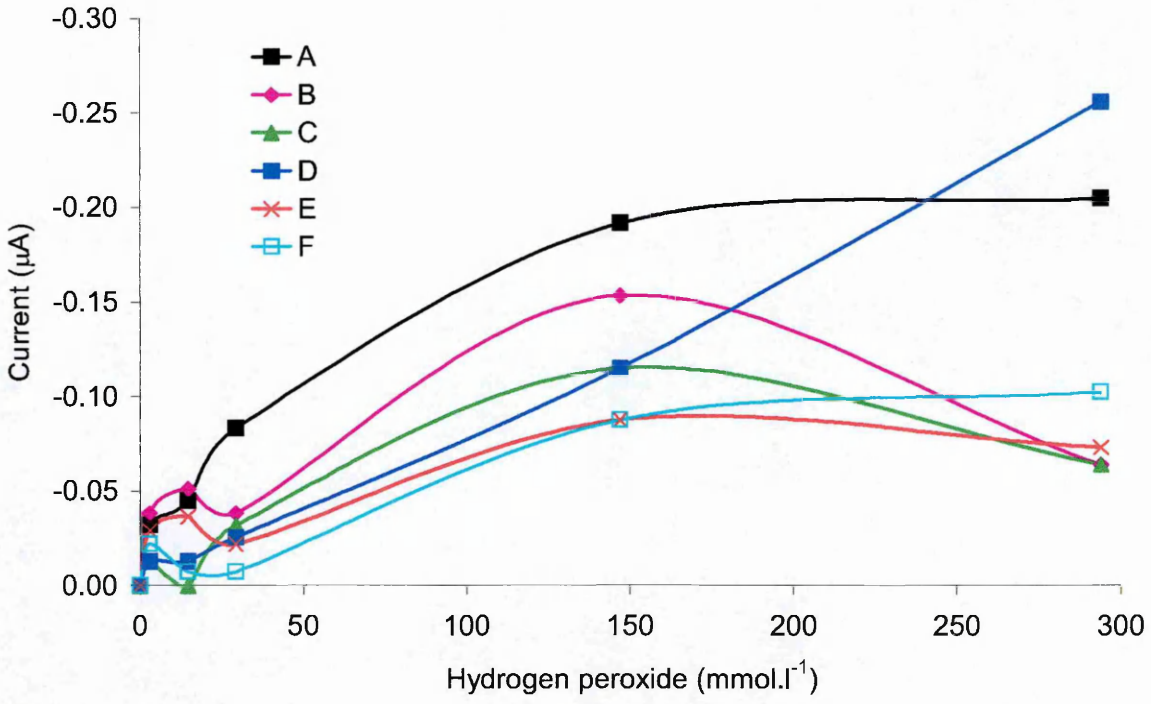

Figure 4.23 Standard deviations at varying concentrations for sensors produced by different procedures

The visual appearance of these sensors compared to those produced by manual pipetting was quite striking, with uneven deposition and a flaky appearance to the white cellulose acetate. From the performance of these sensors while generating the calibration data it would seem that if there had been any losses of the components off the surface it had not caused an unacceptable loss of sensitivity. With this borne in mind, if the sensor was to be put into commercial production it may be possible to reduce the loading of the components.

The optimisation performed in chapter 3 was carried out using sensors produced by manual deposition with testing in a beaker rather than the flow cell. It is quite likely that the proportions of the components would remain the same and that it is the more efficient deposition process that is giving full coverage of the graphite base with a thinner layer allowing more efficient diffusion of analyte through the cellulose acetate. Unfortunately, this theory cannot be validated without having long term access to a synQUAD™ dispensing platform.

The variation in visual appearance could be used as a manufacturing control process with the imaging software rejecting sensors with too great a contrast range indicating the 'coffee ring' effect or simply spots of uneven coverage.

4.8 Summary

The sensor has been shown to perform well compared to other methods in the inter-method comparison carried out at the König Brewery. The stability testing has shown that the sensor will work in a continuous monitoring environment for a minimum of four days.

The flow-cell arrangement has been shown to give a larger analytical range with better reproducibility than dipping the sensor into a stirred solution in a beaker.

The use of a synQUAD™ dispensing platform has been shown as a suitable device for the deposition of the component mix onto the base graphite electrode, producing sensors with a better sensitivity and sensor to sensor reproducibility than those manually pipetted. The comparison of visual appearance and performance has shown that this is probably due to a more efficient coverage of the graphite surface. The scanning electrochemical microscope will be used in the next chapter to investigate this hypothesis.

The variation in the appearance of the sensors using the microscope and video camera arrangement has also demonstrated a possible manufacturing control process.

5. Scanning Electrochemical Microscopy

5.1 Introduction

At the end of the previous chapter, the performance of the sensors was related to their visual appearance by comparing the calibration curves produced against the same series of hydrogen peroxide standard solutions. There were considerable differences in their appearance with only a slight variation in the measured responses to hydrogen peroxide. The sensors that performed slightly better had been produced using the Biodot X-Y3000™ or synQUAD™ dispensing platforms and had a visually more even coverage with the component mix.

The aim of this chapter is to describe the development of the scanning electrochemical microscope as a technique for the characterisation of the surface of a sensor, to establish whether the bioelectrochemical activity is evenly dispersed over the whole surface or whether there are localised areas of increased or decreased activity that can be attributed to the fabrication process.

The technique is not widely used and the instrumentation used in this work, although purchased commercially, still has many operational issues to be resolved. The issues affecting this work are described at the appropriate stage in the chapter with descriptions as to how they were overcome.

5.1.1 The Principles of Scanning Electrochemical Microscopy

Scanning electrochemical microscopy is a relatively new technique allowing the study of electrochemical activity at surfaces (Bard *et al*, 1989). It is a scanned probe microscope related to scanning tunnelling and atomic force microscopes. All scanned probe microscopes operate by scanning or "rastering" a small probe tip over the surface to be imaged. (Wipf, D. O., 2001).

In scanning electrochemical microscopy, imaging occurs in an electrolyte solution with an electrochemically active tip. In most cases, this tip is an ultramicroelectrode usually of 10 μm or less in diameter and the tip signal is the current from the electrolysis of a

species in the electrolyte solution. By studying the current that flows as this ultramicroelectrode is moved near the surface of a conductive, semi-conductive or insulating substrate in solution it is possible to obtain an electrochemical image of the surface.

The response of the scanning electrochemical microscope is dependent on mass transport between the ultramicroelectrode and the sample that, in turn, is governed by the chemical reactions occurring at the sample surface. Although the spatial resolution is not as advanced as for atomic force microscopy and scanning tunnelling microscopy, the technique can probe both the topography and the reactivity of a surface. The resolution of the technique is governed primarily by the size and shape of the ultramicroelectrode tip with mass and charge transfer process rates that affect the current density distribution and the solution resistance also having a lesser, but important influence.

5.1.2 The Tip Current

The current carried by the redox processes at the tip and sample is controlled by the electron transfer kinetics at the interfaces and mass transfer processes in solution. Thus, as the tip approaches the sample surface, the changes in current observed are related to the diffusion layer. By studying this current, it is possible to characterise processes and structural features of the sample. Also, these changes are used to control the approach of the tip to the sample surface before scanning commences.

To explain this process, the redox reaction given in equation 1.7 is considered again.

$$\underset{\textit{solution (s)}}{\text{Oxidised}} + \underset{\textit{electrode (m)}}{ne^-} \rightleftharpoons \underset{s}{\text{Reduced}} \qquad (1.7)$$

When the ultramicroelectrode is well away from the substrate surface, the normal solution effects are observed. Figure 5.1 illustrates this with 'O' representing the oxidised form and 'R' the reduced form.

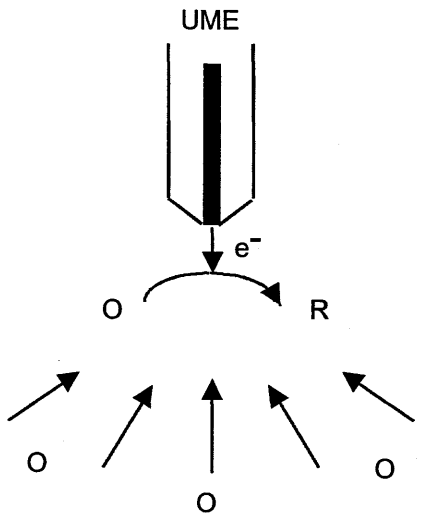

Figure 5.1 An ultramicroelectrode in solution

As the tip approaches the surface of an insulating surface, the tip current decreases because the insulating sheath of the tip blocks the diffusion of 'O' to the tip from the bulk solution (figure 5.2). This decrease in current is illustrated in figure 5.3 for a 10 μm probe held at –0.3 V referenced to a silver-silver chloride electrode, approaching a glass surface in a 20 $mmol.l^{-1}$ potassium ferrocyanide solution in the same buffer as used for the sensor development chapters.

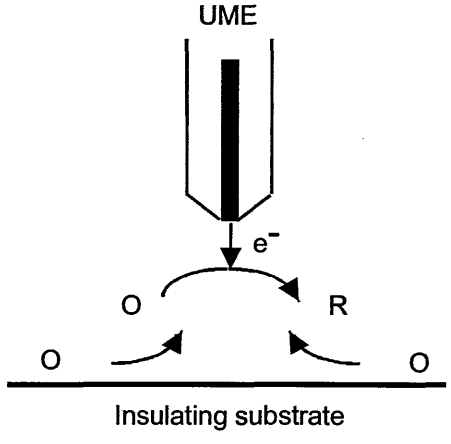

Figure 5.2 An ultramicroelectrode approaching an insulating surface

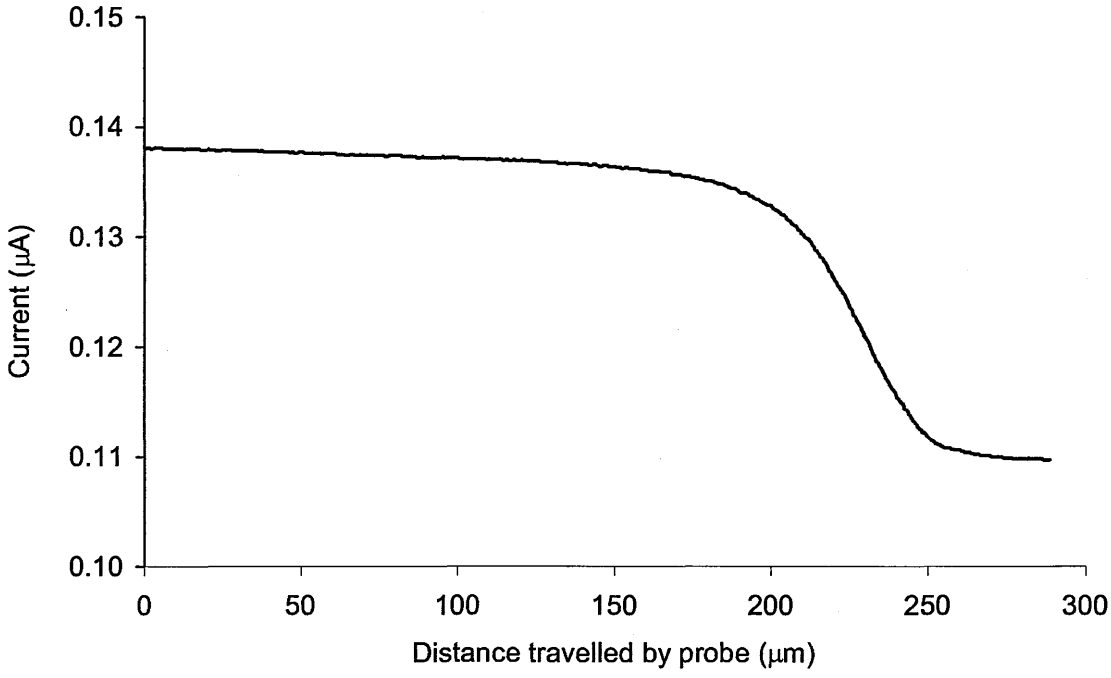

Figure 5.3 The current change as a tip approaches an insulating surface

As the tip approaches the surface of a conducting surface, 'R' can be oxidised back to 'O' producing a flux of 'O' to the tip (figures 5.4) and thus an increase in the observed current. This increase in current is illustrated in figure 5.5 for a 10 μm probe under the same conditions as for the generation of figure 5.3.

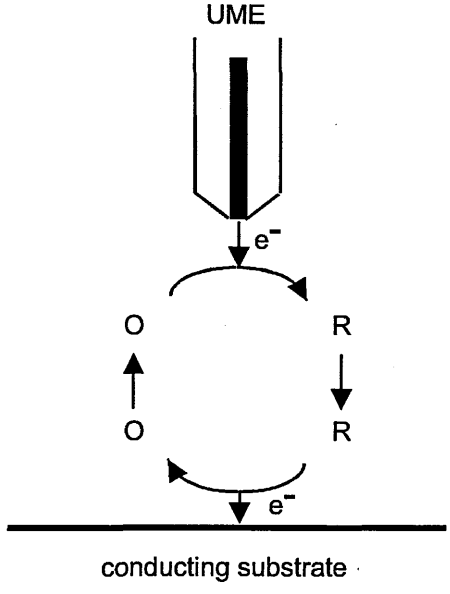

Figure 5.4 An ultramicroelectrode approaching a conducting surface

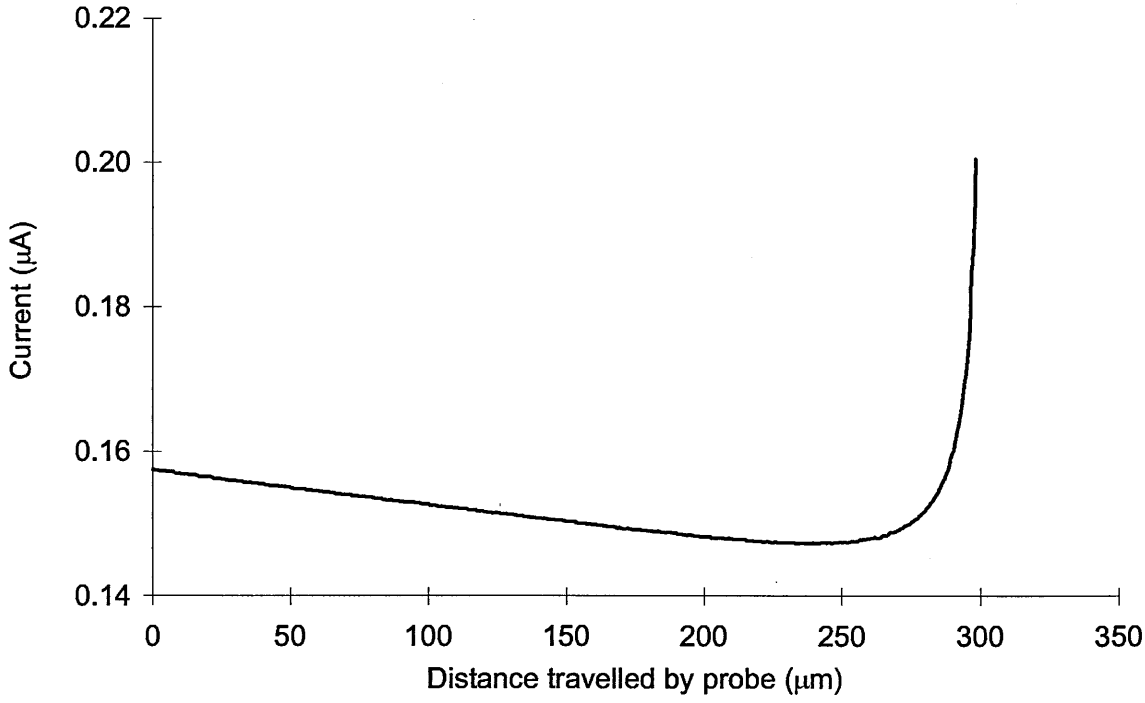

Figure 5.5 The current response as a tip approaches a conducting surface

5.1.3 Imaging Techniques

For an image of the surface to be obtained, the current that is monitored at the ultramicroelectrode tip must be affected in some reproducible fashion by the surface of the material being observed. There are two imaging methods that can be used:

1) Feedback imaging uses the current that flows from the electrolysis of a mediator species such as ferrocene or ferrocyanide at the ultramicroelectrode tip. The surface affects the tip signal depending on whether it is an insulating or conducting surface in a similar way to that shown above as the tip approaches an insulating or conducting surface (figures 5.2, 5.3, 5.4 and 5.5)

   Negative feedback occurs by the physical blocking of the diffusion of the mediator molecules to the tip electrode by the surface. This produces the drop in tip current seen in figure 5.3; thus if the surface becomes more insulating as the tip scans across, the current will also drop. Equally, if the surface has even insulating characteristics but uneven topography, then the current will drop when the gap between tip and surface becomes smaller.

Positive feedback is the opposite and occurs when the mediator is restored to its original oxidation state at the surface by an electrochemical, chemical, or enzymatic reaction. This produces the increase in tip current seen in figure 5.5; thus if the surface becomes more conducting as the tip scans across, the current will also increase. Equally, if the surface has even conducting characteristics but uneven topography, then the current will increase when the gap between tip and surface becomes smaller.

Experiments have demonstrated that the microscope can be used to map variations in electron-transfer rate at metallic electrode surfaces and for enzymes in biological materials (Wipf, D. O., 2001).

2) Generation/collection mode imaging uses the current produced at the tip by a species generated at the surface of the imaged material. Ideally, the tip acts only as a passive sensor with the ability to produce concentration maps of a particular chemical species near the substrate surface. In amperometric generation/collection, the electroactive species emitted or 'generated' by the substrate are detected or 'collected' by electrolysis at an ultramicroelectrode tip.

5.1.4 Ultramicroelectrodes

The ultramicroelectrode tip is one of the most important components of the scanning electrochemical microscope. Commonly tips are based on an embedded disk-shaped geometry. The disk-shaped tips are made by heat-sealing microscopic wires (usually gold, platinum or carbon) into glass tubes. The end of the glass tube is then polished to expose an embedded disk. The tip must then be ground such that the glass insulator forms a truncated cone. This allows the tip to approach more closely the substrate surface. A typical disk electrode will have a radius of between 1 to 25 μm. An insulator radius of 3 to 10 times larger than the electrode radius is desirable (Wipf, D. O., 2001).

5.2 Instrument Description

The instrument used in this work was supplied by CH Instruments Inc., 3700 Tennison Hill Drive, Austin, TX 78733 USA

It consists of four modules including a personal computer to coordinate the movement control and electrochemical data gathering. The layout is shown in figure 5.6 below.

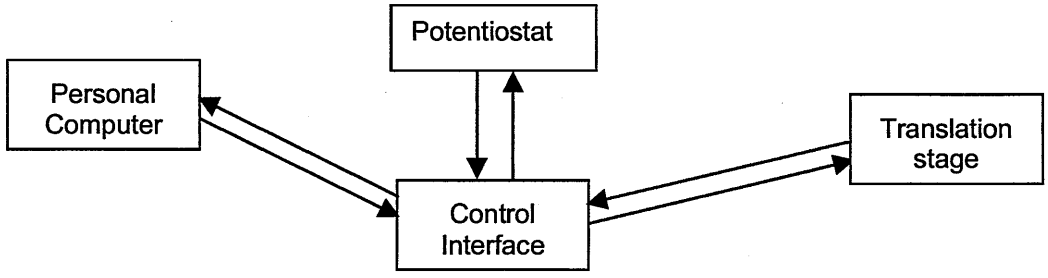

Figure 5.6 Layout of the scanning electrochemical microscope

The operating software is a small programme (under 2 Mbytes in size) that will run on any personal computer running Windows 95, 98 or NT™ and controls the hardware via one of the serial ports. This unfortunately does give rise to problems in routine operation as the communication between the personal computer and control interface is prone to error causing a software freeze with loss of data from the current scan. CH Instruments have recently responded to this problem with a software update that will allow for data recovery under most conditions. Unfortunately, it was released too late for use in this work.

The translation stage consists of three Burleigh IW-700 Series Inchworm motors arranged on two Burleigh TS-100 translation stages to allow control of X and Y directional movement over a 50 mm range with a resolution of 1 μm (Burleigh Instruments, Inc., Burleigh Park, Fishers, New York 14453-0755. USA). The Z motor is clamped to a bracket made by CH Instruments bolted to the X and Y stages to allow the same range and resolution of movement.

The inchworm motors (figure 5.7) have mechanical resolution of 4 nm over their entire range of motion; their minimum speed is 4 $nm.s^{-1}$ going up to a maximum speed of 1.5 $mm.s^{-1}$. They also have a non-rotating shaft with forward and reverse limit switches and a weight limit of 100 g. The translation stages use crossed roller bearings to allow the high precision motion created by the Inchworm motor. The Inchworm Motors are mounted to the stages by highly rigid, self-aligning couplings that eliminate side loads. The translation stage dimensions are 100 mm x 100 mm and with the layout used by CH Instruments, the movement errors due to the mechanical shift of the stages and brackets should be less than ± 1 μm.

Figure 5.7 Inchworm Motors

An Inchworm motor contains three piezoelectric actuators to create the movement. These are electro-mechanical devices that undergo a dimensional change when voltage is applied. This conversion of electrical energy into mechanical motion takes place without the need for any moving electrical contacts and without the generation of a significant magnetic field, thus making them an ideal choice where very low level electrochemical measurements are being taken.

Motion is created by the sequential activation of the three piezoelectric elements as shown in figure 5.8

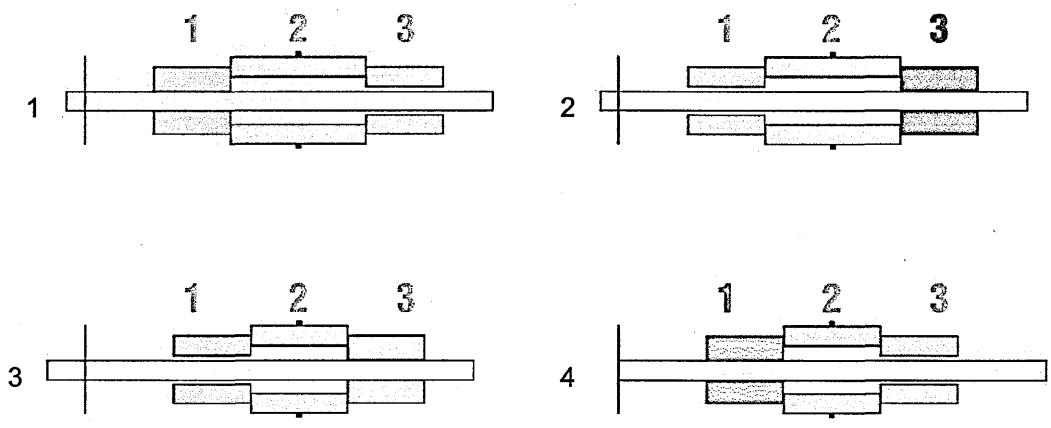

Figure 5.8 The sequence of piezoelectric actuation to produce Inchworm motor movement

The outer two elements, numbers 1 and 3, act as clamps. The central piezoelectric element, number 2, expands and contracts along the motor shaft when voltage is applied. Though all three elements operate independently, they are physically connected.

1. When a voltage is applied to piezoelectric element 1, it clamps the shaft. Then a variable rate staircase voltage is applied to element 2, causing it to change length in discrete steps of a few nanometres. This motion is directly coupled to the output shaft. The staircase takes hundreds of steps from its upper to lower limit and may be stopped and reversed at any point on the ramp.

2. At the end of the staircase ramp, a voltage is applied to element 3, causing it to grip the shaft. Voltage is removed from element 1, releasing it from the shaft.

3. The staircase starts downward until it reaches its lower limit,.

4. Element 1 is reactivated, element 3 is released and the staircase begins again. Thus, only the length of its shaft limits the maximum stroke of the motor.

The layout of the translation stage with the 3 inchworm motors is shown in figure 5.9.

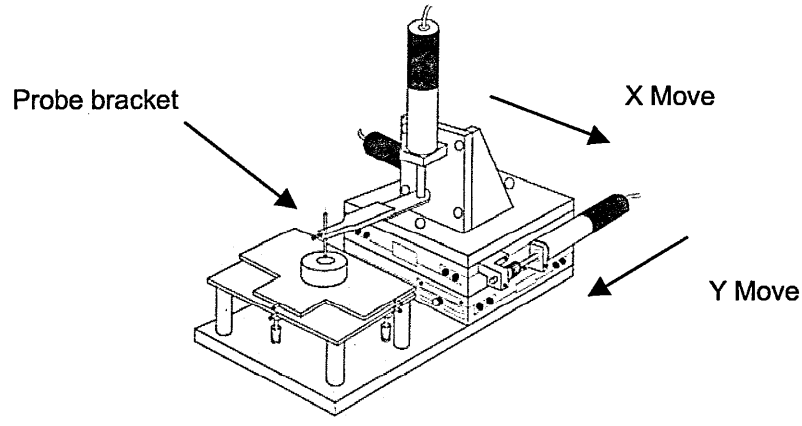

Figure 5.9 Burleigh translation stage layout

When scanning a surface, the control software gives the option of selecting which direction (X or Y) is the 'long travel direction'; this is the direction that is scanned for each incremental step in the other direction. Due to the physical design of the microscope, there was a risk of movement of the probe bracket when there was movement in the X direction and for this reason all scans were performed with the 'long travel direction' setting in the control software set to Y. Thus the X direction movement was kept to a minimum, incrementing after each pass in Y and then returning to the origin at the end of the whole scan.

5.3 Ultramicroelectrode Probe Fabrication

As there was only a limited range of ultramicroelectrodes available commercially, it was decided to make them as required in the laboratory. Various techniques were found in the literature.

Russell *et al* (1986) painted an organometallic gold complex onto quartz fibres to produce ring electrodes. As ring electrodes are not suitable for scanning electrochemical microscopy, this was not a suitable technique.

Fernandez *et al* (1991) sealed carbon fibres in glass capillaries using epoxy resin and Chen and Wang (1994) etched platinum-iridium wires and then insulated them in epoxy resin. A modification of these techniques was tried by sealing a platinum wire in a glass

capillary with epoxy resin. The electrodes were produced successfully but they could not be polished and ground to produce a good tip as the epoxy resin we had available did not become sufficiently hard for this process and the resin smeared across the tip and rapidly fouled the whetstone used for grinding and polishing.

Slevin *et al* (1999) etched platinum wires and then insulated them with an electrophoretic paint. This technique was able to produce electrodes with sub-micron tips but required equipment not available in the laboratory for their production. It was also considered that they would not be very easy to clean and polish should they become fouled during use.

Thus a modification to the technique used at Warwick University (McPherson, personal communication) was considered to be best suited to our requirements. The platinum wire is sealed in glass so there is no epoxy resin to foul the tip or whetstone and the tips can be readily cleaned, polished and re-ground.

1) A 100 mm long thick walled glass capillary tube with 2 mm external diameter and 1.2 mm internal diameter (Clarke Electromedical, UK) was 'pulled' into two fine-pointed halves using a Narishige PP-830 electrode-puller (Narishige Co. Ltd., Tokyo, Japan). Each half had a tapered end where the original glass capillary had been heated until soft and then pulled to a taper as the capillary was stretched until it broke. Each half was used to produce an electrode (figure 5.10).

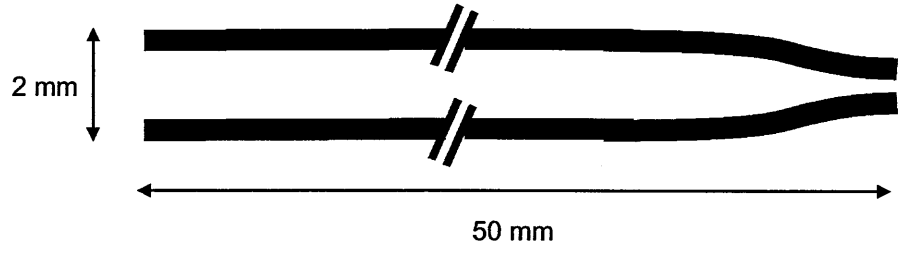

Figure 5.10 Pulled glass capillary

2 a) To produce a 10 μm disk electrode:

The tip (pulled end) of the capillary was then sealed by passing it briefly through a bunsen flame. A 10 to 15 mm length of 10 μm diameter platinum wire (Goodfellow, Cambridge, UK) was then inserted into the capillary, which was then gently tapped on the bench until the wire had dropped down to the sealed end.

2 b) To produce a 1 μm electrode:

A 10 to 15 mm length of 1 μm platinum wollaston wire (Goodfellow, Cambridge, UK) was twisted into a small loop similar to that in figure 5.11 This was found to be much easier if viewed using the low power magnification of the microscope. Wollaston wire is a very thin wire of under 10 μm diameter that is coated with a layer of another metal, in this case silver, to give a wire with an outside diameter of between 50 and 100 μm.

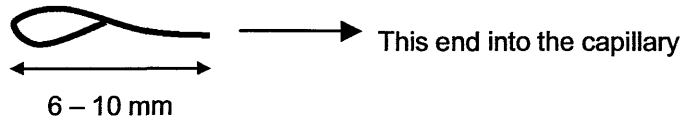

Figure 5.11 Approximate shape of loop of wollaston wire

This loop was then inserted into an unsealed 'pulled' capillary tube that was then gently tapped until the wire had dropped down to the unsealed tip with the wire loop stopping it from passing all the way through. The tip of the capillary was then touched carefully onto the surface of an approximately 1.5 $mol.l^{-1}$ solution of nitric acid; capillary action sucked the acid up around the platinum wire and care had to be taken to ensure that it went no higher than the bottom of the loop. The nitric acid rapidly etched the silver coating away to leave a platinum wire that was no longer visible to the naked eye. Because of the small sizes involved, the etching process was monitored at intervals under a microscope and it was assumed to be complete when there was no longer any visible gas production on the surface of the wire. The capillary was then gently flushed with distilled water to remove excess nitric acid, placed tip down in a small beaker and put in a drying oven for at least one hour to ensure there were no traces of moisture left inside the capillary when it was heated later.

After drying, the tip (pulled end) of the capillary was then sealed by passing it briefly through a Bunsen flame.

3) The sealed capillary was then put back into the electrode puller so that the tip was just inside the heating element. A length of thin wall plastic tube with internal diameter large enough to fit over the end of the capillary yet narrow enough to give a seal was pushed over the non-tapered end of the capillary. The other end of the plastic tube was connected to a low-pressure vacuum pump. Once a slight vacuum had been produced, indicated by the walls of the plastic tube being sucked in, the bottom end of the capillary where the platinum wire was situated was then heated. As the glass softened, the vacuum pulled in the wall of the capillary to form a seal around the platinum wire. The tip of the capillary was gradually lowered through the heating element until all but 2 to 3 mm of the 10 μm platinum wire or the tip of the Wollaston wire loop for the 1 μm wire was embedded in the glass.

4) A 2 to 3 mm length of ready-fluxed solder (RS Components, Corby, UK) was then put into the capillary followed by a 70 to 80 mm length of normal electrical single strand steel wire. The wire was pushed up to the piece of solder and then gently pushed the solder further into the capillary until it was in contact with the exposed end of the platinum wire. The probe was then turned tip up, the wire preventing the solder from falling out.

5) The tip of the capillary was then heated with a soldering iron whilst pushing gently on the wire from underneath. When the solder inside the capillary melted, the steel wire suddenly passed through the liquid solder making contact with the platinum wire. The soldering iron was then removed from the tip and on cooling, the solder maintained electrical contact between the platinum and steel wire.

6) The open end of the capillary was then sealed with 'shrink-fit' insulating plastic (RS Components, Corby, UK) to grip the steel wire and help prevent it from being pulled away from the platinum at the tip.

7) The tip of the glass capillary was then ground down using emery paper to expose the platinum wire. This was then flattened and polished using a Narishige EG-400

micropipette grinder (Narishige Co. Ltd., Tokyo, Japan). The glass point of the tip of the glass capillary was then ground at an angle of approximately 45 degrees until it was approximately ten times the diameter of the embedded platinum wire (Wittstock and Schuhmann, 1997).

5.4. Instrument Control Parameters

5.4.1 Choice of Mediator and Operating Potential

In order to obtain an image of the surface of a sensor, there was still a requirement for a mediator to be in the solution even with the mediator present in the component mixture on the sensor surface. As potassium hexacyanoferrate (II) had been shown to work well with hydrogen peroxide and horseradish peroxidase in section 2.6, a solution containing 20 mmol.l^{-1} in phosphate buffer was considered appropriate for use in this work.

Using cyclic voltammetry, the optimum potential for amperometry with the platinum probe and sensor surface in potassium ferrocyanide was found to be –0.3V referenced against a silver-silver chloride electrode.

5.4.2 Probe Approach

Due to the very close proximity of the probe to the surface under examination, manual positioning is not possible. Thus, the control software has a routine called 'Probe Approach Curve'. This routine monitors the tip current at the applied potential as it approaches the surface under investigation. The shape of these curves was shown in figure 5.3 for an insulating surface and figure 5.5 for a conducting surface. As the forward and reverse distance ratio cannot be calculated for the 'Z' axis (probe approach), it is not possible to accurately move the probe into position at a set distance above the surface using the probe control panel. To overcome this, the probe approach current is monitored and the percentage change from the start current to the current seen at the desired height above the surface, extrapolated back from when it has made contact with the surface, is calculated. This figure is then entered into the scanning electrochemical microscope parameters panel as the 'End i ratio (%)' value along with the approach step size and a withdraw distance to ensure that the probe is not in contact

with the surface before an approach is made. When a scan is initiated, a probe approach is run until this percentage current change is reached, then the scan continues.

5.4.3 Scan Dimensions and Rate

The size of a scan was limited to a maximum of 512 data points in each direction. Thus for scans of over 512 μm in either direction the step size was automatically increased reducing the effective resolution of the instrument.

The rate at which the probe was scanned across the surface had to be slow enough for a steady state to be established before the current was measured after each incremental step. This was found to be 0.04 seconds per step using potassium ferrocyanide.

5.5 Calibration of Translation Stage Movement

5.5.1 Calibration with a Micrometer

Since the Inchworm motor design has no direct indication of position it is necessary to calibrate the movement. The software has a routine, described in the instrument manual, to perform this individually on each of the three motors (Model 900 Scanning Electrochemical Microscope, Users Manual. CH Instruments).

In order to achieve this measurement, a micrometer is required. As there are several designs available, several different ones were tested for the purpose. A Mitutoyo micrometer head, 150 - 190 MHN1-25V with a range of 0 – 25 mm and an accuracy of 1 μm (Mitutoyo, Japan) was found to be most suited for the purpose when fitted into a special stand (figure 5.12) made to our specifications (Model Products Ltd. Wooton, Bedfordshire. UK).

The translation stage stood on the micrometer stand as shown in figure 5.13 for the calibration process to ensure maximum stability and accuracy of measurement.

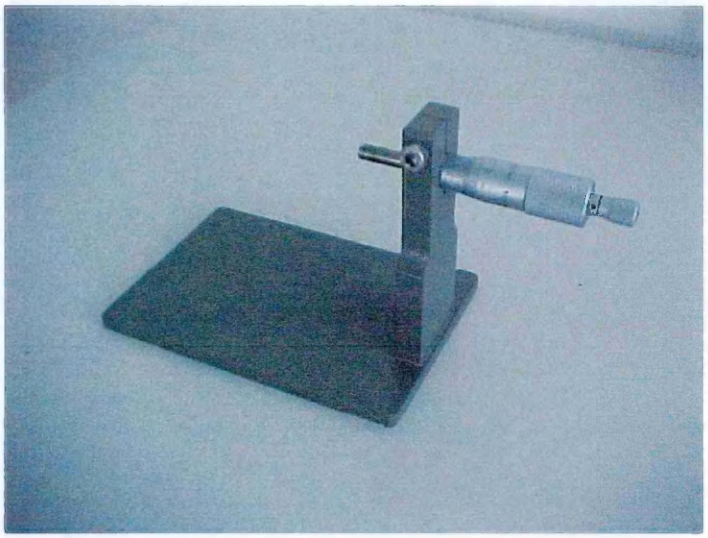

Figure 5.12 Micrometer fixed in purpose designed stand.

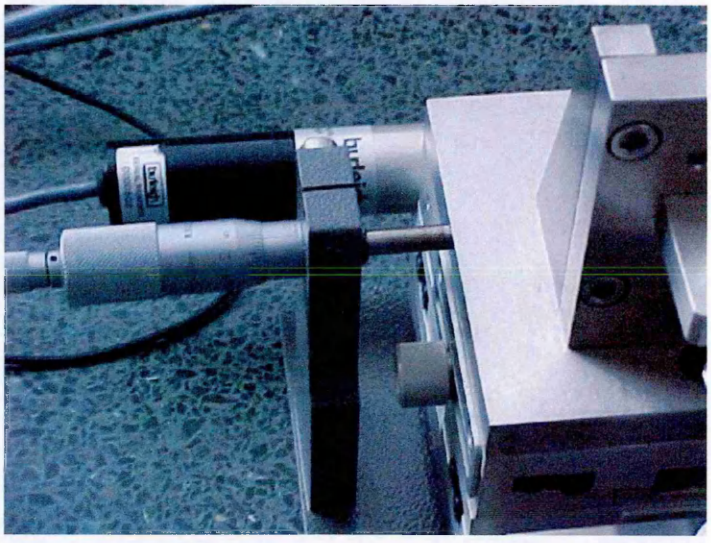

Figure 5.13 The translation stage standing on the micrometer stand for calibration

After clicking on the "calib" button for the motor the operator wishes to calibrate, the control interface causes the motor shaft to fully retract until it hits the reverse limit. A small message box then appears on the computer screen asking the operator to 'measure the motor position and then press OK'. After measuring the fully retracted position of the translation stage relative to the fixed micrometer, the "OK" button is then clicked. The control interface then causes the motor to move forward for a default of 10000 'clicks' (the 'click' is the smallest movement that the control interface can signal to an individual motor). After the motor has stopped moving, another message box will then

appear on the computer screen asking the operator to measure the second position. Once this measurement has been made, the "OK" button is clicked and the difference between the two measurements is entered into the box on the left side of the appropriate "calib" button. The control software uses this information to calculate the probe position and moving distance. In practice this forward movement of 10000 "clicks" was found to be about 13000 μm.

The movement produced by a 'click' when retracting (reverse movement) is different to that produced when extending due to the hysteresis of the piezoelectric motors and unequal grabbing force of the clamps. This difference can be as large as a few percent causing a straight line to slope or a circle to appear as an ellipse. Thus, there is also a 'Forward and Reverse Distance' ratio (F/R ratio) that needs to be entered into the control interface software. In the instructions, this is calculated by measuring the distance actually moved in each direction when the motor has been instructed to move the same distance. This process was found to be ineffective in all the software versions used, as entering the ratio of the two distances never resulted in an accurate return to the origin; in practice, this ratio had to be deduced empirically (see section 5.6.1). At present, the software only has the facility for this correction in the X and Y directions and not Z, the probe approach. It was also found that a different F/R ratio had to be determined for each scan rate used, probably due to changes in hysteresis and grabbing force of the clamps in the piezoelectric motors.

5.5.2 Calibration Check with an Interdigitated Gold Array

When running the scanning electrochemical microscope under analytical conditions, the distance travelled is different to that used at calibration although the software is using the entered travel distance from the calibration to calculate the number of clicks required for the entered length of movement. Also, the speed of movement is not defined at calibration and as the F/R ratio is affected by speed, it was assumed that the calibration would also vary with speed.

For these reasons a calibration control check was devised by using an interdigitated gold array with 15 μm spacing as shown in figure 5.14

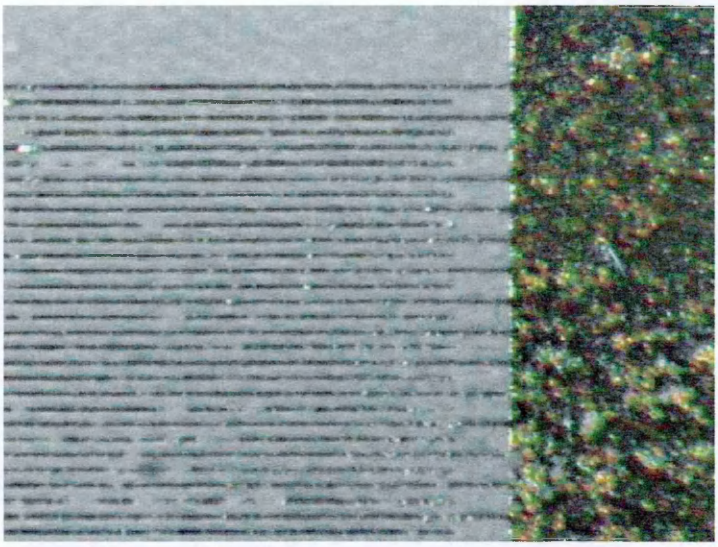

Figure 5.14 Photomicrograph of an interdigitated gold array

The array was fixed in place in the sample well on the scanning electrochemical microscope stage and covered by a 20 $mmol.l^{-1}$ potassium ferrocyanide solution in the same buffer as used for the sensor development chapters. The micro silver/silver chloride reference electrode supplied with the microscope was placed in the cutout at the side of the well and the embedded platinum wire used as the counter electrode.

An example of the expected image when the system is running correctly is shown in figure 5.15. As the probe passes over the gold stripes, there is an increase in current due to positive feedback over the conducting surface and this will appear yellow on the scanning electrochemical microscope image; the lower current that is measured over the insulating glass support is green.

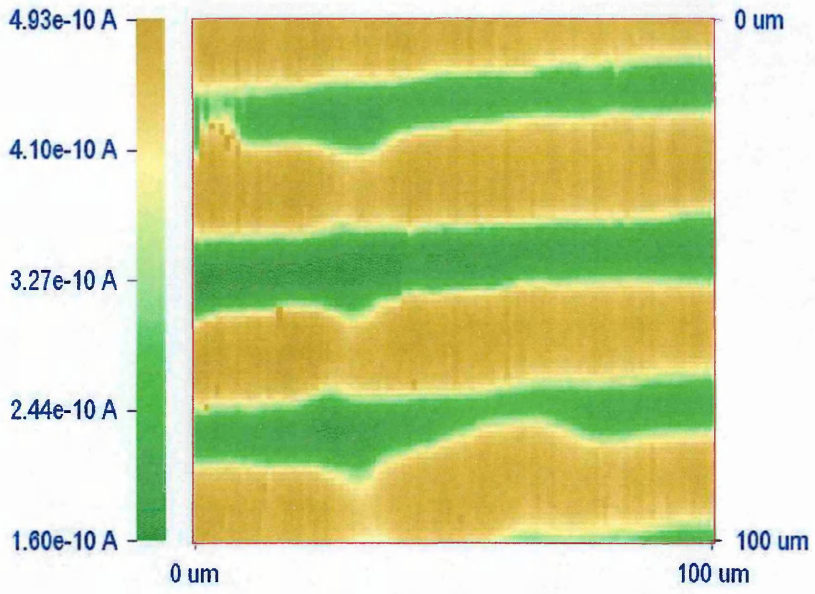

Figure 5.15 Scanning electrochemical microscope scan of a 100 x 100 μm^2 area of an interdigitated gold array (false colour map)

5.6 Investigation of Instrument Calibration Problems

When the instrument was first commissioned, the above procedure for checking the calibration with an interdigitated gold array was followed and all seemed to be working well. However, there were occasions when the image of the array used for calibration would be irregular such as in figure 5.16.

The cause of this was not apparent and thus possible causes were investigated.

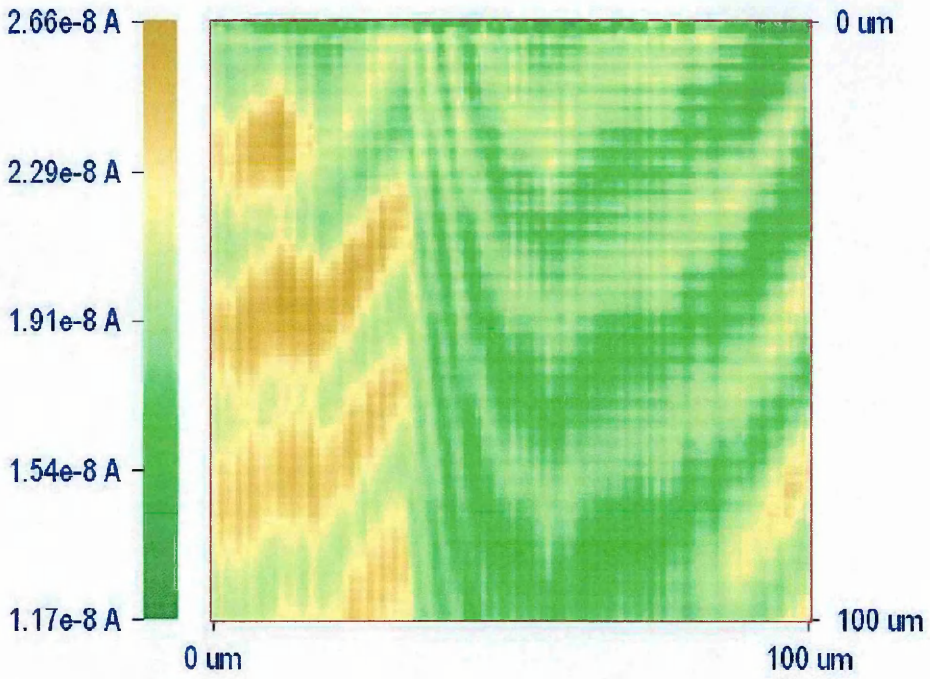

Figure 5.16 Example of irregular movement (false colour map)

5.6.1 Accuracy and Reproducibility of Y Direction Movement.

The movement in the Y direction was first calibrated following the manufacturer's instructions. A series of ten forward movements of 1000 μm at 200 μm per second were then made and each extension measured with the micrometer having a quoted accuracy of 1 μm. As this did not give a satisfactory length of move, the value for the calibration value in the control software was adjusted by an estimate based on the percentage error in the observed movement compared to the programmed movement. This procedure was repeated until satisfactory move lengths were achieved. An example of the results obtained by this process is shown in table 5.1

Table 5.1. Example of data obtained during motor movement calibration

Source	Calibration Value	First Estimated Adjustment	Second Estimated Adjustment
µm for 10000 clicks	13599	13789	13806
Step	**Distance moved (µm)**		
1	1010	999	1002
2	1011	1002	1003
3	1014	1001	999
4	1015	1006	1000
5	1011	999	1000
6	1018	1002	997
7	1015	1001	999
8	1014	1001	997
9	1014	1000	997
10	1018	1001	998
Mean	1014	1001	999
Standard Deviation	2.61	1.89	1.99
Coefficient of Variation (%)	0.26	0.19	0.20

A similar process was then applied to the reverse movement starting with an F/R ratio of 1. An example of the results obtained in this process is shown in table 5.2

Table 5.2. Example of data obtained during motor reverse movement calibration (F/R ratio)

		First Estimated Adjustment	Second Estimated Adjustment
F/R ratio	1.0000	1.0128	1.0098
Step	**Distance moved (μm)**		
1	995	1002	1006
2	989	1012	997
3	990	1010	1008
4	991	1007	1003
5	987	1003	1000
6	987	1003	1000
7	987	1004	1000
8	987	1002	996
9	982	998	994
10	979	988	999
Mean	987	1003	1000
Standard Deviation	4.2474	6.3159	4.1243
Coefficient of Variation (%)	0.4302	0.6298	0.4123

When the calibration was applied to a scan of 50 μm for the X movement and 1000 μm for the Y movement with a step of 2 μm, after only 25 cycles of Y movement there was already a reverse excess of 108 μm. This process was repeated several times and similar results obtained. Such a large error meant that the instrument could not be used to obtain scans of area large enough to give the required information. The size of the scans made was gradually reduced to 100 x 100 μm at which point the error in movement had negligible impact on the resulting scan and allowed the return of the probe back to the origin at the end.

Even after reducing the length of a scan to 100 μm in each direction, the procedure described in the manual for establishing the F/R ratio did not work in practice. Once this ratio value had been entered in the appropriate box in the software window, it was then necessary to modify it by 'trial and error' scanning of the interdigitated gold array and then adjusting the value until a good image was obtained.

For example, figure 5.17 shows a series of scans of an interdigitated array. In 5.17a the array was scanned with the null F/R ratio = 1.0000 and the measurements made with the micrometer, using the procedure given in the manual. This was then changed to 1.0100 and as 5.17b shows this was still insufficient. Two further increases were required to reach a useable ratio of 1.030, shown in 5.17d

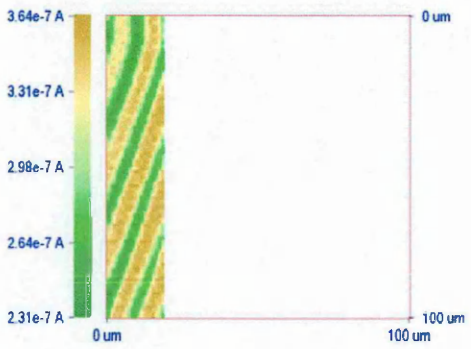

a) F/R = 1.0000

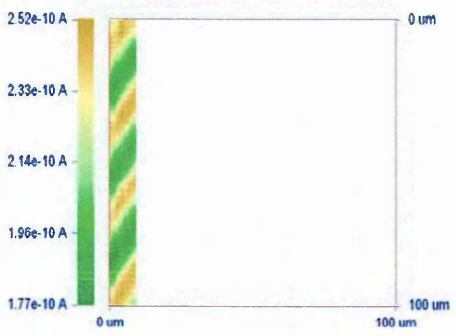

b) F/R = 1.0100

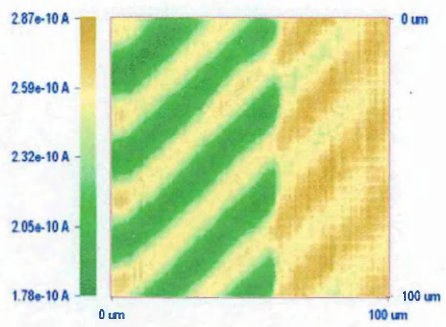

c) F/R = 1.0150

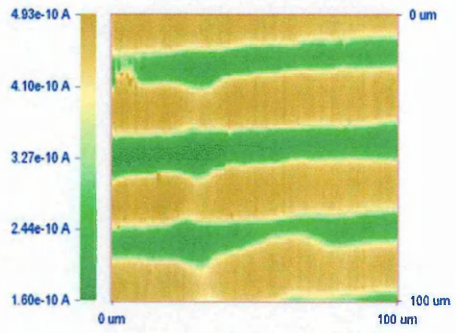

d) F/R = 1.0300

Figure 5.17 Series of scans made in order to achieve a good F/R ratio

5.6.2 Environment Temperature and Movement

Even when the instrument had been calibrated and checked, there were still occasions when the instrument was being used routinely that similar scans to figure 5.16 were obtained.

As there was no obvious cause for the apparently random incidence of these poor quality scans, the effect of temperature on calibration was investigated. A digital thermometer with thermocouple probe (Robin, UK.) was used to monitor the ambient temperature whilst a calibration event was taking place. There was no measurable change in temperature during any of the calibrations but as there was no temperature control in the laboratory all calibrations had to be done on different days when the prevailing weather conditions dictated the temperature. The results obtained are shown in figure 5.18 and table 5.3 below.

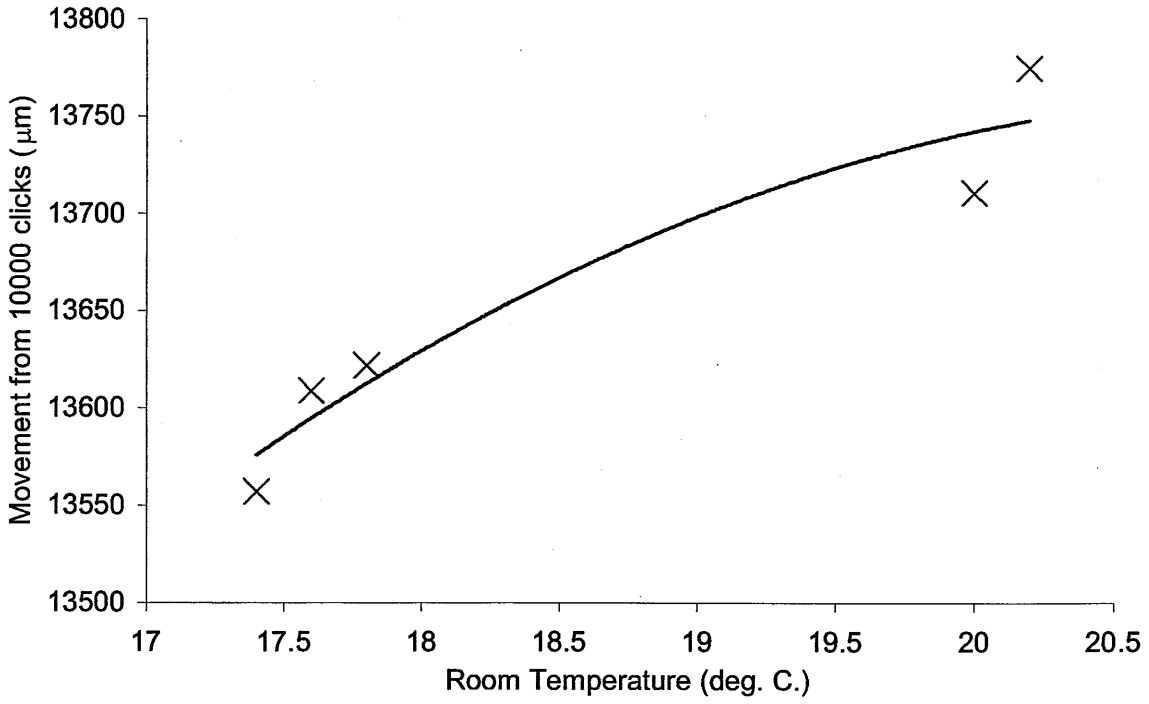

Figure 5.18 The effect of temperature on the calibration of the Y motor movement

From figure 5.18, it can be seen that there was a significant change in calibration value with temperature, with a change of 2.8 degrees Celsius giving rise to a 1.6 % change in calibration value. This in turn would give rise to a significant error in the dimensions of any scanned area.

Table 5.3. The effect of temperature on the calibration of the Y motor movement

Temperature (deg. C)	Y move Calibration value (µm)
17.4	13557
17.6	13609
17.8	13622
20	13711
20.2	13775

Without temperature control in the laboratory, this level of error would prevent an accurate day-to-day comparison of scans. However, it was considered that with the large mass of the translation stage blocks and relative stability of the room temperature over a short period of time, that there should not have been the level of error seen in several scans. Also, the sudden and random nature of some of the errors such as in figure 5.16 after approximately 30 cycles of Y movement could not be explained by temperature fluctuations.

5.6.3 Random Movement Errors

As there was no obvious cause for the apparently random incidence of these poor quality scans, it was decided to visually monitor the scanning process. To achieve this, the microscope and video camera described in chapter 4, section 4.7 was used to monitor the tip movement throughout the scanning process.

The observations made using the microscope and camera were significant.

1) Although the instrument was on a heavy marble table in the laboratory, this was on a wooden floor. As people walked down an adjacent corridor and went through the door at its end, there was severe vibration affecting the probe movement.

2) The environment in which the instrument was situated was also very unstable; whenever the door to the laboratory was opened there were strong air currents and despite being installed in a cabinet, some of these air currents could be seen to affect the probe.

3) Although the probe approach curve for the instrument was used to avoid crashing into the surface under investigation, if the surface was not horizontal to the plane of X-Y movement, contact could be made with the surface during a cycle. Also, when scanning the array, if the approach was made to the glass support rather than a gold stripe, the tip could be too close to the surface and catch on the slightly raised gold array stripes. This was shown as a small flick of the probe as it released itself when the pull or push overcame the resistance of the stripe.

To overcome some of the environmental issues, some experiments were performed at night and at weekends when there were no other people walking around to disturb the system. Although this did improve the performance a little, there were still random errors to the apparent probe movement.

During a discussion with an engineer (E. Brown, Cranfield precision, personal communication) it was discovered that piezoelectric actuators are very sensitive to changes in environmental temperature. As the equipment was to be relocated into a new laboratory with a solid floor and air-conditioning, no further investigation was made until the move to this location had been completed. Once the instrument had been installed and calibrated in the new environment, the results obtained when scanning the gold array were much more reproducible and acceptable for small scans of no more than 100 x 100 $\mu m.^2$ There was however, no improvement on the precision shown earlier in tables 5.1 and 5.2 and the calibration procedure still required the modifications developed earlier in order to give the accuracy required.

5.7 Imaging and Interpretation

The graphical capabilities of the scanning electrochemical microscope control software package are limited. Figure 5.19 shows the image obtained using the control software of a typical scan of a graphite electrode. Such a two-dimensional image does not readily show all the features that can be interpreted from the scan, nor does the software allow any manipulation of the data. In order to overcome this limitation, the data was exported from the control software as Excel 3D formatted files with comma separation and then imported into the Matlab software package (version 5.3, The MathWorks Inc., 24 Prime Park Way, Natick, MA 01760-1500, USA). This package allowed the data to be visualised as a three-dimensional image, using the current response to give the third dimension and thus giving the data a more visual impact. For an example, figure 5.20 shows the same data from figure 5.19 in this three dimensional format.

Matlab also allowed the data to be manipulated in such a way that scans of the same surface under different conditions could be subtracted from each other in order to interpret the effect of the changes in conditions without the effect of the topography of the surface. This was also one of the reasons why the calibration of the translation stage movement in the earlier sections was so important.

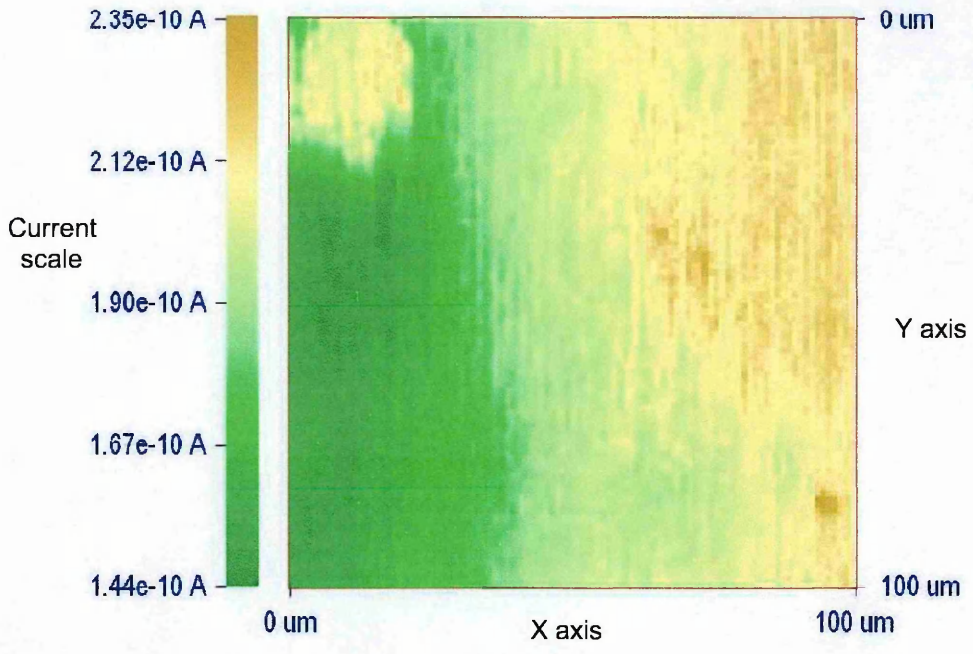

Figure 5.19 An example scan of a coated graphite electrode

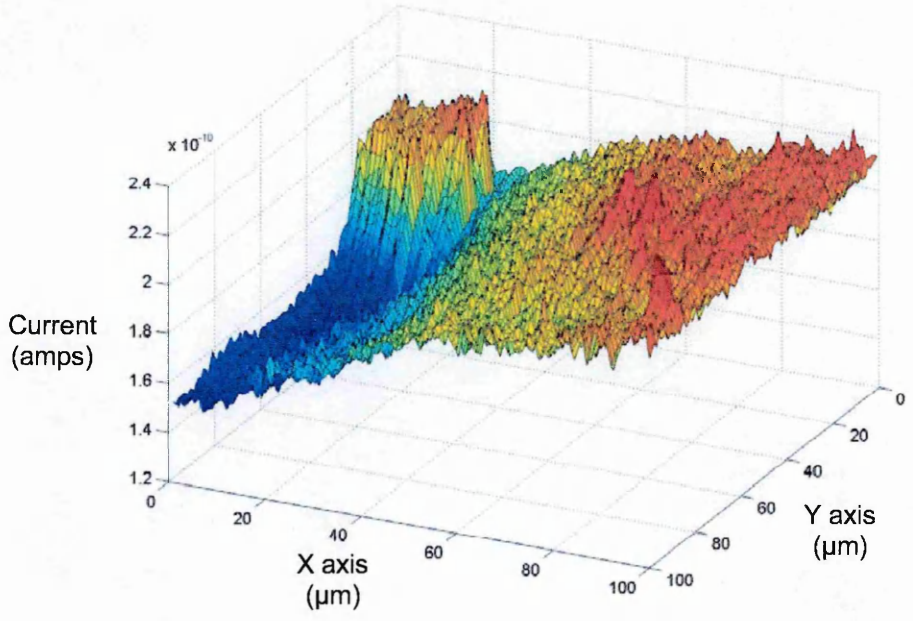

Figure 5.20 Data from figure 5.19 imported into and displayed using Matlab

5.7.1 Measurement in both Forward and Reverse Directions

The instrument control software has the facility to measure the current at the probe whilst scanning in both the forward and reverse directions. The use of this facility was investigated, as it would reduce the time taken to complete a scan. Unfortunately, due to a 'carryover' effect, there was some trailing as the current fell as the probe moved from a 'hot spot' to an area of lower activity. This was not obvious when the current was monitored only when scanning in the forward direction, however, when current was monitored in both directions, the effect became quite significant as shown in figure 5.21 for the control software images and figure 5.22 when the data had been imported into Matlab.

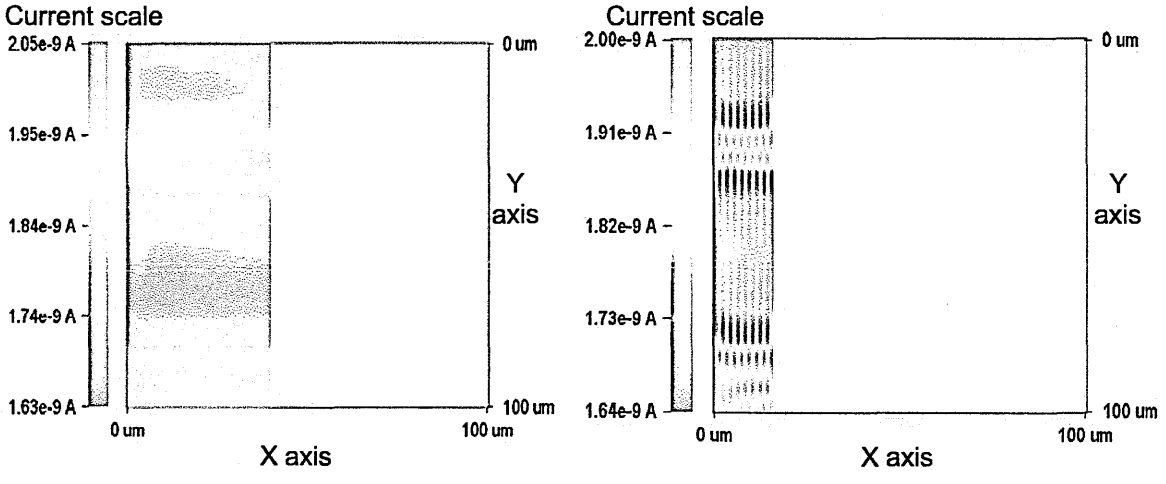

a) Current monitored in forward direction

b) Current monitored in both directions

Figure 5.21 Control software imaging comparing current monitoring options

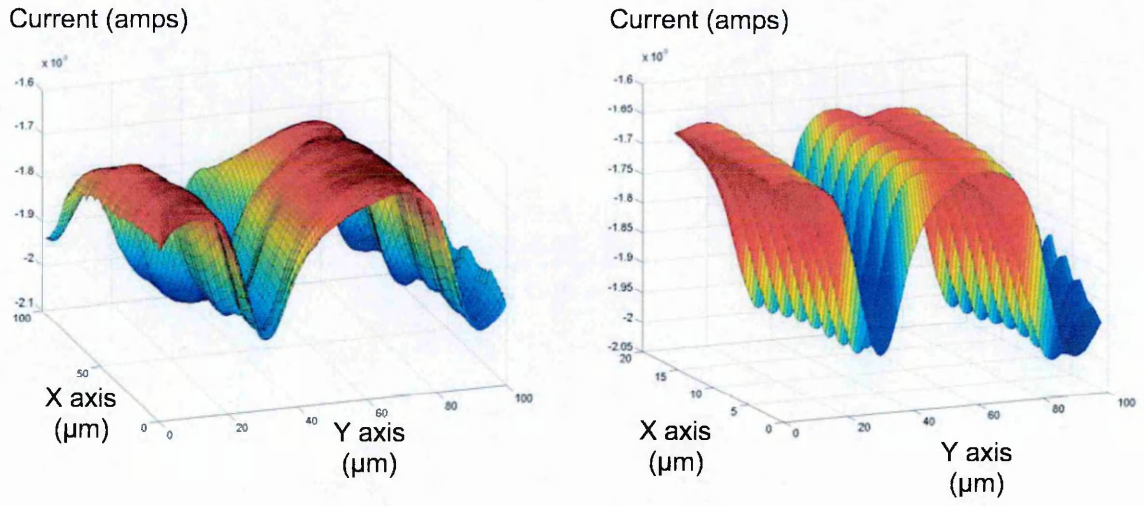

a) Current monitored in forward direction

b) Current monitored in both directions

Figure 5.22 Data from figure 5.21 imported into Matlab

The most probable cause of this trailing was considered to be the slight disturbance of the diffusion layer at the surface of the sensor caused by the movement of the ultramicroelectrode probe. It might have been reduced by slowing the scan rate from 0.04 $s.\mu m^{-1}$ to the slowest allowed by the control software at 0.2 $s.\mu m^{-1}$. Unfortunately, when tested, this delay was not sufficient for the disturbance to have significantly settled before the current was measured but did create a five-fold increase in the time taken to complete the scan. With only this slight improvement, it was decided to continue scanning at the higher speed, but to monitor the current in the forward direction only.

5.8 Imaging of Peroxide Sensors

There has been some work reported on the use of scanning electrochemical microscopy to localise and image enzymes immobilised on a surface. Kranz *et al* (1997) looked at immobilised monolayers of microperoxidase on a gold electrode. Wittstock and Schuhmann (1997) looked at the formation and imaging of enzyme spots on a gold electrode. In both of these reports the gold surface to which the enzyme had been

immobilised was flat, thus they did not have to contend with the issue of surface topography.

In order to visualise the distribution of horseradish peroxidase activity on the graphite electrode, it was necessary to devise a way of allowing for the uneven nature of the graphite electrode and the expected uneven coating with enzyme, mediator and cellulose acetate in acetone.

The simplest way of achieving this was to scan the surface using 20 $mmol.l^{-1}$ potassium ferrocyanide solution as the mediator in the same buffer used as electrolyte for the sensor development. Changes in the feedback current seen in this scan were then assumed to be due to changes in the topography of the surface and porosity of the insulating layer (cellulose acetate) if present. Then, by adding hydrogen peroxide at a concentration of 1 $mmol.l^{-1}$ and re-scanning the same area, any changes in the feedback current that did not match the pattern obtained without hydrogen peroxide could be assumed to be due to activity on the sensor surface.

By importing the feedback current data for the two scans into Excel, the difference in current at each point could be calculated and saved as a separate data set. This in turn was imported into Matlab and an image produced.

As described in the previous chapter, there was a difference in performance observed between manually pipetted sensors and those produced using the biodot or SynQUAD™ dispensing platforms. Sensors produced by all processes were therefore studied using the scanning electrochemical microscope. All of the scans in the following sections were of a 100 x 100^2 μm area of the electrode surface with 1 μm steps using a 1 μm probe at a potential of –0.3 V relative to the reference electrode screen-printed on each sensor. Unfortunately, the z-axis scale (feedback current) labelling could not be controlled as version 5.3 of Matlab automatically defaulted numbers to the nearest factor of 10, although the current ranges for each sensor were in the same order of magnitude.

5.8.1 Base Graphite Electrode

Figure 5.23 shows a scan of a base graphite electrode and figure 5.24 shows the same area of the electrode scanned with hydrogen peroxide in the solution. Figure 5.25 is the image obtained from the calculated difference in feedback current at each point.

It can be seen that although there is possibly some error in the alignment of the scans, the appearance of each of the surfaces is similar. Also the current difference between the two scans is around zero as would be expected with no peroxidase activity on the electrode surface. Also, there is some variation that can be attributed to the uneven surface of the graphite.

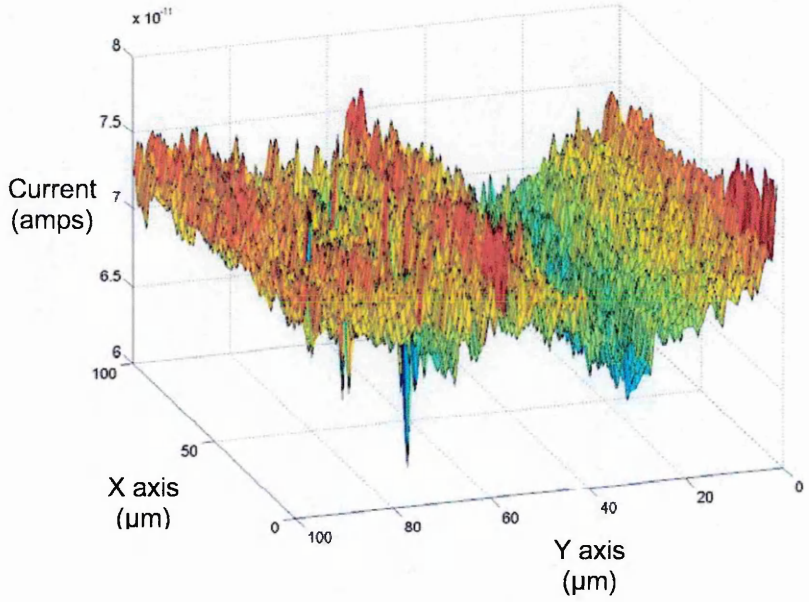

Figure 5.23 Scan of a base graphite electrode in ferrocyanide and buffer

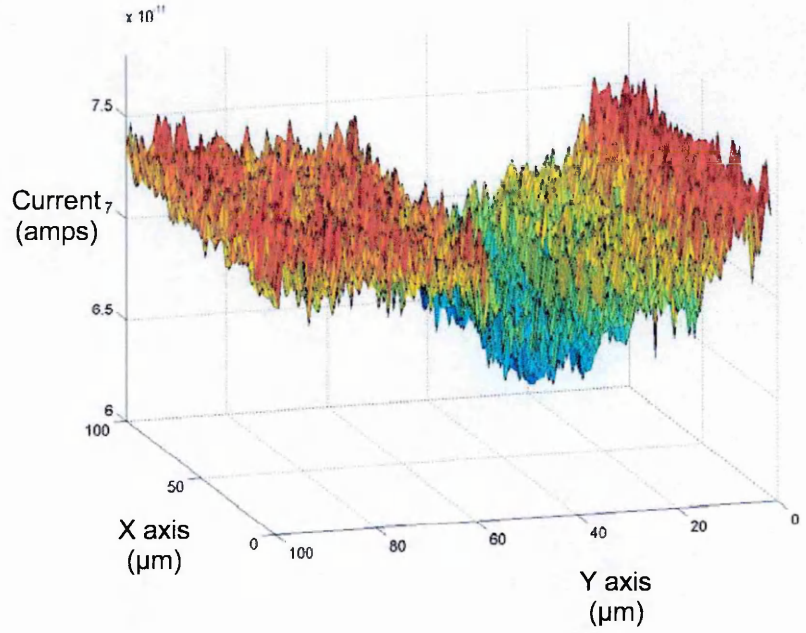

Figure 5.24 Scan of the same area as figure 5.23 with hydrogen peroxide added

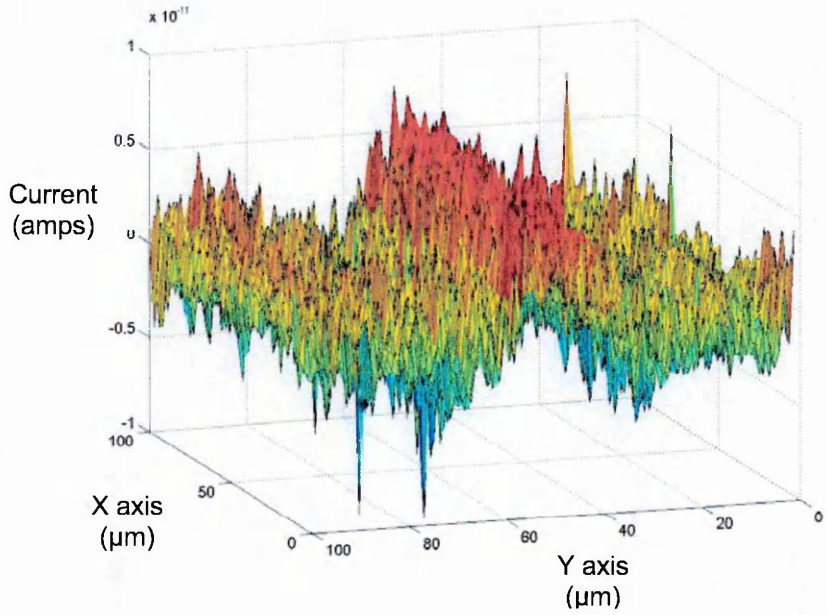

Figure 5.25 Current difference between figures 5.23 and 5.24 representing the effect of hydrogen peroxide

5.8.2 Manually Pipetted Peroxide Biosensors

Figure 5.26 shows the scan of a sensor produced by manually pipetting the enzyme and mediator onto the graphite base. The reduction in feedback current seen to the right of the image (in blue) is most likely due to the sensor coating being thicker causing the probe (at constant height) to become closer to a relatively insulating surface; the area of higher feedback current could be due to a thinner coating of cellulose acetate giving a larger tip to surface distance, or the presence of mediator and enzyme may have created a localised area of greater permeability in the cellulose acetate. When there was hydrogen peroxide present (figure 5.27), there was a three-fold increase in feedback current with an apparently flatter overall response. When the difference in feedback current for each point is plotted (figure 5.28), there is an apparent increase to the right of the image (green through yellow to red) corresponding to the reduction seen in figure 5.26. This suggests that this area had become a relatively more conducting surface in the presence of hydrogen peroxide and this could be attributed to entrapped enzyme and mediator within the cellulose acetate. It could also be due to increased permeability of the cellulose acetate to hydrogen peroxide, but this was considered unlikely because the feedback current obtained for the base graphite electrode (figure 5.25) was a factor of 10 lower and thus, it would be reasonable to conclude that the increase in current is due to the catalytic effect of the enzyme linked to the mediator.

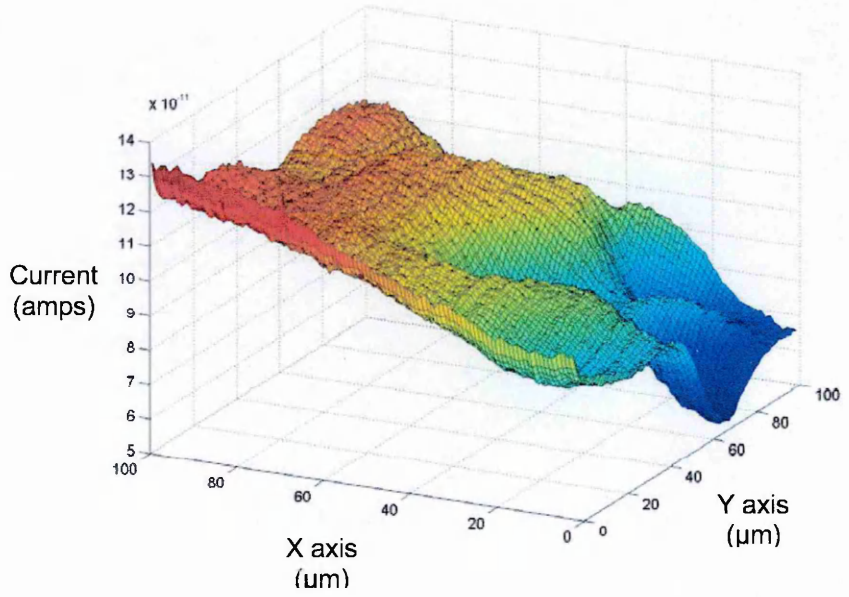

Figure 5.26 Scan of a manually produced peroxide sensor in ferrocyanide and buffer

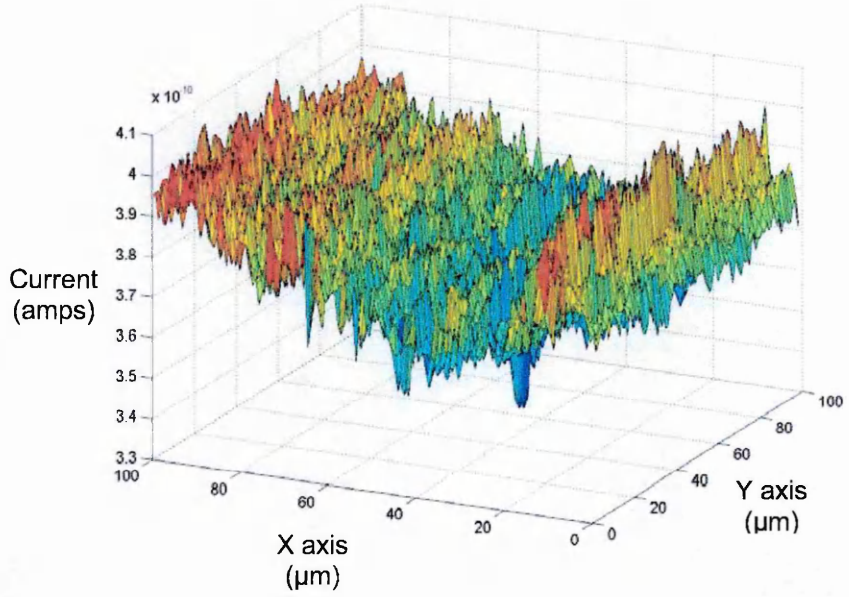

Figure 5.27 Scan of the same area as figure 5.26 with hydrogen peroxide added

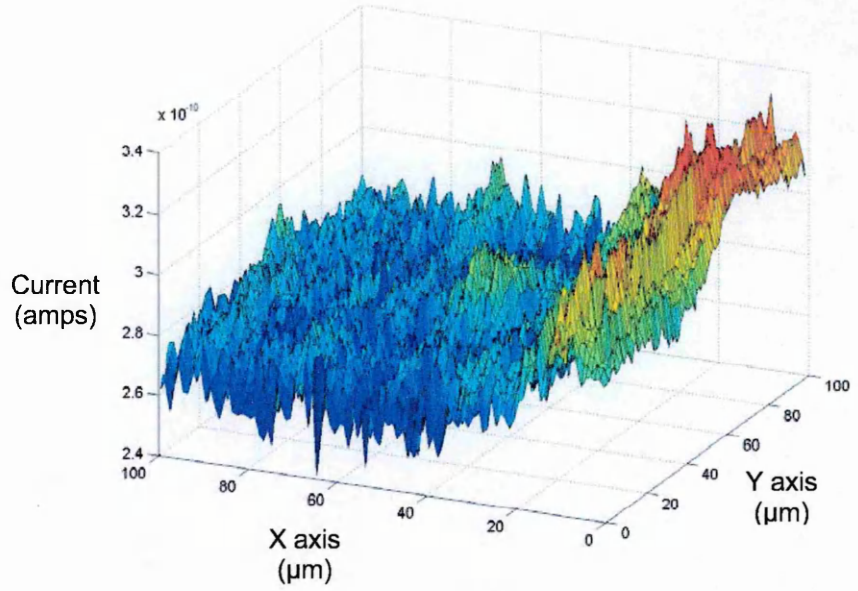

Figure 5.28 Current difference between figures 5.26 and 5.27 representing the effect of hydrogen peroxide

This result would also suggest that there was not an even distribution of enzyme and mediator over the base electrode. This is not surprising considering the appearance of the sensors produced in this way (sensors A, B & C in figure 4.21).

5.8.3 Biodot X-Y3000™ Produced Peroxide Biosensors

Figure 5.29 shows the scan of a sensor produced using the Biodot X-Y3000™ dispensing platform to deposit the enzyme and mediator onto the graphite base. The reduction in feedback current seen as a dip towards the front-left of the scan is again most likely due to the sensor coating being raised above the base electrode causing the probe to become closer to a relatively insulating surface. When there was hydrogen peroxide present (figure 5.30), the back-right part of the scan shows similar feedback current levels to that seen without peroxide present. There is still a fall towards the front-left of the scan but it does not go as low as without peroxide and there is an increase seen at the back-left. When the difference in feedback current for each point is plotted (figure 5.31), there is an apparent increase to the left of the image (orange) corresponding to the reduction seen in both figures 5.29 and 5.30.

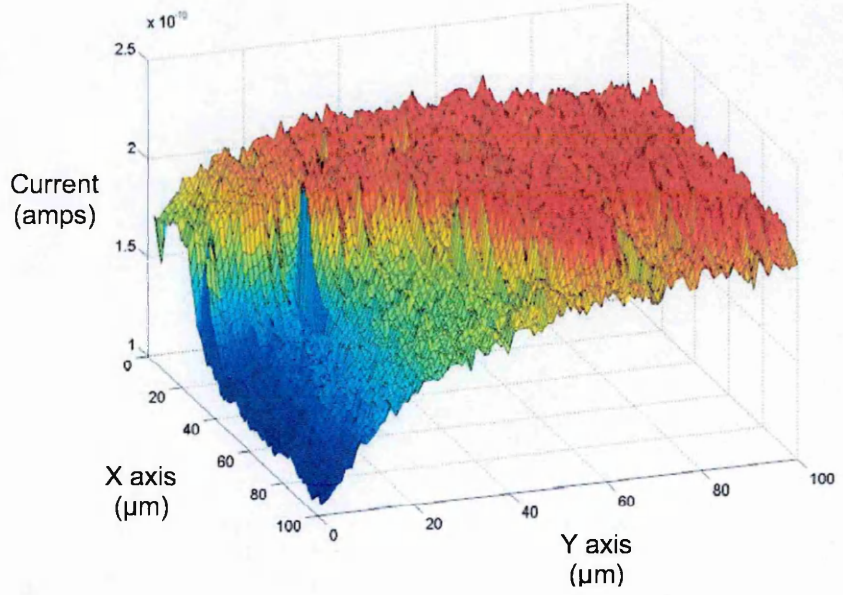

Figure 5.29 Scan of a peroxide sensor in ferrocyanide and buffer

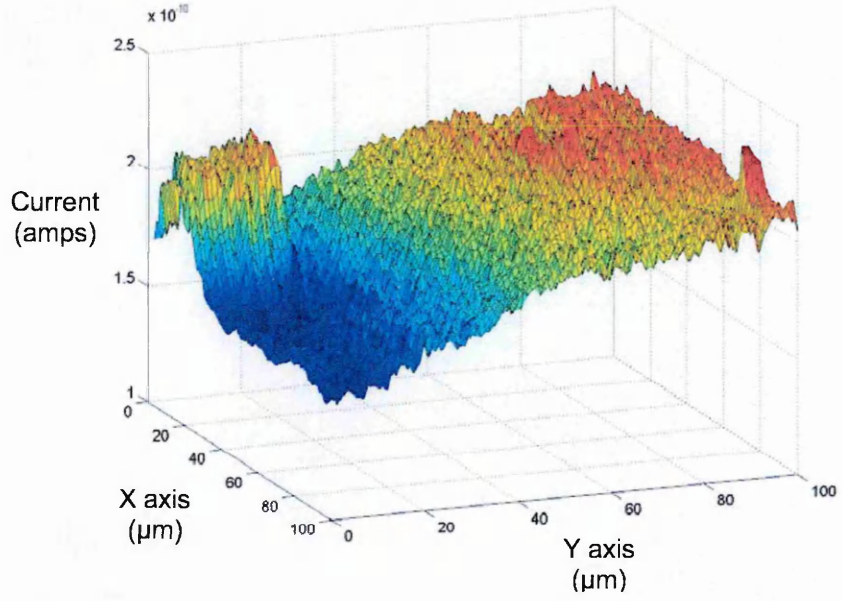

Figure 5.30 Scan of the same area as figure 5.29 with hydrogen peroxide added

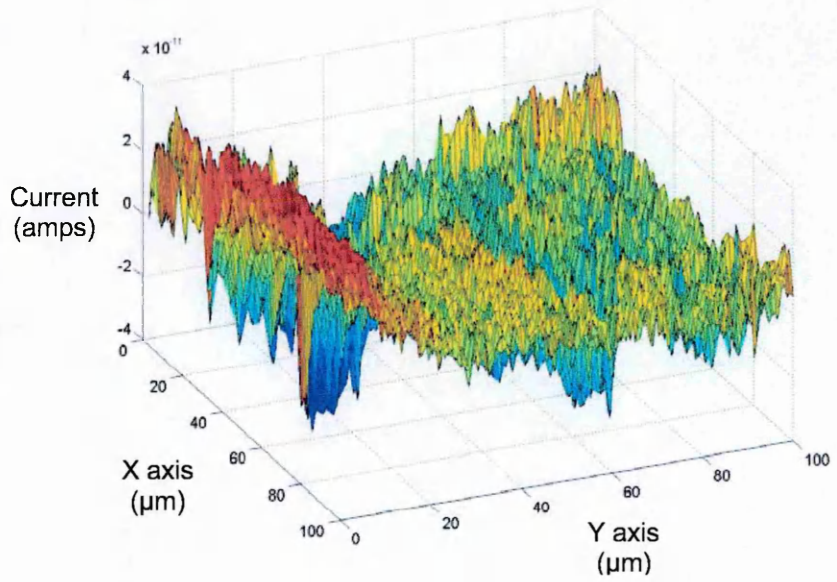

Figure 5.31 Current difference between figures 5.26 and 5.27 representing the effect of hydrogen peroxide

The same possible causes as suggested in section 5.8.2 apply and where there was a smaller increase in feedback current, it would suggest a smaller amount of entrapped enzyme and mediator. This result, as seen with the manually pipetted sensor, suggests that there was an uneven dispersion of enzyme and mediator within the cellulose acetate that was not unexpected with the practical difficulties encountered (section 4.5.1) using the Biodot X-Y3000™ dispensing platform.

5.8.4 SynQUAD™ Dispensing Platform Produced Peroxide Biosensors

As stated earlier in section 4.5.2, the SynQUAD™ dispensing platform allowed the dispensing of much smaller volumes. It thus appeared possible to cover the whole area of the working electrode with 1000 nl of component mixture although the efficiency of the dispersion could not be tested at the production stage. When tested (section 4.7) there was a slightly better performance seen with the application of 4 x 1000 nl compared to 1 x 1000 nl of component mixture. It was hoped that studying the feedback current pattern would indicate if this was due to the effect of loading or dispersion over the surface of the base graphite electrode.

Figure 5.32 shows the scan of a sensor produced with a single 1000 nl application of component mixture using the SynQUAD™ dispensing platform to deposit the enzyme and mediator onto the graphite base. The reduction in feedback current seen as a dip towards the front-right of the scan is, once more, most likely due to the sensor coating being raised above the base electrode causing the probe to become closer to a relatively insulating surface. When there was hydrogen peroxide present (figure 5.33), there was a slight change in the pattern with the peaks at the front left and the back right covering slightly larger areas of the scan and slightly better defined troughs between the peaks. It could also be that some of the peaks at the back right of the scan in figure 5.32 have merged together in figure 5.33. This could be due to the probe scanning at a slightly higher distance above the surface of the sensor, thus reducing the resolution.

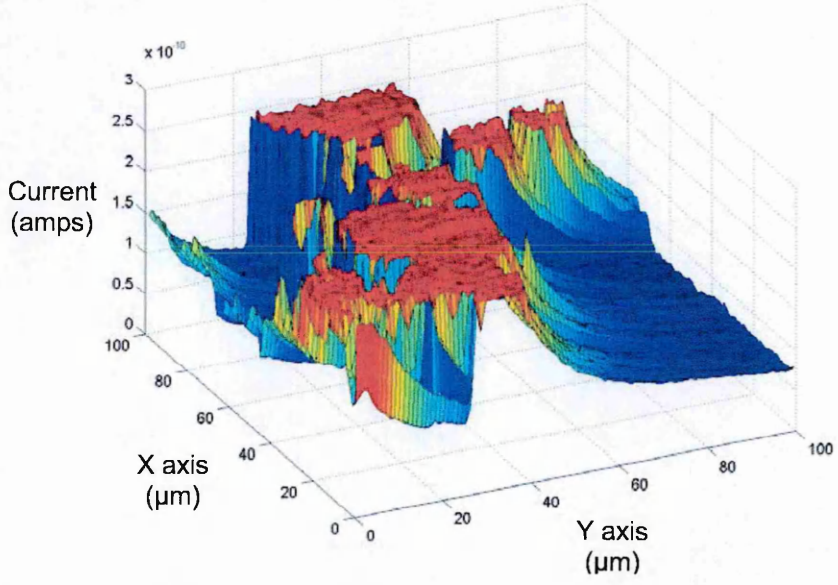

Figure 5.32 Single 1000 nl spot with ferrocyanide and buffer

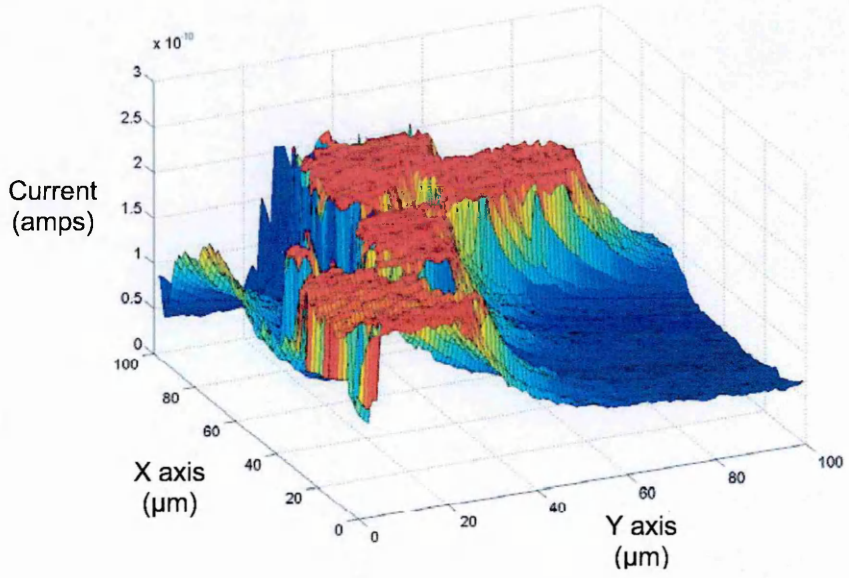

Figure 5.33 Scan of the same area as figure 5.32 with hydrogen peroxide added

When the difference in feedback current for each point was plotted (figure 5.34), the pattern of peaks in feedback current suggested that there was a much better dispersion of enzyme and mediator within the cellulose acetate compared to the sensors produced manually or with the Biodot X-Y3000™ dispensing platform. The areas of lowest feedback current in figure 5.34 are possibly where the cellulose acetate did not spread evenly to cover the base graphite electrode and because of this thinner coating the probe was further away from the surface allowing a greater feedback current due to the disruption of the diffusion layer by the movement of the probe and also the possibility of small areas with no cellulose acetate cover.

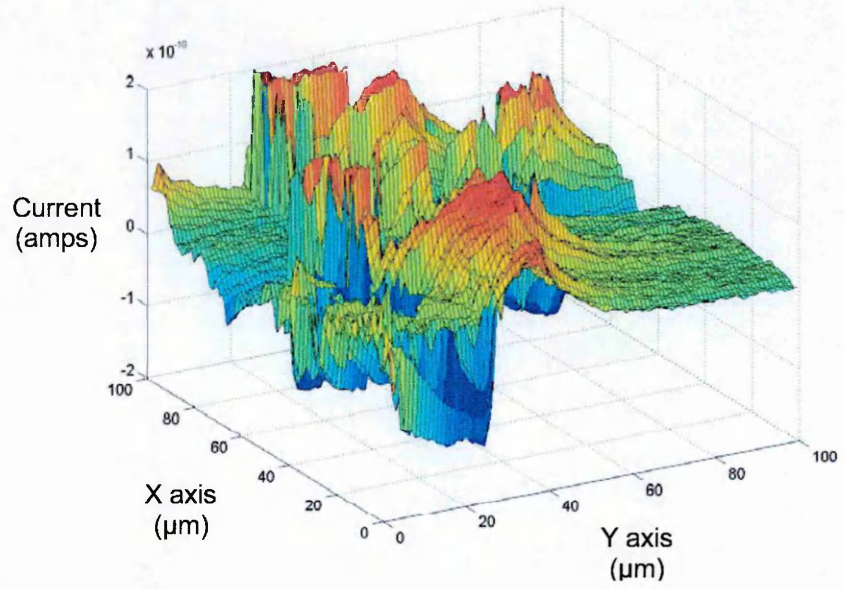

Figure 5.34 Current difference between figures 5.32 and 5.33 representing the effect of hydrogen peroxide

Figure 5.35 shows the scan of a sensor produced with 4 x 1000 nl applications of component mixture using the SynQUAD™ dispensing platform to deposit the enzyme and mediator onto the graphite base.. The reduction in feedback current seen as a trough both to the left and also to the right is again most likely due to the sensor coating being thicker and thus raised higher above the base electrode causing the probe to become closer to a relatively insulating surface. When there was hydrogen peroxide present (figure 5.36), the trough to the left is still apparent, however, the trough to the right has disappeared with just a dip apparent in the middle. When the difference in feedback current for each point is plotted (figure 5.37), the trough to the left is still present and there is still a dip along the right edge. This pattern suggests that the areas of lowest feedback current are where the cellulose acetate is producing an insulating layer at all times and thus no enzyme or mediator is present in these areas. The areas where there is a thinner covering of cellulose acetate with some enzyme and mediator present show a higher background current that becomes more significant in the presence of hydrogen peroxide. The areas of highest feedback current in the absence of hydrogen peroxide are possibly due to the graphite base electrode not being totally covered by a coating of cellulose acetate.

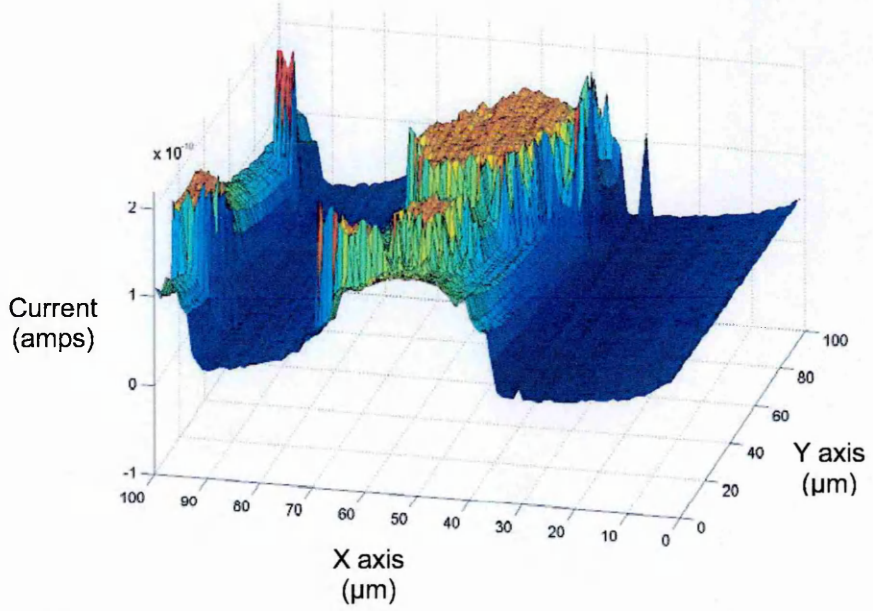

Figure 5.35 4 x 1000 nl spots with ferrocyanide and buffer

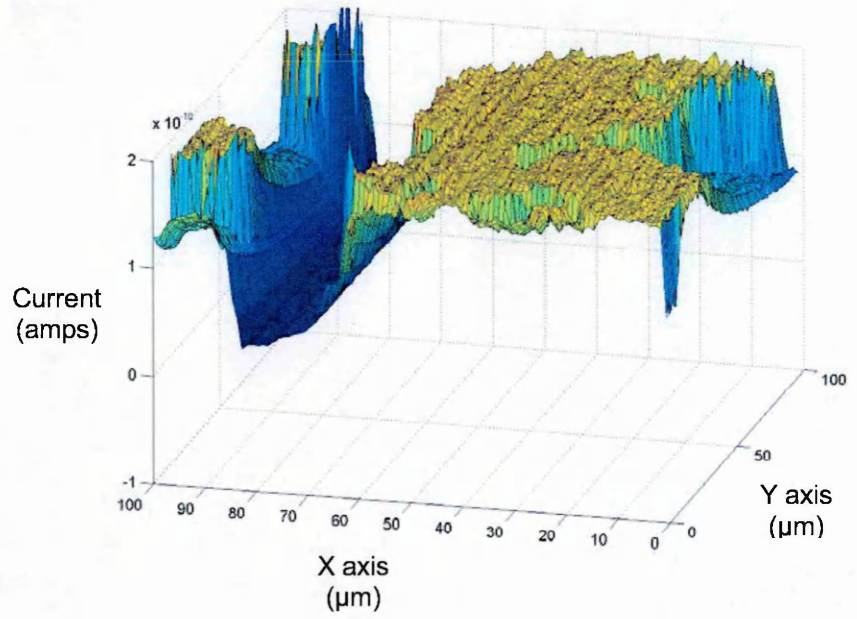

Figure 5.36 Scan of the same area as figure 5.35 with hydrogen peroxide added

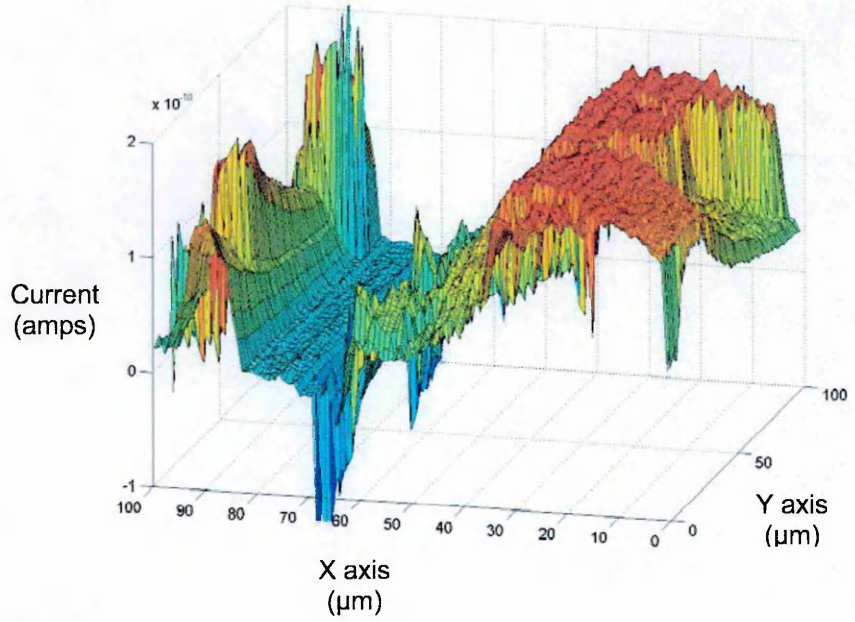

Figure 5.37 Current difference between figures 5.35 and 5.36 representing the effect of hydrogen peroxide

The scan shown in figure 5.38 is of another sensor produced with 4 x 1000 μl application of component mixture and shows a slightly different pattern that still fits the previous analysis. The reduction in feedback current seen as a trough to the right is again most likely due to the sensor coating being raised above the base electrode causing the probe to become closer to a relatively insulating surface. When there was hydrogen peroxide present (figure 5.39), the trough is still apparent. When the difference in feedback current for each point is plotted (figure 5.40), the trough to the right is still present and there are smaller spikes of increased feedback current suggesting a greater dispersion of enzyme and mediator in the coating layer. This pattern again suggests that the areas of lowest feedback current are where the cellulose acetate is producing an insulating layer at all times. The areas where there are localised clumps of enzyme and mediator show a higher background current that becomes more marked in the presence of hydrogen peroxide and the areas of higher feedback current in the absence of hydrogen peroxide are due to the graphite base electrode not being sealed totally by an even coating of cellulose acetate.

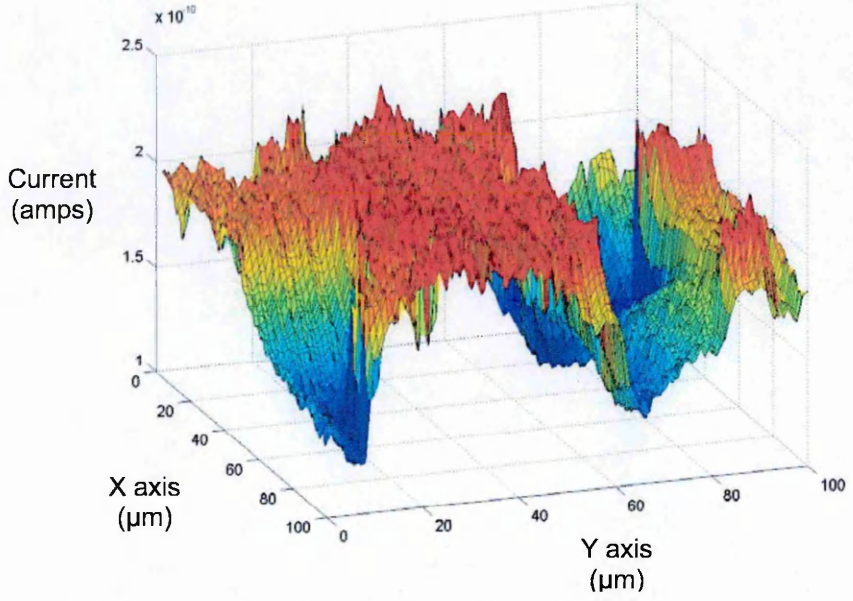

Figure 5.38 4 x 1000 nl spots with ferrocyanide and buffer

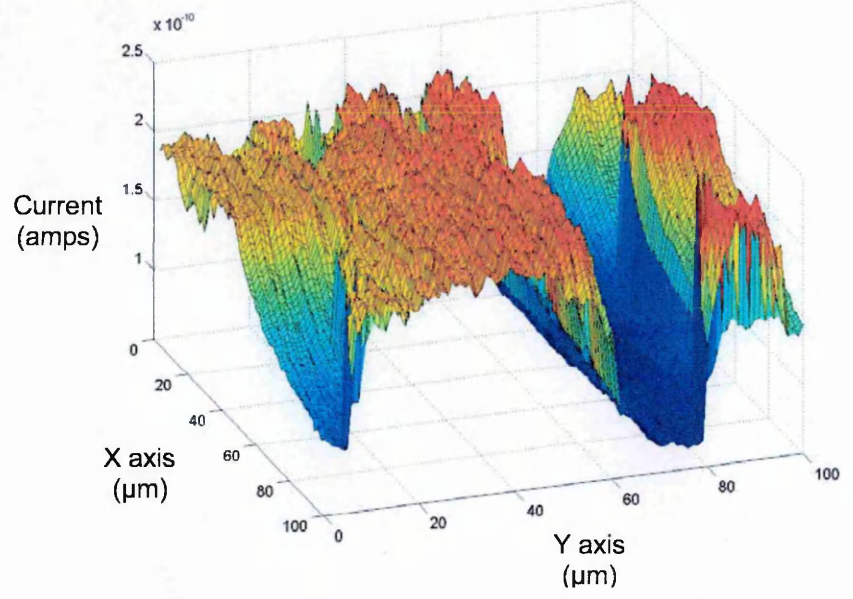

Figure 5.39 Scan of the same area as figure 5.38 with hydrogen peroxide added

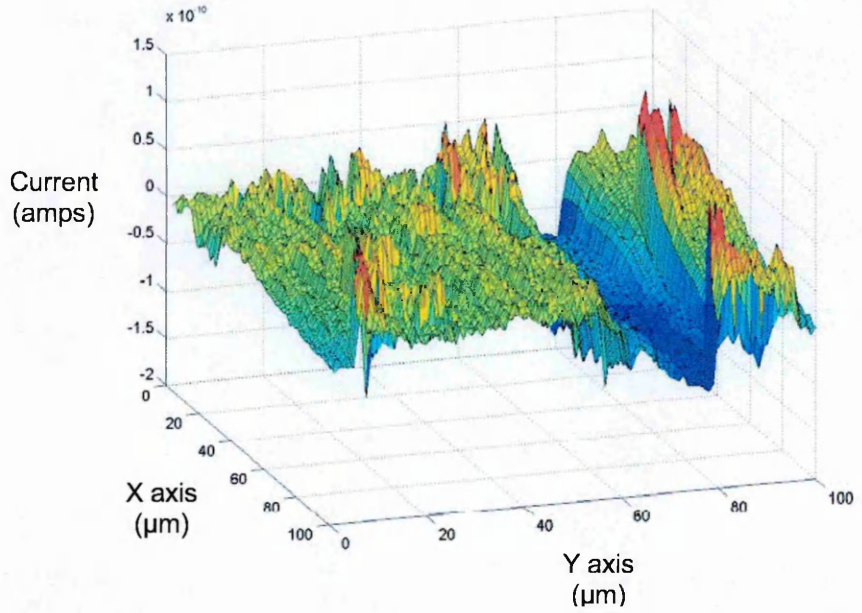

Figure 5.40 Current difference between figures 5.38 and 5.39 representing the effect of hydrogen peroxide

Once again, although an even coverage was not obtained, it appears that sensors produced using the SynQUAD™ dispensing platform had a more even distribution of enzyme and mediator in the cellulose acetate layer. The difference between a single application of 1000 nl of component mixture and four applications of 1000 nl was inconclusive. On the basis of reagent cost however, as the single application produces a working sensor, it would be more cost effective to use this process provided that the performance meets the analytical requirement.

5.8.5 Discussion

By plotting the difference in feedback current between the scans obtained with and without hydrogen peroxide, the image produced is a good representation of the localised change in redox activity at the sensor surface caused by the presence of hydrogen peroxide. It can be hypothesised that this change is due to horseradish peroxidase and 1,1'-dimethylferrocene immobilised within the cellulose acetate layer.

The result of the scans obtained for the base graphite electrode showed no significant current difference between the scans with and without hydrogen peroxide, suggesting

that if there were significant changes seen for the other sensors, then this would most probably be related to the enzyme and mediator within the cellulose acetate layer.

The sensor produced by manual pipetting showed a striking difference between the scans with and without hydrogen peroxide. When the difference between the scans was imaged, there was a relative increase in feedback current corresponding to the area with a fall in feedback current in the absence of hydrogen peroxide; this suggested that the base graphite in this area had a thicker coating containing enzyme and mediator.

The sensor produced using the Biodot dispensing platform showed a lower feedback current in the presence of hydrogen peroxide than the sensor produced by manual pipetting. When the difference due to hydrogen peroxide was imaged, there was a large area that showed little difference in feedback current but the area that showed a fall in feedback current in the absence of hydrogen peroxide still showed a relative increase in feedback current agreeing with the findings for the manually pipetted sensor. The area at the back-left that did not show a fall in feedback current in the absence of hydrogen peroxide but still showed a higher feedback current in the presence of hydrogen peroxide, could be due to an area with a thinner coating of cellulose acetate but still immobilising some enzyme and mediator.

The relatively higher feedback current observed using the manually pipetted sensor with hydrogen peroxide could be due to the tip being further away from the surface of the sensor. The same reason may also be the cause of the higher feedback current observed for the Biodot produced sensor without hydrogen peroxide. Unfortunately, as well as an increase in feedback current, the larger distance between tip and sensor surface results in a lower resolution as suggested in the interpretation of the scans for the single application of 1000 nl of component mix in section 5.8.4, figure 5.33.

When tested as described in section 4.7, there was a slightly better performance seen with the application of 4 x 1000 nl of component mixture compared to the application of 1 x 1000 nl of component mixture. It was hoped that studying the feedback current pattern would indicate if this was due to the effect of loading or dispersion over the surface of the base graphite electrode. The results described above for the two different sensors produced by the application of 4 x 1000 nl of component mixture showed

different levels of dispersion but unfortunately it was not possible to produce more sensors and test them within the time-frame of this work.

As the instrument used for this work has limitations to the size of area that can be scanned with a useful step size, many more scans of adjacent areas need to be performed. Also, repeating the work with alternative bioelectrochemical sensor systems would validate the hypothesis if similar results were obtained.

5.9 Conclusions and Further Work

The scanning electrochemical microscope has been demonstrated as a technique that can be used for the characterisation the surface of a sensor by mapping the distribution of areas of localised electrochemical activity.

The ultramicroelectrode fabrication method developed is inexpensive and robust, producing a probe that can be cleaned and polished several times before it is no longer usable. The diameter of the disc electrode at the tip was reliant upon the manufacturers quoted dimensions for the wire, but with the control resolution of the instrument, this was considered to be sufficient.

With all the problems experienced in commissioning the instrument and its limitations in terms of calibration and data handling there are many modifications that need to be made. Some of these have been suggested to CH Instruments and to date, the only one they have acted upon is to provide a routine to recover the data lost when a scan stops due to a software freeze.

There are many manufacturers of precision positioning devices that can be controlled by a personal computer and also provide a feedback of the current position. When Burleigh Instruments Inc. that manufactured the inchworm motors were contacted, they said that they manufactured such devices and the feedback position data can be used by third-party software for other purposes. CH Instruments claimed that the data could not be used in this way.

As the instrument was only finally commissioned at the end of the time available for this thesis there is a considerable amount of further work that could be performed. If possible, a custom built instrument should be used as this could allow the scanning of much larger areas of a sensor surface. Also, a translation stage using a system with position feedback would improve reproducibility and remove the need for time-consuming calibration processes. If this instrument cannot be built, then adjacent areas should be scanned and the data obtained linked together to provide a much larger surface area to interpret.

6. Final Conclusions and Future Work

6.1 Meeting the Original Objective

The objective of this thesis was to research and develop a biosensor for hydrogen peroxide that could meet the requirements of a food or beverage production facility such as the König brewery in Germany.

6.1.1 Component Selection and Optimisation

In chapter two, the construction of the sensor and selection of the active components was described with consideration towards the analytical needs and cost. The selection of a screen-printed base three-electrode system was made based upon experience within the University department and its suitability for a mass production process. The final choice of horseradish peroxidase as the enzyme was made based on cost compared to other potentially suitable enzymes. The mediator 1,1'-dimethylferrocene was selected after testing three candidates found from a search of the literature and provided the optimum balance between cost, stability and low solubility in aqueous solution. The membrane material, cellulose acetate, was selected after testing two candidates suitable for a mass production process found from a search of the literature and provided the lower cost and better stability required.

These selections met the first key requirement given in the introduction that a commercially viable sensor should have relatively low production costs.

In chapter three, the component proportions were optimised to give the best performance within the desired analytical range.

6.1.2 Sensor Testing and Operation

In chapter four, the testing of the sensor was described. In the laboratory, the sensor was shown to meet the stability requirement by lasting at least 4 days in continuous use in a flow cell environment. The lower limit of detection of the sensor was shown to be low

enough to enable a sufficiently large dilution of the wash solution in the buffer that it did not need additional pH adjustment.

The sensor was compared to the other methods developed within the EUROPEROX project for monitoring hydrogen peroxide levels in wash solutions. It was shown to perform well and was shown to be potentially usable for monitoring peroxyacetic acid levels under similar conditions.

When considering the remaining key requirements given in the introduction, these have also been met:

1. The operating costs of the sensor could not really be lower as the only reagent it requires is phosphate buffer. In addition, with a minimum stability of four days the sensor could not be considered as a high cost item.

2. The sensor was readily incorporated into the on-line monitoring system at the König brewery within minutes for the successful on–line study. The results obtained in this study also corresponded well with a parallel trial performed by one of the industrial partners in the EUROPEROX consortium using a colorimetric technique. Unfortunately, due to the commercial nature of the information, the company do not wish to release these results at this stage of their product development and therefore they cannot be reported here.

3. Routine maintenance is minimal and simple enough for a semi-skilled operator to perform. The only reagent production required is a simple buffer and for a commercial system, the flow cell could be designed for an even simpler exchange of sensors.

6.1.3 Sensor Production

From the outset of the development work, the base electrode was produced economically by screen-printing using readily available inks. In chapter four, several processes were considered for the application of the active components onto the graphite base electrode in a production process; consideration was once more given

towards cost as well as performance in the selection of the synQUAD™ dispensing platform and in pre-mixing all the components before application.

The sensor can be produced in the laboratory at a unit cost of less than £ 0.01 for materials. It is not possible to calculate a full costing projection for a commercially produced sensor as labour costs and equipment overheads would depend on the scale of production. By buying the raw materials in bulk there would be considerable savings in costs taking the unit cost even lower. As the current wholesale price of widely used blood glucose sensors is around £ 0.30, this would indicate that the sensor could be commercially produced at a comparable price even allowing for marketing and distribution overheads.

6.1.4 Surface Characterisation

Having developed a working sensor, light microscopy was used to show that a more even visual appearance to the coated electrode surface resulted in larger signal currents and better reproducibility of sensor-to-sensor response.

A scanning electrochemical microscope was commissioned in the hope that the information gained about the dispersion of localised surface activity could be used to aid in the development of a mass production process for the final sensor. Initial results have indicated that this is possible in the future with further development to the instrument.

6.2 Future Work

6.2.1 Sensor Production

The use of the synQUAD™ dispensing platform showed that the working area of the sensor could be evenly coated with less than 4 µl of the component mix. As this would reduce production costs, it would be worthwhile investigating further. The optimisation process was performed with sensors produced by the manual pipetting of a 4 µl layer, as the dispensing platform was not available for development work within the department and therefore, the optimisation would have to be re-validated.

For mass production, larger quantities of the component mix would need to be made. This would pose the problems of solvent evaporation and suspension settlement. It should be possible to incorporate a chilled reservoir with built-in sonication onto the dispensing platform to overcome both of these issues.

6.2.2 Sensor Validation

The sensor has been shown to work successfully in a single field study and all of its production steps have been developed with the potential for mass-production. If suitable commercial interest could be found, then a pilot production process would need to be developed and a rigidly controlled field evaluation performed.

6.2.2 Flow-cell

The exchange of a sensor in the prototype flow cell requires only that four retaining bolts are released, the sensor replaced and the bolts be tightened. In a commercially produced product, the flow cell could be design to have spring-loaded clamps and the shape of the sensors designed with location pin cutaways to ensure correct placement in the flow cell.

6.2.3 Optical Microscopy

Optical microscopy has been used to demonstrate obvious visual differences between the evenness of coating of the sensor surface using manual and automated techniques. These images have been gathered using a digital camera and thus for quality control procedures in a production process, this could be incorporated using digital image matching techniques that are already in place in many other manufacturing situations.

6.2.4 Scanning Electrochemical Microscopy

In the final chapter, the scanning electrochemical microscope was investigated as a technique for characterising the surface of the final sensor. Unfortunately, the instrument took several months to commission, with various issues that had to be the solved before any sensors could be studied. The preliminary results obtained from a small sample of sensors suggested that the technique might provide useful information regarding the distribution of the active components over the working electrode surface.

To achieve this, better control of the positioning mechanism is needed along with the facility to gather more than 512 data points in each of the X and Y-axes. This could be achieved by the use of inchworm motors with positional feedback and improved control software.

7. References

Abdel-Hamid, L., Atanasov, P. & Wilkins, E. (1995). Development of a needle-type biosensor for intravascular glucose monitoring. *Analytica Chimica Acta.* **313:** 45-54.

Adeyoju, O., Iwuoha, E. I. & Smyth. M. R. (1995). Reactivities of amperometric organic-phase peroxidase-modified electrodes in the presence and absence of thiourea and ethylenethiourea as inhibitors. *Analytica Chimica Acta.* **305:** 57-64.

Alvarez-Icaza, M. & Bilitewski, U. (1993). Mass production of biosensors. *Analytical Chemistry.* **65:** 525-533

Amine, A., Kauffmann, J. M., Guilbault, G. G. & Bacha, S. (1993). Characterisation of mixed enzyme-mediator-carbon paste electrodes. *Analytical Letters.* **26:** 1281-1299.

Bard, A. J., Fan, F. F., Kwak, J. & Lev, O. (1989). Scanning electrochemical microscopy. Introduction and principles. *Analytical Chemistry.* **61:** 132-138.

Barker, A. L., Gonsalves, M., Macpherson, J. V., Slevin, C. J. & Unwin, P. R. (1999). Scanning electrochemical microscopy: Beyond the solid/liquid interface. *Analytica Chimica Acta.* **385:** 223-240.

Benmakroha, Y., Christie, I., Desai, M. & Vadgama, P. (1996). Poly(vinyl chloride), polysulfone and sulfonated polyether-ether sulfone composite membranes for glucose and hydrogen-peroxide permselectivity in amperometric biosensors. *The Analyst.* **121:** 521-526.

Bilitewski, U., Drewes, W., Neermann, J., Schrader, J., Surkow, R., Schmid, R. D. & Bradley, J. (1993). comparison of different biosensor systems suitable for bioprocess monitoring. *Journal of Biotechnology.* **31:** 257-266.

Borgwarth, K., Ricken, C., Ebling, D.G. & Heinze, J. (1995). Surface characterization and modification by the scanning electrochemical microscope (SECM). *Berichte Der Bunsen-Gesellschaft-Physical Chemistry Chemical Physics.* **99:** 1421-1426.

Cardosi, M. F. & Birch, S. W. (1993). Screen printed glucose electrodes based on platinised carbon particals and glucose oxidase. *Analytica Chimica Acta.* **276:** 69-74.

Cardosi, M. F. (1994). Hydrogen peroxide-sensitive electrode based on horseradish peroxidase-modified platinized carbon. *Electroanalysis.* **6:** 89-96

Chen, Z. F. & Wang, E. (1994). Fabrication and characterisation of tips for electrochemical scanning tunneling microscopy. *Electroanalysis.* **6:** 672-676.

CH Instruments. (1998). Scanning electrochemical microscope manual

Christensen, C. S., Brodsgaard, S., Mortensen, P., Egmose, K. & Linde, S. A. (2000). Determination of hydrogen peroxide in workplace air: Interferences and method validation. *Journal of Environmental Monitoring.* **2:** 339-343

Chut, S. L., Li, J. & Tan, S. N. (1997). A mediated turnip tissue-based amperometric hydrogen peroxide biosensor. *Analytical Letters.* **30:** 1993-1998

Collins English Dictionary. (1979).

Conn & Stumpf (1976) Outlines of biochemistry - 4th Edition. John Wiley & sons.

Cosgrove, M., Moody, G. J. & Thomas, J. D. R. (1988). Chemically immobilised enzyme electrodes for hydrogen peroxide determination. *The Analyst.* **113:** 1181-1815.

Csoregi, E., Gorton, L. & Marko-Varga, G. (1994a). Amperometric microbiosensors for detection of hydrogen peroxide and glucose based on peroxidase-modified carbon fibers. *Electroanalysis.* **6:** 925-933.

Csoregi, E., Gorton, L., Marko-Varga, G., Tudos, A. J. & Kok, W. T. (1994b). Peroxidase-modified carbon-fiber microelectrodes in flow-through detection of hydrogen-peroxide and organic peroxides. *Analytical Chemistry.* **66:** 3604-3610.

Dong, S. J. & Li, J. H. (1997). Self-assembled monolayers of thiols on gold electrodes for bioelectrochemistry and biosensors. *Bioelectrochemistry And Bioenergetics.* **42:** 7-13.

Dunford, H. B. (1982). Peroxidases. *Advances In Inorganic Biochemistry.* **4:** 41-68.

Effkemann, S., Brodsgaard, S., Mortensen, P., Linde, S. A. & Karst, U. (1999). Determination of gas phase peroxyacetic acid using pre-column derivatization with organic sulfide reagents and liquid chromatography. *Journal of Chromatography A.* **855:** 551-561.

Effkemann, S., Pinkernell, U. & Karst, U. (1998). Peroxide analysis in laundry detergents using liquid chromatography. *Analytica Chimica Acta.* **363:** 97-103.

Elvers, B., Hawkins, S., Ravenscroft, M. & Schultz, G. (1991). Ullman's Encyclopedia of Industrial Chemistry. 5th edition. VCH Publishers, NY. Volume A13. 443-466.

Engstrom, R. C., Meaney, T., Tople, R. & Wightman R. M. (1987). Spatiotemporal description of the diffusion layer with a microelectrode probe. *Analytical Chemistry.* **59:** 2005-2010.

Epton, R., Hobson, M. E. & Marr, G. (1978). Oxidation of ferrocene and some substituted ferrocenes in the presence of horseradish peroxidase. *Journal of Organometallic Chemistry.* **149:** 231-244.

Ferapontova, E. E., Grigorenko, V. G., Egorov, A. M., Borchers, T., Ruzgas, T. & Gorton, L. (2001). Direct electron transfer in the system gold electrode-recombinant horseradish peroxidases. *Journal of Electroanalytical Chemistry.* **509:** 19-26.

Fernandez, A. I. S., Calzon, J. A. G., Garcia, A. C. & Blanco, P. T. (1991). Simple and reliable fabrication of carbon fiber ultramicroelectrodes. *Electroanalysis.* **3:** 413-417.

Fisher, A. C. (1996). Electrode Dynamics. Oxford Unversity Press.

Forber, C. L. (1992). Twenty-first century bleaching will be a challenging lottery. *Pulp & Paper.* November 1992. Pp.90-97.

Frew, J. E., Jones, J. & Scholes, G. (1983). Spectrophotometric determination of hydrogen peroxide and organic hydroperoxides at low concentrations in aqueous solution. *Analytica Chimica Acta.* **155:** 139-150.

Frew, J. E. & Hill, H. A. O. (1988). Direct and indirect electron transfer between electrodes and redox proteins. *European Journal of Biochemistry.* **172:** 261-269.

Gilmartin, M. A. T. & Hart, J. P. (1995). Sensing with chemically and biologically modified carbon electrodes. *The Analyst.* **120:** 1020-1045.

Goldberg, H. D., Brown, R. B., Liu D. P. & Meyerhoff M. E. (1994). Screen printing: A technology for the batch fabrication of integrated chemical-sensor arrays. *Sensors and Actuators B-Chemical.* **21:** 171-183.

Gooding, J. J. Hall, C. E. & Hall, E. A. H. (1997). Physical study of film-forming acrylate emulsion polymers for biosensor applications. *Analytica Chimica Acta.* **349:** 131-141.

Goral, V. N. & Ryabov, A. D. (1998). Reactivity of the horseradish peroxidase compounds I and II toward organometallic substrates. A stopped-flow kinetic study of oxidation of ferrocenes. *Biochemistry and Molecular Biology International.* **45:** 61-71.

Gorton, L. (1985). A carbon electrode sputtered with palladium and gold for the amperometric determination of hydrogen peroxide. *Analytica Chimica Acta.* **178:** 247-253.

Gorton, L., Bremle, G., Csoregi, E., Jonsson Pettersson, G. & Persson, B. (1991). Amperometric glucose sensors based on immobilized glucose-oxidizing enzymes and chemically modified electrodes. *Analytica Chimica Acta.* **249:** 43-54.

Green, M. J. & Hill, H. A. O. (1986). Amperometric enzyme electrodes. *Journal of the Chemical Society-Faraday Transactions.* **82:** 1273-1243.

Guerrieri, A., De Benedetto, G. E. & Zambonin, P. G. (1998). Electrosynthesized non-conducting polymers as permselective membranes in amperometric enzyme electrodes: A glucose biosensor based on a co-crosslink glucose oxidase/overoxidised polypyrrole bilayer. *Biosensors & Bioelectronics.* **13:** 103-112.

Harms, D., Than, R., Krebs, B. & Karst, U. (1999a). Flow injection analysis of hydrogen peroxide in disinfectants. *Fresenius Journal of Analytical Chemistry.* **364:** 184-188.

Harms, D., Meyer, J., Westerheide, L., Krebs, B. & Karst, U. (1999b). Determination of glucose in soft drinks using its enzymatic oxidation and the detection of formed hydrogen peroxide with a dinuclear iron(III) complex. *Analytica Chimica Acta.* **401:** 83-90.

Harms, D. (2001). König Brewery. Personal Communication.

Hart, A. L., Turner, A. P. F. & Hopcroft, D. (1996). On the use of screen- and ink-jet printing to produce amperometric enzyme electrodes for lactate. *Biosensors & Bioelectronics.* **11:** 263-270.

Heller, A. (1990). Electrical wiring of redox enzymes. *Accounts of Chemical Research.* **23:** 129-134.

Jawaheer, Shobha. (1999). Cranfield University. Personal Communication.

Johansson, K., Jonsson Pettersson, G., Gorton, L., Marko-Varga, G. & Csoregi, E. (1993). A reagentless amperometric biosensor for alcohol detection in column liquid-chromatography based on co-immobilized peroxidase and alcohol oxidase in carbon-paste. *Journal Of Biotechnology.* **31:** 301-316.

Kalab, T. & Skladal, P. (1995). A disposable amperometric immunosensor for 2,4-dichlorophenoxyacetic acid. *Analytica Chimica Acta.* **304:** 361-368.

Karyakin, A. A., Karyakina, E. E. & Gorton, L. (1996). Prussian-blue-based amperometric biosensors in flow-injection analysis. *Talanta.* **43:** 1597-1606.

Kenausis, G., Chen, Q. & Heller, A. (1997). Electrochemical glucose and lactate sensors based on "wired" thermostable soybean peroxidase operating continuously and stably at 37 degrees C. *Analytical Chemistry.* **69:** 1054-1060.

Koochaki, Z., Christie, I. & Vadgama, P. (1991). Electrode responses to phenolic species through cellulosic membranes. *Journal Of Membrane Science.* **57:** 83-94.

Korell, U. & Spichiger, U. E. (1994). Novel membraneless amperometric peroxide biosensor based on a tetrathiafulvalene-p-tetracyanoquinodimethane electrode. *Analytical Chemistry.* **66:** 510-515.

Kranz, C., Lotzbeyer, T., Schmidt, H. L. & Schuhmann, W. (1997). Lateral visualization of direct electron transfer between microperoxidase and electrodes by means of scanning electrochemical microscopy. *Biosensors & Bioelectronics.* **12:** 257-266.

Kröger, S. & Turner, A. P. F. (1997). Solvent-resistant carbon electrodes screen printed onto plastic for use in biosensors. *Analytica Chimica Acta.* **347:** 9-18.

Krüßmann, H. & Bohnen, J. (1994). On-line-analytik für peressigsäure. *Tenside Surfactants. Deterg.* **31:** 229-232.

Kulys, J. J., Schuhmann, W. & Schmidt, H-L. (1992). Carbon-paste electrodes with incorporated lactate oxidase and mediators. *Analytical Letters.* **25:** 1011-1024.

Kunzelmann, U. & Bottcher, H. (1997). Biosensor properties of glucose oxidase immobilized within SiO_2 Gels. *Sensors And Actuators B-Chemical.* **39:** 222-228.

Lee C. M., Wipf D. O., Bard A. J., Bartels K. & Bovik A. C. (1991). Scanning electrochemical microscopy 11. Improvement of image-resolution by digital processing techniques. *Analytical Chemistry.* **63:** 2442-2447.

Liu, H., Kong, J. & Deng, J. (1995a). An amperometric lactate sensor using tetrathiafulvalene in Ppolyester ionomer film as electron transfer. *Analytical Letters.* **28:** 563-579.

Liu, H., Qian, J., Liu, Y., Yu, T. & Deng, J. (1995b). Nickelocene-mediating sensor for hydrogen peroxide based on bioelectrocatalytic reduction of hydrogen peroxide. *Analytical Communications.* **32:** 475-477.

Liu, H. Y., Fan, F. R. F., Lin, C. W. & Bard, A. J. (1986). Scanning electrochemical and tunneling ultramicroelectrode microscope for high-resolution examination of electrode surfaces in solution. *Journal of the American Chemical Society.* **108:** 3838-3839.

Liu, H. Y., Ying, T. L., Sun, K., Li, H. H. & Qi, D. Y. (1997). Reagentless amperometric biosensors highly sensitive to hydrogen peroxide, glucose and lactose based on N-methyl phenazine methosulfate incorporated in a nafion film as an electron transfer mediator between horseradish peroxidase and an electrode. *Analytica Chimica Acta.* **344:** 187-199.

Lotzbeyer, T., Schuhmann, W., Katz, E., Falter, J. & Schmidt, H. L. (1994). Direct electron-transfer between the covalently immobilized enzyme microperoxidase mp-11 and a cystamine-modified gold electrode. *Journal Of Electroanalytical Chemistry.* **377:** 291-294.

Lowe, C. R. (1985). An introduction to the concepts and technology of biosensors. *Biosensors.* **1:** 3-16.

Marzouk, S. A. M., Cosofret, V. V., Buck, R. P., Yang, H., Cascio, W. E. & Hassan, S. S. M. (1997). Amperometric monitoring of lactate accumulation in rabbit ischemic myocardium. *Talanta.* **44:** 1527-1541.

Meyer, J. & Karst, U. (1999). Workplace monitoring of gas phase hydrogen peroxide by means of fluorescence spectroscopy. *Analytica Chimica Acta.* **401:** 191-196

Mirkin, M. V. & Horrocks, B. R. (2000). Electroanalytical measurements using the scanning electrochemical microscope. *Analytica Chimica Acta.* **406:** 119-146

Moore, A. N. J., Katz, E. & Willner, I. (1996). Electrocatalytic reduction of organic peroxides in organic solvents by microperoxidase-11 immobilized as a monolayer on a gold electrode. *Journal Of Electroanalytical Chemistry.* **417:** 189-192.

Morales, A., Cespedes, F., Munoz, J., Martinezfabrega, E. & Alegret, S. (1996). Hydrogen peroxide amperometric biosensor based on a peroxidase-graphite-epoxy biocomposite. *Analytica Chimica Acta.* **332:** 131-138.

Mukerjee, S. (1990). Reviews of applied electrochemistry 23. Particle size and structural effects in platinum electrocatalysis. *Journal of Applied Electrochemistry.* **20:** 537-548.

Myler, S., Eaton, S. & Higson, S. P. J. (1997). Poly(o-phenylenediamine) ultra-thin polymer-film composite membranes for enzyme electrodes. *Analytica Chimica Acta.* **357:** 55-61.

Newman, J. D., White, S. F., Tothill, I. E. & Turner, A. P. F. (1995). Catalytic materials, membranes, and fabrication technologies suitable for the construction of amperometric biosensors. *Analytical Chemistry.* **67:** 4594-4599.

Newman, J. D, White S. F., Tothill, I. E. & Turner, A. P. F. (1997). An instrument for on-line monitoring of fermentations using FIA and amperometric biosensors. *Abstracts of Papers of the American Chemical Society.* **213:** 59-BTEC.

Okawa, Y., Nagano, M., Hirota. S., Kobayashi, H., Ohno. T. & Watanabe, M. (1999). Tethered mediator biosensor. Mediated electron transfer between redox enzyme and electrode via ferrocene anchored to electrode surface with long poly(oxyethylene) chain. *Biosensors & Bioelectronics.* **14:** 229-235.

Ortiz, G., Gonzalez, M. C,. Reviejo, A. J. & Pingarron, J M. (1997). Graphite-poly(tetrafluoroethylene) composite enzyme electrodes as suitable biosensors in predominantly nonaqueous media. *Analytical Chemistry.* **69:** 3521-3526.

Pandey P. C., Upadhyay S. & Upadhyay B. (1997). Peroxide biosensors and mediated electrochemical regeneration of redox enzymes. *Analytical Biochemistry.* **252:** 136-142.

Pinkernell, U., Effkemann, S., Nitzsche, F. and Karst, U. (1996). Rapid high-performance liquid chromatographic method for the determination of peroxyacetic acid. *Journal of Chromatography.* **730:** 203-208.

Pinkernell, U., Luke, H. J. & Karst, U. (1997). Selective photometric determination of peroxycarboxylic acids in the presence of hydrogen peroxide. *The Analyst.* **122:** 567-571.

Popescu, I. C., Zetterberg, G. & Gorton, L. (1995). Influence of graphite powder, additives and enzyme immobilization procedures on a mediatorless HRP-modified carbon-paste electrode for amperometric flow-injection detection of H_2O_2. *Biosensors & Bioelectronics.* **10:** 443-461.

Reddy, S. M., Higson, S. P. J., Christie, I. M. & Vadgama, P. M. (1994). Selective membranes for the construction and optimization of an amperometric oxalate enzyme electrode. *The Analyst.* **119:** 949-952.

Reslow, M., Adlercreutz, P. & Mattiasson, B. (1987). Organic solvents for bioorganic synthesis: 1. Optimisation of parameters for chymotrypsin catalyzed process. *Applied Microbiology and Biotechnology.* **26:** 1-8.

Rohm, L., Genrich, M., Collier, W. & Bilitewski, U. (1996). Development of ultraviolet-polymerizable enzyme pastes: bioprocess applications of screen printed L-lactate sensors. *The Analyst.* **121:** 877-881.

Russell, A., Repka, K., Dibble, T., Ghoroghchian, J., Smith, J. J., Fleischmann, M., Pitt, C. H. & Pons, S. (1986). Determination of electrochemical heterogeneous electron-transfer reaction-rates from steady-state measurements at ultramicroelectrodes. *Analytical Chemistry.* **58:** 2961-2964.

Ryabov, A. D., Goral, V. N., Ivanova, E. V., Reshetova, M. D., Hradsky, A. & Bildstein, B. (1999). Linear free-energy relationships and inverted Marcus region in the horseradish peroxidase-catalyzed oxidation of ferrocenes by hydrogen peroxide. *Journal of Organometallic Chemistry.* **589:** 85-91.

Saini, S. S. (1993). Organic Phase Electrodes. *PhD Thesis.* Cranfield University.

Saini, S. & Turner, A. P. F. (1991). Biosensors in organic phases. *Biochemical Society Transactions.* **19:** 28-31.

Saini, S., Hall, G. F., Downs, M. E. A. & Turner, A. P. F. (1991). Organic phase enzyme electrodes. *Analytica Chimica Acta.* **249:** 1-15.

Sampath, S. & Lev, O. (1997). Membrane-free, rhodium-modified, methyl silicate-graphite amperometric biosensor. *Journal Of Electroanalytical Chemistry.* **426:** 131-137.

Sanchez, P. D., Ordieres, A. J. M., Garcia, A. C. & Blanco, P. T. (1991). Peroxidase ferrocene modified carbon paste electrode as an amperometric sensor for the hydrogen-peroxide assay. *Electroanalysis.* **3:** 281-285.

Schneider, P. M. (1993). Low-temperature sterilization alternatives in the 1990s. *Tappi Journal.* **77**: 115-119.

Schubert, F. Saini, S. Turner, A. P. F. (1991). Mediated amperometric enzyme electrode incorporating peroxidase for the determination of hydrogen-peroxide in organic-solvents. *Analytica Chimica Acta.* **245:** 133-138.

Schubert, F., Saini, S., Turner, A. P. F. & Scheller, F. (1992). Organic-phase enzyme electrodes for the determination of hydrogen-peroxide and phenol. *Sensors and Actuators B-Chemical.* **7:** 408-411.

Scott, E. R., White, H. S. & Phipps, J. B. (1991). Scanning electrochemical microscopy of a porous membrane. *Journal of Membrane Science.* **58:** 71-87.

Slevin, C. J., Gray, N. J., Macpherson, J. V., Webb, M. A. & Unwin, P. R. (1999). Fabrication and characterisation of nanometre-size platinum electrodes for voltammetric analysis and imaging. *Electrochemistry Communications.* **1:** 282-288.

Selkirk, J. Y. (1997). *PhD Thesis*. Cranfield University.

Southampton Electrochemistry Group. (1990). Instrumental methods in electrochemistry. Ellis Horwood.

Spohn, U., Narasaiah, D. & Gorton, L. (1997). Reagentless hydrogen peroxide and L-lactate sensors based on carbon paste electrodes modified with different peroxidases and lactate oxidases. *Journal Fur Praktische Chemie-Chemiker-Zeitung.* **339:** 607-614.

Thévenot, D. R., Toth, K., Durst, R. A. and Wilson, G. S. (1999). Electrochemical biosensors: Recommended definition and classification. *Pure and Applied Chemistry.* **71:** 2333

Turner, A. P. F., Karube, I. & Wilson, G. S. (Eds.) (1987). Biosensors, fundamentals and Applications. Oxford University press.

Vadgama, P. (1990). Membrane based sensors : A review. *Journal Of Membrane Science.* **50:** 141-152.

Vadgama, P. (1992). Designing biosensors. *Chemistry in Britain.* **28:** 249-252.

Wang, F., Schubert, F. & Rinneberg, H. (1995). A fluorometric rate assay of hydrogen-peroxide using immobilized peroxidase with a fiberoptic detector. *Sensors And Actuators B-Chemical.* **28:** 3-7.

Wang, J. (1991). Modified electrodes for electrochemical sensors. *Electroanalysis.* **3:** 255-259.

Wang, J., Lu, F., Angnes, L., Liu, J., Sakslund, H., Chen, Q., Pedrero, M., Chen, L. & Hammerich, O. (1995). Remarkably selective metallized-carbon amperometric biosensors. *Analytica Chimica Acta.* **305:** 3-7.

Wang, J., Pedrero, M., Sakslund, H., Hammerich, O. & Pingarron, J. (1996). Electrochemical activation of screen-printed carbon strips. *The Analyst.* **121:** 345-350.

Wang, J., Chen, L. & Luo, D. B. (1997). Electrocatalytic detection of hydrogen peroxide at a poly(m-phenylenediamine)-modified carbon paste electrode and its use for biosensing of glucose. *Analytical Communications.* **34:** 217-219.

Weston, D. (1999). *PhD Thesis.* Cranfield University.

Wipf, D. O. (2001). Scanning electrochemical microscopy. msstate.edu/dept/chemistry/dow1/secm/secm.html

Wittstock, G. & Schuhmann, W. (1997). Formation and imaging of microscopic enzymatically active spots on an alkanethiolate-covered gold electrode by scanning electrochemical microscopy. *Analytical Chemistry.* **69:** 5059-5066.

Wring, S. A. & Hart J. P. (1992). Chemically modified, carbon-based electrodes and their application as electrochemical sensors for the analysis of biologically important compounds. A review. *The Analyst.* **117:** 1215-1229.

Wurster, P. (1992). Die Peressigsäurebleiche - eine Alternative zu bleichverfahren mit Halogenhaltigen Oxidationsmitteln. *Textil Praxis International, October 1992*, 960-965.

Xu, C. X., Marzouk, S. A. M., Cosofret, V. V., Buck, R. P., Neuman, M. R. & Sprinkle, R. H. (1997). Development of a diamine biosensor. *Talanta.* **44:** 1625-1632.

Yang, L., Janle, E., Huang, T., Gitzen, J., & Kissinger, P. T. (1995). Applications of "wired" peroxidase electrodes for peroxide determination in liquid chromatography coupled to oxidase immobilised enzyme reactors. *Analytical Chemistry.* **67:** 1326-1331.

Zaks, A. and Klibanov, A. M. (1988a). The effect of water on enzyme action in organic media. *Journal of Biological Chemistry.* **263:** 8017-8021.

Zaks, A. and Klibanov, A. M. (1988b). Enzymatic catalysis in nonaqueous solvents. *Journal of Biological Chemistry.* **263:** 3194-3201.

Zaks, A. & Russell, A. J. (1988). Enzymes in organic solvents: Properties and applications. *Journal of Biotechnology.* **8:** 259-270.

Zhang, Y. N., Hu, Y. B., Wilson, G. S., Moattisirat, D., Poitout, V. & Reach, G. (1994). Elimination of the acetaminophen interference in an implantable glucose sensor. *Analytical Chemistry.* **66:** 1183-118.

Appendix

Published Papers and Conference Proceedings.

Peroxide Sensors for On-Line Monitoring in the Food Industry

A P Moody and S Saini
Cranfield Centre for Analytical Science, Cranfield University, Bedfordshire, MK43 OAL, UK.
www.cranfield.ac.uk/ibst/ccas/

Introduction

In recent years, because of their environmental advantages, peroxides such as hydrogen peroxide and peracetic acid have been replacing halogenated substances for disinfection processes in the food and beverage industry. They are however, more expensive (up to 3 times the cost) and thus users need to have more control over their use and thus waste (1, 2, 3).
In the disinfection of food and beverage production facilities or the sterilisation of medical and pharmaceutical instrumentation, it is essential to have error free disinfection to avoid bacterial contamination. To avoid this risk, it is common to add 20% *more* disinfectant than is really necessary. After disinfection, it has to be confirmed that none of the disinfectant is left in the production vessels so that it will not contaminate the products. This requires a method with a low level of detection and a working range over several orders of magnitude. Current methods are not suitable for on-line monitoring at the concentrations found.

Aim

The aim of this work was to develop a biosensor that could be used for the on-line determination of hydrogen peroxide in such a situation, thus reducing consumption and costs by up to 20%.

Sensor Production

The sensor is for use in an on-line system, thus over time, the sensor's active components will gradually be removed or contaminated.
Various approaches can be taken to retain the components on the surface of a sensor but many do not lend themselves readily to economical mass production.
We decided to entrap the enzyme and mediator using a polymer as membrane material and selected cellulose acetate as it is inexpensive and readily available.
The base sensors were produced by the well established technique of thick film screen printing (Figure 1)
The central (working electrode) then had the active components (horseradish peroxidase in buffer mixed with dimethylferrocene and cellulose acetate in acetone to produce a suspension) printed onto it using a BIODOT printer. This was set to print 4 dots of 400nl on the working electrode surface where they spread to give an even cover before the acetone evaporated.

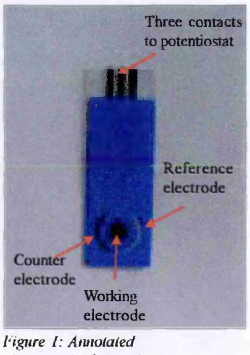

Figure 1: Annotated photograph of a single sensor

Results

When immersed in a vessel of constantly renewed buffer solution, the sensor retained its sensitivity for at least a week. When placed in a small sealed flow-cell (Figure 2) this was reduced to 4 days. Figure 3 shows the peaks obtained in a typical 10 point calibration and Figure 4 shows the calibration curves obtained initially from a fresh sensor and after 4 days in the flow cell.


Figure 2: Photograph of a sensor fixed in the flow cell

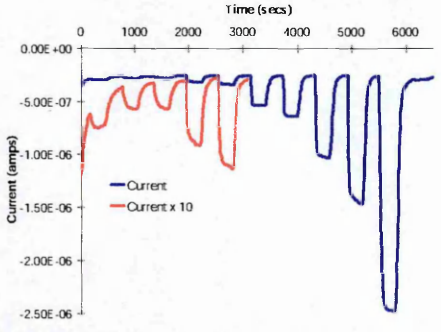

Figure 3: Peaks obtained with a 10 point calibration (blue) and then with a 10-fold mathematically increased gain (red) for the lower levels.

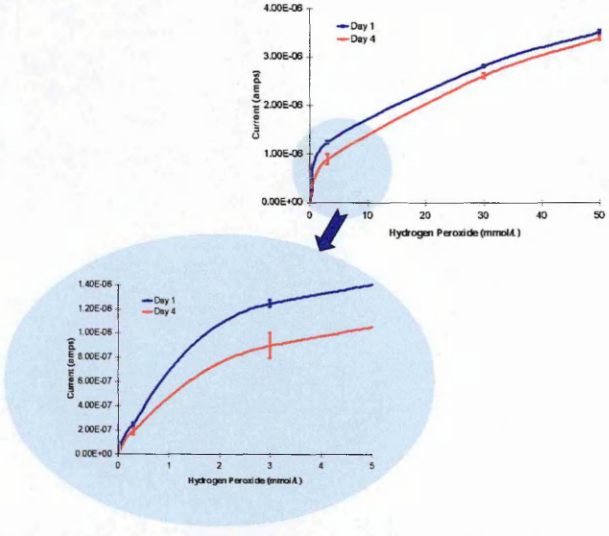

Figure 4: Calibration curves obtained with a fresh sensor (blue) and the same sensor after 4 days continuous use (red)

Conclusion and Prospects

The above results show that entrapping horseradish peroxidase and dimethylferrocene within a cellulose acetate membrane enables us to economically produce a peroxide sensor for on-line monitoring in the food industry; the four-day operation that we have achieved being considered as adequate. This technique of sensor production may also be used for other analytes of interest to the food and beverage industries.

Acknowledgements

We acknowledge the financial support of the EU Standards, Measurements and Testing programme, Europerox project (SMT4 - CT97 - 2153)

References

1. Forber, C. L. *Pulp & Paper*, November 1992. pp. 90-97
2. Wurster, P. *Textil Praxis International*, October 1992. pp. 960-965.
3. Krüßmann, H. & Bohnen, J. *Tenside Surfactants. Deterg.* 1994 **31** 229-232

FULL PAPER
THE ANALYST
www.rsc.org/analyst

Peroxidase enzyme sensor for on-line monitoring of disinfection processes in the food industry

Andrew Moody, Steven Setford and Selwayan Saini*

Cranfield Centre for Analytical Science, Cranfield University at Silsoe, Silsoe, Bedfordshire, UK MK45 4DT. E-mail: s.saini@cranfield.ac.uk

Received 23rd April 2001, Accepted 11th July 2001
First published as an Advance Article on the web 5th September 2001

For desirable environmental reasons, peroxides have replaced halogenated substances for disinfection purposes in the food and beverage industry. However, cost issues and the requirement to remove these agents completely after disinfection necessitate simple, low-cost and sensitive test methods with a wide dynamic range and on-line capability. The development and performance of such a method is detailed here. Low-cost peroxide sensors were fabricated using a single deposition procedure, in which horseradish peroxidase enzyme and dimethylferrocene mediator were entrapped within a cellulose acetate membrane, over the working electrode area of a screen-printed three-electrode assembly. Optimum performance was obtained using HRP and DMFc loadings of 25 U and 0.03 μmol per electrode, respectively, and a mean cellulose acetate molecular weight of 37000. The device had a detection limit of 49.5 μM hydrogen peroxide and mean RSD values of 21% across the concentration range 49.5–368 μM. In laboratory studies the sensor was shown to have a stability of ≥4 d in continuous flow-mode maintaining an accuracy of ±16% that was considered acceptable for the intended on-line monitoring of the disinfection process. In a field study, it was successfully used on-line within a flow-cell to measure peroxide levels during disinfection of an industrial fermentation vessel.

1. Introduction

A wide range of chemicals are routinely used for disinfection purposes in the food and beverage industry, including alcohols, aldehydes, gaseous agents, phenolics and halogenated compounds, with the last group being most widely employed for reasons of cost and efficiency. However, in recent years, peroxides such as hydrogen peroxide (HPx) and peracetic acid have been increasingly used since they are more potent oxidising agents than many of the routinely used halogenated disinfectants. HPx readily decomposes into water and oxygen and therefore poses no threat to the environment and removes the possibility of disinfectant contamination due to inadequate rinsing of production vessels.

However, these benefits are at a price since peroxides typically cost up to three times more than their halogenated counterparts. Therefore, in order for peroxide disinfection to be cost-effective, industrial users require simple, low-cost and effective methods for monitoring their usage. Furthermore, manufacturers achieve error-free disinfection and avoid biological contamination, by working with excess levels of disinfectant (typically ~20%). Therefore, on-line measurement procedures would allow the manufacturer to maintain accurately disinfectant levels above a desired threshold value, thereby minimising excess disinfectant usage. Such an approach would also allow the end-user to confirm rapidly and routinely that all disinfectant residues have been removed from the production vessel prior to commencement of the next production cycle.

There are a number of off-line methods available for the determination of peroxides. Chemical methods include the spectrophotometric measurement of oxidised products arising from peroxide activity.[1]

The inherent electroactivity of these compounds also allows their simple measurement using electroanalytical techniques, notably amperometry in which an electrode is poised at a suitable operating potential and the current due to the reduction of the peroxide is measured. A problem with this approach is the overpotential required to facilitate the oxidation process. The operating potential can be reduced using noble metals such as gold or platinum or more inexpensively using electrocatalytic materials such as metallised carbons[2–5]

However, even with such approaches, a significant potential is required and signal interference due to the presence of other electroactive compounds in a given sample can occur. Whilst a further reduction in operating potential will reduce the magnitude of the interference signal, this will also be at the expense of the analyte signal.

The interference problem can be effectively eliminated *via* the use of biological rather than electrochemical catalysts, allowing the application of very low operating potentials. For peroxides, this is routinely achieved using the redox enzyme horseradish peroxidase (HRP). HRP is able to reduce HPx to water, with the concomitant oxidation of a suitable electron donor, the reducing equivalents being transferred to the peroxide via the active site of the enzyme:

$$H_2O_2 + 2DH \xrightarrow{HRP} 2H_2O + 2D$$

where DH and D are the reduced and oxidised forms of the added electron donor, respectively. In electroanalytical systems, the electron donor is often termed a mediator since it mediates the transfer of electrons from the working electrode to the active site of the enzyme. In biosensor systems, HRP is typically immobilised or entrapped at or near the electrode surface. Many different mediators, capable of undergoing reduction at electrode surfaces at very low potentials, have been evaluated.[6–19] The use of chromogenic electron donors also allows the enzymatic reduction of peroxidase to be monitored colorimetrically using free peroxidase and a spectrophotometer. The enzymes catalase and microperoxidase have also been used for peroxide determination.

The choice as to whether an electrochemical or colorimetric approach is used to determine peroxide activity is dependent upon the application. The latter approach predominates in centralised testing facilities since it is well established but

DOI: 10.1039/b103591f

relatively complex, requiring a number of sequential liquid handling steps and an incubation procedure. In contrast, the electrochemical biosensor approach is simple, inexpensive and rapid and consequently is ideal for deployment in an at-line or on-line capability.

Consequently, the key aim of this study was to develop an on-line biosensor tool, incorporating HRP and mediator, for the simple, real-time monitoring of peroxide disinfection processes for usage by the food and drinks industries. Currently, no such continuous on-line peroxide determination system is commercially available. The basal electrochemical transduction devices were produced by screen-printing, a reproducible, routine and low-cost method for the mass manufacture of electrodes.[2,3] The devices were intended to be disposable, thereby addressing issues related to electrode fouling and enzyme stability. The performance of the optimised sensor device was tested under real on-line process conditions within an industrial production environment.

2. Experimental

2.1. Reagents

Phosphate buffer solution (PBS) was composed of 0.1 M KH_2PO_4–K_2HPO_4, pH 7.2, whilst phosphate buffer–electrolyte (PBE) solutions also contained 0.1M KCl, all supplied by Merck (Poole, Dorset, UK). Horseradish peroxidase (EC 1.11.1.7, 200 U mg^{-1}) was obtained from Sigma (Poole, Dorset, UK), Nafion and 1,1-dimethyferrocene from Aldrich (Gillingham, Dorset, UK), hydrogen peroxide (HPx, 30% w/v), hexacyanoferrate(II) (HCF) and tetrathiafulvalene (TTF) from Merck and cellulose acetate (CA, various average MWs) from Fluka (Buchs, Switzerland). Water was purified by de-ionisation and reverse osmosis (Elgastat system, Elga, High Wycombe, UK).

2.2. Sensor fabrication

Three-electrode devices were mass manufactured in-house by a multi-stage screen-printing process using a DEK 248 machine (DEK, Weymouth, UK) and screens with appropriate stencil designs (60 per screen) fabricated by DEK Precision Screen Division. The stainless-steel screen mesh was mounted at 45° to the print stroke with 77 wires cm^{-1} (125 wires cm^{-1} for graphite ink) with an emulsion thickness of 13 μm. Devices were printed on to 250 μm thick polyester sheet (ICI Melinex ST275, Cadillac Plastic, Swindon, UK). The circular working electrode (WE) (planar area 0.16 cm^2), counter electrode and basal tracks were fabricated from graphite ink (Electrodag 423SS, Acheson Colloids, Plymouth, UK). The reference electrode ink contained 15% silver chloride in silver paste (Ag/AgCl, MCA Services, Cambridge, UK). The basal tracks were insulated from the measurement solution using 242-SB epoxy-based protective coating ink (Agmet ESL, Reading, UK). The electrodes were heat treated at 125 °C for 2 h to cure the epoxy resin to allow prolonged device usage in solution.[2]

2.3. Preparation of peroxide sensor surface

The screen-printed bare carbon WE surface was adapted to HPx detection using an appropriate enzyme–mediator system and membrane. Previous characterisation studies coupled with cost, durability, stability and ease of use considerations resulted in the choice of the mediators hexacyanoferrate(II) (HCF)[6,7], tetrathiafulvalene (TTF)[8–11] and dimethylferrocene (DMFc).[8,16,17]

The final device was intended to function in a flowing stream over a complete disinfection cycle. In order to minimise electrode fouling and loss of immobilised HRP activity due to desorption, coverage of the WE with a membrane was evaluated. The prime criteria for the selection of the membrane material were reduced fouling and enzyme desorption coupled with enhanced protection of the biolayer, acceptable sensor sensitivity and detection limit, rapid response, cost and amenability to mass manufacture.

Various polymers have been used as membrane materials in conjunction with HRP,[20] including acrylate,[21] polyurethane and poly(vinyl chloride)[22] with Koochaki *et al.*[23] showing cellulose acetate to be superior to polycarbonate and acetate butyrate for reasons of selectivity or magnitude of response. Electro-polymerisation of poly(*o*-phenylenediamine) to give ultra-thin layers has been suggested, but the process is not amenable to mass manufacture.[6]

Nafion is a highly negatively charged perfluorinated sulfonate polymer that acts as a strongly acidic cation exchanger. It acts to repel anionic species whilst allowing the passage of cations, particularly divalent hydrophobic cations[24]. Ink-jet printing can be used for the deposition of Nafion, giving membranes of defined and reproducible geometry. Cellulose acetate (CA) works by size exclusion with the thickness of the coating affecting the response time of the sensor[23]. It can be used alone[2,22–24] or in combination with other membrane materials, including Nafion[25]. Application may be by dip coating or ink-jet printing and thus is suited to mass production. For these reasons and also for reasons of cost and availability, it was decided to investigate the use of Nafion and CA membranes in this work.

Three approaches, described below, were examined for the optimised deposition of these materials on the circular WE surfaces. DMFc and polymer (2% w/v) were prepared in acetone and HRP in PBS.

All solutions were applied in 4 μl doses, the minimum volume necessary to cover the WE surface. Applied solutions were thoroughly dried (> 1 h) prior to application of proceeding liquids. Reagents were either applied in a single dose or diluted 1 + 2 and applied as a double dose with drying in between. Three deposition regimes were examined, as follows.

2.3.1. Sequential addition of mediator, enzyme, then membrane. Single application: DMFc and HRP and CA were sequentially dried on to the WE surface. Double application: the solutions were sequentially (DMFc × 2, HRP × 2, CA × 2) dried on to the WE surface.

2.3.2. Pre-mixing, then application of enzyme–mediator, then membrane. Single application: the HRP and DMFc solutions were mixed before application. The CA solution was then dried over the enzyme–mediator film. Double application: the HRP and DMFc solutions were diluted before being mixed and two applications of the mix were dried on to the WE. The diluted CA solution had two applications dried over the enzyme–mediator film.

2.3.3. Pre-mixing then application of all components. Single application: DMFc, HRP and CA were mixed then dried on to the WE. Double application: the DMFc, HRP and CA solutions were diluted to half that previously, before being mixed and two applications dried on to the WE.

Four CA materials of different MW (29000, 37000, 52000 and 61000) were evaluated. The final electrodes each contained 25 U HRP and 0.03 μmol DMFc and the equivalent of a 2% w/v CA film. All acetone solutions were used immediately after preparation to avoid solvent evaporation.

2.4. Measurement procedure

The test procedure was performed at ambient temperature using an Autolab Electrochemical Analyser with GPES3 software (Ecochemie, Utrecht, The Netherlands). The screen-printed electrodes were connected to the analyser using IDE edge connectors (RS Components, Corby, UK). Characterisation of the enzyme–mediator systems with the screen-printed devices using cyclic voltammetry and chronoamperometry indicated that the optimum potential for amperometric HPx detection was −300 mV for DMFc, −175 mV for HCF and −150 mV for TTF (all *vs.* Ag/AgCl reference). Tests were performed by immersion of the three-electrode system in process solutions appropriately diluted in PBE. HPx solutions were maintained below 2.5 mM in order to prevent HRP deactivation.[26,27]

2.5. Testing of flow-cell system

The fermenter evacuation stream was sampled *via* a bleed line then mixed and diluted in two steps using a peristaltic pump and tubes as in Fig. 1. Air segments were introduced into the stream to reduce carry-over and facilitate mixing as the stream passed through the coils. A two-step dilution process was required to achieve a suitably large dilution (×432) of the sample such that the HPx concentration fell within the dynamic range of the sensor and was compatible with the available range of pump tube flow rates. The diluted sample stream was fed to the HRP electrode housed in a Perspex flow-cell at a rate of 0.42 ml min^{-1}. The flow-cell had channel dimensions of 24 × 10 × 0.5 mm (measured volume of 120 μl using RO water at ambient temperature; see Fig. 2).

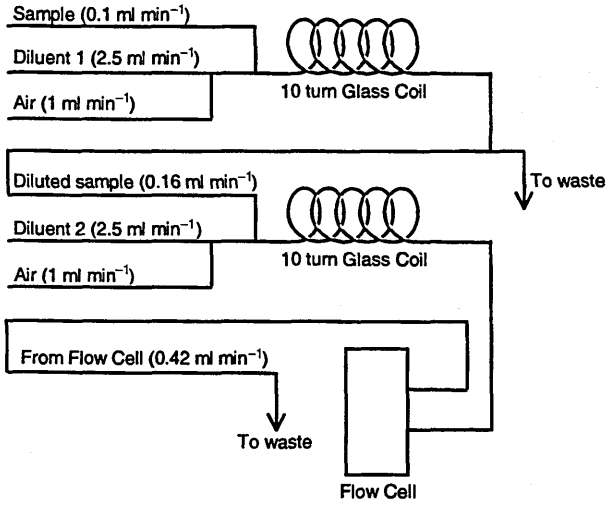

Fig. 1 Schematic diagram of the peristaltic pump tubing layout for the flow-cell assembly.

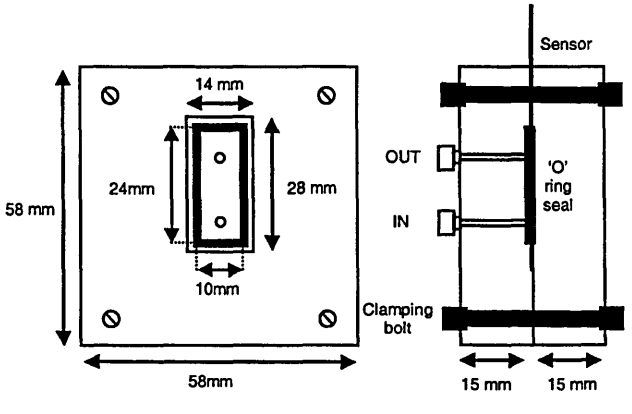

Fig. 2 Schematic diagram of the flow-cell body.

In the off-line study, 'synthetic' samples consisting of HPx and 'real' samples consisting of actual process solutions containing HPx were tested. In the on-line study, the stirred fermentation vessel was filled with ~180 l of 2% w/v NaOH in water and 10 l of spent fermentation broth (total volume ~190 l) and the mixture heated to 60–80 °C. After 245 s, 1.5 l of 10 M (34%) HPx were added to the vessel (final volume ~191.5 l, giving a diluted HPx concentration of about 1.5 × 10000/191.5 = 78 mM) for the cleaning process. This was then diluted by the pump tube system (Fig. 1) at the sampling stage and the sensor response to this diluted sample (~180 μM) was recorded. The sample stream from the fermentation vessel was passed through a refrigeration unit prior to dilution to ensure that samples were at ambient temperature (~25 °C) on entering the flow-cell. The flow-cell was calibrated on-line by sampling pure HPx solutions of 29–220 mM prior to sampling from the bleed line and the addition of HPx to the fermentation vessel.

2.6. Standard method

An HPx stock standard solution used as a common calibration standard and spiked samples were analysed before and after analysis by titration with thiosulfate after addition of potassium iodide. Iodimetric titration with dichromate was used for the standardization of the titrant.[28]

3. Results and discussion

3.1. Selection of mediator and membrane material

Preliminary experiments were performed in order to select the most appropriate mediator and membrane materials. Of the three mediators evaluated, TTF was found to give the poorest sensor sensitivity and HCF was found to be highly water soluble and thus prone to leaching into the aqueous sample medium, despite the presence of a protective membrane layer. Consequently, the low-cost mediator DMFc was selected. CA proved more suitable than Nafion for membrane fabrication purposes, owing to a more stable signal and baseline and lower cost, important considerations when considering mass manufacturing issues.

3.2. Application of mediator, enzyme and membrane

As with all enzyme-electrode devices, determination of the optimum reagent deposition protocol is essential in order to maximise the sensor response. The three protocols described in the Experimental section, were studied with solutions being applied in a single or double application.

The current *versus* concentration plots for the HRP sensor are shown in Fig. 3. In effect, the greater the gradient, the more responsive the sensor is to HPx. Thus, the sensor response is enhanced by pre-mixing and co-depositing HRP, DMFc and CA membrane, as opposed to pre-mixing and applying HRP and DMFc prior to the CA membrane and also applying the three reagent components individually. Application of the three components together results in the entrapment of enzyme and mediator within, as opposed to under, the membrane film. This method of application facilitates a more intimate contact between the mediator and enzyme with enhanced accessibility of HPx to the enzyme, which is in, as opposed to under, the membrane.

Furthermore, application of the reagents in two discrete doses as opposed to a single dose further enhanced the signal. A number of factors may contribute to this effect, including the fact that the membrane pore size, which is a function of drying time, will be influenced by the amount of liquid sample

deposited on the electrode. Given the fact that ease and economy of mass manufacture are important factors in disposable sensor fabrication, single-dose reagent application was selected over the double-dose method.

3.3. Selection of optimum sensor parameters

Three key sensor parameters were optimised during the course of this work: enzyme loading, mediator loading and CA membrane MW. A large-scale optimisation experiment was initiated in which all combinations of these parameters were assessed, in triplicate, across a suitable range of values over an analytically valid HPx concentration range. That combination of parameters giving the highest signal *versus* reproducibility ratio coupled with an acceptable dynamic range and limit of detection (LOD) was considered optimal with regard to sensor performance. The following sections detail the effect of varying each of these three variables in turn, with the remaining two variables being maintained at the optimum levels determined by the overall large-scale experiment. In all cases the performance was evaluated over the HPx range 0–368 μM.

3.3.1. Optimisation of horseradish peroxidase loading. The response of the sensors, loaded with various amounts of HRP and an optimised amount of mediator (0.03 μmol per electrode) and a CA MW of 37000 is shown in Fig. 4. It can be seen that the largest responses were obtained at enzyme loadings of 20 and 25 U; the latter loading was selected for further experimentation, based on a superior signal : *s* ratio (19.0 *vs.* 15.8) and greater reproducibility, based on a lower RSD value across the HPx concentration range (6.9 *vs.* 11.3%).

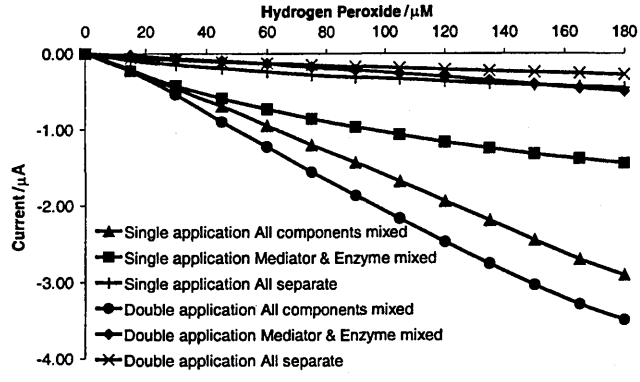

Fig. 3 Effect of the three different application processes used to deposit HRP, DMFc and CA on sensor response across 0–368 μM HPx. Each sensor had an HRP and DMFc loading of 25 U and 0.03 μmol per electrode, respectively, with a mean CA MW of 37000.

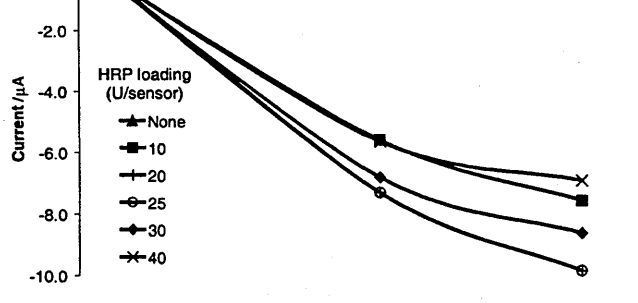

Fig. 4 Effect of HRP loading on sensor response across 0–368 μM HPx. Each sensor had a DMFc loading of 0.03 μmol per electrode and a mean CA MW of 37000.

Higher signal : *s* ratios were recorded at other HRP loadings, but were accompanied by larger RSD values (Table 1).

3.3.2. Optimisation of dimethylferrocene mediator loading. The response of the sensors, loaded with various amounts of mediator, an optimised amount of enzyme (25 U) and a CA MW of 37000, to HPx is shown in Fig. 5. The largest responses were obtained at a DMFc loading of 0.1 μmol per sensor. However, over the evaluated HPx range a DMFc loading of 0.03 μmol per sensor gave demonstrably superior performance with regard to signal : *s* ratio and RSD (35.7 and 9.2%, respectively) (Table 2). Only at low HPx concentrations (0–2.2 μM) did the data suggest an optimum mediator loading of 0.10 μmol per electrode (signal : *s* ratio 5.0; RSD 8.9%). The optimum choice of mediator loading is therefore dependent on the level of analyte in the sample. As the sample dilution for the cleaning process can be controlled, with the superior signal : *s* ratio at the higher concentrations, the 0.03 μmol/sensor loading was used.

Table 1 HRP electrode response using enzyme activity loadings of 0–40 U per working electrode. The mean signal : *s* ratio and mean RSD values across the HPx range 0–368 μM are shown. Sensors were fabricated using 37000 MW CA membrane and a DMFc loading of 0.03 μmol per electrode; $n = 3$

	Horseradish peroxidase enzyme loading/U per electrode					
	0	10	20	25	30	40
Mean signal : *s* ratio[a]	3.0	24.6	15.8	19.0	7.3	6.7
Mean RSD[b] (%)	41.9	26.0	11.3	6.9	14.1	28.0

[a] Mean response/mean *s* of the sensor for each HPx concentration tested. [b] Mean RSD of the sensor response for each HPx concentration tested.

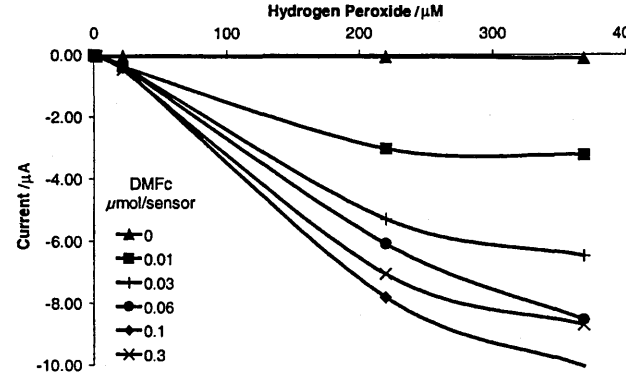

Fig. 5 Effect of DMFc loading on sensor response across 0–368 μM HPx. Each sensor had an HRP loading of 25 U and a mean CA MW of 37000.

Table 2 HRP electrode response using mediator loadings of 0–0.3 μmol per working electrode. The mean signal, mean *s* and mean RSD values across the HPx ranges 0–2.2 and 0–368 μM are shown. Sensors were fabricated using a 37000 MW CA membrane and an enzyme loading of 25 U; $n = 3$

	1,1-Dimethylferrocene loading per sensor/ μmol per sensor					
	0.00	0.01	0.03	0.06	0.10	0.30
0–368 μM hydrogen peroxide range						
Mean signal : *s* ratio	6.0	6.0	35.7	8.0	21.7	6.7
Mean RSD (%)	17.3	22.3	9.2	16.6	6.7	18.0
0–2.2 μM hydrogen peroxide range						
Mean signal : *s* ratio	3.1	4.9	4.7	3.4	5.0	4.0
Mean RSD (%)	19.6	4.7	14.1	22.6	8.9	22.5

3.3.3. Optimisation of cellulose acetate membrane molecular weight. The response of the sensors, loaded with the four CAs with different mean MWs, an optimised amount of enzyme (25 U) and an optimised amount of mediator (0.03 μmol per electrode), to HPx is shown in Fig. 6. It can be seen that acceptable sensor performance characteristics were recorded for all of the CA MWs examined, with the 29000 and 52000 MW CA sensors giving larger signals than the 37000 and 61000 CA MW sensors. However, when the mean signal:s ratio and mean RSD data (Table 3) are examined, then the selection of the most appropriate MW for membrane fabrication becomes dependent upon the analytical performance required. For example, whilst the mean RSD values were comparable between the sensors for each MW examined, the 52000 MW CA sensors gave the largest mean signal:s ratio, whilst those fabricated with 37000 MW CA gave the lowest HPx detection limit. For the present application, it was decided to select the 37000 MW CA for the benefit of the lowest HPx detection limit with a better mean signal:s ratio than the 29000 MW CA.

3.4. Flow-cell format

The performances of the fully optimised HPx sensors (25 U HRP, 0.03 μmol DMFc, 37000 MW CA membrane) were examined in the flow-cell format. Fig. 7 shows the sensor response to increasing concentrations of HPx. A typical calibration curve for the flow-cell mounted sensor is shown in Fig. 8 along with a typical calibration curve for the non-flow-cell mounted electrode. A ~10-fold reduction in the current response of the sensor in the flow system with a concomitant increase in the dynamic range is apparent. These different response profiles were considered to be due primarily to differences in boundary layer diffusion profiles. An electrode mounted within a flow-cell channel with a constant flow of solution will experience laminar flow conditions and have a significantly different boundary layer to that experienced by the same sensor in a stirred beaker experiencing turbulent flow conditions.

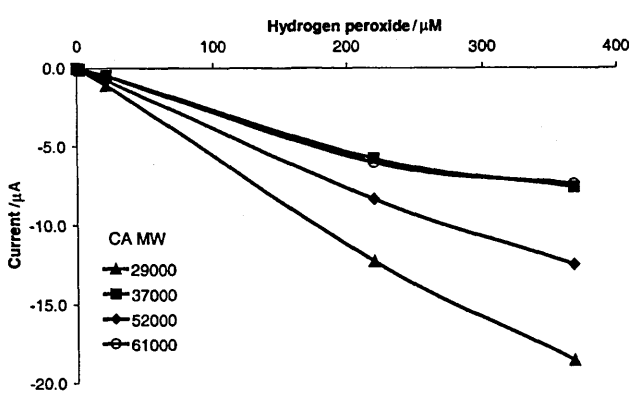

Fig. 6 Effect of mean MW of cellulose acetate on sensor response across 0–368 μM HPx. Each sensor had an HRP and DMFc loading of 25 U and 0.03 μmol per electrode, respectively.

Table 3 Analytical performance characteristics of the HRP enzyme electrodes with membranes fabricated using CA of various mean MW. HRP and 1,1-dimethylferrocene loadings of 25 U and 0.03 μmol per electrode, respectively, were used; n = 3

	Mean cellulose acetate MW			
	29000	37000	52000	61000
Mean signal:s ratio	4.34	5.74	8.24	6.60
Mean RSD (%)	26.07	21.01	20.42	21.87
LOD/μM[a]	49.53	49.49	76.58	116.41

[a] LOD (limit of detection): 2.5 × s at zero HPx.

The flow-cell mounted sensor system was used in a large-scale disinfection process within a real production environment at the König Brauerei, Duisberg, Germany. The flow-cell system was initially tested off-line by addition of the synthetic HPx samples into the buffer–ethanoic acid carrier stream and comparing the resultant responses with suitable calibrational data. Next, the system was tested, again off-line, with the real samples obtained from the standard process-scale disinfection procedure. Key results are given in Table 4.

The off-line performance of the flow-cell system was very encouraging. Sensor HPx measurements were within ±16% of those determined by the standard permanganate titration method for both the synthetic and real samples at the higher and lower analyte concentrations. Furthermore, the good agreement between the sensor and standard method for the real samples indicated no significant matrix or interference effects. In all cases the RSDs of the measured samples (n = 6) were ≤7.3%. The flow-cell method was considered to be sufficiently accurate and repeatable to allow meaningful evaluation of the system in an on-line capacity. The on-line experimental procedure detailed in the Experimental section was followed. The sensor response profile to the HPx wash solution with yeast extract is shown in Fig. 9. For the purpose of this industrial trial, the significant factor was the response seen after addition of HPx to the wash and then a gradual fall in response as the peroxide was broken down during the wash cycle.

3.5. Interferences and matrix effects

Whilst the developed sensor has wide applications for the detection of peroxides and peracetic acid in a wide variety of

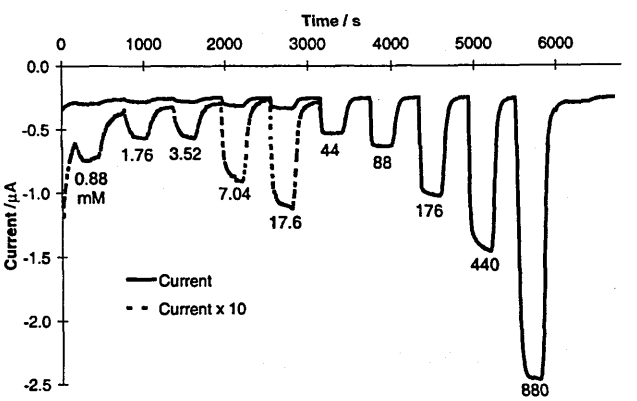

Fig. 7 Flow-cell mounted sensor response to increasing concentrations of HPx solution. The sensor response profiles at the lower HPx concentrations have been multiplied ×10 to aid interpretation.

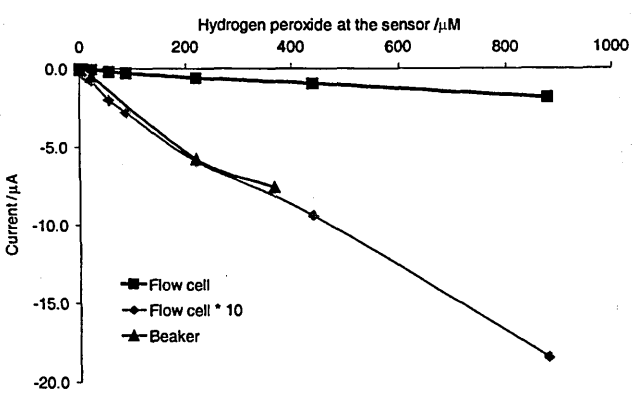

Fig. 8 Calibration curve for the flow-cell mounted optimised HPx sensor. Also shown is the response of the same sensor in a stirred beaker. The sensor responses for the flow-cell mounted sensor are also shown ×10 to aid data comparison.

Table 4 Response of flow-cell mounted HRP sensors to HPx samples and operated in an off-line capacity. Synthetic samples contained HPx only, whereas real samples were those obtained from a standard process-scale disinfection process. Samples were diluted as described in the Experimental section

	Spiked HPx concentration		Sensor data			
Sample	mg l^{-1}	mM	mg l^{-1}	mM	Accuracy (%)	RSD[a] (%)
Synthetic	264	7.8	227	6.7	−14.0	6.7
Synthetic	4803	141.3	4656	136.9	−3.1	3.1
Real	4715	138.7	4459	131.1	−5.4	4.3
Real	4797	141.1	5069	149.1	+5.7	7.3
Real	4800	141.2	4031	118.6	−16.0	5.6
Real	960	28.2	927	27.3	−3.4	5.2

[a] $n = 6$.

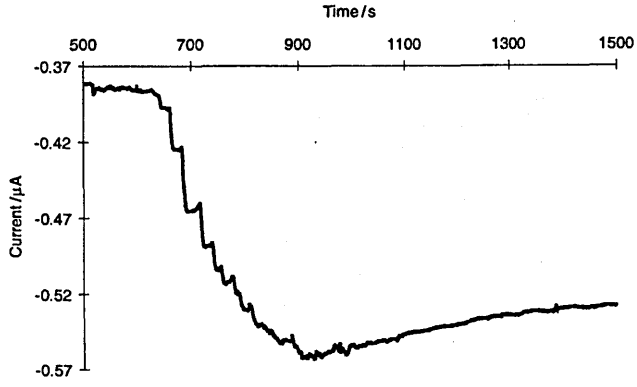

Fig. 9 Response profile of the flow-cell mounted HPx sensor operated in an on-line capacity for measurement of a real wash solution containing HPx removed at the end of a process-scale disinfection process.

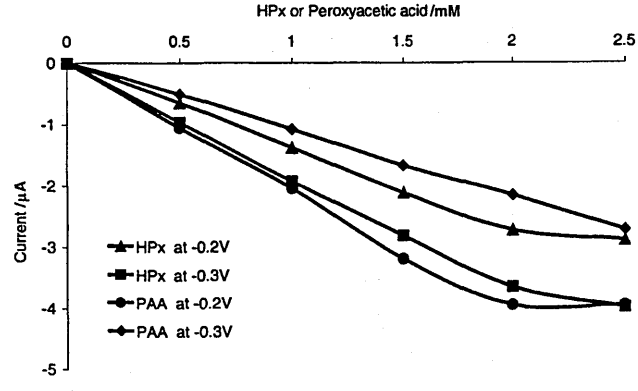

Fig. 10 Calibration curves for the sensor responses to HPx and peracetic acid at operating potentials of −0.2 and −0.3V *vs.* Ag/AgCl.

applications, the real samples from the industrial disinfection process consisted of a highly alkaline wash solution that were shown not to contain significant levels of interferents or matrix effects. Application of the sensor to alternative measurement problems where interferents or matrix problems may occur would necessitate a detailed evaluation of these issues on an application-by-application basis. The mediator approach, with DMFc undergoing reduction at −300 mV (*vs.* Ag/AgCl), ensures minimisation of undesirable electrochemical reactions.

As part of the optimisation process, the operating potential for the sensor was set at −300 mV (*vs.* Ag/AgCl) to give the best relative response to HPx (as opposed to peracetic acid with an optimum detection potential of −200mV *vs.* Ag/AgCl). Fig. 10 shows the relative responses of both compounds. As only one compound would be used at any one time in a disinfection process, specificity was not an issue. In the study at the König Brauerei,[28] the sensor was shown to respond to peracetic acid as the sole oxidising agent with similar precision and accuracy to

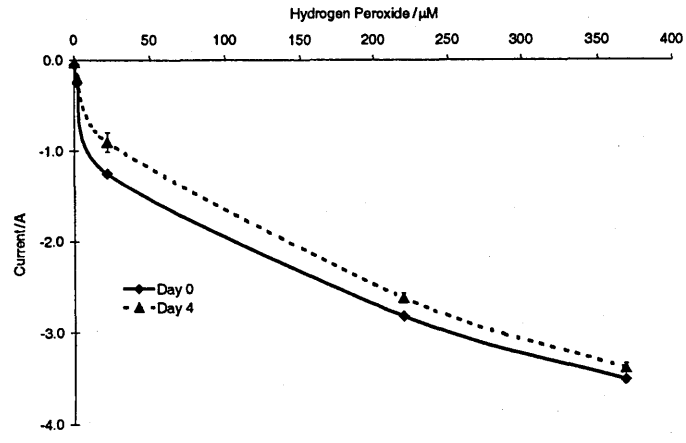

Fig. 11 Calibration curves for the flow-cell mounted optimised HPx sensor at time zero and after 4 d of continuous operation.

those found when HPx was used. The sensor showed no response to ascorbic acid or acetic acid (present in solution when peracetic acid is used) at either potential.

3.6. Sensor lifetime and stability

The sensor showed no decline in either response or sensitivity when run in 0.1 M phosphate buffer for 7 d at 25 °C. The response of the sensor after 4 d of continuous operation within the flow-cell is shown in Fig. 11. Comparison of the sensor response at the commencement of the stability test and after the 4 d test period is shown in Table 5. A very small decline in signal magnitude (<7.1%) was observed at high HPx concentrations (30–50 mM), but became more noticeable at lower HPx concentrations (45.6% loss of signal at 0.03 mM HPx). Since most HPx disinfection processes are completed in a few hours, the observed stability characteristics of the HPx sensor were deemed acceptable. The slight decline in sensor performance may be due to a number of factors including leaching of enzyme and/or mediator, loss in enzyme activity and membrane and/or electrode fouling.

4. Conclusions

Flow-cell mounted screen-printed peroxide sensitive sensors provide acceptable analytical performance for the on-line monitoring of residual peroxide levels during industrial-scale fermentation vessel disinfection processes. Optimum sensor performance was obtained using 25 U of horseradish peroxidase enzyme and 0.03 μmol dimethylferrocene mediator per electrode, entrapped within a 2% w/v cellulose acetate membrane (mean MW 37000) with all three reagents being co-deposited in a single step. The low cost of the reagents and sensor fabrication

Table 5 Response and RSD data for flow-cell mounted sensor at commencement of measurement process and after 4 d of continuous operation. The percentage decrease in sensor response after 4 d is shown in the last column. The zero analyte response from the sensor is the baseline prior to HPx addition in each case

	Day 0		Day 4		
HPx/μM	Mean response/A	RSD (%) (n = 3)	Mean response/A	RSD (%) (n = 3)	Loss from day 0 response (%)
0.03	5.15×10^{-8}	22.4	2.80×10^{-8}	7.6	45.6
0.30	2.55×10^{-7}	5.5	1.96×10^{-7}	14.9	23.1
3.00	1.25×10^{-6}	2.4	9.06×10^{-7}	11.8	27.7
30.00	2.82×10^{-6}	1.1	2.62×10^{-6}	2.1	7.1
50.00	3.52×10^{-6}	1.1	3.40×10^{-6}	1.4	3.5

and simplicity of reagent deposition makes this approach amenable to the high-volume production of these disposable elements. The sensor can be used continuously over at least a 4 d period. This technique represents a novel and genuine advance in the monitoring of peroxide disinfection processes since no commercial alternatives are currently available.

5. Acknowledgements

We acknowledge the financial support of the EU Standards, Measurements and Testing programme, Europerox project (SMT4 – CT97 – 2153) and partners therein: Skalar Analytical; Cees Bonis for the on-line testing studies; Miljo-Kemi; König-Brauerei, especially Dr Frank Nitzsche and Dr Diedrich Harms; Dr Uwe Karst, University of Munster; and Prof. Karyanis, University of Ioannina, Greece.

References

1 J. E. Frew, J. Jones and G. Scholes, *Anal. Chim. Acta*, 1983, **155**, 139.
2 S. Kröger and A. P. F. Turner, *Anal. Chim. Acta*, 1997, **347**, 9.
3 J. D. Newman, S. F. White, I. E. Tothill and A. P. F. Turner, *Anal. Chem.*, 1995, **67**, 4594.
4 S. Sampath and O. Lev, *J. Electroanal. Chem.*, 1997, **426**, 131.
5 J. Wang, F. Lu, L. Angnes, J. Liu, H. Sakslund, Q. Chen, M. Pedrero, L. Chen and O. Hammerich, *Anal. Chim. Acta*, 1995, **305**, 3.
6 K. Johansson, G. Jönsson Pettersson, L. Gorton, G. Marko-Varga and E. Csöregi, *J. Biotechnol.*, 1993, **31**, 301.
7 G. Ortiz, M. C. Gonzalez, A. J. Reviejo and J. M. Pingarron, *Anal. Chem.*, 1997, **69**, 3521.
8 P. C. Pandey, S. Upadhyay and B. Upadhyay, *Anal. Biochem.*, 1997, **252**, 136.
9 U. Bilitewski, W. Drewes, J. Neermann, J. Schrader, R. Surkow, R. D. Schmid and J. Bradley, *J. Biotechnol.*, 1993, **31**, 257.
10 H. Liu, J. Kong and J. Deng, *Anal. Lett.*, 1995, **28**, 563.
11 U. Korell and U. E. Spichiger, *Anal. Chem.*, 1994, **66**, 510.
12 M. J. Green and H. A. O. Hill, *J.Chem. Soc., Faraday Trans.*, 1986, **82**, 1273.
13 P. D. Sanchez, A. J. M. Ordieres, A. C. Garcia and P. T. Blanco, *Electroanalysis*, 1991, **3**, 281.
14 S. L. Chut, J. Li and S. N. Tan, *Anal. Lett.*, 1997, **30**, 1993.
15 U. Kunzelmann and H. Bottcher, *Sens. Actuators B*, 1997, **39**, 222.
16 A. Amine, J. M. Kauffmann, G. G. Guilbault and S. Bacha, *Anal. Lett.*, 1993, **26**, 1281.
17 J. J. Kulys, W. Schuhmann and H.-L. Schmidt, *Anal. Lett.*, 1992, **25**, 1011.
18 A. A. Karyakin, E. E. Karyakina and L. Gorton, *Talanta*, 1996, **43**, 1597.
19 H. Y. Liu, T. L. Ying, K. Sun, H. H. Li and D. Y. Qi, *Anal. Chim. Acta*, 1997, **344**, 187.
20 P. Vadgama, *J. Membr. Sci.*, 1990, **50**, 141.
21 J. J. Gooding, C. E. Hall and E. A. H. Hall, *Anal. Chim. Acta*, 1997, **349**, 131.
22 L. Abdel-Hamid, P. Atanasov and E. Wilkins, *Anal. Chim. Acta*, 1995, **313**, 45.
23 Z. Koochaki, I. Christie and P. Vadgama, *J. Membr. Sci.*, 1991, **57**, 83.
24 M. A. T. Gilmartin and J. P. Hart, *Analyst*, 1995, **120**, 1020.
25 Y. N. Zhang, Y. B. Hu, G. S. Wilson, D. Moattisirat, V. Poitout and G. Reach, *Anal. Chem.*, 1994, **66**, 1183.
26 E. Csöregi, G. Jönsson Pettersson and L. Gorton, *J. Biotechnol.*, 1993, **30**, 315.
27 L. Gorton, G. Bremle, E. Csöregi, G. Jönsson Pettersson and B. Persson, *Anal. Chim. Acta*, 1991, **249**, 43.
28 P. Mortensen, S. Brødsgaard, C. Stenholt, A. Moody, D. Harms, C. Bonis, J. Meyer, T. Steinkamp and G. Diehl, *Anal. Chim. Acta*, submitted.